On the basis of sex: Impact of biological sex on the *Plasmodium* parasite liver stage

Caroline J. Duncombe

A dissertation

submitted in partial fulfillment of the

requirements for the degree of

Doctor of Philosophy

University of Washington

2025

Reading Committee:

Sean C. Murphy, Chair

Paul Edlefsen

Naeha Subramanian

Program Authorized to Offer Degree:

Pathobiology

University of Washington

Abstract

On the basis of sex: Impact of biological sex on the *Plasmodium* parasite liver stage

Caroline J. Duncombe

Chair of the Supervisory Committee:

Sean C. Murphy

Department of Laboratory Medicine and Pathology and Department of Microbiology

The enclosed dissertation lies at the intersection of three fields of study: sex differences, malaria, and hepatology (study of the liver). Biological sex and gender are critically important factors affecting health and disease throughout the human lifespan. Malaria is a deadly disease caused by *Plasmodium* parasites, a pathogen with a complex lifecycle, including a brief but critical liver stage. The liver is the largest solid organ in the body, and the site of complex spatial heterogeneity and important endocrine and immunological function. Biological sex influences the liver. As a sexually dimorphic organ, the liver sustains baseline differences in function, cell composition, and gene expression profiles on the basis of sex. And the liver niche impacts the *Plasmodium* parasite's liver stage. As a hepatotropic pathogen, *Plasmodium* parasites interact within the heterogenous liver microenvironment in a series of host-pathogen interactions that permit survival in the face of innate and adaptive immune responses. However, a knowledge gap remains regarding whether

biological sex impacts the liver stage of the *Plasmodium* parasite. Understanding this connection – between host biological sex, the hepatotropic *Plasmodium* parasite, and the liver – could uncover a new perspective on fundamental liver stage biology and inform the design and execution of liver-targeting vaccines. Thus, the overall goal of this dissertation is to add sex-specific hepatotropic pathogen to the definition of *Plasmodium* parasites. Additionally, this dissertation aims to underscore the need for sex-informed research that transcends outdated biases, ensuring that host-pathogen profiling and vaccines evolve to serve all people.

This thesis demonstrates that *Plasmodium* parasites trigger a sex-specific host response, which holds significant implications for research and clinical interventions. Three key points will be demonstrated. First, humans exhibit sex-specific *Plasmodium falciparum* liver stage outcomes. Second, murine models exhibit sex-specific inflammatory and cellular responses during the rodent *Plasmodium* liver stage, which subsequently impacts parasite survival. Third, murine models also exhibit sex-specific protection from malaria liver stage vaccines, which is connected to the impact of androgens on $CD8^+$ T cell effector mechanisms. Furthermore, we apply a three-part framework for understanding sex differences—encompassing the roles of sex hormones, sex chromosomes, and physiology—to offer a comprehensive, mechanistic view of how biological sex influences host responses to *Plasmodium* infection, with particular emphasis on the impact of sex hormones.

The findings of this thesis reveal the complex impact of biological sex on liver stage immunity and *Plasmodium* liver stage outcomes. In humans, a pooled analysis across 13 Controlled Human Malaria Infection (CHMI) trials in malaria-naïve populations found that males are more likely to

experience a delayed time to blood-stage positive parasites following challenge with *Plasmodium falciparum* compared to females. In mice, no difference in susceptibility of infection was identified. However, *Plasmodium* parasites had higher rates of survival in mice, leading to enhanced liver burden during later liver stage development. We spatially profile the liver stage and identify higher survival of infected hepatocytes in males, linking to a restricted inflammatory response and innate cell recruitment in male mice. Furthermore, the presence of androgens in males suppresses this innate immune response and alters liver stage survival. Next, this study sought to evaluate the impact of biological sex on *Plasmodium* liver stage vaccines. We discovered that male mice vaccinated with prime-and-trap, a whole organism-based vaccine strategy, exhibit poorer protection against *Plasmodium* sporozoite challenge than females. We investigated this sex difference, and identified that vaccinated male mice have fewer hepatic memory $CD8^+$ T cells than females when scaling for liver biomass. We further investigated the impact of sex hormones, and identified that the presence of androgens did not affect memory $CD8^+$ T cell quantity nor quality, but directly inhibited protective $CD8^+$ T cell effector response during sporozoite challenge. The contrast in liver stage infection between mice and humans—where male mice show a *higher* liver parasite burden, whereas male humans experience an extended liver stage, suggesting a *lower* liver burden—highlights the critical role of model selection in sex difference research. Our findings reveal that baseline differences in cellular composition and tissue homeostasis must be accounted for to understand the underlying host-parasite interactions accurately. Bridging insights from mouse infection models to human observations remains essential. Overall, this research shows that sex differences in host responses significantly impact *Plasmodium* liver stage biology in both humans and mice. Sex hormones emerge as powerful modulators of these differences, shifting immunological baselines and influencing protection against infection in both natural-acquired and

vaccine-induced immunity. This work underscores the importance of biological sex as a key variable in liver stage malaria studies and vaccine development.

DEDICATION

To Ruth Bader Ginsburg, a trailblazer who saw a path to justice where others only saw barriers. I dedicate this thesis, *On the Basis of Sex: The Impact of Biological Sex on the Plasmodium Liver Stage*, to her. I began my PhD journey in September 2020, the month Justice Ginsburg passed away, surrounded by family, at age 87. She was more than a Supreme Court Justice – she was a champion for gender equality, a strategist of unyielding purpose, and a leader who fought tirelessly for rights that generations had been denied.

RBG's pivotal brief in *Weinberger v. Wiesenfeld* marked a turning point in dismantling discriminatory statutes. By tackling gender bias where it had historically disadvantaged men, she helped lay the groundwork for protections that would extend to all. My research mirrors her approach, exploring sex-biased immune responses in males to expose gaps in basic infection mechanisms and vaccine efficacy. Her work underscored the idea that addressing inequity for one group can lead to advancements for all.

When I started my thesis research, I focused on the *Plasmodium* liver stage vaccines in a mouse model, investigating the role of biological sex in modifying vaccine responses. My findings revealed an overlooked dimension: testosterone reduced vaccine efficacy, rendering male mice more susceptible to infection. As my research continued, I uncovered additional complexities in human immune responses to *Plasmodium* parasites on the basis of sex. Together, this line of inquiry, rooted in a deep respect for sex differences data, calls for a shift in vaccine development that considers both biological differences and the biases that have long shaped this field.

Historically, vaccine research has disregarded the complexity of immune responses between sexes, favoring a one-size-fits-all approach skewed toward male biology. Only recently have more women been included in clinical trials, yet the foundational knowledge still privileges male immune responses. In a twist of irony, this imbalance has ultimately harmed both sexes. Females, studies now show, typically mount a stronger and more lasting defense against pathogens—an immunity advantage that could have offered insights had it not been neglected for so long.

Through this work, I aim to underscore the need for sex-informed research that transcends outdated biases, ensuring that vaccines and other interventions evolve to serve all people, regardless of sex or gender. It is my hope that the strides I have made here reflect RBG's commitment to advancing justice for everyone by strategically addressing inequities, one insight at a time.

ACKNOWLEDGMENTS

I am deeply grateful to everyone who has supported and contributed to this dissertation. I want to express my heartfelt appreciation to the past and present members of the Murphy Laboratory for their invaluable feedback, suggestions, and stimulating discussions. Special thanks to Dr. Melanie J. Shears, whose guidance in study design, meticulous editing, and ongoing encouragement throughout this project were invaluable. I admire Melanie's thoughtful approach to scientific inquiry and consider her a role model in the field. I am also immensely grateful to the undergraduate and master's students—Nilasha Sen, Ethan Conrad, and Alen Poleman—who brought joy to my work environment and provided vital support to the research projects within this thesis. I couldn't have accomplished so much without your dedication. Additionally, I thank Ken Boey for his essential assistance with survival surgeries, which were crucial to my research. My appreciation also goes to Dr. Dianna Hergott and Weston Staubus for their statistical insights and advice, and to Mariko Seilie for always managing to locate misplaced items and experiments assistance. Lastly, I extend my deepest gratitude to Dr. Sean C. Murphy for his mentorship, passion for malaria research, and willingness to support a project that expanded beyond the lab's usual scope.

I would also like to acknowledge the statisticians and bioinformaticians who have supported my journey into large data analysis. My deepest thanks to Dr. Paul Edlefsen, who taught me to approach statistics with purpose and care; his enthusiasm for studying sex differences has greatly influenced my own path. I am also grateful to Dr. Kim Dill-McFarland and GW McElfresh for guiding me through transcriptomic analysis and helping me develop as an independent bioinformatician. Thank you to Shui Ma for giving me the opportunity to be a Teacher Assistant for *Bioinformatics and Gene Sequence Analysis*, which allowed me to deepen my understanding of the field.

I am immensely grateful to all the experts who have shared their knowledge and taught me so much about various assays. Special thanks to Erik Layton for his invaluable training and guidance in flow cytometry analysis—my PhD thesis would not be what it is today without his thoughtful mentorship and expertise. I am also thankful to Dr. John Amory and Dr. Katya Rubinow for their insightful endocrinological perspectives on this project.

Thank you to all the collaborators who contributed to this project. I am grateful to Dr. Nana Minkah at Seattle Children's Research Institute (SCRI) for providing experimental insights and antibodies essential for Digital Spatial Profiling. I would also like to thank Dr. Alexis Kaushansky for their experimental input and for allowing us to use their lab space for microscopy, as well as Lizzie Glennon for additional microscopy and experimental advice. I appreciate Dr. Meta Roestenberg and Mirte Balke at Leiden University for their support and trust in sharing data with us.

Additional thank you all the cores for providing expertise and support on projects. A big thank you to the insectary teams at SCRI and the University of Washington (UW), whose dedicated support in providing sporozoites was critical to these studies. Special thanks go to the UW Department of Comparative Medicine for managing the mouse colonies. Additional thank you to Dr. Chetan Shesdari and Erik Layton for their expertise in flow cytometry, and to the UW Cell Analysis

Facility for additional flow cytometry support. I am also grateful to Brendy Fountaine and Marina Ivanova at the Histology and Imaging Center Support for their assistance with histology preparations. I would like to thank Drs. Emily Beirne and Ram Akilesh from the Department of Laboratory Medicine and Pathology (DLMP) Spatial Biology Core Facility for their technical expertise and for executing the NanoString GeoMx Digital Spatial Profiling. Lastly, I am grateful to Dr. Jenna J. Klug for her assistance with interpreting histopathology on immunohistochemistry slides. This work would not have been possible without the invaluable support and contributions of these essential cores.

I am grateful to the UW Department of Laboratory Medicine and Pathology (DLMP) for providing grant awards that supported my pursuits in omics research. I also thank the National Science Foundation for awarding me the Graduate Research Fellowship (GRFP), which funded my stipend in the Murphy lab for three years. I also extend my gratitude to the National Institutes of Health and the Bill and Melinda Gates Foundation for their financial support of my research. Additionally, I acknowledge that portions of this thesis were edited for clarity and style with the assistance of OpenAI's ChatGPT, an AI-based language model that enhanced its readability and flow. I also acknowledge that schematic figures were made with BioRender. I am especially thankful to OpenAI for developing such a valuable tool for writing and code development, which greatly facilitated my data analysis and communication efforts.

I am grateful to the Pathobiology graduate program for their encouragement and support. Special thanks to Ernie Lefler, the program manager, and Dr. Jennifer Lund, the program director, for their guidance in navigating graduate school policies. I would also like to thank Jamie Kadri, the grants and research specialist in the Murphy Laboratory, for expertly managing funding.

I am deeply appreciative of my dissertation committee—Drs. Sean C. Murphy, Whitney Harrington, Naeha Subramanian, Dan Campbell, and Paul Edlefsen—for their insights and guidance. Finally, a heartfelt thank you to my family and friends for their unwavering support throughout my academic journey.

TABLE OF CONTENTS

LIST OF FIGURES

LIST TABLES

ABBREVIATIONS

7DW8-5 = [(2S,3S,4R)-1-O-(α-D-galactopyranosyl)-N-(11-(4-fluorophenyl)undecanoyl)-2-amino-1,3,4-octadecanetriol)]
Acy = Acyline
AIM = absent in melanoma
APC = antigen presenting cells
AR = androgen receptor
BH = Benjamini-Hochberg correction
CD = cluster of differentiation
CHMI = controlled human malaria infection
CI = confidence interval
CSP = circumsporozoite protein
CXCR = CXC chemokine receptor
CYP = cytochrome P450 superfamily enzymes
DC = dendritic cell
DEG = differentially expressed genes
DHT = dihydrotestosterone
DMSO = dimethyl sulfoxide
DMSO = Dimethylsulfoxide
DNA = deoxyribonucleic acid
DSP = digital spatial profiler
DVI = direct intravenous infection
E2 = 17β - estradiol
EDTA = Ethylenediaminetetraacetic acid
ELISA = enzyme-linked immunosorbent assay
ELISPOT = enzyme-linked immunosorbent spot
ER = estrogen receptor
FBS = fetal bovine serum
FCG = four-core genotype
FDR = false discovery rate
FOXP3 = Forkhead box P transcription factor
GAPDH = glyceraldehyde 3-phosphate dehydrogenase
GDP = gross domestic product
GG = gene gun
GH = growth hormone
GMP = Good manufacturing practice
GnRH = gonadotropin releasing hormone
GS = glutamine synthetase
GSEA = Gene set enrichment analysis
GZMB = granzyme B
H = Hallmark pathways
HBV = hepatitis B virus
HCV = hepatitis C virus
HGF = hepatocyte growth factor

HPG = hypothalamic-pituitary-gonadal
hpi = hours post injection
HR = hazard ratio
hr = hour
HRE = hormone response elements
HSC = hepatic stellate cells
HSD = hydroxysteroid dehydrogenases
HSPG = heparan sulphate proteoglycan
IACUC = Institutional Animal Care and Use Committee
ICS = intracellular cytokine staining
ID = intradermal
IFN = interferon
IFNAR = interferon alpha and beta receptor
IL = interleukin
IP = intraperitoneal
IRF = interferon regulatory factors
ISG = interferon stimulated genes
IV = intravenous
IVIS = in vivo imaging system
IZ = interzonal zone
K = KEGG pathways
KC = Kupffer cells
KLRG = Killer cell lectin-like receptor subfamily G member
KM = Kaplan-meier
LAG = Lymphocyte-activation gene
logFC = Log Fold Change
LSEC = liver sinusoid endothelial cells
LT = labile toxin
Luc = luciferase
LUMC = Leiden Controlled Human Infection Center
MAVS = mitochondrial antiviral signaling protein
MDA5 = melanoma differentiation-associated gene 5 protein
MDSC = myeloid-derived suppressor cells
MHC = major histocompatibility complex
MMDL = Malaria Molecular Diagnostic Laboratory
MPEC = memory precursor effector cells
mRNA = messenger RNA
mSIGDB = Molecular Signatures Database
NAAT = *Plasmodium* 18S nucleic acid amplification tests
NIH = National Institute of Health
NK = natural killer cell
NKT = natural killer T cell
ns = non-significant
OLAW = Office of Laboratory Animal Welfare
OR = odds ratio
ORX = orchiectomy (removal of testes)

OVX = ovariectomy (removal of ovaries)
P&T = prime-and-trap
Pb = *Plasmodium berghei* (*P. berghei*) (change to not italics)
PBS = phosphate buffered saline
PBS = Phosphate Buffered Saline
PC = pericentral zone
PD = programmed cell death
PE = pre-erythrocytic
PE = pre-erythrocytic
Pf = *Plasmodium falciparum* (*P. falciparum*) (change to not italics)
PfSPZ = Sanaria's cryopreserved radiation attenuated sporozoite vaccine
PP = periportal zone
PRRs = pattern recognition receptors
PV = parasitophorous vacuole
Pv = *Plasmodium vivax* (*P. vivax*) (change to not italics)
Py = *Plasmodium yoelii* (*P. yoelii*) (change to not italics)
QC = quality control
qPCR = quantitative PCR
R21 = malaria subunit vaccine undergoing phase 3 clinical trials
RAS = radiation attenuated sporozoite
RBC = red blood cell
RNA = ribonucleic acid
RNAseq = RNA sequencing
ROI = region of interest
RP = Ribosomal protein
RT-PCR = qRT-PCR = reverse transcription polymerase chain reaction
RTS,S = World Health Organization recommended malaria subunit vaccine
SC = subcutaneous
SCRI = Seattle Children's Research Institute
SD = standard deviation
SFU = spot-forming unit
SHBG = sex hormone-binding globulin
SLEC = short-lived effector cells
Spz = sporozoite
STAR = Spliced Transcripts Alignment to a Reference
T = testosterone
TCF = T cell factor
Tcm = T central memory
Tem = T effector memory
Tet = tetramer
Th = T helper
TLR = Toll-like receptor
TNF = tumor necrosis factor
TRAP = thrombospondin-related adhesion protein
Treg = Regulatory T cells
Trm = T resident memory

TTP = time to positivity
UW = University of Washington
WHO = World Health Organization
WT = wildtype
XCI = X-chromosome inactivation

Chapter 1. INTRODUCTION

1.1 BIOLOGICAL SEX & IMMUNITY

Biological sex and gender are among the most important factors affecting health and disease throughout the human lifespan[1]. Sex refers to biological characteristics such as chromosomes, reproductive organs, and sex hormones, whereas gender encompasses gender identity, expression, roles, and stereotypes, many of which are shaped by societal perceptions and behavioral norms[2]. Both biological sex and gender contribute to sex differences, which shape human health over time. Sex differences involve overlapping but shifted phenotypic traits in males and females, as opposed to sex dimorphism, which refers to non-overlapping phenotypic differences. For example, gonads and breasts are sexually dimorphic characteristics, while differences in disease prevalence between sexes are considered sex differential characteristics[3]. Studying sex differences is essential for advancing equitable medicine. Understanding the biological basis of these differences helps clarify health disparities, guides therapeutic interventions, and reveals novel mechanisms of pathogenesis. Although both biological sex and gender contribute to sex differences and subsequent health disparities in humans, this thesis will focus on the implications of biological sex on immunity.

Biological sex is a dramatic mediator of the quality and magnitude of immune responses[4]. Sex influences immune responses to pathogens and vaccines, resulting in sex-specific outcomes. Generally, males are more susceptible to infection and produce reduced vaccine responses compared to their female counterparts, although this observation shifts across the human lifespan[5]. Three main intrinsic factors influence sex differences: sex hormones, sex-chromosome linked genes, and physiology. Each of these elements play a role in shaping immune responses,

potentially driving sex-specific effects on both innate and adaptive immunity. In this section, we will explore how these three factors contribute to immune response to pathogens and vaccines, highlighting their general mechanisms of action.

Sex hormones

Sex hormones are steroid molecules derived from cholesterol that regulate a vast repertoire of biological functions. There are three main classes of sex hormones - progestogens, androgens, and estrogens[6]. Sex hormone production is regulated by the hypothalamic-pituitary-gonadal (HPG) axis, which controls androgen synthesis in the testes for males and estrogen synthesis in the ovaries for females[7]. However, peripheral tissues also have the capacity for sex hormone biosynthesis[8,9]. Notably, all sex hormones are present in both females and males. Sex hormone concentrations vary significantly across tissues[10] and fluctuate throughout life, influenced by key events such as puberty, pregnancy, menopause, and aging[11].

Sex hormones regulate immunity through both direct and indirect mechanisms, leading to differences in immune cell production, maintenance, and function[3,4]. Directly, sex hormones interact with nuclear hormone receptors—such as the androgen receptor (AR) and estrogen receptor (ER)—present in immune cells. These ligand-bound receptors bind to hormone response elements (HREs) in the promoters of target genes, thereby regulating gene expression[12,13]. Additionally, sex hormones can modulate gene expression through non-genomic pathways[14]. Indirectly, sex hormones influence the microenvironment surrounding non-immune cells, altering the signals received by innate and adaptive immune cells during activation and development[15,16].

Testosterone and estrogen exert distinct effects on the immune system. Numerous studies in both humans and mice have demonstrated that testosterone generally has anti-inflammatory effects, which may contribute to the reduced immune responses in males to infections and vaccinations[4,14]. Estrogen's effects, however, are more nuanced and depend on factors such as the form of estrogen, its concentration, biological sex, and the cell type involved. In general, low levels of estradiol (a form of estrogen) enhance pro-inflammatory responses in both humans and mice, while supraphysiological levels suppress inflammation[17]. Klein et al. provide an in-depth review of how sex hormones influence various immune cell types[4]. An in-depth review of the impact of sex hormones on T cells will be discussed in **Chapter 1.6**. A common starting point for studying the impact of sex hormones on human health is by comparing immune responses before and after puberty, when sex hormone levels rise significantly[14]. Although pubertal onset involves other non-hormone related changes, comparing adolescents to adults is still one common indicator of the impact of sex hormones on immune responses.

Sex chromosomes

Sex chromosomes drive sex differences through gene dosage with males (XY) and females (XX) having distinct sets of X- and Y-linked genes[3-5]. The human X chromosome contains over 1400 genes, while the Y chromosome has over 200 genes[18]. To balance X-linked gene expression and prevent a harmful double dose of proteins, females undergo X-chromosome inactivation (XCI), randomly silencing one X chromosome in each cell. Some X-linked genes escape this process with mechanisms involving inactivation, disrupted maintenance of X inactivation, and XCI skewing[19]. The influence of sex-linked genes plays a significant role in biological sex differences, especially in immune responses and susceptibility to disease.

Many genes on the X chromosome regulate immune function and play an important role in modulating sex differences in the development of immune-related disease. These genes code for proteins ranging from Pattern Recognition Receptors (PRRs) to cytokine receptors and transcriptional factors[20]. Additionally, escape from XCI-inactivation on the immune-related genes has been implicated in differential immune outcomes by sex[21,22]. The Y chromosome contains regulatory genes that may impact immune function, and variations within this chromosome can contribute to sex-specific susceptibilities to viral infections[23]. However, the specific influence of Y-linked genes on immune responses remains relatively unknown[1].

Physiology

Physiological factors contributing to sex differences include variations in body size/mass, cell composition, and organ structure. Those first two factors are intrinsically linked. Males are generally larger in size compared to females in both humans and mice[24]. The impact of size differences is a difference in baseline level of cells. Male and females differ in cell density for several immune cells categories[4], for example females have higher $CD4^+$ T cells numbers and higher CD4/CD8 ratios compared to males[25], and T_{reg} frequencies are higher within males[26]. Additionally, sex dimorphism in reproductive organs results in divergent regulatory pathways and biological systems[27]. For example, gonadal organs also play a role in production and memory response in the body, and undergo different processes by sex[28].

This thesis introduces a three-part framework for studying sex differences in immunity. However, additional factors also contribute to phenotypic sex differences in immune responses. Variations in epigenetics, microRNA expression, genetic architecture[1], and environmental factors such as nutrition, stress, and microbiota can also differ between sexes and modulate

immune responses[4,5]. While these factors will not be explored here, they play an important role in driving sex differences in immunity.

1.2 MALARIA

Plasmodium parasites, the causative agent of malaria, are unicellular eukaryotes that are transmitted to people through the bites of mosquitoes. Malaria is a major global health problem and resulted in an estimated 249 million cases and 608,000 deaths in 2022[29]. Around 95% of malaria-related deaths happen in Sub-Saharan Africa, with 76% of these fatalities occurring in children under the age of five[29].

Moreover, the social and global health effects of the malaria burden are significant and enduring, as a 10% decrease in malaria cases was associated with a 1.8–1.9% increase in GDP per capita between 2000 and 2017[30]. Reducing the social, global health, and economic impacts of malaria remains a high priority for the World Health Organization (WHO), with a focus on prevention, treatment, and ultimately, the elimination of the disease[31]. To achieve this, innovative new approaches that are grounded in the unique lifecycle and biology of the *Plasmodium* parasite are necessary.

Plasmodium **parasite lifecycle**

While there are over 200 species of *Plasmodium* that infect vertebrates and insects, two species, *P. falciparum (Pf)* and *P. vivax (Pv)*, are responsible for most malarial morbidity and mortality in humans worldwide[32]. Rodent *Plasmodium* parasites are widely used as surrogates to study infection and therapeutics. The three primary species employed in murine systems are *P. berghei* (*Pb*), *P. chabaudi* (*Pc*), and *P. yoelii* (*Py*)[33]. In both human and murine hosts, *Plasmodium* parasites undergo a complex lifecycle (**Figure 1.1**). In brief, the cycle begins with a bite of a

mosquito carrying infectious sporozoites (spz). Spz migrate from the dermis to the bloodstream and are transported to the liver where they invade hepatocytes[34]. During this liver stage (discussed more in depth in **Chapter 1.5**), spz replicate over 10,000-fold. This process lasts 2 days in mice and ~6.5 days in humans[33]. At the conclusion of the liver stage, infected hepatocytes release infectious exoerythrocytic merozoites into the bloodstream, which initiates the disease-causing phase of *Plasmodium* infection and eventually enables transmission to mosquitoes[35].

Malaria vaccines

Preventative measures are a core strategy in combating the global malaria burden[29]. These measures broadly include vector control, antimalarial chemotherapies, insecticide-treated bed nets[36], monoclonal antibody therapies[37], and vaccines. While all are vital tools in the fight against malaria, this section focuses on recent advances in malaria vaccines. Vaccines are designed to enhance natural immunity and provide additional protection against malaria[38,39]. Given the complex lifecycle of *Plasmodium*, malaria vaccines fall into three categories: infection-blocking, disease-blocking, and transmission-blocking. Although vaccines can target any stage of the parasite's lifecycle, the most advanced efforts have focused on the pre-erythrocytic (PE) stages, leading to potential prevention of disease and downstream transmission[40] (**Figure 1.1**).

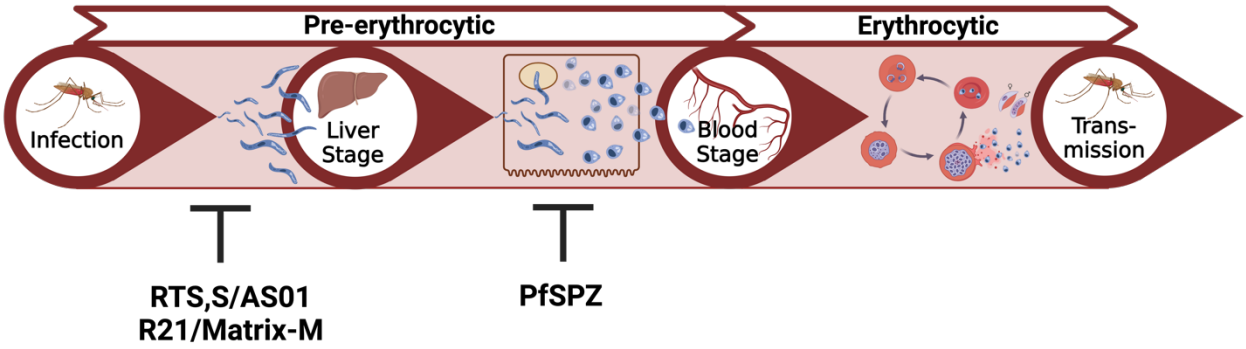

Figure 1.1. Schematic of the *Plasmodium* lifecycle as a target for vaccines. Created with BioRender.com.

The two most clinically advanced malaria vaccines are RTS,S/AS01[41,42] and R21/Matrix-M[43]. Both vaccines induce humoral responses that can block spz invasion of the liver. These vaccines completed phase 3 clinical trials and received WHO recommendations for pediatric use in malaria-endemic regions[44]. RTS,S has shown a 35% reduction in severe malaria cases[45], while R21/Matrix-M demonstrated 75% efficacy over one year[46]. Although both vaccines induce strong immune responses, their efficacy wanes quickly over time – their net benefit may be limited to preventing severe malaria rather than completely eliminating infection or stopping transmission[38]. Thus, at this time, the primary goal for many developers of next-generation malaria vaccines is to achieve durable, sterilizing immunity that exceeds that of RTS,S/AS01 and R21/Matrix-M.

Malaria liver stage vaccines

The liver stage is a promising target for next-generation vaccines because this stage naturally has a small number of parasites that are vulnerable to T cell-mediated killing of infected hepatocytes prior to further replication[47]. If development of the parasite in the liver is completely stopped, there is no blood stage infection, no clinical disease, and no onward transmission. One promising

liver stage vaccine is the PfSPZ vaccine, based on an attenuated whole sporozoite strategy, described in detail more in **Chapter 1.6**[40]. In brief, PfSPZ aims to provide long-lasting protection by leveraging the unique biology of *Plasmodium* parasites in the liver during both primary infection and post-vaccination reinfection (secondary infection). Clinical trials with PfSPZ have demonstrated potential for complete sterile protection in adults, with efficacy rates ranging from 50% to 100%, depending on participant demographics[48]. Despite decades of research into the *Plasmodium* parasites' hepatotropic properties, the complex role of the liver microenvironment in shaping the vaccine outcomes remains under investigation. This environment is essential for the parasite's survival and function, and studying it may yield insights into both natural *Plasmodium* biology (addressed more in **Chapter 1.5**) and potential vaccine strategies (addressed more in **Chapter 1.6**). The first step in understanding these effects is to examine the liver in its steady state, as this foundational knowledge could inform future vaccine design and implementation.

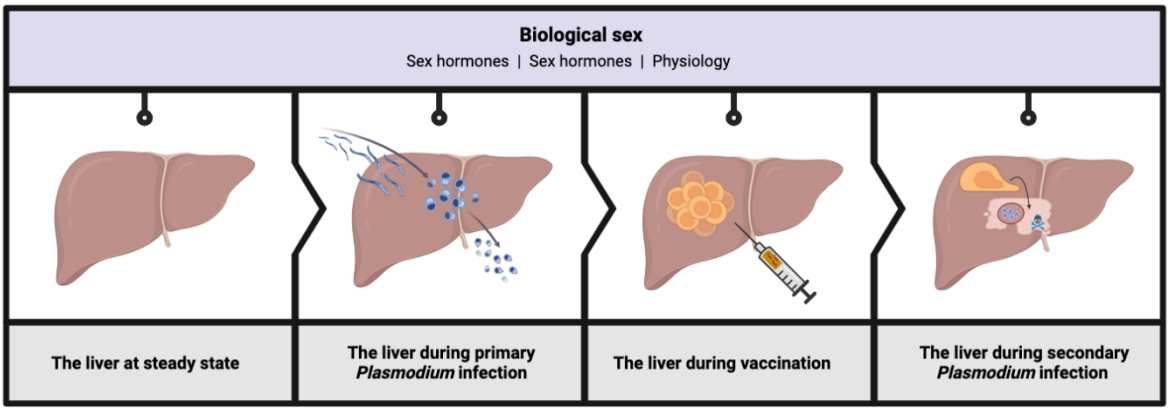

Figure 1.2: A framework of the types of the *Plasmodium* parasite's liver interaction that may be influenced by biological sex. Created with BioRender.com.

1.3 THE LIVER AT STEADY STATE

At steady state, the liver maintains a unique microenvironment, made distinct by its architecture, function, and immunogenic properties.

Liver architecture

The liver is the largest internal organ in the body. While the architecture of the liver differs between mice and men, both share the same basic structural unit: hepatic lobules comprised of layers of hepatocytes arranged around a central vein[49] (**Figure 1.3**). As the major organ stroma, hepatocytes comprise up to 80% of the total volume of the liver[50]. Hepatocytes radiate from the central vein, forming a hexagon shape. Branched to the corners is the portal triad, which is composed of the portal vein (supplies oxygenated blood), hepatic artery (carries blood rich in nutrients), and bile duct (collects bile products). The hepatic sinusoids are liver microvessels that facilitate mixing of blood from the portal triad before draining to the central vein, and recirculating to the heart[51]. The hepatic sinusoid contains three main cells types: 1) liver sinusoid endothelial cells (LSECs), which constitute the walls of microvessels; 2) hepatic stellate cells (HSCs), which regulate microvasculature and synthesize the extracellular matrix; and 3) Kupffer cells (KC), which are resident macrophages[51]. Additionally, the liver sinusoid is a uniquely porous endothelial layer with slower blood flow compared to other organs. This features allows circulating T cells to directly interact with hepatocytes, bypassing the need to extravasate to eliminate cells[52]. This unique characteristic is one reason T cells are a primary focus for malaria vaccine development (discussed further in **Chapter 1.6**).

Liver function

The liver performs a plethora of vital physiological functions. Included amongst these functions is the breakdown of waste products and foreign substances, as well as glucose, lipid, and cholesterol metabolism, and blood volume regulation[53]. The liver is also a dynamic endocrine organ. It is involved with important endocrine pathways via direct roles in hormone production and metabolism of hormone binding proteins[54]. With the high vascularity of the liver, it is optimally placed to participate in multiple signaling pathways with other endocrine organs, including the pituitary, pancreas, gut, thyroid, and adrenal glands, to modulate the liver's metabolic and synthetic functions[54].

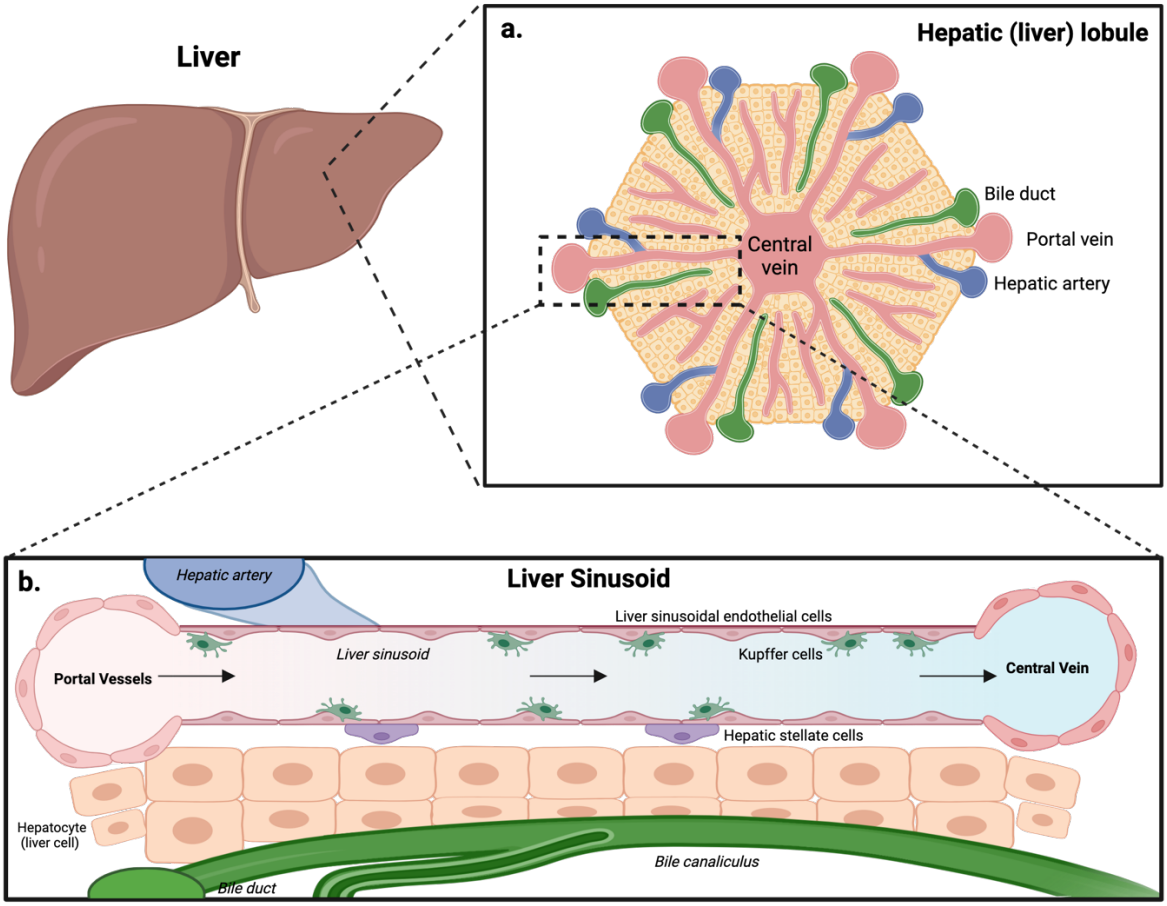

Figure 1.3: Architecture and cell composition of the liver. a. The macro structure of the liver lobule, which is composed of the bile duct, portal vein, central vein, and hepatic artery. b. Further examination depicts the nutrient flux and cellular composition of the liver sinusoids. Adapted from Bram et al[55]. Created with BioRender.com.

Liver immunology

The liver is a hub of immune activity. It hosts a diverse array of immune cells that contribute to homeostasis, tolerance, and inflammation[56,57]. Constantly exposed to dietary antigens and bacterial products, the liver must tolerate benign stimuli while maintaining surveillance for pathogens and malignant cells[58]. Its unique structure, cellular composition, and continuous exposure to gut-derived molecules shape a distinct microenvironment where tolerance and inflammation coexist. This regulated immune activity ensures that the liver remains primed to respond to threats, such as infections or toxic metabolic byproducts, without compromising its homeostatic functions[56,57].

The liver's immune complexity arises from its high density of both myeloid and lymphoid cells, including Kupffer cells (KC), dendritic cells (DC), neutrophils, and adaptive and innate lymphocytes such as T cells, natural killer (NK) and natural killer T cells (NKT). KCs, which make up a significant portion of the liver's non-parenchymal cells, act as primary detectors of microbial molecules and drivers of inflammation[59]. These resident macrophages, equipped with an array of PRRs[60], play a critical role in phagocytosis, cytokine production, tissue repair, and regeneration[59,61]. DCs, including myeloid and plasmacytoid subsets, stimulate robust T-cell responses in the liver and liver-draining lymph nodes[62], while neutrophils primarily appear in the liver during infection and inflammation[63].

The lymphoid compartment also contributes to liver heterogeneity. The liver is enriched in $CD8^+$ T cells, memory T cells, and various innate lymphocyte populations[64]. These cells are crucial for

a productive innate and adaptive immune response in the liver[47]. The role of memory $CD8^+$ T cells in adaptive immunity will be discussed more in **Chapter 1.6.** B cells are present as well, contributing to the liver's immune landscape[65]. Beyond immune cells, non-hematopoietic cells—hepatocytes, hepatic stellate cells, and liver sinusoidal endothelial cells—are key players in both local and systemic immune regulation, serving as sensors and responders to immune challenges through their expression of PRRs[66].

The liver's tolerogenic ability to balance inflammatory and regulatory responses is crucial for maintaining homeostasis, both locally and systemically[58,67]. KCs[68] and hepatic DCs[69] promote tolerance by producing anti-inflammatory cytokines like IL-10 and favoring regulatory T cell (T_{reg}) responses. Myeloid-derived suppressor cells (MDSCs) further enhance this tolerogenic environment, particularly during the liver's acute phase response[70]. This intricate immunological equilibrium allows the liver to ensure protection from harmful agents while fostering tolerance to non-threatening stimuli in this unique microenvironment.

Liver is a sexually dimorphic organ

We have examined the diverse properties of the liver microenvironment, but an essential element of its complexity is its sexually dimorphic nature. The liver is one of the most sexually dimorphic organs, with differences in function and composition between males and females in mice[71] and humans[72]. This dimorphism is primarily driven by sex hormones, sex chromosomes, and physiology which results in two critical sex differences: 1) cell composition and 2) gene expression patterns in hepatocytes. The diverse liver cell types contribute significantly to sex-specific liver functions. Under steady-state conditions, the liver exhibits sex-based differences in cell numbers, with hepatocytes and KCs more abundant in females than in males[73]. This

bicellular composition bias is accompanied by notable sex differences in gene expression profiles. Hepatocytes account for most of the observed sex-biased gene expression. In contrast, non-parenchymal cells—including immune cells like KC, NK cells, NKT cells, dendritic cells, T and B lymphocytes, and LSECs—show less baseline gene expression bias between sexes[74]. Although these immune cells exhibit subtler gene expression differences, sex-specific immune activities have been documented in other tissue microenvironments[75]. Investigating how variations in cell density and activity influence host-parasite interactions remains an important yet underexplored area.

Sexual dimorphism plays an important role in sex-specific liver function and is dynamically linked to the endocrine system and sex hormone production. For example, the primary regulators of sex-biased gene expression are androgen and estrogen signaling[76] and sex-dependent expression of growth hormone (GH)[77]. Thus, we will further review in-depth how the liver participates in most steps of steroid hormone regulation, starting from being the primary site of cholesterol biosynthesis[78]. Cholesterol translocation to the mitochondrial membrane is the first step of sex hormone biosynthesis within a cell (**Figure 1.4)**[79]. Following this rate limiting step, cholesterol is converted to pregnenolone by *Cyp11a1*, a member of the cytochrome P450 superfamily (CYP) of enzymes. A cascade of enzymatic steps conducted by hydroxysteroid dehydrogenases (HSD) and CYP enzymes result in the generation of estrogens and androgens. Many of the HSD and CYP enzymes responsible for this conversion are expressed in the liver. Critically, the liver is a major source of expression of 5α-reductase (*Srd5a*), the enzyme responsible for converting testosterone (T) to its potent form dihydrotestosterone (DHT). Aromatase (*Cyp19a1*), the enzyme responsible for catalyzing conversion of testosterone to

estradiol is also expressed in the liver[80]. Thus, while steroid hormones are mostly synthesized by the gonads and adrenals, the liver tissue is another main site for metabolic conversion of estrogens, progesterones, and androgens.

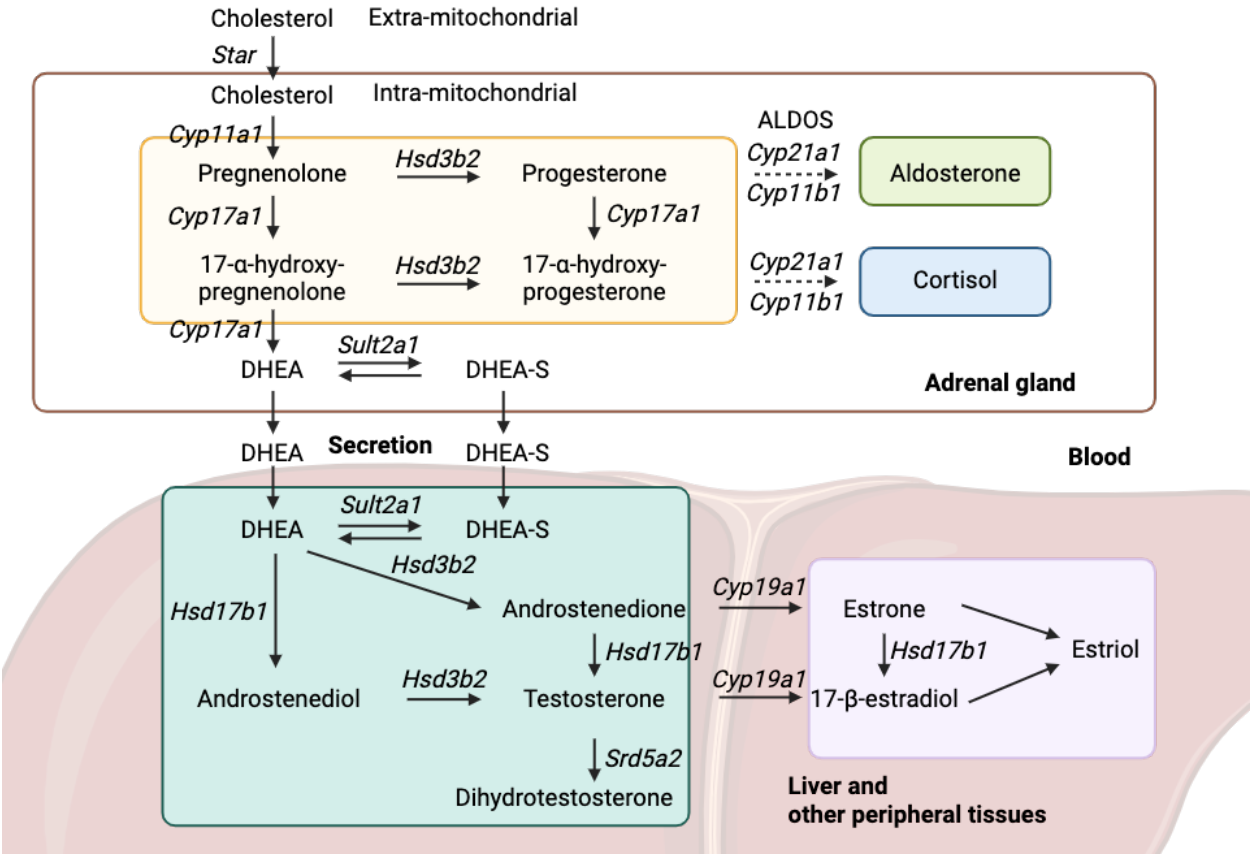

Figure 1.4: Schematic of hormone biosynthesis pathways in the liver and resulting endocrine axis. Created with BioRender.com.

Sex steroid biosynthesis is intrinsically linked to other essential liver functions such as fatty acid, lipid, and glucose metabolism. Here we will discuss the intersections between sex hormones and glucose metabolism in the liver as a well-studied example of endocrine-metabolism interactions. Androgens for example are regulators of glucose metabolism[54]. In male mice, targeted deletion of the aromatase gene resulted in glucose and insulin intolerance[81]. In female mice, aromatase

deficiency led to impaired liver metabolism and was correlated to elevated T levels[55]. In castrated male rats blood glucose levels increase since glucose is exported out of the liver more[82]. The exact impact of sex hormones on the liver is sex-specific: high testosterone levels are associated with decreased risk of insulin resistance and Type II Diabetes in men, but increased risk in women[83]. This example emphasizes the importance of considering endocrine contributions to sexual dimorphism of metabolic diseases in the liver.

In summary, the liver is a complex sexually dimorphic organ, and as a hepatotropic pathogen, *Plasmodium* is likely influenced by these sex-based differences during its liver stage (**Figure 1.2**). This intersection—between biological sex, *Plasmodium*, and the liver—forms the foundation of this thesis. In the next section, we will explore current knowledge on sex differences induced by liver and attenuated *Plasmodium* parasites and other hepatotropic pathogens.

1.4 SEX-BASED DIFFEERENCES IN MALARIA

Sex-based differences in malaria

Although malaria poses a significant global burden, there is limited information available regarding sex-specific differences during the *Plasmodium* lifecycle and malaria disease. Available evidence indicates that sex-linked differences exert a multifaceted influence throughout the human lifespan, showing distinct divergences between children and adults. This suggests that puberty may play a significant role in mediating these sex differences.

There is insufficient evidence of sex-based differences in malaria in children and infants. Several studies evaluated the prevalence, incidence and disease severity by sex in children. The hallmark Garki Project, spanning from 1969 to 1976 in the rural lowlands of Nigeria, was a longitudinal study that documented malaria prevalence through repeated cross-sectional surveys. In this high transmission setting, there was no sex difference in *Pf* prevalence in children prior to 5 years of age[84]. A similar study in India and Thailand on children in low-burden area also found no difference of prevalence and incidence of *Pv* and *Pf*[85,86]. An observational prospective cohort study in Uganda that enrolled febrile children aged 2 months to 5 years also found that there was no difference by sex in disease severity scores or in frequency of diagnosis of malaria[87]. Some conflicting studies have also been reported where female[88,89] or male[88,90–92] children were at greater risk of malaria. Overall, there is conflicting and insufficient evidence to suggest sex-difference in malaria risk in children.

There is sufficient evidence of sex-based differences in malaria risk in older children and adults. Specifically, several studies have reported male bias in malaria prevalence during adolescence and adulthood. Prevalence of infection (often measured by cross-sectional studies) is a reflection of both the number of new infections (incidence) and the duration of those infections. The Garki Project found that after 5 years of age, males have higher *Pf* malaria prevalence than females, and these differences were most significant in the age groups of 9 -18 years and 19 - 28 years[84]. Several other studies in low and high-burden areas found similar male biases in *Pf* and *Pv* prevalence[88,90,93–96]. There are however mixed results related to sex bias in *Plasmodium* incidence[97]. Some studies have also found a higher incidence of *Pf* or *Pv* malaria in male older children and adults[85,86,91,92], while other studies have reported higher incidences in females[98] or

observed no difference based on sex[89,99]. Related to disease severity, it has been found that females are at higher risk of presenting symptoms[100]. Briggs et al[97] hypothesized that the reason older males experience higher prevalence of malaria is related to a reduced ability to clear blood-stage infection, and females are less able to tolerate parasite without fever, leading to a higher probability of symptoms upon infection. Indeed, one cohort study in Uganda intensively followed *Pf* infections and modeled the rate of clearance. They found that females cleared asymptomatic infections at nearly twice the rate as males, after accounting for age, timing of infection onset, and parasite density[101]. For more information on epidemiological trends, find a thorough review in Briggs et al[97]. Overall, prevalence of malaria is higher in males in adult populations, but the same trend is not observed in infants and neonates.

While the epidemiological evidence points to higher malaria burden in adolescent and adult male populations, these studies capture sex differences related to blood-stage infection and malaria disease, overlooking potential differences related to the liver stage of the *Plasmodium* lifecycle. Measuring the liver stage infection rates is difficult within the scope of available measurement on human populations. Perhaps the greatest evidence of sex-specific differences to liver infections would be observed following the liver stage in CHMI trials of naïve and exposed populations. We hypothesize that sex differences exist in the host response to the liver stage of *Plasmodium*, given that the liver is a highly sexually dimorphic organ and sex biases are documented for other hepatotropic pathogens. However, to our knowledge, no sex-specific studies have evaluated this in humans. Therefore, to explore known sex differences during the *Plasmodium* liver stage, animal models are essential.

Sex-based differences in *Plasmodium* murine model

Murine models of malaria infection are most frequently employed to study mechanisms underlying immunity. These tools' main benefit is their ability to provide access to the liver for immunological assessments. As previously discussed there are three main strains of rodent *Plasmodium* employed in studies (*P. berghei, P. yoelii,* and *P. chabaudi*) and administered to the inbred mouse strains, like C57BL/6 and BALB/cJ mice, or outbred mouse strains[33]. Sex differences in blood stage infection outcomes has long been observed. In studies involving the lethal malaria model of C57BL/6 mice challenged with *P. chabaudi*-infected red blood cells, male mice were significantly more likely to die and exhibited slower recovery than female mice[102,103]. A similar trend is found within CBA/Ca mice infected with *P. berghei*-infected red blood cells, where males exhibited slower recovery compared to a female counterpart[104] and higher parasitemia nine days post-infection[105].

Further evaluation of the impact of sex hormones in malaria blood stage infection has also been conducted. The surgical approach of orchiectomy (ORX – removal of testes in male mice) and ovariectomy (OVX – removal of ovaries in female mice) to remove the major source of sex hormones in murine models has also been employed. Ovariectomy in females reversed sex-specific responses to *P. chabaudi* infection, suggesting that estradiol and progesterone might influence the response to blood stage infection [102,106]. Add-back studies of estradiol and progesterone in mice found a pro-inflammatory role during *Plasmodium* infection[103]. Orchiectomy in males reduced sex differences in immune response to *P. chabaudi* infection as well, suggesting a role of testosterone in mediating infection[107]. Indeed, administration of testosterone to females significantly reduced survival outcomes following blood stage

challenge,[108] which has been linked to suppressed immune responses during *Plasmodium* blood stage infection in the liver and blood[108–110]. While the potential to use mice to study sex bias during liver stage is clear, to our knowledge this topic has never been previously studied in detail. While evidence regarding sex differences to *Plasmodium* during the liver stage is limited, hints of sex-based differences might exist in the literature of liver-targeting vaccines or other hepatotropic pathogens.

Sex-based differences to liver stage vaccines

Liver stage vaccines are often employed as a tool for studying the *Plasmodium* liver stage[111]. Sex-specific responses to vaccination are a well-documented phenomenon, with adult females generally producing more robust immune responses than males [1,5,112,113]. Though the question remains, what is the impact of biological sex on liver stage vaccines? A recent meta-analysis of clinical trials on the attenuated sporozoite vaccine PfSPZ, found higher levels of antigen-specific antibodies in adult females compared to males[114]. However, no difference in PfSPZ vaccine efficacy based on sex was identified. No sex difference evaluation of the presumed mechanism of protection, $CD8^+$ T cells, was included within the paper. Interestingly, since these PfSPZ human challenge clinical trials began in 2011, 343 adults have been vaccinated. Of those enrolled, 238 (69.4%) were male[114]. However, almost all pre-clinical studies of spz-based vaccines have almost exclusively relied on female mice. For example, in a review[115] of 17 papers on spz immunization in mice, none reported using male mice, 11/17 reported using exclusively female mice, and 6/17 reported no sex information (Error! Reference source not found.). This underscores the need to consider sex as a biological variable and delineate protection requirements in male mice. The limited data we do have on the impact of sex on immune responses to liver stage malaria vaccines in mice come from a single pre-clinical study[116].

Following repeated radiation attenuated sporozoite-based vaccination (reviewed in **Chapter 1.6**), female mice were found to have more hepatic IFN-γ-producing $CD8^+$ T cells and greater protection against *P. berghei* spz challenge than male mice. This reduced protection in males could be overcome by removal of testicular hormones via orchiectomy prior to vaccination[116]. Given the paucity of information about how biological sex interacts with the immune-parasite axis during *Plasmodium* liver stage infection in mice and humans, further evaluation of the basic biology of how male and females respond to liver stage vaccination is warranted.

Sex-based differences in hepatotropic pathogens

Sex-based differences in the prevalence and pathogenesis of liver-targeting diseases are extensively documented. In this section we will briefly review general trends is sex-bias to pathogen-induced hepatotropic diseases (amebiasis, schistosomiasis, and viral hepatitis) and other liver diseases.

Amebiasis

Amebiasis is a parasitic disease caused by *Entamoeba histolytica* which spreads to various organs, leading to significant liver tissue destruction known as amebic liver abscess. Amebiasis serves as a classic example of a parasitic disease that exhibits a notable sex bias towards males[117]. Over 80% of amebic liver abscess cases occur in adult men, with the disease being rare among children and women[117,118]. Testosterone has been implicated in mediating these sex differences, with risk increasing significantly post-puberty and gradually declining with age, reaching its peak in men around 40 years old[118].

Schistosomiasis

Schistosomiasis is most commonly caused by the trematodies such as *Schistosoma mansoni* that cause adnominal pain, diarrhea, blood in the stool, and liver enlargement in advanced stages[119]. Infection occurs after contact with water, linking access to water as a major confounding factor in epidemiologic studies on sex-related differences. For example, a study in Uganda found that correcting for exposure to water reduced sex-differences in infection intensity and prevalence[120]. Despite this, a study found late-stage liver fibrosis occurs predominately in adult men[121]. Additionally, schistosomiasis is more commonly diagnosed in male travelers than female travelers[122].

Viral hepatitis

Viral hepatitis is an infection caused by nucleic acid-based viruses that causes liver inflammation and damage. While there are six types of viral hepatitis, hepatitis B and C (HBV and HCV) pose the most significant public health threat due to the persistence of chronic infection, which can lead to liver cirrhosis, failure or cancer[123]. Several meta-analyses have identified a male bias in hepatitis infection, with higher HCV and HBV prevalence in males compared to females[124–127]. One study further identified no gender difference in children[124], implicating sex hormones in modulating response to chronic viral hepatitis.

Other liver diseases

Compared to adult males, human females generally experience a degree of protection against chronic liver fibrosis, irrespective of its cause, with lower rates of nonalcoholic fatty liver disease[128], cirrhosis and liver transplant[129], as well as a reduced risk of hepatocellular

carcinoma.[127] Additionally, metabolic associated fatty liver disease is more common in males, with a loss of protection in post-menopausal females[130] when hormone levels naturally deplete.

Overall, there is resounding evidence of sex dimorphism of disease in the liver. Moreover, sex hormones have also been implicated in shaping the male response to hepatotropic pathogens and related diseases. Yet, this story has not been comprehensively told for *Plasmodium* liver stage infection and vaccination. In the next section, we will further describe *Plasmodium* liver stage infection and discuss how the unique sex-specific physiology of the liver may alter downstream outcomes.

1.5 THE LIVER DURING PRIMARY *PLASMODIUM* INFECTION

This section provides context about the biology of the liver stage of *Plasmodium* in the setting of the unique immunological properties of the liver. First, we will review the bi-directional interaction between parasite metabolic re-modeling and hepatocyte micronutrient composition. Second, we will describe the innate immune response during primary *Plasmodium* infection, from the inflammatory and cellular level. In each part, we discuss how biological sex might shape the outcomes.

The *Plasmodium* liver stage

The saga between *Plasmodium* parasites and mammalian host begins with the bite of a thirsty female mosquito. Spz, the pre-erythrocytic form of *Plasmodium,* are introduced into the dermis and within one hour, approximately half will use gliding motility to migrate to blood vessel[131]. After entering the circulatory system, spzrapidly and efficiently arrive at the liver sinusoids[132]. Spz leverage specific interactions between its surface proteins and host molecules to arrest

within the liver sinusoid. The main mechanism described is the interaction between the parasite's circumsporozoite protein (CSP) and heparan sulphate proteoglycan (HSPG) expressed on the surface of hepatocytes[65]. After arresting in the sinusoid, the spz must navigate through two potential obstacles prior to invasion of hepatocytes: endothelial cells and KCs. In theory, spz could traverse through either cell type, however the exact mechanism of spz traversal out of the sinusoid is actively debated[133,134]. Regardless, once a spz accesses a hepatocyte, it migrates through several hepatocytes before forming a parasitophorous vacuole (trophozoite and schizont phase) in its final hepatocyte host cell. Puncturing of the plasma membrane as sporozoites migrate through hepatocytes causes microenvironmental liver damage[133], possibly inducing secretion of infection-susceptibility-inducing factors like hepatocyte growth factor (HGF)[135]. Following the final invasion, surviving spz proliferate within the hepatocyte, resulting in the production of thousands of new parasites in the merozoite form. Importantly though, not all parasite-infected hepatocytes survive. Some infected hepatocytes self-abort[136] or are detected by the host immune cells and are killed[136]. The liver stage takes about 2 days in mice and around a week in humans (Schematic in **Figure 1.5**). Once merozoites are released from infected hepatocytes into the blood stream, the erythrocytic stage of the *Plasmodium* lifecycle begins[132].

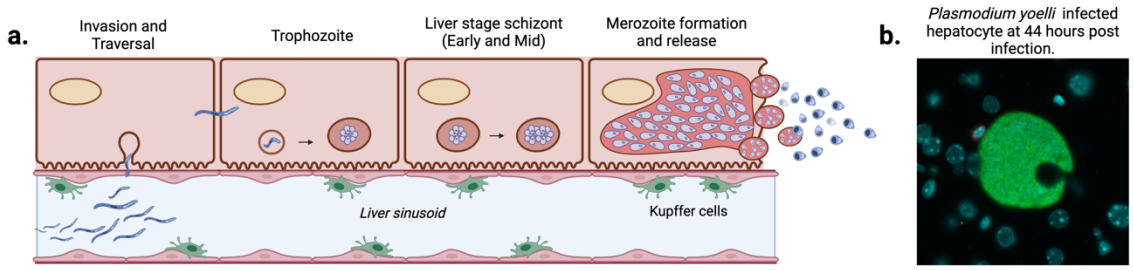

Figure 1.5: Detailed schematic of the *Plasmodium* liver stage. a. Schematic of the *Plasmodium* liver stage from invasion to merozoite release. b. Fluorescent microscopy image of a schizont during later liver stage development, with a clear depiction of a parasitophorous vacuole (PV).

Image was taken on tissue harvested 44 hours post *P. yoelli* infection in BALB/cJ mice. Created with BioRender.com.

Micronutrients and zonation direct the liver stage

The unique microenvironments in the liver are mediators of the parasite development in hepatocytes and actively shapes replication into daughter cells. Hepatocytes are storehouses for excess nutrients, capable of internalizing and metabolizing proteins and molecules for later usage[137]. Since *Plasmodium* is auxotropic for specific nutrients (amino acids, sterols, fatty acids, etc), the parasite capitalizes on the nutrient rich environment of hepatocytes[138–140]. During replication process tens of thousands of merozoites end up occupying 90% of the host cell volume[141] (**Figure 1.5**), the parasites undergo a dramatic metabolic re-configuration. Mechanistic studies on liver stage infection of *Plasmodium* revealed its capacity for sequestration and metabolism of glucose, sterols, and fatty acids, highlighting key adaptations that support parasite survival and growth[138,139,142]. Alongside with parasite re-configuration, hepatocytes also undergo significant shifts. Gene expression studies on infected hepatocytes found various host pathways that are manipulated by the parasite such as cholesterol synthesis, amino acid metabolism, and nutrient metabolism[143–145]. While the bi-directional feedback between parasite and hepatocyte has been extensively studied[146], one question that remains is if sex hormones and their biosynthesis, which begins with cholesterol (**Chapter 1.3**), is leveraged by *Plasmodium* during development for growth and replication. While parasite sequestration of sex hormones has been hypothesized before, a lack of sex-powered murine studies has shrouded a potential endocrine-*Plasmodium* interaction in the liver.

Liver zonation is an important mechanistic clue for how *Plasmodium* might interact under different nutrient environments. As previously described, the liver is structured in hexagonal lobules, where different metabolic processes are concentrated in specific areas. Hepatocytes near the portal region (portal) primarily handle gluconeogenesis and ureagenesis due to their proximity to a fresh supply of oxygen and nutrients. In contrast, hepatocytes near the central vein (central) are focused on glycolysis and xenobiotic metabolism (**Figure 1.6**). An important implication of studies evaluating *Plasmodium* interaction within micronutrient environments is the biased zone localization within a hepatic lobule[147]. A key paper found that *Pf* spz had a selective preference for pericentral hepatocytes, in part due to more abortive hepatocyte state in the periportal location[148]. One explanation for this bias has been that glutamine synthetase (GS), which is highly expressed in the pericentral region, is imported for the parasite and further supports a beneficial metabolic state[136].

Liver zonation, however, also exhibits sex-biased gene expression[149]. A detailed spatial analysis of the impact of sex on liver zonation in gene expression revealed that many transcripts exhibit sex-specific zonation patterns within the liver lobule[74]. For example, one study found that 46% of zone-biased genes are sex-biased, particularly affecting pathways in lipid metabolism, cytochrome P450, and ion transport[74]. Some of these sex-biased pathways may be exploited by *Plasmodium* parasites, enhancing its development within this spatially heterogeneous liver environment. A growing body of literature on *Plasmodium*'s liver stage has underscored the pivotal role of liver zonation and metabolism in shaping infection[136,150]. However, none of these studies have explored the impact of the liver's sexually dimorphic microenvironment on bi-directional interaction between parasite and hepatocyte.

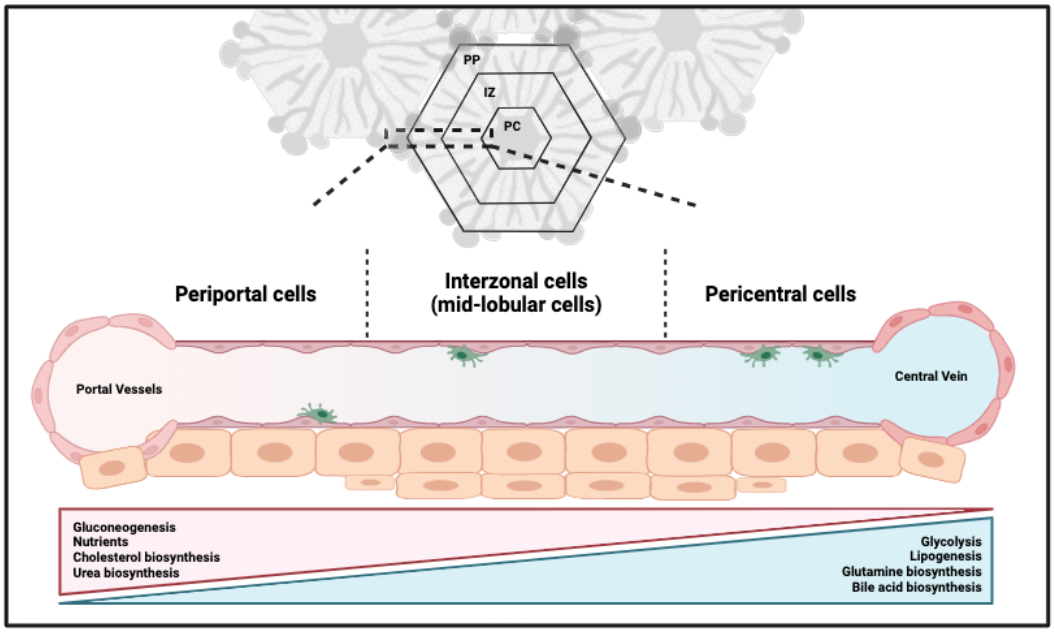

Figure 1.6: Liver lobule anatomy and nutrients composition. Highlights nutrient flux across its three distinct zones: Periportal (PP), Interzonal (IZ), and Pericentral (PC). These zones are defined by their relative positions within the lobule, ranging from the portal vessels to the central vein. Metabolic nutrient flux varies significantly across these zones, reflecting their unique roles in hepatic function. Adopted from Cunningham and Porat-Shliom[151]. Created with BioRender.com.

Innate immune response to the liver stage

The innate immune response induced by *Plasmodium* infection is another factor potentially influenced by biological sex. There are two main components to this innate response: 1) sensing and initiation of inflammation within infected hepatocytes; and 2) innate cell recruitment and activation toward infected hepatocytes.

First is the sensing and initiation of inflammatory responses within infected hepatocytes (**Figure 1.7**). Hepatocytes infected with rodent *Plasmodium* have been demonstrated to sense and initiate a type I interferon (IFN) response[152]. *Plasmodium* RNA is likely detected via melanoma differentiation-associated gene 5 protein (MDA5) and signaling occurs via the mitochondrial

antiviral signaling protein (MAVS) to activate the transcription factors IRF3 and IRF7. Type I IFNs are then released in the extracellular environment, where they bind to *Ifnar* on the surface of hepatocytes in an autocrine or paracrine manner, leading to the upregulation of IFN stimulated genes (ISGs) via IRF9 transcription factor. This process is portrayed in **Figure 1.7**[152].

Plasmodium DNA is also detected by pathways such as cytosolic AIM2 (absent in melanoma 2) receptor activation of inflammasome-mediated Caspase-1 activation[153].While these processes likely play a crucial role in recruiting immune cells to infected hepatocytes, it is noteworthy that the hepatocyte-mediated response alone likely isn't sufficient to eliminate the parasite. One experiment in *P. berghei*-infected mice lacking *Ifnar1* specifically on myeloid cells (neutrophils and macrophages), found reduced innate cell recruitment to infected hepatocytes. This indicates that hepatocytes indirectly act against *Plasmodium* parasites by recruiting and inducing leukocytes to execute elimination[152].

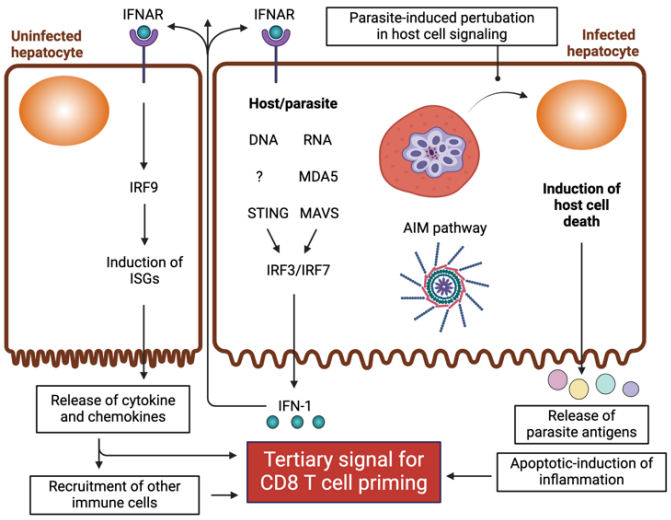

Figure 1.7: Schematic of hepatocyte innate inflammatory response to *Plasmodium* infection by hepatocytes. Innate immune response may be autocrine or paracrine toward other hepatocytes and could influence downstream $CD8^+$ T cell production. Created with BioRender.com.

Secondly, four key types of innate immune cells are abundant in the liver and play crucial roles in controlling *Plasmodium* infection in a naïve host. (1) Natural killer (NK) and (2) natural killer T (NKT) cells increase in the liver within three days post-*Pb* infection and are capable of eliminating the infection[111,154]. (3) Monocyte-derived dendritic cells increase in number 36 hours post-*P. yoelii* infection,

facilitating antigen presentation and initiating an adaptive immune response[155]. (4) Kupffer cells, while not increasing in total number following *Plasmodium* infection[155], are recruited to infected hepatocytes[156], potentially propagating a type I IFN response that aids in recruiting additional effector cells[152].

Biological sex impacts innate immune cells

Biological sex plays a key role in regulating innate immune responses, affecting both inflammation and immune cell activity. Generally, females develop a more robust innate immune response, that escalates to a higher magnitude[14,16,157]. The three main sex factors—sex hormones, sex chromosomes, and physiology—may all influence this, but here we will focus on the significant impact of sex hormones on the innate immune response. Sex hormones can alter the costimulatory tissue environment by modulating type I IFN signaling, a critical signal for the production of functional resident memory $CD8^+$ T cells[158]. Multiple studies have described sex-specific effects on induction of type I IFN by innate immune cells[16,159]. In autoimmune liver diseases where T cells are thought to play an important pathogenetic role, both estrogens and androgens have been implicated in their role in mediating inflammatory responses in the liver[159,160]. In a model of autoimmune liver inflammation, female mice produced more type I IFN signaling than male counterparts leading to more severe liver pathology[157]. In light of a well-established female bias in the type I IFN responses upon active inflammation, a sex-specific balance of sex hormones and type I IFN signaling underlie sexual dimorphism in autoimmunity and potentially primary immune response to *Plasmodium* infection.

While the innate immune response is an important tool against liver stage infection, by itself the innate response is not sufficient to arrest spz during the liver stage prior to emergence into the

blood stage. It is also important to note that the hepatic microenvironment in naïve and previously exposed (immune) animals is distinct. In the next section we will review how liver stage vaccines have sought to leverage the unique biology of the immune liver to advance a protective immune response for parasite elimination.

1.6 THE LIVER DURING VACCINATION & SECONDARY *PLASMODIUM* INFECTION

We have established that the liver is sexually dimorphic, and the *Plasmodium* liver stage can exploit this heterogeneity to its advantage. One of the most significant impacts of these sex differences may be observed in liver-targeted malaria vaccination. In this section, we will discuss malaria liver stage vaccines, the adaptive immune responses they aim to elicit, and how biological sex might influence these responses. The implications of sex differences extend beyond natural immunity and could also affect vaccine efficacy.

Attenuated-sporozoite based vaccines

The goal for many vaccine developers against malaria is to induce long-lived and sterile protection. The liver stage is a promising target because this stage naturally has a small number of parasites that are vulnerable to T cell-mediated killing of infected hepatocytes prior to further replication[47]. Additionally, if the development of the parasite in the liver is completely stopped, there is no blood stage infection, clinical disease, or onward transmission.

Attenuated spz are a leading class of vaccines that leverage the ability of spz to home to and invade the liver but then arrest prior to completion of the liver stage – in doing so, attenuated spz deliver thousands of parasite antigens to the liver[161]. There are two major categories of these

liver-targeting live attenuated-sporozoite based vaccines: homologous and heterologous. Homologous strategies involve repeated delivery of attenuated spz. Various attenuation strategies have been employed on spz, though overall they can be further categorized as early arresting and late arresting spz[115]. Repeated vaccination with radiation-attenuated sporozoites (RAS), an early arresting strategy, serves as the most protective experimental malaria vaccine tested in humans to date that confers sterile immunity against the liver stage[162–164]. The ability of RAS to protect against infection was first demonstrated in mouse models of *Plasmodium*[165]. Subsequent studies of liver stage vaccination primarily use *P. berghei* and *P. yoelli* in BALB/c or C57BL/6 mice[115]. Since this discovery, decades of research have sought to deconvolute the mechanisms of immune protection conferred by RAS and other similar attenuated spz-based liver stage vaccines.

The collective data indicate that sufficient memory $CD8^+$ T cells are a defining requirement for a protective immune response in the liver. In particular, eliciting liver-targeted, tissue-resident memory $CD8^+$ T (Trm) cells and effector memory $CD8^+$ (Tem) cells are important for durable protection[164,166]. Knowledge of these immune correlates of protection inspired the design of next-generation heterologous liver stage vaccines using a 'prime-and-trap' (P&T) strategy. The priming component of P&T vaccines is designed to induce peripheral antigen-specific $CD8^+$ T cells, and the trapping component is intended to later recruit or 'trap' circulating antigen-specific memory $CD8^+$ T cells in the liver to become liver Trm cells[166,167]. Although various non-sporozoite-based liver vaccine strategies exist, the immunity produced by both homologous attenuated-sporozoite strategies and heterologous P&T vaccination is highly liver-specific. Spz-

based regimens can be utilized to study sex-specific adaptive immune responses, while also simultaneously serving as a tool to study the adaptive immune response to virulent spz infection.

Plasmodium-specific CD8$^+$ T cells

As previously mentioned, *Plasmodium*-specific CD8$^+$ T cells are a critical correlate of long-term protection against sporozoite challenge in mice and humans[52,164,165]. The most compelling evidence for the important role of CD8$^+$ T cells is observed when depletion of CD8$^+$ T cells at the time of vaccination[168] and at the time of sporozoite challenge[169] sharply reduces protection in all tested combinations of a vaccine regimen across all mouse and parasite strains[170]. In immunized mice and humans, *Plasmodium*-specific cytotoxic CD8$^+$ T cells eliminate infected hepatocytes following recognition of parasite derived antigens bound to MHC class I molecules presented on the hepatocyte surface[161]. Naive CD8$^+$ T cells are not sufficient to clear spz, due to slow development of effector function and low frequency in the liver[171]. One study adoptively transferred naïve and memory/activated CSP-specific CD8$^+$ T cells and found the naïve cells were unable to reduce parasite liver burden in contrast to the memory/activated cells[171]. Titration studies on the number of antigen-specific CD8$^+$ T cells needed to confer protection is dependent on the number of infected hepatocytes and the ability to locate infected hepatocytes[172,173]. Due to their scarcity, infected hepatocytes are vastly outnumbered by non-infected cells, making them difficult to target. Even one infected hepatocyte escaping immune detection can trigger blood-stage infection, necessitating a hyper-abundance of memory CD8$^+$ T cells for effective protection[172]. Consequently, a robust pool of memory parasite-specific CD8$^+$ T cells is essential for immunity against sporozoite challenge.

Memory $CD8^+$ T cells can be divided into three main subsets based on phenotypic heterogeneity in expression of homing markers: central memory T cells (Tcm), which patrol secondary lymphoid organs; Tem cells, which recirculate through the blood and peripheral tissues; and Trm cells, which remain stationed in a respective tissue compartment[174]. Tem and Trm cells are ideally situated to respond to malaria challenge, whereas little evidence has demonstrated a role of Tcm in protective immunity against malaria parasite[175,176]. Tem cells recirculate throughout the liver sinusoids and can quickly exert effector function within 6 hours after *Pb* infection to facilitate clearance of liver stage malaria infection in female mice[176]. Tem cells are defined by lack of secondary lymph node organ-homing markers such as L-selectin (CD62L)[177]. In a series of elegant experiments by Lefebvre et al., it was found that Tem recruitment into the liver is independent of antigen, liver Trm cells, Kupffer cells, CD11c+ cells (marker of DCs), IFNγ signaling, NK and NKT cells, type I IFN signaling, platelets, and CD44 (memory marker) blockade[176]. Instead, Tem cell recruitment to the liver from the periphery is dependent on liver resident and circulating macrophages, including KCs and $CD8^+$ T cell-intrinsic LFA-1 expression[176].

Trm cells are like sentinels, patrolling the liver sinusoids for their cognate antigen anatomically poised to recognize and initiate effector function[166,178]. Trm cells in mice are distinguished from other subsets by the expression of chemokine receptors like CXCR6 and CXCR3 , activation marker CD69, and the senescence like $KLRG1^{lo}$ phenotype. Residency status of liver Trm cells are clearly assessed via parabiosis, where only Trm defined cells in the liver ($CD69^+KLRG1^{lo}$) were not mixed between vaccinated and unvaccinated parabiotic mouse[166]. Trm cells are clearly critical for protection against sporozoite challenge; depletion studies with anti-CXCR3, a Trm

marker, at time of challenge abrogated sterile protection in previously vaccinated mice[166]. While Trm cells confer sterilizing immunity, two possible mechanisms could explain this essentiality: by enacting intrinsic cytotoxic and cytokine pathways to directly kill hepatocytes or by initiating a "sensing and alarm" function to recruit other cytotoxic cells[178], or both. Thus, both $CD8^+$ Trm and Tem cells play roles in adaptive protection during liver stage vaccination.

Fate and function of *Plasmodium*-specific $CD8^+$ T cells.

There are two main phases that could influence the fate and functions of *Plasmodium*-specific cytotoxic $CD8^+$ T cells: the **Production phase** (time of vaccination) and the **Effector phase** (time of challenge) (**Figure 1.8**). In this section, we will briefly introduce the current understanding of the role of these two phases in shaping memory $CD8^+$ T cell responses to liver stage vaccines, noting how the liver microenvironment plays a role in shaping fate and function.

Production phase (Time of vaccination)

Contrary to previous assumptions[179], $CD8^+$ T cell responses are not likely to be primed by *Plasmodium*-infected hepatocytes. Instead, during natural infection there is an essential role for monocyte-derived $CD11c^+$ cells in acquiring *Plasmodium* in the liver and delivering liver stage antigens to $CD8^+$ T cells in the liver-draining lymph node[155]. In RAS vaccinated mice, this priming process also occurs in both the spleen and liver-draining lymph node[52]. Once activated in the spleen or liver-draining lymph node, naïve $CD8^+$ T cells home back to the liver and can differentiate into short-lived effector cells (SLEC) or memory precursor effector cells (MPEC) to facilitate clearance of parasites. Generally, SLEC are good at producing effector proteins, but decline after clearance of *Plasmodium* infection, whereas MPEC produce less effector proteins and can be observed to develop into true memory T cells[180].

The acute inflammatory response of hepatocytes and innate immune cells in the liver microenvironment following liver stage malaria immunization shapes the fate and function of sporozoite-specific $CD8^+$ T cell responses. From the perspective of fate, the magnitude and decision to convert into a SLEC or MPEC is dependent on the liver microenvironment and the transcription factors the cell is expressing[180]. Typically, SLEC develop in high inflammatory conditions (high levels of inflammatory cytokines like IFNγ and IL-12) and MPEC develop in low inflammatory conditions[180,181]. Additionally, immunizing IFNγ receptor KO mice with RAS does not result in protection[182] and is linked to attenuated contraction of the $CD8^+$ T cells[183]. From the perspective of function, studies comparing early and late arresting whole sporozoite vaccines in female mice have determined that the presence of a type I IFN gene signature at the time of immunization impairs hepatic $CD8^+$ T cell memory via a $CD8^+$ T cell extrinsic mechanism[184]. IFN-1 signaling-deficient mice immunized with replication-competent spz exhibited superior protection against infection compared to similarly vaccinated C57BL/6 mice with *Py.* Additionally, these mice also expressed less exhaustion markers like PD-1 and LAG-3 and had an increased number of memory $CD8^+$ T cells in the liver[184]. This finding is further corroborated by two recent studies in spz-immunized humans, which found a negative correlation between type I IFN signaling in peripheral blood and protection against malaria infection[185,186]. The same paper concluded that the detrimental role for the parasite-engendered IFN-1 signaling is due to IFN-1 signaling in a cell type other than $CD8^+$ T cells[184].

In addition, the presence and frequency of other cells are important to the priming process. For example, depletion of γδ T cells at time of RAS vaccination in mice hindered the influx of

$CD11c^+$ DCs into the liver and prevented optimal effector $CD8^+$ T cell responses and sterilizing immunity to future sporozoite challenges[187]. NK cells[188] and $CD4^+$ T cells[189] may also mediate the fate and function of $CD8^+$ T cells during the production phase. Overall, the acute inflammatory environment via a $CD8^+$ T cell-extrinsic mechanism influences functional $CD8^+$ T cell responses.

Effector phase (Time of challenge)

The mechanisms by which cytotoxic $CD8^+$ T cells enact their effector mechanisms against infected hepatocytes involve three mechanisms: cytolytic pathways, cytokine pathways[190], and "sensing and alarm"[178]. Cytolytic pathways involved direct lysis of infected hepatocytes via granzymes and perforin. Cytokine pathways involve the direct production of IFNγ and TNF to help control parasites[191]. Redundancy is present across these effector pathways; studies on depletion at the time of challenge, which evaluate the role of cytokines and cytotoxic proteins in protection outcomes, are highly dependent on the recipient mouse strain and the *Plasmodium* species[162,170,191]. This significant variation suggests that an effective $CD8^+$ T cell response is influenced by factors extrinsic to the $CD8^+$ T cells and by the natural defense mechanisms of the host[192]. Yet, this also points to the importance of polyfunctional T cells, able to enact both cytolytic and cytokine pathways. "Sensing and alarm" function is unique to Trm cells, and involved Trm cells serve as a local sensor of *Plasmodium* antigen presentation by hepatocytes to initiate an innate-like alarm signal to recruit more memory $CD8^+$ T cells[178]. This might be of especial importance in *Py* infection, where it was demonstrated *in vivo* that *Py* undergoes a lengthy process that requires multiple $CD8^+$ T cells per parasite and independent of contact with hepatocytes (contact independent)[193].

The contribution of acute inflammatory environment in the liver microenvironment at time of challenge is less clearly defined. This is an important consideration, since the T cell response in the liver is suppressed by diverse mechanisms, any of which might be an obstacle to $CD8^+$ T cell-mediated *Plasmodium* elimination. IFNγ depletion at time of challenge reduces protection outcomes. While this effect is often attributed to impaired $CD8^+$ T cell function, IFNγ is also produced by other liver-resident cells, such as NK and NKT cells[111], and may synergize with TNF to activate additional innate immune cells. Type I IFN signaling is not required for protection in a C57BL/6 / *Py* mouse model. IFNAR and IRF3 knockout mice vaccinated with two doses of late-arresting attenuated spz were able to confer complete protection[83]. Other cells types have been assessed for their role in mediating protection during this phase: γδ T cells are dispensable[187] and generally bystander activation is thought to not play an essential role in hepatocyte clearance at time of challenge[194].

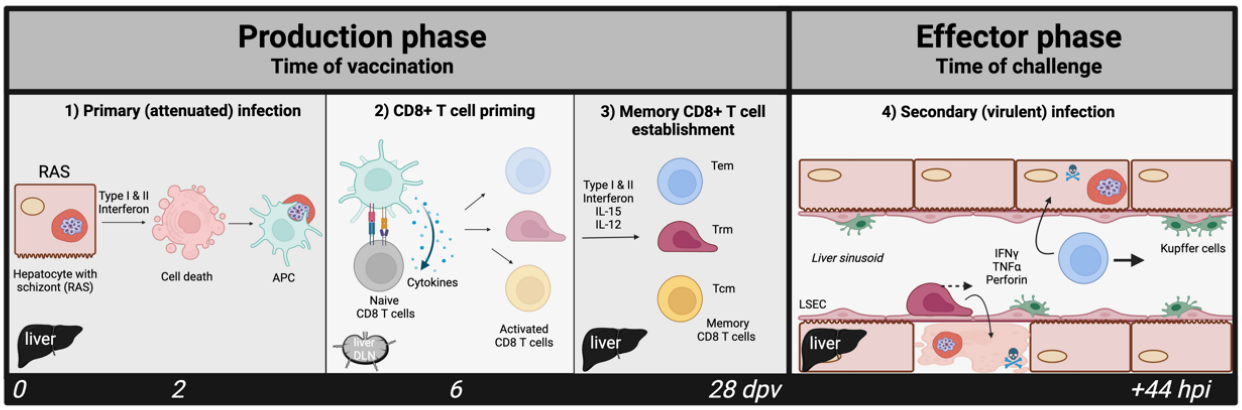

Figure 1.8: Schematic summarizing the time course of the priming and effector phase of T cells responses in the liver following attenuated whole spz-based vaccination. Created with BioRender.com.

Overall, designing a vaccine that induces polyfunctional T cells that can contribute to cytokine production, cytolytic action, and sensing and alarm is the ideal goal of vaccination. To design a

vaccine effective in all populations, one must overcome sex-specific differences in intrinsic and extrinsic factors influencing $CD8^+$ T cell fate and function.

Biological sex and $CD8^+$ T cells

Biological sex influences the human T cell repertoire. Generally, females have higher number of activated T cells, cytotoxic activity, greater proliferation, higher $CD4^+$ T cell counts and a bias toward Th2 $CD4^+$ T cells. Whereas, males tend to have more T_{reg} and $CD8^+$ T cell counts (reviewed in [4]). An important consideration to these trends is that they occur in an age-dependent manner. For example, while adolescent females and males have similar $CD4^+$:$CD8^+$ T cell ratios, as opposed to the higher $CD4^+$:$CD8^+$ T cell ratio in females in adulthood[4]. While many differences exist in the T cell repertoire, due to their importance in liver stage vaccine strategies, the rest of this section will focus on the implications of biological sex on memory $CD8^+$ T cells.

Biological sex influences $CD8^+$ T cells via three potential mechanisms: sex hormones, sex chromosome-linked genes, and physiology. Sex hormones could skew $CD8^+$ T cells either by direct action on $CD8^+$ T cell transcription or epigenetic modifications or indirectly via altering the cytokine and inflammatory signals delivered to $CD8^+$ T cells[195] during the priming and effector phase to direct fate and recall response. Sex chromosome-linked genes have the potential to alter $CD8^+$ T cell fate and function via intrinsic differences in either XCI escape, expression of Y-linked genes in males, or epigenetic differences produced over the life course.[196] Physiological differences could be related to the impact of murine size to cell ratio and baseline differences in density of T cells, such as naïve $CD8^+$ T cells or T_{reg} cells[197].

Sex hormones and $CD8^+$ T cells

Androgens and estrogens are also known to modulate $CD8^+$ T cells via direct and indirect mechanisms. At the direct level, sex hormones mediate transcriptional regulation and post-translational modifications[198]. Via binding to their respective receptors (ERα, ERβ, AR) or non-genomic signaling pathways, sex hormone modifications can significantly impact T cell function[4]. Of key interest to vaccination is the impact of androgens and estrogens on $CD8^+$ T cell fate and function. The most developed literature comes from the fields of prostate cancer, female reproduction, and autoimmunity. Recent studies on prostate cancer found that androgen signaling pathways decreased $CD8^+$ T cell effector function and routed $CD8^+$ T cells toward exhaustion[199,200]. In a tumor model of chronic antigen stimulation, the frequency of $CD4^+$ and $CD8^+$ T cells were comparable between sexes, but male mice had fewer polyfunctional $CD8^+$ T cells able to produce effector cytokines such as IFN-γ, TNFα, and granzyme B in tumors[199]. Estrogens likewise modulate $CD8^+$ T cell function. Estrogen regulates the IFNγ promoter[201], with higher estrogen levels in females driving increased T cell IFNγ production. Estrogen also suppresses cytotoxic activity of human endometrial $CD8^+$ T cells. This was exhibited when 17β-estradiol-treated $CD8^+$ T cells exhibited inhibition of perforin and granzyme A, regardless of endometrial tissue-residency states as defined by the CD103 tissue resident memory marker[202]. Relating to impact on fate, a recent paper demonstrated that in females these cells have a propensity to become SLEC, whereas male $CD8^+$ T cells give rise to more MPEC, linking this phenotype to the innate propensity of female $CD8^+$ T cells to respond to IL-12 . As far as we know, no one has reported the impact of biological sex and sex hormones on Trm frequency, number, and function in any tissue-type.

At the indirect level, sex hormones can alter the costimulatory tissue environment by modulating type I IFN signaling, a critical signal for the production of functional resident memory $CD8^+$ T

cells[158]. Additionally, another indirect mechanism could be related to the differential activity of innate immune cells in assisting or delivering signals to CD8+ T cells during the priming or effector phase[14,15,204].

Sex chromosomes and $CD8^+$ T cells

Many genes on the X chromosome regulate immunity and are important for the development of functional $CD8^+$ T cells. Immunological X-linked genes involved in CD8+ T cell memory response include: immune response related proteins like CD40L (CD40 ligand), transcriptional control effectors like FOXP3 (associated with the development and function of T_{reg} cells), receptors like IL-2RG, AR (Androgen receptor), and the pattern recognition receptor, TLR7 (reviewed in [196]). Further investigations into the contribution of these ligands in modulating memory $CD8^+$ T cell formation is warranted.

Physiological differences and $CD8^+$ T cells

Finally, the physiological differences - different size, organs, and cell composition of the host – could also influence the production and effector function of $CD8^+$ T cells[4]. Different densities or frequencies of immune cells could impact the sensing and alarm function of $CD8^+$ T cells, time course of recruitment of T cells toward site of infection, or skewing of certain signaling immune cells. This process is likely impacted by the surrounding tissue microenvironment. For example a recent study found that female mice had a higher density of skin-resident T cells than males and found this was tissue specific[197].

In conclusion, the intrinsic differences between a male and female liver have the potential to shape protection outcomes to CD8-T cell-dependent liver stage vaccines via three potential mechanisms - sex hormones, sex chromosomes, and physiological differences. The direct and indirect effects on protection could occur during the priming and/or effector phase of the CD8 T cell response.

1.7 THESIS GOALS

Epidemiological studies on sex-based differences in *Plasmodium* infection capture only one stage of the parasite's lifecycle, the blood stage infection. It is unclear whether sex-based differences exist during the liver stage of *Plasmodium* lifecycle. Given biological sex significantly alters infection outcomes of other hepatotropic pathogens, the story of sex differences in the host response to *Plasmodium* parasites has yet to be told. **Chapter 1** has summarized the intersection of several fields of study - sex differences, malaria, hepatology (study of the liver), immunology, and endocrinology – to provide frameworks and background for the rest of this thesis. The remaining chapters of this dissertation will investigate the impact of biological sex on the host response to *Plasmodium* liver stage and liver stage vaccines. Combined, this body of work seeks to add sex-specific hepatotropic pathogen to the definition of *Plasmodium* parasites, and inspire the study of the impact of host sex on mechanisms, therapeutics and vaccines targeting the *Plasmodium* liver stage.

Chapter 2 will evaluate the impact of biological sex on the duration of *Plasmodium falciparum* liver stage infection in humans. **Chapter 3** will seek to evaluate sex-specific and sex hormone-mediated immune responses to *Plasmodium* parasite's liver stage in rodent malaria models. **Chapter 4** will evaluate the impact of biological sex on protection by malaria liver stage

vaccines in mice. Further work will also deconvolute the molecular and cellular mechanism underlying androgen-mediated protection to liver stage vaccination. **Chapter 5** will conclude by summarizing the dissertation, discussing the significance of the results, and outlining limitations as well as potential future directions for the project.

Chapter 2. SEX-BASED DIFFERENCES TO PLASMODIUM INFECTION IN THE PLACEBO ARMS OF CONTROLLED HUMAN MALARIA INFECTION (CHMI) TRIALS IN MALARIA-NAÏVE POPULATIONS: A POOLED ANALYSIS

2.1 ABSTRACT

Plasmodium falciparum, while most known for the clinical manifestations of malaria during blood stage infection, is a hepatotropic pathogen with a complex liver stage. Sex-based differences in pathogenesis by hepatotropic pathogens are well-documented, but unstudied for *P. falciparum.* We conducted a pooled analysis on data from participants in placebo arms and infectivity controls of Controlled Human Malaria Infection (CHMI) trials in malaria-naïve populations to evaluate the impact of biological sex on the time to blood stage positivity and initial parasite density as indicators of liver stage dynamics and parasite replication. In this study, we pooled data from 102 placebo controls (48 female and 54 male) across 13 CHMI studies conducted between 2010 and 2024. We found that males are more likely to experience a delayed detection of blood-stage parasites following challenge with *Plasmodium falciparum* compared to females. Similar replication rate during blood-stage infection implicates sex-based difference in liver stage biology as the culprit of a delayed time to parasitemia. Thus, *Plasmodium falciparum* induces a sex-specific host-pathogen response in the liver, similar to what is observed with other hepatotropic pathogens.

2.2 INTRODUCTION

Biological sex, defined by characteristics such as chromosomes, reproductive organs, and hormones, significantly influences immune responses to infectious diseases[4]. Typically, females exhibit more robust innate and adaptive immune responses than males, often resulting in

increased susceptibility and more severe disease progression among males for various pathogens[4,205–207]. This disparity is particularly evident with hepatotropic pathogens, where sex-based differences in liver disease prevalence and pathogenesis are well documented. Pathogens such as *Entamoeba histolytica*[117,118], *Schistosoma* spp.[120–122], and hepatitis-inducing viruses[124–127] lead to higher rates of fibrosis and liver damage or increased infection frequency in males compared to females. Despite extensive evidence of these sex-specific effects on hepatotropic pathogens, the impact of biological sex on the liver stage of *Plasmodium* species in humans remains largely unexplored.

Plasmodium parasites, the causative agents of malaria, pose a significant global health threat, with an estimated 249 million cases and 608,000 deaths reported in 2022[29]. These parasites have a complex lifecycle that begins when sporozoites are transmitted to humans by mosquito bites[34]. Infectious sporozoites migrate from the dermis to the bloodstream and are transported to the liver to initiate an asymptomatic liver stage that lasts about a week[208,209]. This is followed by the symptomatic blood stage, where parasites cyclically replicate in red blood cells, leading to clinical malarial illness. Eventually parasites develop into gametocytes that when transmitted to mosquitoes can facilitate the rest of the parasite lifecycle[35]. Although *Plasmodium* parasites are mostly known for their clinical malaria manifestations during the blood stage, they are also considered to be hepatotropic because of the preceding liver-targeting stage of their lifecycle.

Despite the significant global burden of malaria, there is limited information on sex-specific differences throughout the *Plasmodium* lifecycle, with most evidence focused on blood stage outcomes[97]. Several studies show higher malaria prevalence in males, especially among older

children and adults, but this bias is not seen in all study settings[84,88]. Similarly, findings on sex differences in malaria incidence are mixed, with some studies indicating higher incidence in males[85,86,91,92], one higher in females[98] and some showing no sex-based differences[89,99]. Potential variations in liver stage infection by biological sex remain underexplored due to challenges like limited access to liver samples, underrepresentation and underreporting of biological sex in study designs, and immunodominant effects of existing and prior blood stage infection.

A critical tool for assessing the duration of liver stage infection without directly sampling the liver involves measuring the day of the first blood stage infection in Controlled Human Malaria Infection (CHMI) studies[210]. In CHMI trials, human volunteers are safely and deliberately infected with *P. falciparum* parasites under close medical supervision to evaluate the efficacy of experimental drugs and vaccines[211]. During the acute blood stage infection window, these trials include at least daily monitoring of participants to diagnose infections and monitor for clearance after treatment with approved antimalarial medications. To evaluate the efficacy of the biologic product and ensure that the challenge product is infectious, many CHMI trials include a placebo control group and/or infectivity controls. These participants do not receive any products known to block parasite development, but do receive challenge with wild-type infectious sporozoites.

When CHMI is conducted in malaria-naïve populations, the placebo participants provide a unique set of samples to study parasite emergence into the blood stage. These participants provide a minimally biased and available set of samples to assess the impact of biological sex on *Plasmodium* liver stage dynamics. Malaria-naïve participants represent a unique population with no pre-existing immunity, allowing us to isolate the contribution of biological sex without

confounding effects of prior *Plasmodium* infections. Here, data from CHMI trials conducted in malaria-naïve populations in the United States and the Netherlands were used to investigate the effect of biological sex on time to positivity (TTP) of *P. falciparum* parasites as an indicator of sex-specific liver stage outcomes in *P. falciparum* infection. Additionally, the effect of biological sex on parasite replication in the blood stage was examined. This analysis offers valuable insights into sex-specific differences in liver stage outcomes, which could have significant implications for the development and assessment of vaccines that target liver stage parasite development. Understanding these differences is also important for identifying sources of heterogeneity in liver stage infections that may influence outcomes in vaccine and drug efficacy trials.

2.3 METHODS

Data Sources and Participants

Data were compiled from all CHMI clinical trials where testing was conducted at the Seattle Malaria Molecular Diagnostic Laboratory (MMDL) or the Leiden Controlled Human Infection Center (LUMC) using *Plasmodium* 18S nucleic acid amplification tests (NAAT) as infection detection assays[208,212–220]. The MMDL assay targeted 18S rRNA by quantitative reverse transcription PCR (qRT-PCR) and the LUMC assay targeted the 18S rRNA coding genes by quantitative PCR (qPCR); the assays are hereafter referred to as '18S NAAT' tests. All studies enrolled healthy, malaria-naïve adults between age 18 and 48 years old.

For each study, the route of CHMI administration (intravenous or mosquito bite), *Plasmodium* challenge strain, challenge dose, placebo given, start day and frequency of blood draws post

CHMI, treatment criteria, study year(s), and method for parasite detection were abstracted from study protocols and publications. For each participant in the placebo or infectivity control groups, sex, age (if available), date of anti-malarial treatment, and date and parasite densities for all post-CHMI blood draws were obtained.

Patient Consent Statement

The study designs and consent forms for future research were previously approved by local ethics committees. Informed consent for each clinical study was described in previously published reports[212–216,219–224]. No further documentation was needed for the analyses presented in this report.

Data Processing and Outcome Variables

The main outcome of interest was the TTP for each participant, defined as the day which corresponded to the first positive 18S NAAT result at any parasite density. Day of CHMI was coded as Day 0 for all studies. For studies that sampled twice per day, the second daily samples were coded as half days (e.g. Day 6.5). Any participant who did not experience the outcome was excluded from these analyses.

Given that previous analyses have suggested the liver stage is 6-7 days[209,225], we reviewed TTP distributions, blinded to biological sex, and confirmed most participants had parasites detected by PCR by Day 7. Then, we created a binary variable, delayed parasitemia, to classify if TTP occurred greater than seven whole days post-CHMI. For this outcome measure, the analytic data set was restricted to include only the first sample of the day. This was done to create uniformity with studies that sampled daily and minimize possible biases.

As an exploratory analysis, we analyzed parasite densities at TTP and one and two days post-TTP to assess blood stage replication rate. Parasite densities were reported in estimated parasites/mL by the testing laboratories for all received samples and then transformed to $\log_{10}$ densities for analyses. Only samples drawn prior to the initiation of antimalarial treatment were considered.

Statistical Analysis

To explore possible differences in the distribution of TTP by sex, we compared whether there was a difference in TTP by sex with a log-rank test using interval-censored Kaplan-Meier survival. The start of the interval was the time of the last negative test prior to testing positive. The end of the interval was the time that a participant tested positive. If a participant tested positive on their first day of sampling, the start of their interval was set to Day 6, which was the most common sampling start day in the studies. No positives were observed before Day 6 in studies that began sampling earlier. We estimated a hazard ratio (HR) and 95% confidence interval (CI) using a semi-parametric interval-censored Cox-proportional hazard model. We fit an unadjusted model, as well as a model that included vector and CHMI strain. Finally, Z-tests were used to compare the likelihoods of developing parasitemia by Days 6, 7 or 8 between males and females, based on survival probabilities from the interval-censored survival model.

To explore the relationship between delayed parasitemia (first positive >7 days post-CHMI) and sex, we fit a generalized linear mixed-effects model with a logit link that accounted for the correlation within studies. The final model was adjusted for route of CHMI administration and strain, coded as a binary variable indicating if NF54 or another strain was used (3D7 or 7G8).

Prior to model fitting, we assessed possible effect modification by administration route and CHMI strain using chi-squared tests for homogeneity within stratum of route and vector. To explore if any single study was especially influential on the outcome, we performed a sensitivity analysis in which each study was removed from the data set one-by-one and the adjusted and unadjusted model was refit. Odds ratios and confidence intervals from each iteration were plotted to look for influential studies.

Finally, to examine if blood stage replication rates may differ between males and females, we compared the fold change in parasite density over one-day (~24 hours) and two-day (~48 hours) intervals. The fold change was calculated as the difference in $\log_{10}$ parasite density relative to density at first positive. Both full-day and half-day samples were considered. For example, if a participant was first positive on Day 7, samples considered were Days 7, 8 and 9. If the first positive was on Day 6.5, samples considered were Days 6.5, 7.5, and 8.5. Fold changes were compared between males and females using t-tests after verifying that the distributions were approximately normal.

All analyses were performed using R Statistical Software, version 4.3.2[226]. Survival analysis was conducted using the *survival* R package version 3.7-0, *icenReg* package version 1.0.1[227] and *interval* package version 1.1-1.0[228]. Generalized linear mixed effects models were fit using the *lme4* package version 1.1-35.5[229].

2.4 RESULTS

CHMI demographics

Data from 103 controls from 13 different studies carried out between 2010 and 2024 with samples tested by molecular assays at the MMDL or LUMC were available for this study (**Table 2.1**). One infectivity control from the GAP3KO study did not develop parasitemia following CHMI[216] and was not included in this analysis, resulting in 102 controls included. Nine (69%) of the studies challenged participants using infectious mosquito bites, three (23%) used direct venous inoculation (DVI) of PfSPZ Challenge sporozoites, and one (DSM265) challenged two participants with mosquito bites and two participants via DVI of PfSPZ Challenge. All mosquito bite challenges were conducted using bites from five infectious mosquitoes. All DVI PfSPZ Challenge were conducted using aseptic, cryopreserved, vialed *P. falciparum* strain with NF54[230] or 7G8[231] sporozoites. The DVI challenge dose was $3.2x10^3$ PfSPZ Challenge in all studies. Most studies (11/13) used the NF54 challenge strain, while one used 3D7 strain by mosquito bites and another used PfSPZ Challenge 7G8 by DVI. Two studies began monitoring participants for parasites beginning five days post-CHMI, nine began monitoring on Day 6, and one (USSPZV6) began monitoring on Day 7. Ten studies took samples once daily, and three studies drew samples twice daily (MC-003/Cvac, ZonMW1, ZonMW2)[212–214]. Participants in the placebo groups in most studies received normal saline, non-infectious bites, or no product at all (infectivity controls) during the experimental product administration phase of the study that preceded the CHMI phase. Three studies administered placebo products in conjunction with an antimalaria medication with CHMI performed later after the prophylactic effects of the drug had worn off (MC-003, ZonMW1, ZonMW2)[212–214]. The reagents and conditions of the NAATs differed between sites and evolved over time[208,220,222,232]. However, the tests had similar limits of

detection (10-100 parasites per mL) and used standard curves for absolute quantification, allowing for pooled and comparative analysis across trials.

clinicaltrials.gov identifier	Shorthand name	Year(s)	Total Placebos (M +F)	Challenge route	CHMI strain	Monitoring start day	Sampling frequency
NCT01058226	MC-001/Demo	2010-2011	6 (4+2)	Mosquito bite	NF54	5	daily
NCT01500980	MC-003/Cvac	2012	6 (3+3)	Mosquito bite	NF54	6	twice daily
NCT01218893	ZonMW1	2012	5 (0+5)	Mosquito bite	NF54	6	twice daily
NCT01422954	ZonMW2	2012-2013	4 (0+4)	Mosquito bite	NF54	5	twice daily
NCT04072302	KAF156	2014-2017	22 (22+0)	Mosquito bite	NF54	6	daily
NCT02562872	DSM265	2016	6 (0+6)	DVI or Mosquito bite	NF54	6	daily
NCT02511054	NIH Cvac-Pyr	2016	5 (3+2)	DVI	NF54	6	daily
NCT02773979	DMID 11-0042	2017	6 (4+2)	DVI	NF54	6	daily
NCT0316121	GA1	2017	9 (3+6)	Mosquito bite	NF54	6	daily
NCT03168854	VTEU 14-008 GAP3KO	2018-2019	9 (3+6)	Mosquito bite	NF54	6	daily
NCT04966871	USSPZV6 Warfighter	2021-2022	11 (6+5)	DVI	7G8	7	daily
NCT04577066	GA2	2022	3 (1+2)	Mosquito bite	NF54	6	daily
NCT05468606	CoGA	2023-2024	5 (3+2)	Mosquito bite	3D7	6	daily

Table 2.1 Summary of Controlled Human Malaria Infection (CHMI) Studies. Studies included in the pooled analysis, along with meta-data about each study.

Of 102 participants, 54 (52%) were male. There were no notable differences in age, challenge route, or challenge strain between male and female participants (**Table 2.2**). However, females were overrepresented in studies that sampled twice per day (15/48) compared to males (5/54).

	Female	Male	All
Participants	48	54	102
Mean age (SD)	26.67 (7.51)	28.06 (5.66)	27.27 (6.77)
Challenge route			
DVI (%)	13 (27.1)	13 (24.1)	26 (25.5)
Mosquito bite (%)	35 (72.9)	41 (75.9)	76 (74.5)
CHMI strain (%)			
3D7	2 (4.2)	3 (5.6)	5 (4.9)
7G8	5 (10.4)	6 (11.1)	11 (10.8)
NF54	41 (85.4)	45 (83.3)	86 (84.3)

Abbreviations: SD= standard deviation; DVI= direct venous inoculation; CHMI = Controlled Human Malaria Infection

Table 2.2. Baseline characteristics for male and female subjects included in the pooled analysis of time to parasitemia following controlled human malaria infection (CHMI).

Sex difference in time to parasitemia

The data indicate that males have an overall longer time to the first NAAT-positive test compared to females. The distribution of TTP by sex is shown in **Figure 2.1.** Considering all samples drawn, the mean day of first positivity for females was 7.2 (SD=0.9), and for males was 7.6 (SD=1.2), with no discernable differences by route of CHMI administration and strain (**Table 2.3** and **Table 2.4**). Additionally, the risk of TTP is presented by Kaplan-Meier (KM) curves in **Figure 2.2.** A log-rank test of the interval-censored survival curves showed a significant difference in the distribution of TTP between males and females (p=0.04), with males tending to develop parasitemia at later time points than females. A Cox proportional hazards model suited for interval-censored data also suggested that males were 37% less likely to develop parasitemia at any time point compared to females in an unadjusted model (HR=0.63, 95%CI: 0.39, 1.05), but the result only bordered on significance (p=0.08). Adjusting for vector and strain of CHMI did not change the HR estimate for sex, but did increase the confidence interval (adjusted HR=0.63, 95%CI: 0.33, 1.2, p=0.16).

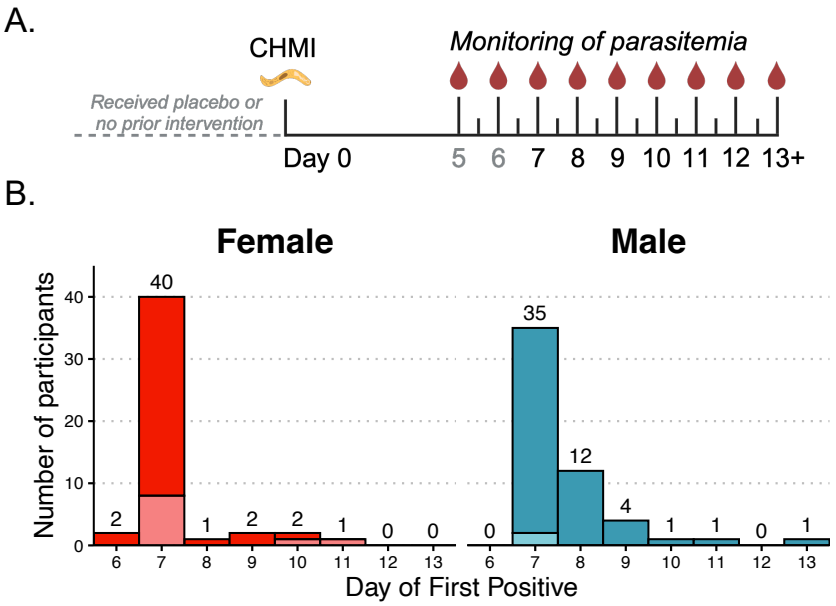

Figure 2.1. Distribution of the day after CHMI that each participant was first positive for *P. falciparum* by NAAT, divided by sex. A. Schematic of placebo or infectivity control arms of CHMI clinical trial. B. Histogram of the day after CHMI that each participant was first positive for *P. falciparum* by NAAT, divided by sex. For studies that sampled twice daily, the lighter shaded section of the bar indicates participants that had their first positive during the second sample of the day.

	Female			Male			Overall
	Mosquito Bite	DVI	All	Mosquito Bite	DVI	All	
Total Participants	35	13	48	41	13	54	102
Day First Positive[1]	7.14 (1.01)	7.23 (0.60)	7.17 (0.91)	7.63 (1.27)	7.46 (0.66)	7.59 (1.15)	7.39 (1.06)
Log_{10} parasite density at first positive[1]	2.21 (0.48)	1.92 (0.56)	2.13 (0.51)	2.41 (0.59)	1.91 (0.68)	2.29 (0.64)	2.21 (0.59)
Time to first positive 18S NAAT[2]:							
> 7 days	4 (0.11)	2 (0.15)	6 (0.13)	14 (0.34)	5 (0.38)	19 (0.35)	26 (0.25)
≤ 7 days	31 (0.89)	11 (0.85)	42 (0.88)	27 (0.66)	8 (0.62)	35 (0.65)	76 (0.75)

[1]Presented as mean (standard deviation) ; [2]Presented as n (%)

Table 2.3. Summary of *Plasmodium falciparum* 18S NAAT data in CHMI studies.

	Female			Male			Overall		
	3D7	7G8	NF54	3D7	7G8	NF54	3D7	7G8	NF54
Total Participants	2	5	41	3	6	45	5	11	86
Day First Positive[1]	8.00 (1.41)	7.00 (0.00)	7.15 (0.94)	9.00 (2.00)	7.50 (0.84)	7.51 (1.09)	8.60 (1.67)	7.27 (0.65)	7.34 (1.04)
Parasite density at first positive[1]	2.40 (0.52)	2.49 (0.27)	2.07 (0.52)	2.21 (0.30)	2.29 (0.73)	2.29 (0.66)	2.29 (0.35)	2.38 (0.55)	2.19 (0.60)
Time to first positive 18S NAAT:									
> 7 days	1 (0.5)	0 (0)	5 (0.12)	2 (0.67)	2 (0.33)	15 (0.33)	3 (0.6)	2 (0.18)	20 (0.23)
<= 7 days	1 (0.5)	5 (1)	36 (0.88)	1 (0.33)	4 (0.67)	30 (0.67)	2 (0.4)	9 (0.82)	66 (0.77)

[1]Presented as mean (standard deviation) ; [2]Presented as n (%)

Table 2.4. Summary of Plasmodium 18S NAAT data in CHMI studies by parasite strain.

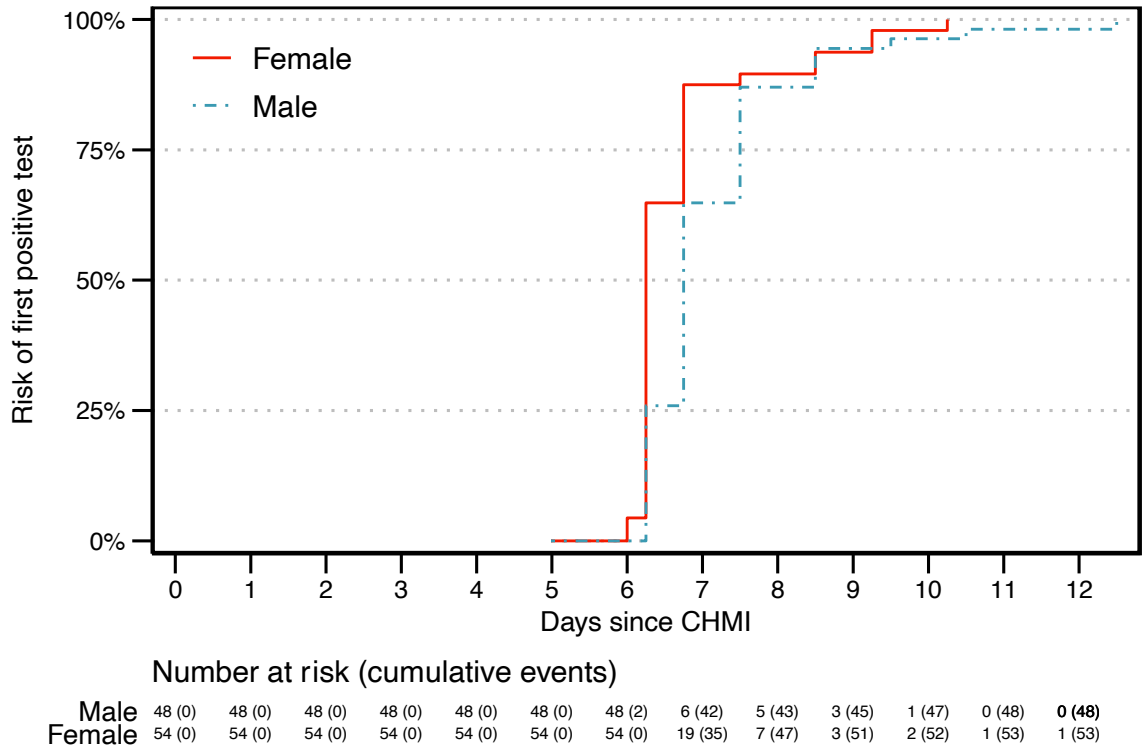

Figure 2.2. Risk of parasitemia following CHMI. Kaplan-Meier plot showing time to first positive NAAT-positive test for males (blue dashed line) and females (red solid line). All samples were included when determining the first positive sample. Samples began to be collected starting on Days 5, 6 or 7.

Drawing on prior literature indicating a liver stage duration of approximately seven days, we assessed the probability of TTP within the expected detection window of seven days post-CHMI, plus or minus one day. The probability of developing parasitemia by Day 7 estimated with the interval-censored survival model was significantly higher in females (86.7%) compared to males (63.5%) (p=0.005). There was no difference between females and males in the probability of first positive by Day 6 or Day 8 (**Table 2.5**).

Day	Probability of first positive		p-value
	Female	Male	
6	4.40%	0.00%	0.26
7	87.50%	64.80%	0.005
8	89.60%	87.00%	0.1

Table 2.5. Interval-censored Kaplan-Meier survival curve estimates of probability of first positive by Day 6, 7 and 8 post CHMI, separated by sex.

In parallel with the survival analysis, a binary variable, delayed parasitemia, to classify an over seven-day TTP was developed. Using data only from the first sample of each day, there were 19 males (35%) who experienced delayed parasitemia, compared to six females (13%), with proportions similar when stratifying by route of infection (**Table 2.3**). There was no difference in classification of each participant when half-day samples were considered. There was no evidence of differences in the proportions of delayed parasitemia by sex within stratum of route of infection or CHMI strain, and all data were used in a single model. In the unadjusted model, males were 3.71 times more likely to experience delayed parasitemia compared to females (95%CI: 1.28, 10.77). Males were 3.67 times more likely to experience delayed parasitemia when adjusting for route of administration and challenge strain (95%CI: 1.24, 10.79). Results were similar when stratifying by route of challenge, but results were no longer significant with the smaller sample sizes (**Figure 2.3**).

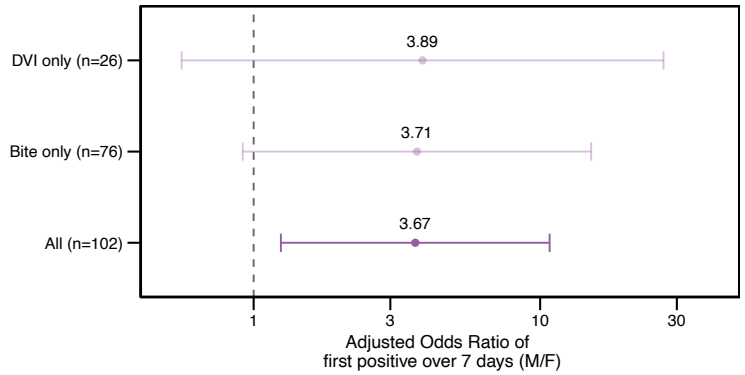

Figure 2.3. Adjusted odds ratio of first positive after seven days in males compared to females. The odds ratio (OR), adjusted for CHMI vector and strain, is presented as a point, and the limits of the 95% confidence intervals as lines. The adjusted ORs are presented just in those that received CHMI via DVI or mosquito bite, and all participants combined.

Removing studies one-by-one revealed no studies that were heavily influencing the results (**Supplemental Figure 2.7**). Adjusted odds ratios (aOR) of odds of delayed parasitemia comparing males to females ranged from 2.8 to 4.9 with each data set. The greatest impact was seen when removing KAF156, which only had male placebo participants. Without this study in the data, the aOR was 2.8, and was the only estimate that was not significant (95%CI: 0.84, 9.33).

No sex difference in parasite density and replication

Evaluation of parasite densities indicate no sex-specific difference in density at day of first positive. The $\log_{10}$ parasite density for all first-positive samples was not significantly different between males and females ($p = 0.16$) (**Figure 2.4**). Similarly, no significant differences in parasite density were observed when data were stratified by route and strain. However, males exhibited a trend toward slightly higher parasite densities compared to females in the mosquito bite group ($p = 0.1$) and NF54 strain recipients ($p = 0.08$) (**Figure 2.4**). Additionally, parasite density was higher in those challenged by mosquito bite compared to DVI for both females and males (**Table 2.3**). Similarly, the $\log_{10}$ parasite density at first positive was comparable across *P. falciparum* strains (3D7, 7G8, and NF54) in both females and males (**Table 2.4**).

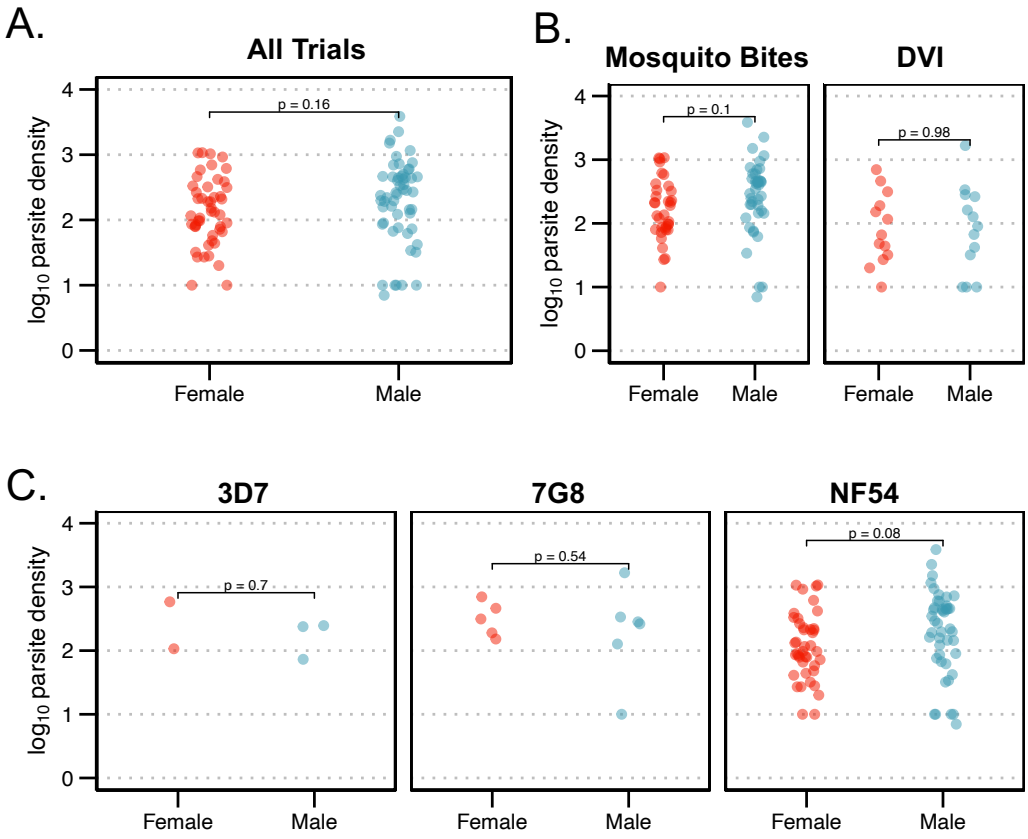

Figure 2.4: Parasite densities of first positive NAAT test following CHMI. Jitter plots show the parasite densities (log_{10} parasites/mL) of males and females at first positive NAAT test for all clinical trials (A), or divided by challenge route (B) and strain (C). P-values displayed are from an unpaired t-test.

Further evaluation of parasite replication capacity within the first two days of parasitemia found no difference between males and females. Parasite density measurements unaffected by rescue drug treatment were available one and two days after first positive for 90 and 63 participants, respectively. For those with a sample one day after the first positive, mean log_{10} density in females (2.03 +/- 0.48 log_{10} parasites/mL) was slightly lower compared males (2.26 +/-0.66 log_{10} parasites/mL) at first positive. One day after, mean log_{10} density increased by an average 0.44 log_{10} parasites/mL in females and 0.17 log_{10} parasites/mL in males, but the difference in log_{10} fold change was not significant (p=0.3). For those with samples two days after the first positive,

mean log_{10} density in females (1.89 +/- 0.41 log_{10} parasites/mL) was similarly lower compared to males (2.04 +/- 0.60 log_{10} parasites/mL) at first positive (**Supplemental Figure 2.8**). Two days after, mean log_{10} density increased by an average 0.70 log_{10} parasites/mL in females and 0.71 log_{10} parasites/mL in males. The log_{10} fold change between first positive and two days later was not significantly different between sexes (p=0.98) (**Figure 2.5**).

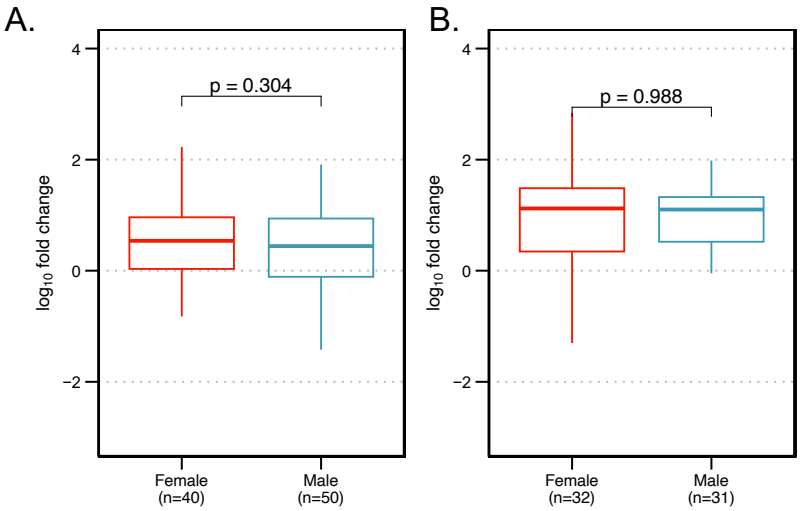

Figure 2.5. Fold change relative to first positive of log_{10}-transformed parasite densities. Box plots show the median log_{10}-fold change in parasite densities for males and females one day (A) and two days (B) after first positive. The top and bottom of the boxes represent the third and first quartiles of the distribution, respectively, with lines extending to the 95% of the distribution. Points outside of the 95% are presented as points. P-values displayed are from an unpaired t-test.

2.5 DISCUSSION

We analyzed the impact of biological sex on the time to positivity after CHMI and the *P. falciparum* blood stage replication rate following CHMI in the placebo arms of clinical trials conducted in malaria-naïve adults. We pooled data from malaria-naïve participants in 13 clinical studies across two locations. Overall, males tended to develop parasitemia later than females, and males were 3.7 times more likely than females to have TTP greater than seven days post CHMI. Results did not change when stratifying by CHMI challenge route, nor when adjusting analyses for challenge route and strain. Evaluation of changes in parasite density following patency, which is a proxy for blood stage replication, showed that that replication in the blood did not

differ by biological sex. These results suggest that the *Plasmodium* liver stage serves as the source of the sex difference in patency, which to our knowledge, is the first evidence of a biological sex difference in liver stage infections in humans.

Our results highlight the unknown impact of biological sex of participants on *Plasmodium* infection, and subsequent interpretation of CHMI clinical trials and vaccine efficacy. CHMI has a long history as a tool to quickly and effectively evaluate clinical interventions such as vaccines and drugs[233,234]. Delay of parasitemia, defined as a delay in time to blood stage parasitemia during a pre-defined follow-up period compared with infectivity controls, is a frequently applied primary or secondary analysis for partial treatment efficacy[235–240]. The *P. falciparum* liver stage is understood to have a biological duration of 6 to 7 days[209,225]. Here we find that biological sex modifies the duration of the liver stage and the emergence of blood stage infections, highlighting the need to account for biological sex in malaria clinical trials and analyses.

Two general biological phenomena could explain why males are more likely to experience a longer time to positivity compared to females: parasites have a slower replication capacity within the blood stage of male hosts or parasites experience a delayed or reduced liver stage in male hosts. Previous clinical studies have sought to evaluate differences in parasite densities by sex. A longitudinal cohort study conducted in a malaria endemic region of Uganda intensively followed *P. falciparum* infections in members from 80 households over two years and found no evidence for differences in parasite density as determined by qPCR between male and females after adjusting for age[101]. The same conclusion was found in a cross-sectional study of school children in Cote d'Ivoire where mean parasite densities by PCR did not differ between sexes[95]. We

observed similar findings in our analyses. There were no differences in parasite density of the first positive test result between males and females. Additionally, we saw no difference in the $\log_{10}$ change in parasite densities in samples taken one and two days after first positive, suggesting that blood stage replication is not altered by biological sex. The lack of evidence for difference in blood stage replication leaves one to consider the impact of biological sex on the *Plasmodium* liver stage.

The liver is a sexually dimorphic organ[71,75,241], due in part to its critical role as an endocrine organ responsible for biosynthesis of certain sex hormones[54,77,242]. Five biological host-pathogen liver stage mechanisms could explain why males might be more likely to experience delayed TTP: 1) decreased susceptibility during initial infection; 2) lower replication rate within hepatocytes; 3) higher threshold needed for merozoite egress; or 4) higher clearance by intrinsic and extrinsic immune mechanisms. One additional explanation could be that fewer *P. falciparum* parasites reach the male liver during migration from the dermis, reducing downstream liver burden. While this study does not address these questions directly, our results highlight the need to differentiate these outcomes by sex and adjust the current paradigm to accommodate the heterogeneity introduced by biological sex.

For the results of a pooled analysis to be valid, one must assume that the data collected across studies are sufficiently similar to be combined. While all studies in our sample set utilized *P. falciparum* sporozoite CHMI, there were differences in the use of vialed PfSPZ Challenge products or infectious mosquito bites and the *P. falciparum* strain utilized. Route of administration is a known modifier of TTP and parasite density at TTP, with mosquito bite

challenge introducing more variability and longer TTP[243]. We observed a wider range of TTPs in both males and females in those challenged by mosquito bite compared to DVI (**Supplemental Figure 2.6**). However, there was no evidence of an interaction between sex and challenge route that differentially impacted time to parasitemia. Previous literature found a reduced patency period for 7G8 compared to NF54; however, we found no difference in TTP between these strains (**Table 2.4**). In our sample set, the minimum pre-patency period for those challenged with NF54 was six days, compared to seven days for 3D7 and 7G8. However, it should be noted that the one study that used 7G8 did not start sampling before Day 7, so it is possible that patency occurred prior to Day 7, but was not measured. Even though there was a slight difference in TTP by strain observed, it did not differ by sex and showed no modifying effect on our analysis.

Another difference between studies was the frequency of sample collection and the first day of sampling. Two studies began monitoring on Day 5, ten on Day 6, and one on Day 7. Most studies sampled participants once per day, but three studies conducted twice daily sampling. Notably, two of the three studies that did twice daily sampling only had female placebo subjects. As such, the TTP is potentially biased by the timing and frequency of sampling, as the true TTP exists between the time of the last negative and first positive. Interestingly, 12/20 (60%) participants who were sampled twice per day had their first positive on the second sample of the day. This suggests that participants sampled once per day may have developed parasitemia prior to their test positive date. To account for this, we utilized interval censoring for survival analyses. For the odds ratio analyses, we limited the analysis to include only the first samples in studies that sampled twice per day. Shifting to only using the first sample of each day did not

change whether a participant was positive before or after seven days, suggesting our results would not change if more frequent sampling had occurred.

Despite long-standing observations of biological sex differences in malaria prevalence[97], there is little known about sex-based differences during the liver stage of *P. falciparum* infection. Our analysis shows that malaria-naïve males are more likely to experience a delayed detection of blood stage parasites following CHMI compared to malaria-naïve females. The controlled design of CHMI trials minimizes environmental influences on infection outcomes, making observed differences more directly attributable to biological factors. The sex-based delay in patency is likely due to differences in liver stage biology rather than blood stage replication. CHMI trials remain critical decision-making tools for treatment efficacy, with time to positivity often serving as an important primary endpoint metric. We propose that biological sex may be a demographic characteristic that could influence the interpretation of such results, such that the sex of participants should be considered during randomization and analysis. Re-analysis of CHMI trials with sex-disaggregated data and consideration of biological sex in appropriately-powered future studies may reveal other potentially sex-based differences.

2.6 ACKNOWLEDGMENTS

I would like to thanks the co-authors on this paper that was written based on this work: Dianna E.B Hergott, Weston Staubus, Mirte Balke-Buijs, James G. Kublin, Patrick E. Duffy, Sara A. Healy, Angela Talley, Lisa Jackson, Meta Roestenberg, Sean C. Murphy. I especially would like to thank Dianna E.B. Hergott for conducting the statistical analyses and helping draft the manuscript on this topic. I also extend a heartfelt thank you to the clinical site staff, the

molecular team headed by Els Wessels (LUMC) and A. Mariko Seilie (MMDL) performing the NAAT assays in CHMI trials, and the participants involved in each of the original studies.

2.7 SUPPLEMENTAL FIGURES

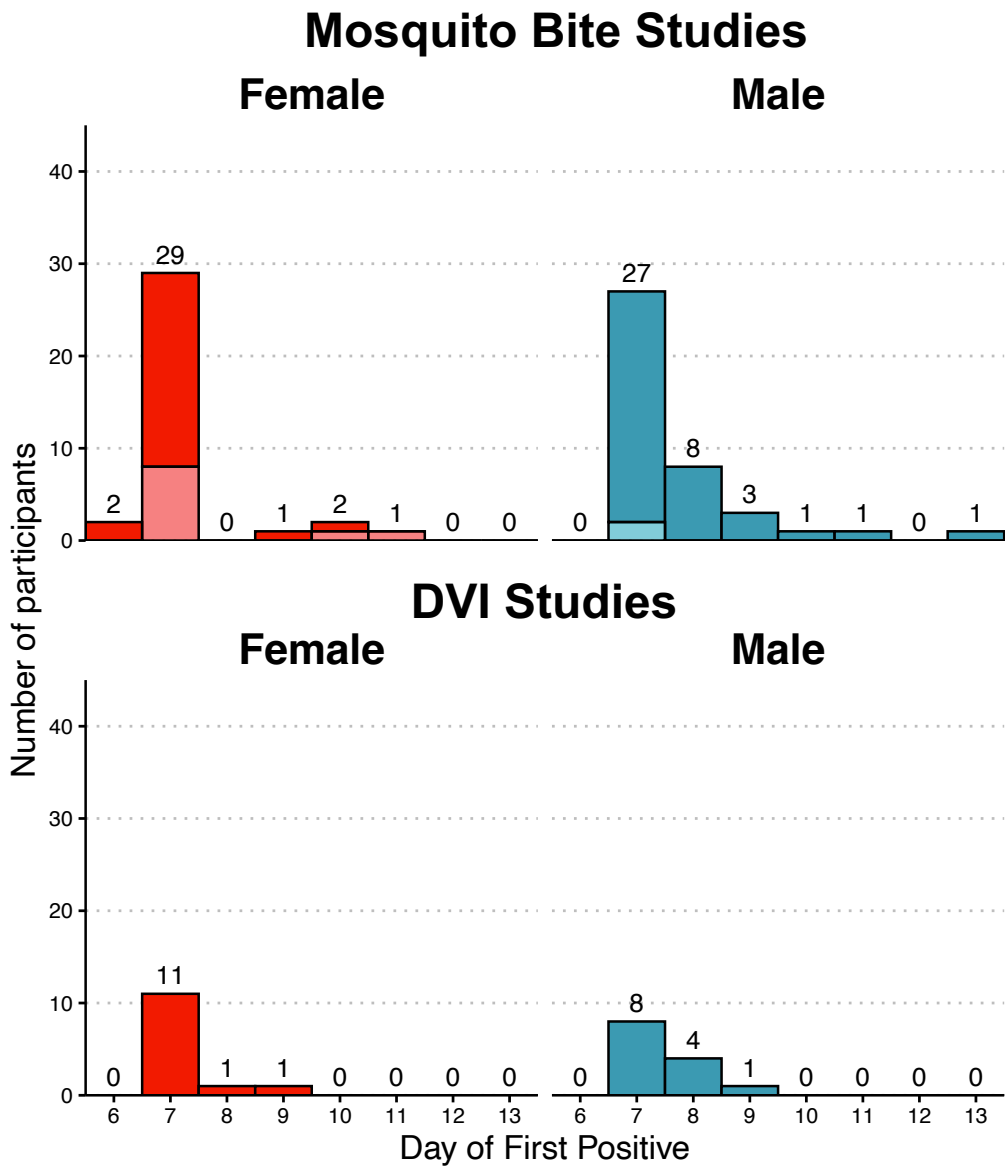

Supplemental Figure 2.6. Distribution of the day after CHMI that each participant was first positive for P. falciparum by 18S NAAT, divided by sex and route. For studies that sampled twice daily, the lighter shaded section of the bar indicates participants that had their first positive during the second sample of the day.

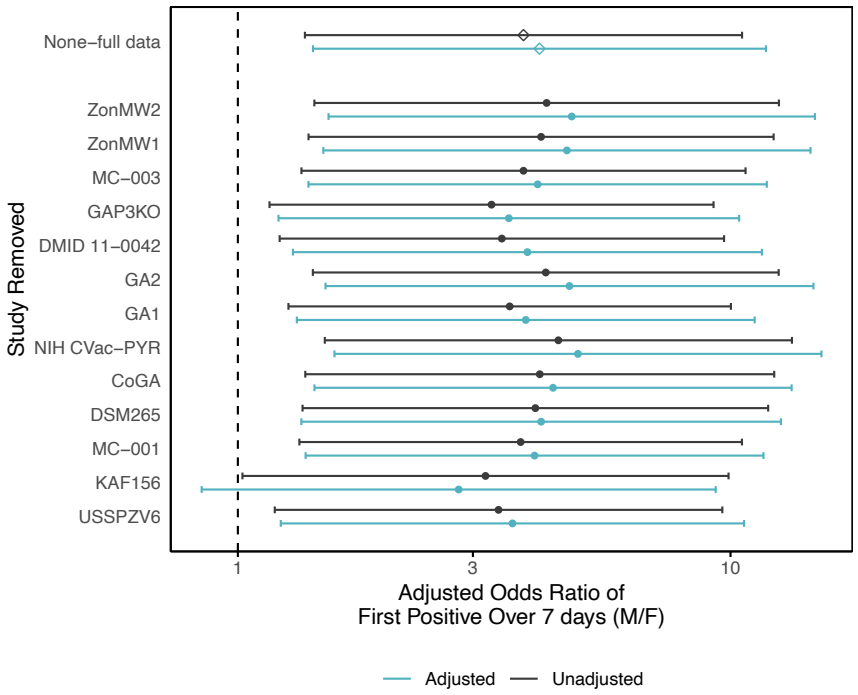

Supplemental Figure 2.7. Sensitivity analysis of adjusted odds ratio. Odds ratios comparing odds of delayed parasitemia (parasite detected more than 7 days after CHMI) between males and female control subjects in CHMI studies. Unadjusted (black) and adjusted for strain and route (teal) are presented for the full data set, and then with one study removed, shown on the y-axis. Lines show the 95% confidence interval for each estimate.

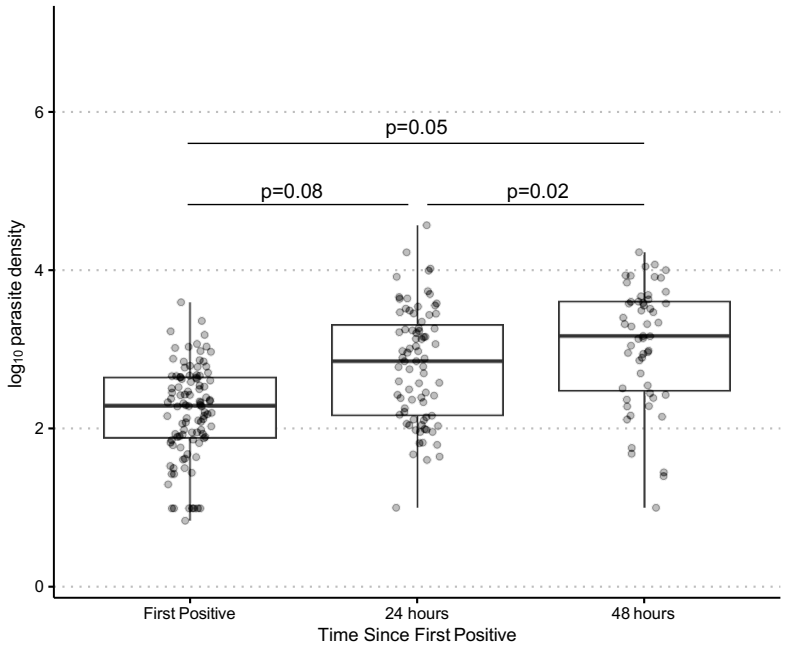

Supplemental Figure 2.8. Log_{10}-transformed parasite density (parasites/mL) measured at time of first test positive (TTP), 1-day post-TTP, and 2-days post-TTP. P-values displayed are from a paired t-test.

Chapter 3. HOST BIOLOGICAL SEX DIRECTS IMMUNE CONTROL OF *PLASMODIUM* PARASITE LIVER STAGE IN MICE

3.1 ABSTRACT

Plasmodium parasites, the causative agents of malaria, undergo a complex liver stage involving replication influenced by the spatial heterogeneity of the liver. The liver is known to be one of the most sexually dimorphic organs in the body, yet how the biological sex and androgens alters host responses to parasites in the liver remains unclear. Here, we investigated how biological sex and androgen levels influence host-parasite interactions during *Plasmodium yoelii* liver-stage infection. Using spatial transcriptomics, we mapped sex-specific gene expression and cellular composition in the BALB/cJ mouse liver. We found that androgens significantly impact parasite survival by reducing infected hepatocyte numbers, with females and castrated (ORX) males showing greater immune activity compared to intact males. At homeostasis, males exhibited lower baseline densities of Kupffer cells, monocytes, and dendritic cells in the liver; during infection, these disparities persisted and amplified. Intact males displayed impaired recruitment of immune cells and reduced antigen presentation activity, alongside a deficient Type I interferon response, which was robust in females and ORX males. Interestingly, despite similar magnitudes of Kupffer cell recruitment during infection, sex differences were driven by baseline innate immune cell densities mediated by androgens. Our findings highlight the critical role of biological sex in shaping immune responses during *Plasmodium* infection, and highlight the importance of considering sex as a biological variable in malaria infection studies.

3.2 INTRODUCTION

Plasmodium spp., the unicellular eukaryotic parasites responsible for malaria, are transmitted to mammalian hosts through the bite of infected *Anopheles* mosquitoes[34]. This transmission introduces *Plasmodium* sporozoites into the dermis, a highly motile stage of the parasite that quickly travels through the host's circulatory system to reach the liver via the portal vein[131]. The sporozoite traverses across multiple hepatocytes, until infection is established within a final hepatocyte. Upon entering a hepatocyte, the sporozoite forms a parasitophorous vacuole (PV), a protective enclosure within the cell's plasma membrane, allowing it to replicate rapidly in a process called schizogony while evading host defense mechanisms[132]. *Plasmodium* parasites actively modify the host hepatocyte to access nutrients that support its growth and development[143–145]. At the end of this transformation, the schizont form matures into merozoites, which are then released into the bloodstream, initiating the symptomatic blood stage of malaria[35].

The liver is a sexually dimorphic organ, characterized by differential gene expression patterns and ensuing function on the basis of sex[149]. The male and female liver during homeostasis maintains hundreds of genes that are differentially expressed in mice[71] and humans[72], including genes encoding xenobiotic and fatty acid metabolic enzymes, immune signaling pathways, and immune cells markers. Sex-differential patterns in function are most commonly characterized for sex-bias in metabolism[76,77] and endocrine function, where the liver plays an important role in sex hormone biosynthesis and hormone protein production[54,244]. Due to its high vascularity, the liver is well-suited for inter-organ signaling, modulating metabolic and synthetic functions in concert with other endocrine organs[54]. Sex differences also characterize the prevalence and severity of several hepatotropic pathogens, including *Entamoeba histolytica*[117,118], trematodes[119–122], and

hepatitis-causing viruses[124–127], which are either more prevalent or more severe, or both, in males. A hormonal basis for these sex differences is indicated by lower prevalence and severity in prepubertal populations, as is the case for Amebiasis is a parasitic disease caused by *Entamoeba histolytica,* where risk in men increases significantly post-puberty and gradually declining with age[118].

Biological sex also modifies the spatial heterogeneity within the liver[74]. The liver's basic anatomical unit, the lobule, consists of layers of hepatocytes arranged around a central vein, forming a hexagonal structure[49]. Hepatocytes, which make up about 80% of liver volume[50], radiate from this vein, with portal triads at each corner containing the portal vein, hepatic artery, and bile duct[51]. To optimize metabolism and prevent futile cycles, liver cells express different proteins along the axis from each portal node to the central vein, creating spatially defined metabolic zones known as zonation[245]. Sex-biased gene expression also follows a zonal pattern in the lobule; for example, one study found that 46% of zone-biased genes are sex-biased, particularly affecting pathways in lipid and xenobiotic metabolism[74].

The diverse liver cell types contribute significantly to sex-specific liver functions. Under steady-state conditions, the liver exhibits sex-based differences in cell numbers, with hepatocytes and Kupffer cells (KC) more abundant in females than in males[246]. This bicellular composition bias is accompanied by notable sex differences in gene expression profiles. Hepatocytes account for most of the observed sex-biased gene expression[74]. In contrast, non-parenchymal cells—including immune cells like KCs, Natural Killer (NK) cells, dendritic cells (DC), T and B lymphocytes—show less bias in baseline gene expression between sexes[74]. Although these

immune cells exhibit subtler gene expression differences, sex-specific immune cell activities have been documented in other tissue microenvironments[197].

Prior studies have mapped a spatially-resolved host response to *Plasmodium* liver-stage infection using rodent *Plasmodium* parasites[136,150,156]. Other studies found that during *P. berghei* infection, the host liver initiates a sequential response, including interferon-mediated immune gene activation in later stages of parasite development[111,145,152]. Additionally, parasite growth dynamics, including pace and survival, vary between pericentral (PC) and periportal (PP) hepatocytes[136]. Another study found immune cell infiltrates have also been observed, gathering around infected hepatocytes following *P. berghei*[150,152] infection. These insights have deepened our understanding of *Plasmodium* infection, hepatic zonation, and tissue-wide immune responses. However, despite the pronounced sexual dimorphism of the liver, these previous studies on *Plasmodium* liver-stage heterogeneity have focused mostly on female mice. Thus, the effects of sex-specific factors and hormones on gene expression across hepatic zones and the involvement of liver-resident immune cells so far remains unexplored.

Here, we examine the impact of biological sex on the susceptibility, development, and survival of the rodent parasite *Plasmodium yoelii*. Building on prior evidence for androgen effects on infection outcomes, we further characterize how androgens influence *P. yoelii* infection in male mice. To elucidate the effects of sex and sex hormones on the host response, we conducted spatial gene expression analysis of *P. yoelii*-infected mouse livers 44 hours post-infection. We investigate genes, pathways, and immune cell dynamics influenced by biological sex, by comparing male and female, and androgen levels, by comparing male and orchiectomized (ORX) male. Our findings are further corroborated through immunofluorescence microscopy.

Altogether, this study provides a comprehensive analysis of host-parasite interactions within the sexually dimorphic liver microenvironment.

3.3 METHODS

Ethics statement

Animal studies were performed according to the regulations of the institutional animal care and use committee. Approval was obtained from the University of Washington Institutional Animal Care and Use Committee (IACUC) under protocol 4317-01. The University of Washington IACUC adheres to the NIH Office of Laboratory Animal Welfare standards (OLAW welfare assurance # D16-00292).

Mice

Male and female BALB/cj mice (4-6 wk old) were obtained from Jackson Laboratories (Barr Harbor, ME) and housed at the University of Washington in an Institutional Animal Care and Use Committee (IACUC)-approved animal facility. All mice were used under an approved IACUC protocol (4317-01 to SCM).

Plasmodium sporozoites for challenge

Female *Anopheles stephensi* mosquitoes infected with wild-type (WT) *Py* (strain 17XNL) and unattenuated *P. berghei* ANKA (*Pb*) were reared at Seattle Children's Research Institute (Seattle, WA) or UW Medicine (Seattle, WA). Fresh spz were obtained by salivary gland dissection 14-18 days post-infection. All spz were diluted in Schneider's insect media for administration (Gibco, Thermo Fisher Scientific). Figure legends specify the dose for each

experiment. For *Py*-WT spz challenge administrations, $1x10^5$ freshly dissected *Py*-WT spz were injected unless state otherwise. For *Pb*-WT spz challenge administrations, $0.5x10^5$ freshly dissected *Pb*-WT spz were injected unless state otherwise.

Liver Fixations for Microscopy

Following infection with either *Py* or *Pb* or mock injection with loading media (Schneiders), livers from mice were harvested at 12, 24, or 44 hours post infection (hpi) and left lateral lobe was fixed in formalin solution (MilliporeSigma) for 24 hours. Tissue were then paraffin embedded, cut into 5μm sections, and mounted on positively charged glass slides. Mounted liver slices were then used for digital spatial profiling or immunofluorescence staining.

Immunofluorescence Staining

Slide-mounted liver slices were washed twice in xylene for 3 minutes followed by washes in 100%, 95%, 70% and 50% ethanol for 3 minutes each. Slides were then washed with DI water and heated to 90°C for 30 minutes in 1% citrate-based antigen unmasking solution (Vector Laboratories) using a Biocare Medical Decloaking Chamber. Slides were washed with Tris-buffered saline (TBS) and 1% Triton X-100 and then blocked for 2 hours in a solution containing 1.5% BSA and 15% goat serum (Sigma Aldrich). Slides were incubated in primary antibodies at 4°C overnight. Following primary antibody staining, slides were washed with TBS and 1% Triton X-100 then incubated with secondary antibodies and DAPI (1:2,000) for 1 hour at room temperature. Because the conjugated CLEC4F antibodies also come from a mouse host, slides were washed again with TBS and 1% Triton X-100 followed by an overnight incubation at 4°C with the CLEC4F antibodies separately. Slides were washed and autofluorescence quenched using Vector TrueView (Vector Labs). Fluoromount G mounting media was used to preserve

fluorescence signal. Primary antibodies were used at the following concentrations: *Py*Hsp70 1:500, Conjugated CLEC4F-647 1:100 (BioLegend 156804). Secondary antibodies, anti-mouse AlexaFluor-488, were used at a 1:1,000 dilution.

For experiments on quantification of spatial localization and parasite size at 44hpi, the following method was employed. Slide-mounted liver slices were washed twice in xylene for 3 minutes followed by washes in 100%, 95%, 70%, and 50% ethanol for 3 minutes each. Slides were then washed with DI water and heated to 90C for 30 minutes in 1% citrate-based antigen unmasking solution (Vector Laboratories) using a Biocare Medical Decloaking Chamber. Slides were washed with PBS and blocked for 1 hour in PBS containing 0.3% Triton-X, 1% BSA, and 10% natural goat serum (Jackson ImmunoResearch). Slides were incubated in primary antibodies and Hoescht (1:1000) and DAPI (1:400) (Invitrogen) at room temperature for 1 hour. Following primary antibody staining, slides were washed with PBS and incubated with secondary antibodies for 1 hour at room temperature. Slides were washed with PBS and autofluorescence quenched using Vector TrueView (Vector Laboratories). Fluoromount G mounting media was used to preserve fluorescence signal. Primary antibodies were used at the following concentrations: PvHsp70 1:500, anti-Ass1-AF488 1:250 (Abcam ab208412), anti-GS 1:500 (Abcam ab64613). Secondary antibodies anti-rabbit AlexaFluor-594 and anti-mouse AlexaFluor-647 were used at 1:500 dilution.

Imaging and Quantification

Images (40X) were acquired using a high-resolution widefield focused on encompassing infected hepatocytes and uninfected regions. For cell quantification within Ring ROIs 4x4 image panels were taken with a 60-pixel overlap and stitched together using the DAPI channel. Images were

stitched and deconvolved using the NIS-Elements software and were visualized using ImageJ software. ImageJ was used to quantify fluorescence intensity within defined ROIs of 200μm radii. Distances from parasites to Kupffer cells were measured between nucleus centers, using ImageJ/FIJI. Only Kupffer cells with a visible, stained nucleus (DAPI) and a clear surrounding CLEC4F signal were included in counts. Size quantification and frequency at 24 hours post *Py* infection used whole lobe images for quantification of number of parasites images were acquired at 10X, and image panels were generated based the size entire liver lobe.

Images for spatial localization were acquired in the following method. Images (20X) were acquired and stitched using a Keyence Automated Microscope. For liver zonation, periportal, interzonal, and pericentral regions were identified by Ass1 and GS staining. Periportal regions were classified as $Ass1^{hi}GS^{lo}$, interzonal regions were classified as $Ass1^{int}GS^{lo}$, and pericentral regions were classified as within 3 nuclei of $Ass1^{lo}GS^{hi}$.Images were visualized for analysis using ImageJ software. ImageJ was used to count the number of parsitess in each liver region and define ROIs around parasites in order to measure parasite area. Only parasites with visible, stained nuclei were included in counts and measurements.

Liver burden quantification by RT-qPCR

To quantify liver burden by reverse transcription polymerase chain reaction (RT-qPCR), mice were sacrificed, half of the liver was excised and pulverized by bead beating NucliSENS lysis buffer, and nucleic acid was extracted as previously described (bioMérieux, Durham, NC, USA). RNA was subjected to RT-PCR using the SensiFAST™ Probe Lo-ROX Kit (Bioline, London, UK) using a predesigned HEX-labelled mouse GAPDH RT-PCR assay (IDT Inc, Coralville, IA) multiplexed with a Pan-*Plasmodium* 18S rRNA assay as described[222]. Conditions of 45°C for 10

min, 95°C for 2 min and 45 cycles of 95°C for 5 s, 50°C for 35 s were run on a QuantStudio 5 real-time PCR machine (Thermo Fisher Scientific). Data were normalized to mouse GAPDH, and copy numbers per reaction were determined using custom lot of quantified Armored RNA encoding full-length *Plasmodium* 18S rRNA (Asuragen, Austin, TX).

Acyline and testosterone administration

Acyline (lot # RDZ001) was provided by John K. Amory, MD, MPH at the University of Washington. The lyophilized vials were stored at -20°C until resuspension. At the time of use, Acyline was resuspend to a concentration of 2mg/mL with sterile Molecular Biology Grade Water (Cytiva). Resuspended vials were stored for a maximum of 1 week at 4°C. Mice were subcutaneously injected 5 and 4 days prior to treatment to give time for the hormone environment to equilibrate. For testosterone treatment, testosterone propionate (Sigma Aldrich) was dissolved in sesame oil (Sigma Aldrich) at a concentration of 20 ug/uL. Mice were weighed to determine average weight per group, and then subcutaneously injected with 100 ug testosterone/g body weight at 2 timepoints (3- and 1-day pre-challenge).

Testosterone quantification in serum

Serum was collected via chin bleed day of harvest and stored in -20°C until testing. To measure testosterone levels in serum, Testosterone ELISA kits (Crystal Chem) were used per manufacturer guidelines. Singlet absorbance values of each sample were measured with CLARIOstar Plus Microplate Reader (BMG Labtech) and analyzed using MARS data analysis interface. A calibration curve was generated using manufacturer provided standards (0,0.1, 0.4, 1.5, 6.0, and 25 ng/mL) and a four parametric logistic curve fit was used to calculate sample values.

Orchiectomy

Male mice were orchiectomized at least 30 days prior to treatment. For orchiectomy (ORX), male mice were anesthetized by isoflurane inhalation (Isoflurane, USP, Dechra Veterinary Products), with doses of 4-5% for induction and, 2-3% for maintenance. A 5 mg/kg dose of meloxicam (Pivetal® Alloxate™, Aspen Veterinary Resources®, LTD) was administered subcutaneously (SC) to each mouse for systemic analgesia. Lubricant ophthalmic ointment (Pivetal® Artificial Tears, Aspen Veterinary Resources®, LTD) was applied to both eyes to prevent corneal desiccation. Thermal support was provided using a warm water circulating heating pad. The intended incision site was surgically prepped with three alternating scrubs of 10% povidone-iodine and 70% ethanol. A small, midline, scrotal incision was made with tissue scissors. Each testicle was identified singly, and the associated spermatic cord was clamped with hemostats for at least 10 seconds, and the testicle removed. The incision was closed using surgical tissue adhesive (3M™ Vetbond Tissue Adhesive 1469, 3M). Sham ORX surgeries were performed using the same surgical protocol without surgical removal of the testicles.

Digital Spatial Profiling

Experimental execution of DSP

Spatial transcriptomic analysis was completed using the Nanostring GeoMx Digital Spatial Profiler. Tissues were cut onto positively charged slides at a 5 micron thickness, dried overnight, and baked at 65°C for 1 hour. All subsequent steps were performed in an RNAse-free environment with DEPC water. Slides were de-paraffinized with xylenes, rehydrated using graded alcohols, and held in 1X PBS for 1 minute. Tissues were incubated in Tris/EDTA pH 9.0 antigen retrieval solution (Invitrogen #00-4956-58) pre-heated to 100°C for 15 minutes, washed

in 1X PBS for 5 minutes, and transferred to 37°C 1.0 ug/ml proteinase K (Ambion #AM2546) for 15 minutes. Slides were washed in 1X PBS for 5 minutes, then post-fixed with a 5 minute incubation in 10% neutral-buffered formalin followed by two 5 minutes incubations in Tris-glycine fixation stop buffer and one 5 minute wash in 1X PBS. Slides were hybridized overnight at 37°C with the Mouse Whole Transcriptome Atlas probe set (Nanostring #121400313) diluted in Buffer R (Nanostring #121300313) and DEPC water. Unbound probes were removed using two 25 minute incubations in stringency wash buffer comprised of 50% deionized formamide (Sigma #4650) and 50% 4X SSC buffer. Slides were washed twice with 2X SSC buffer for 2 minutes, then incubated in Buffer W for 30 minutes. Slides were stained overnight in morphology marker HSP70 antibody (Rabbit polyclonal, 1:42 dilution, StressMarq #SPC-186D), washed twice with 2X SSC for 5 minutes, and detected with a 1 hour incubation in secondary antibody conjugated to AlexaFluor 647 (Goat polyclonal, 1:200 dilution, Jackson ImmunoResearch #111-605-144). This was followed by two 5 minute 2X SSC washes and 1 hour incubation of labeled antibodies ASS1-AlexaFluor 488 (Rabbit clone EPR12398, 1:250 dilution, Abcam #ab208412) and GS-AlexaFluor 594 (Mouse clone 3B6, 1:60 dilution, Abcam #ab64613) cocktailed with nuclear counterstain Syto83 (2 uM, 1:10, Invitrogen #S11364). Slides were held overnight in 2X SSC buffer, then re-stained for 10 minutes with Syto83 immediately prior to loading the instrument.

Following whole-slide fluorescent imaging, circular ROIs were placed on tissue areas. Syto83 immunofluorescence was utilized for autofocus of GeoMx imaging. Immunofluorescence for Ass1 was used to identify periportal, pericentral, and interzonal regions and *Pf*HSP70 was used to identify the location of parasites. ROIs were generated using the circle tool and measured to a

diameter of 200µm, 100µm, 75µm, and 50µm. Each ROI was selectively exposed to UV light, cleaving the barcode sequences and collecting them in a unique well in a 96-well collection plate (three plates in total). Libraries were prepared with Nanostring SeqCode construction kits according to manufacturer instructions, sequenced using NovaSeq 6000 SP flowcell, and processed using the GeoMX NGS Pipeline.

Quality control

In the mouse GeoMx experiment, 278 segments were collected in total from 18 mice, and 5 of these segments failed Quality Control (QC) analysis and were removed from the dataset. One segment was removed for sequence stitching <80% and aligned sequence reads <80%. Two additional segments were removed for aligned sequence reads <80% alone, and two segments were removed for sequence saturation <50%. A secondary blinded reviewer conducted a follow-up quality control (QC) evaluation of the liver zones after initial collection. ROIs with identified discrepancies in accordance between initial and secondary reviewers were excluded from subsequent analyses (14 ROIs removed). Additionally, we excluded 60 ROIs with diameters that deviated from the specified 200 µm radius threshold and were collected for exploratory purposes. Final analysis included 199 ROIs.

		PP	IZ	PC
Parasite	**F**	9	9	6
	M	9	7	3
	ORX	8	9	7
Bystander	**F**	8	9	9
	M	9	9	9
	ORX	9	9	9
Mock	**F**	6	6	5
	M	5	6	6
	ORX	6	6	6
			Total	**199**

Table 3.1. Table of final number per condition following QC and exclusion criteria

Of the 20175 gene targets contained in the GeoMx Mouse Whole Transcriptome Atlas, all were included in the downstream analyses following QC analysis. No genes were removed as a global outlier and local outlier (Grubbs test). Sample size was determined based on pilot data. No statistical method was used to determine sample size. Experiments did not involve multiple experimental conditions.

Normalization and Batch Correction

The dataset was processed using the Seurat package. Gene expression data were normalized using Seurat's NormalizeData function, which scales and log-transforms the data. Variable features were identified with the FindVariableFeatures function, selecting the top features for downstream analysis. The selected features were then scaled using the ScaleData function to standardize expression values across cells.

To correct for batch effects, raw count data were extracted from the Seurat object and converted into a matrix format compatible with the Surrogate Variable Analysis (SVA) package. Batch variables were defined based on the experimental block, and covariates (sex/hormone status and infection status) were incorporated into a covariate matrix. Batch correction was performed using the ComBat_seq function from the SVA package, and the adjusted count matrix was then used for subsequent analyses.

Differential expression

Differential expression of gene targets in the GeoMx experiments was determined via a linear regression model. The regression model implemented was as follows:

$$Y = gene \sim Group + Group{:}\,liver\ zone + liver\ zone$$

Where group is a combined designation for sex/hormone status and infection type (e.g. F mock, F parasite, M mock, M parasite, ORX mock, ORX parasite). This model robustly tests for differential gene expression for comparisons of interest (ex. mock vs. parasite, sex and hormone status within mocks, etc.) while controlling for liver zone. Prior iterations of this model included bystander with an interaction term to evaluate the impact of bystander activation of gene expression, where Group was composed of mock, bystander, and parasite ROIs.

$$Y = gene \sim Group * Type + Group{:}\,liver\ zone + liver\ zone$$

However, with the limited difference between parasite and bystander (**Supplemental Figure 3.13**) led us to exclude the bystander ROIs from the main DE analysis in **Figure 3.4**. Differentially expressed genes (DEGs) were defined as genes with a false-discovery rate (FDR) < 0.05 and |logFC| > 1.0.

Pathway analysis

Hypergeometic enrichment against Broad MSigDBHallmark (H) and KEGG (K) pathway gene sets was completed for significant genes. Gene set enrichment analysis (GSEA) was performed again H and KEGG gene sets with contrast fold changes using fast GSEA.

Cell-type deconvolution

We used BayesPrism via InstaPrism[247] cell-type deconvolution algorithm to determine the cell-type proportions in our spatial transcriptomics data. We determined cell-type proportions in our data via comparison of our data to single-cell data from Hildebrandt et al[150], which was

conducted on C57BL/6 mice during *P. berghei* infection and included 14 cell types. We pseudo bulked the scRNAseq data by calculated the average expression per cell type in dataset. To determine statistical significance of difference in cell type proportions, we compared groups with a Wilcoxon test since proportions do not hold up to assumptions of normality.

Statistics

Details of the statistical tests applied to datasets shown in figures can be found in the above methods and in corresponding figure legends. All data points and n values reflect biological replicates. Data analyzed included outliers unless these could be explained by technical error. GeoMX data collection and analysis were not performed blind to the conditions of the experiments. Fluorescent microscopy with CLEC4F antibody and liver zonation were counted blinded to experimental conditions. Fluorescent microscopy and 18S rRNA data were assumed to be not normal thus non-parametric test were employed. Where relevant, statistical tests were two-sided. Individual p values are provided in the figures. Statistical analyses were performed in R (version 4.3.2) or GraphPad Prism 9.1.2 Software. Plots used in this manuscript were generated with GraphPad Prism and the following R packages: ggplot2, ggpubr, and UpSet[248].

3.4 RESULTS

Time-dependent sex differences in *Plasmodium yoelli* liver infection

To test if biological sex modifies susceptibility to infection or subsequent liver stage development, we used a model where adult male and female BALB/cJ mice were infected with 1 x10^5 *P. yoelli* sporozoite intravenously. Twelve, twenty-four, and forty-four hours post infection (hpi), the liver was isolated for quantification of a *Plasmodium* parasite RNA by 18S RT-qPCR

as a surrogate for liver burden (**Figure 3.1a**). At 12 and 24 hpi, no significant sex difference was observed. However, at 44 hpi, males maintain a about 3- fold higher liver burden compared to female age-matched mice (**Figure 3.1b**), indicating a sex difference in growth or survival and not frequency of initial infection. Two factors potentially influence the quantity of *Plasmodium* rRNA at 44 hours: 1) the number of parasite infected hepatocytes or 2) the replication capacity of schizont within the hepatocyte. To evaluate if sex influenced these factors, the number of infected hepatocytes were counted and measured size with fluorescence microscopy (**Figure 3.1c**). Similar to our previous findings, there were more parasites in males compared to females at 44 hours, but not at 24 hours (**Figure 3.1d**). The size of parasites was not significantly different between sexes at 44 hours, suggesting growth was unaffected by sex (**Figure 3.1e**). Interestingly, parasite size was significantly higher in males at the 24-hour timepoint, indicating that rate or initiation of replication might differ initially, but other factors influence schizont size at 44 hours. Taken together, this data suggests that higher liver burden at 44 hours in males is related to survival, rather that differences in susceptibility to infection or parasite replication capacity.

Androgen-linked variation in *Plasmodium* parasite survival

Previous data has implicated androgens in modifying liver-stage vaccination outcomes[116]. We therefore sought to evaluate whether androgens in males contribute to higher liver burden at 44 hours. To evaluate whether androgens in males contributed to susceptibility or survival of infection, we removed the gonads in adult male mice at least 14 days prior to challenge and then later quantified liver burden at 12, 24, and 44 hours post-spz challenge by *Plasmodium* 18S rRNA RT-PCR (**Figure 3.1a)**. Orchiectomy (ORX) is a common method for removing testicular hormones, and is frequently applied to reduce androgen levels in murine systems[249]. For males,

ORX led to higher liver burden in male mice at 44 hpi (**Figure 3.1b**). Also similar to previous data, no significant difference in 18S rRNA parasite burden at 12 and 24 hpi between intact and ORX male mice was observed (**Figure 3.1b**). We further identified that ORX male mice maintained more infected hepatocytes at 44 hours compared to intact counterparts, with ORX male mice having a similar number to that of female mice (**Figure 3.1d**).

To further confirm the confirm that testosterone increased parasite survival, we developed an acute and reversible model to suppress testosterone production in male mice. Acyline is a gonadotropin releasing hormone (GnRH) antagonist that suppresses downstream production of testosterone in a dose-dependent manner and has previously been applied in mice[250], and humans[251,252]. We depleted testosterone prior to infection with *P. yoelli* and measured liver burden via 18S RT-qPCR at 44 hpi. We found reducing testosterone (**Supplemental Figure 3.7a**) was sufficient to increase liver burden outcomes in male mice (**Supplemental Figure 3.7c**). To further confirm that testosterone during infection changes liver burden at 44 hpi, we added back testosterone and once again saw a reduced 18S rRNA levels in androgen treated groups compared to Acyline treated group (testosterone depleted) (**Supplemental Figure 3.7c**)**.** Together, these findings lead us to conclude that testosterone during liver infection is a significant factor influencing the survival of parasites during the liver stage.

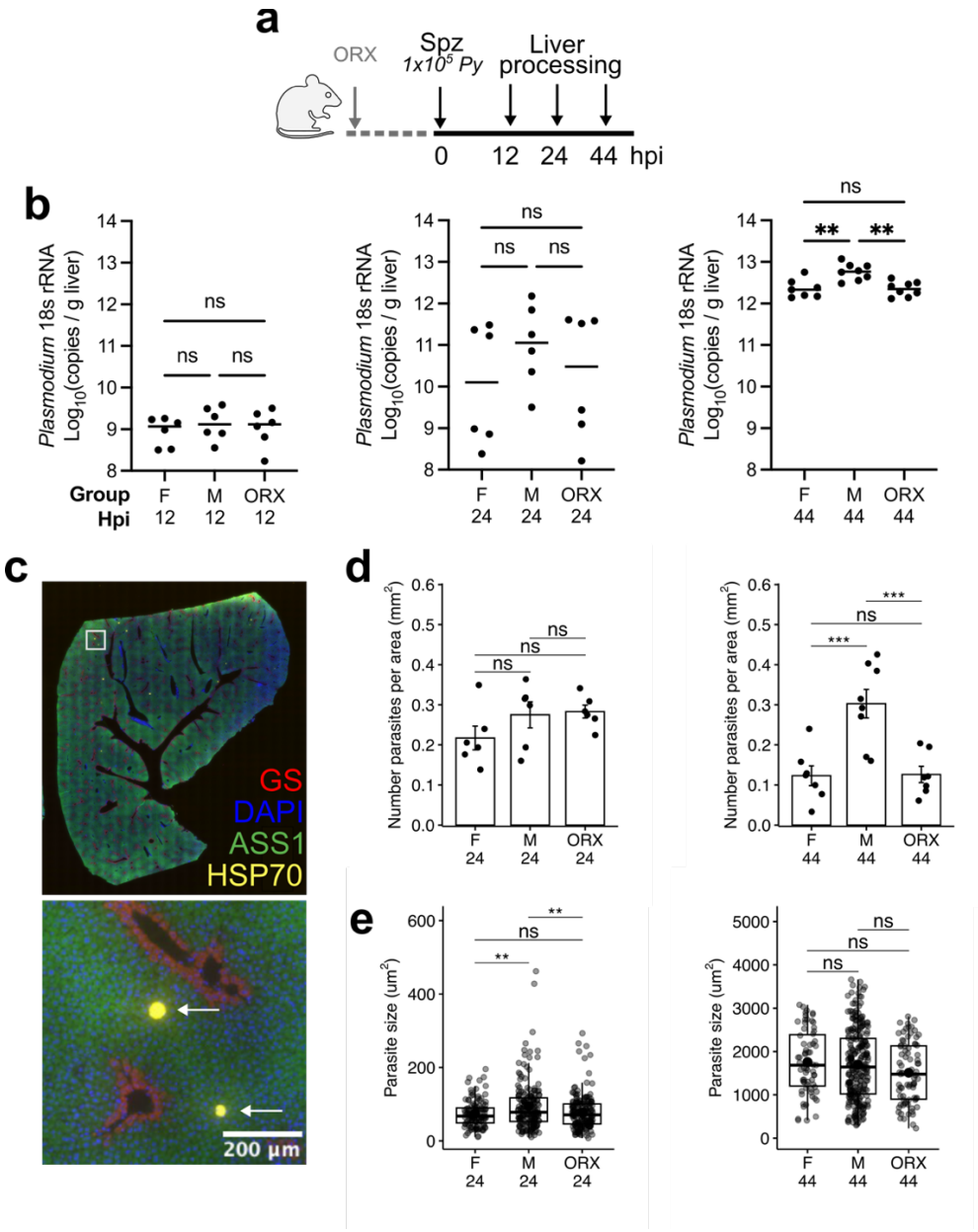

Figure 3.1: Sex bias in survival of *Plasmodium yoelli* infection in BALB/cJ mice. a. Schematic of male, female, and orchiectomized (ORX) male BALB/cJ mice infected with 1x10^5 *Py*-WT spz intravenously (IV) and harvested at 12, 24, and 44 hours post infection (hpi). b. Livers were excised for absolute pan-*Plasmodium* 18S rRNA quantification at 12 hpi (left), 24hpi (middle) and 44hpi (right); c. Liver stage parasites were visualized by fluorescence microscopy with HSP70 in yellow, DAPI shown in blue, ASS1 (zonal marker) in green, and GS (zonal marker) in red. d. Density of liver stage in tissue quantified by microscopic counting at 24hpi (left) and 44hpi (right). e. The size of each parasite was quantified in each sample with fluorescence microscopy at 24hpi (left) and 44hpi (right). Data are shown from two independent experiments (n= 6-8). Statistical significance for data was determined by One-way ANOVA with Tukey multiple comparison. Error bar represents mean ± s.e.m; box plot depicts median with interquartile range. ***p<0.001, **p<0.01, *p<0.05, ns p≥0.05.

Spatial transcriptomics captures sex-specific responses induced by *Plasmodium* parasite infection

To interrogate the impact of sex and sex hormones on host response to *Plasmodium* infection, we performed GeoMX spatial genome-wide transcriptomic profiling on *P. yoelli*-infected BALB/cj mouse liver tissue. Adult intact male, female and ORX male mice were intravenously infected with 3 x10^5 *Py* sporozoites or mock injected. The comparison with mock-infected sections enabled us to evaluate the baseline contributions of biological sex in this mouse model. At 44 hpi, 18 liver sections from the left lateral lobe were collected and prepared for digital spatial profiling with GeoMX.

The design of GeoMX is to capture transcripts in tissue regions, which we employed to capture regions of interest (ROIs). These ROIs were selected based on staining with fluorescent microscopy with three markers, one for *Plasmodium* parasites (HSP70 -cytosolic marker), one for liver zonation (ASS1 – periportal marker), and one nuclear stain (SYTO83). ROIs were selected from infected and mock infected mice. Within the infected mice, two additional ROIs were collected to evaluate both direct and indirect effects of *Plasmodium* on liver-stage outcomes: one surrounding the parasites and another distant from parasites (bystander, without encircling parasites). (**Figure 3.2a**). As zonal location (Periportal (PP), Interzonal (IZ), and Pericentral (PC)) is known to influence the host response to infection[136,150], we selected at least 3 ROIs per mouse per zone per infection type. We confirmed clear zonated expression were exhibited by pre-annotated ROIs (**Supplemental Figure 3.8**). This was evidenced from the mutually exclusive expression of the pericentrally zonated hepatocyte gene *Cyp2e1* and *Glul* and the periportally zonated gene *Cyp2f2* (**Supplemental Figure 3.8a**). We further confirmed with

differential gene expression analysis that these genes were differentially expressed between Periportal and Pericentral regions (**Supplemental Figure 3.8b**). Cell proportion analysis also accurately predicted the pericentral and periportal regions, though the interzonal (midlobular) region was more unclear (**Supplemental Figure 3.8c**). Gene-set enrichment analysis also found that within the PP region, primary bile acid biosynthesis was upregulated, in part due to the proximity of the bile duct to the portal vein (**Supplemental Figure 3.8d**).

First, we performed unsupervised clustering analysis to identify overall trends in the data. We identified 5 clusters (0-4) (**Figure 3.2b**). Many of these clusters represented the hormone status of the mouse, with intact males (Cluster 0) differentiating from females (Clusters 1, 3, 4) and ORX males (Clusters 1, 2, 4) regardless of infection status (**Figure 3.2c**). Clusters associated with Females and ORX males clearly differentiate on infection status (Cluster 4 – uninfected; Cluster 0,2, and 3 – infected). We found genes enriched in these clusters are connected to the cytochrome P450 superfamily, fatty acid metabolism, and hormone biosynthesis (**Figure 3.2d**). In contrast, the clusters associated with intact males did not separate out by infection status (Cluster 0). Liver zone did not drive cluster expression at this resolution. With these clusters defined, we next conducted a supervised analysis to further investigate the impact of biological sex on gene expression outcomes.

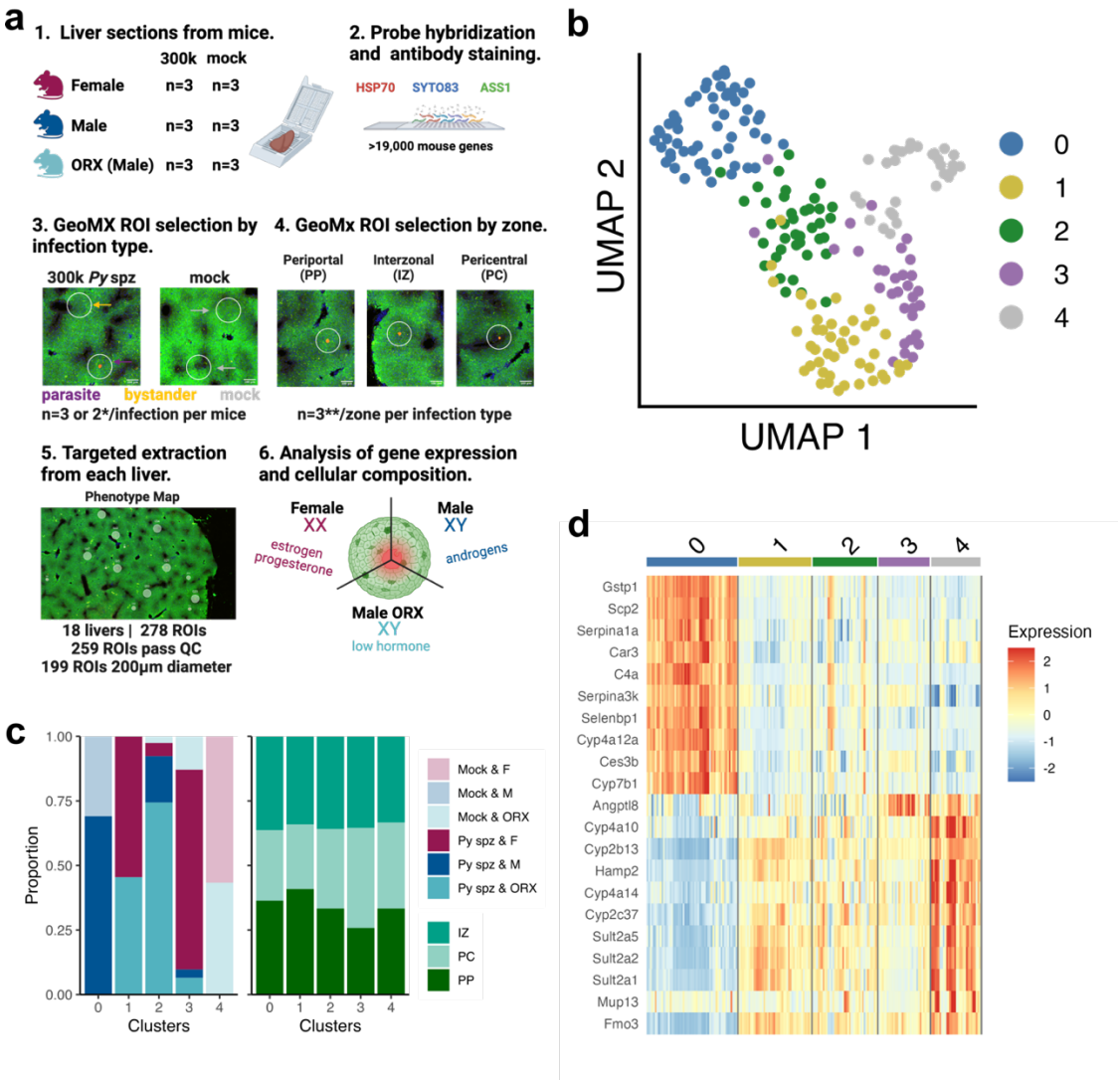

Figure 3.2: Digital spatial profiling facilitates evaluation of transcriptomes in *Plasmodium yoelii* infected tissues. a. The workflow to evaluate fixed liver samples from BALB/sJ mice infected with *Py* sporozoites. 1) Biopsies from 18 mice were fixed and assembled to evaluate mice challenged with 300k *Py* spz IV (3 per group) or mock infected (3 per group) in three groups, adult female, male, and ORX male mice. 2) Liver section was stained with anti-ASS1, anti-SYTO83, and anti-HSP70 to visualize the liver zone and the presence of *Plasmodium* parasite and then hybridized with a >19,000 RNA probe panel targeting mouse genes for GeoMX assay. 3 - 4) Region of interests (ROIs) were selected based on the infection status of the mouse and the zonal location of the parasite. To ensure representation from each zone, at least 3 ROI were selected per infection type (bystander, parasite, mock) and per liver zone (PC, IZ, PP). 5) Targeted extraction of whole transcriptomes within each region that enables differentiation of targeted mouse groups. 6) Computationally dissect the key differences underlying response to infection by biological sex and hormone status. b. After dimensionality reduction, the normalized and batch-corrected data were embedded in Uniform manifold approximation and projection (UMAP) space and colored by clusters identified through unsupervised clustering. c. Proportion of spots of original conditions (Infection status, sex and hormone status, and zonal location) across all identified clusters from analysis. Original conditions are indicated by color. d. Heat map for top marker genes per cluster. *Py spz samples had 3 ROIs per infection type and mock samples each had 2. **Up to 3 zones if enough parasites were present at time of collection.

Sex-bias in gene expression and cell composition in the liver at steady state

To further evaluate how sex and sex hormones impact the liver at steady state, we then overlaid phenotypic information of all ROIs collected. Globally, male mice clearly differentiate from female and ORX male mice with mutually exclusive expression of *Cyp7b1*, a cytochrome p450 family gene that is known to be regulated by biological sex in the murine liver[253]. Female and ORX male mice also differentiate from intact male mice with higher expression of *Cyp2b13,* a gene connected to lipid and fatty acid metabolism[254](**Figure 3.3a**). Thus, we were able to capture known differences in gene expression by biological sex and hormone status[74,253,255], and identified that androgen presence better differentiated clusters than biological sex.

Next, to identify differentially expressed genes, we performed pairwise comparisons between all intact males and females and intact males and ORX males, while accounting for covariates of infection, and liver zone. We found most genes differentially expressed between females and intact males were also differentially expressed between ORX and intact males (**Figure 3.3b, Supplemental Figure 3.9**). Up regulated genes in females and ORX males are linked to fatty acid metabolism (e.g. *Acot3*, *Hao2*) and xenobiotic metabolism (e.g. *Fmo3* and *Gstp1*). Up regulated genes in males were linked to bile acid metabolism (e.g. *Cyp7b1*, *Scp2*) complement and coagulation cascades (e.g. *C4a, C9*) (**Figure 3.3c**) corroborating previously identified sex-biased pathways[256].

Thirdly, since GeoMX does not provide data at the individual cell level, we leveraged single-cell RNAseq data set from livers of C57BL/6 mice infected with *P. berghei* published by Hildebrandt et al[150]. This dataset defined liver cell populations based their differential gene expression

patterns, which we deconvoluted[247,257] and used to estimate cell type proportions across the tissue in spatial gene expression data. We focused on mock-infected groups to define cellular composition by sex in the liver at baseline/steady state (**Figure 3.3d**). Comparing the proportions of 14 annotated cell types, we found that within our selected ROIs, hepatocytes comprised 20 – 40% (and remaining cells type comprised 60 – 80%) within the mock infected samples (**Supplemental Figure 3.10**). We note this was different than Hildebrandt et al., likely due to differences in sequencing platform because we uniquely targeted ROIs in immune rich regions. Four immune cell categories were captured with this method, KCs, monocytes and DCs, T and NK cells, and B cells. Analysis of cell proportions revealed that females and ORX males have higher levels of KCs, monocytes and DCs, and T and NK cells compared to intact males. Thus, this analysis revealed similar sex-biased differences in baseline immune cell proportions in tissues as previously identified in rodent models[246,258].

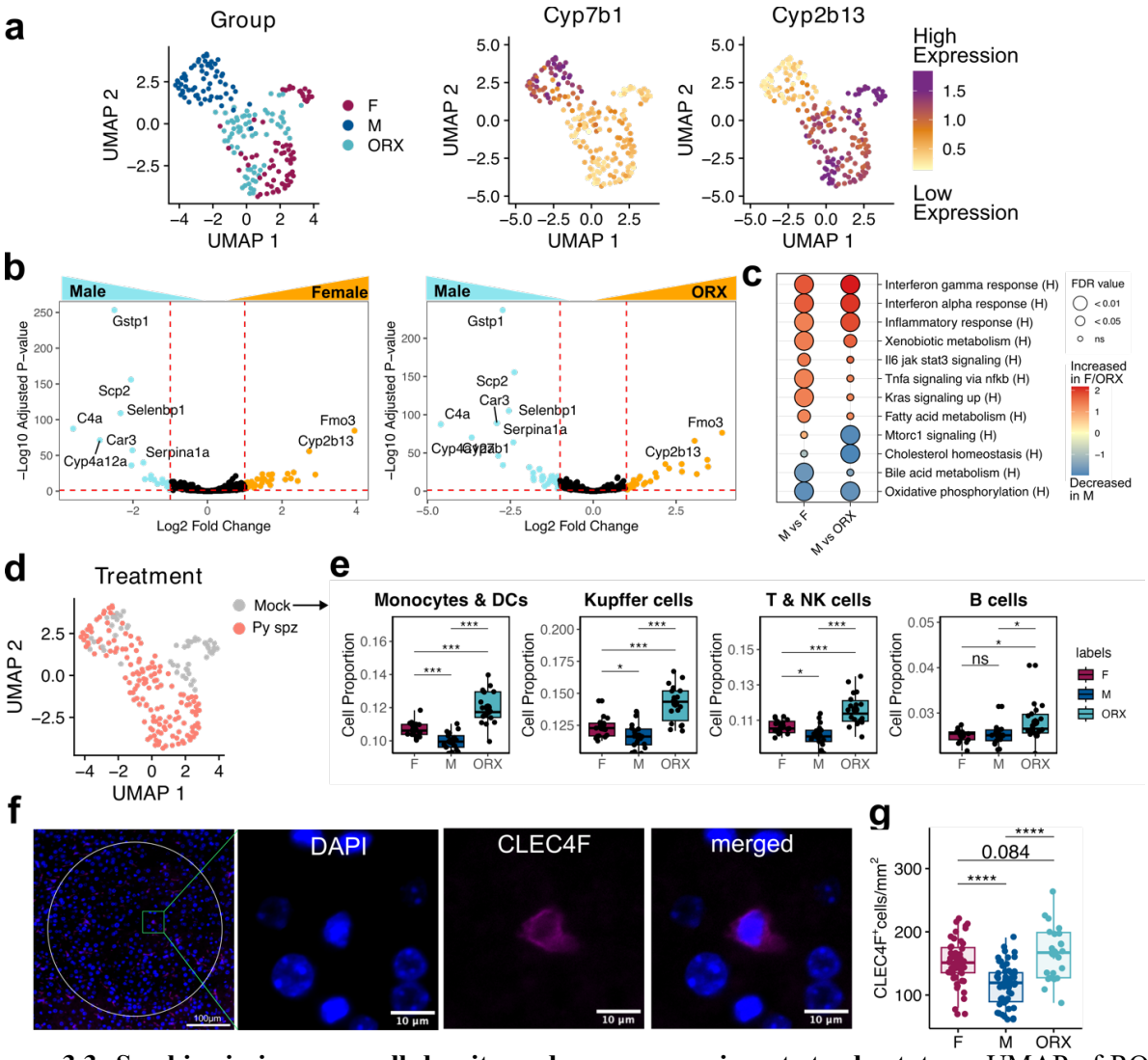

Figure 3.3: Sex bias in immune cell density and gene expression at steady state. a. UMAP of ROIs, colored by biological sex and hormone status (left), and by expression of the male-biased genes *Cyp7b1* and androgen-naïve biased-gene *Cyp2b13*. b. Volcano plot showing differentially expressed genes conserved across all females and males (left) and orchiectomized males and intact males (right). The y-axis shows the $\log_{10}$ of the adjusted p value (Bonferroni corrected). The x-axis shows the $\log_2$ fold change relative to all males. Gene significantly increased or decreased in ROIs are plotted in orange or blue, respectively (false discovery rate (FDR) p-value< 0.05 and Log_2Fold Change +/- 1). Gene symbols are shown for selected genes. c. Gene set enrichment analysis (GSEA) shows pathways differentially regulated between Females and Males, and ORX Males and Males. H, Hallmark gene sets. d. UMAP of ROIs, colored by infection status. d. Immune cell type proportions calculated with BayesPrism method for each ROI in mock-infected mice, separated by biological sex and hormone status. e. An independent Wilcoxon test was used to compare the mean cell type proportions between female, male, and ORX male samples, and the resulting p values are shown. f. Representative image of CLEC4F$^+$ staining within a mock-infected liver. Tissue Nuclear DAPI staining is shown in blue, CLEC4F (Kupffer cell marker) in red. Ring captures a 200um diameter randomly selected within a mock-infected tissue. 10 ROI sets were counted for each of the mice. g. Number of CELC4F$^+$ cells normalized by area of ring in infected and uninfected tissue at 44hpi (Two independent replicates, n = 5 – 8; up to 10 circles per mouse). One-way ANOVA with Tukey multiple comparison was applied for g. box plot depicts median with interquartile range. ***p <0.001, **p<0.01, *p<0.05, ns p>0.05.

To confirm the finding that females and ORX males have higher density of KCs compared to males in mock-infected tissues, we used fluorescent microscopy and quantified KCs with a CLEC4F marker (**Figure 3.3f**). We found that females and ORX males have higher baseline levels of CLEC4F+ cells compared to the males (**Figure 3.3g**). Overall, this suggests that differences in baseline gene expression and immune cell composition between intact male and female mice are strongly influenced by androgen status, establishing a distinct metabolic and immune homeostatic state.

Biological sex does not impact *P. yoelli* liver zonal patterns

Next, we explored if biological sex and hormone status modified gene expression patterns by liver zone. Previous studies have identified sex-biased gene expression patterns by liver zones[74,259]. Thus, we investigated if including liver zone as an interaction term was able to identify differentially boosted genes by biological sex and hormone status (**Supplemental Figure 3.11a**). Three genes were identified to be modified by biological sex and hormone status and down regulated between PC and PP region, *Csad, Cyp2c29,* and *Cyp2a4* (**Supplemental Figure 3.11b**). While previous single-cell studies have shown that biological sex can influence liver zone-specific gene expression, the non-single-cell resolution of the GeoMX platform may have diluted this signal, potentially preventing us from detecting the effect if it exists.

While we did not identify gene expression differences based on zonal location, we had yet to evaluate potential sex differences in zonal patterns in infection rates. We quantified the location of parasites in the liver in a separate set of validation mice that were infected with 1 x10^5 *Py* IV and harvested 44 hpi (**Supplemental Figure 3.12a**). Here, zonation was determined with the

markers Hsp70, Ass1 (periportal marker), and GS (pericentral marker) (**Supplemental Figure 3.12b**). Across all samples, regardless of biological sex and hormone status, there were more periportally located schizonts than pericentral (**Supplemental Figure 3.12c**). A slight difference in localization was observed between intact and ORX male mice and female mice, though no detectable difference was observed for the PC region. Additionally, quantification of parasite size was not significantly different regardless of the location of the parasite (**Supplemental Figure 3.12c**). This indicates that the relative contribution of liver zonation is minimal on the basis of sex and hormone status, though if anything there might be some skew towards parasites in female mice being more concentrated in the PP relative to the IZ region**.**

P. yoelli infection impacts both proximal and bystander immune responses

We next sought to confirm that genes expected to respond to rodent malaria infection were indeed induced. Upon visual inspection, cluster analysis was unable to differentiate gene expression patterns between ROIs selected around parasites or around peripheral bystander regions on the same tissue (**Supplemental Figure 3.13a**). We further confirmed that few significant differences were found in immune cell proportions between parasite and bystander regions (**Supplemental Figure 3.13b**). This observation of global gene expression instead of distinct spatial effect has been observed previously[150]. Thus, for differential gene expression analysis, we focused on identifying the uniquely expressed genes between *P. yoelii* parasites and mock ROIs, and excluded bystander selected ROIs from further analysis.

We further aimed to connect the observed patterns of immune cell enrichment in infected liver tissues with the data disaggregated by infection status only. Kupffer cells and monocytes and DCs were significantly induced between mock infected samples and parasites, confirming

previously identified trends in immune cell recruitment in the liver during *Plasmodium* infection (**Supplemental Figure 3.13c**). Interestingly, we also found a potential downregulation of B cells and fibroblasts in infected tissue compared to mock injected samples (**Supplemental Figure 3.13c**). This suggests that our assay was able to capture known fluctuations in the liver cell proportions during *Plasmodium* infection[156].

Biological sex impacts inflammatory response to *P. yoelii* infection

After establishing that biological sex and androgens alter innate immune cells and gene expression patterns at baseline, we next aimed to evaluate whether these effects extend to influencing the host response to *P. yoelii* infection. We conducted pairwise comparisons between parasite and mock ROIs for each female, male, and male ORX mice (**Figure 3.4a**). Differential gene expression analysis found that regardless of zonal location, IFNα responses were upregulated in females, males, and ORX males. Gene enrichment analysis conducted separately for females, males and ORX males confirmed inductions of pathways previously identified as induced in response to *P. berghei* in female C57BL/6 mice[136]. For example, all groups demonstrated an upregulation of response to type I IFNs and antigen processing and both females and males showed downregulation of metabolism of fatty acids and bile acid in response to parasite infection (**Figure 3.4b**).

Further investigation of the specific genes differentially induced between groups revealed a restricted inflammatory response within intact male mice. Overall, fewer genes were differentially induced in males, compared to female and ORX males (**Figure 3.4c**). While all groups demonstrated an upregulation of genes associated with cellular stress response (*Saa1, Saa2, Orm2*), we found a significantly restricted interferon response in intact male mice

compared to female and ORX male counterparts (**Figure 3.4d**). Upregulated genes at 44 hpi that were shared between female and ORX male mice, but not intact male mice, were linked to cellular stress responses and inflammation (e.g. *Saa3*, *Cxcl9*) and type I IFN response (e.g. *Irf7, Tgtp1, Gbp6, Ly6e*) (**Figure 3.4e**, **Supplemental Table 3.3**). Females exhibited an even stronger interferon response at 44 hpi compared ORX males and intact males (**Figure 3.4d**). Many differentially expressed genes in females were interferon stimulated genes (ISGs), including transcription of *Cxcl10, Isg15, Bst2,* and *Ifitm3* and ISGs connected to autophagy*,* including *Igtp, Gbp2, Irmg1, Irmg2,* and *Ifi47* (**Figure 3.4e**, **Supplemental Table 3.3**). Thus, females and ORX mice both mount more robust inflammatory responses compared to intact male counterparts.

Biological sex impacts other key pathways in response to *P. yoelii* infection

Gene enrichment analysis further revealed pathways associated with antigen processing and presentation were uniquely produced withing female mice. Upon further inspection, however, we identified a coordinated set of expression of genes connected to antigen presentation via MHC class II (*Cd74, H2-Eb1, H2-Ea),* MHC class I (*H2-D1, Tap1*) (**Figure 3.4f**)*.* Additionally, *Mpeg1,* macrophage-expressed gene1, which is a pore-forming protein that plays a central role in antigen cross-presentation in DC[260,261], which is an important process for priming CD8 T cells in the liver[179]. Further evaluation identifies a trend toward significance with ORX mice, but not male mice, possibly indicating either reduced activity by DCs and monocytes or higher recruitment of these antigen presenting cells (APCs).

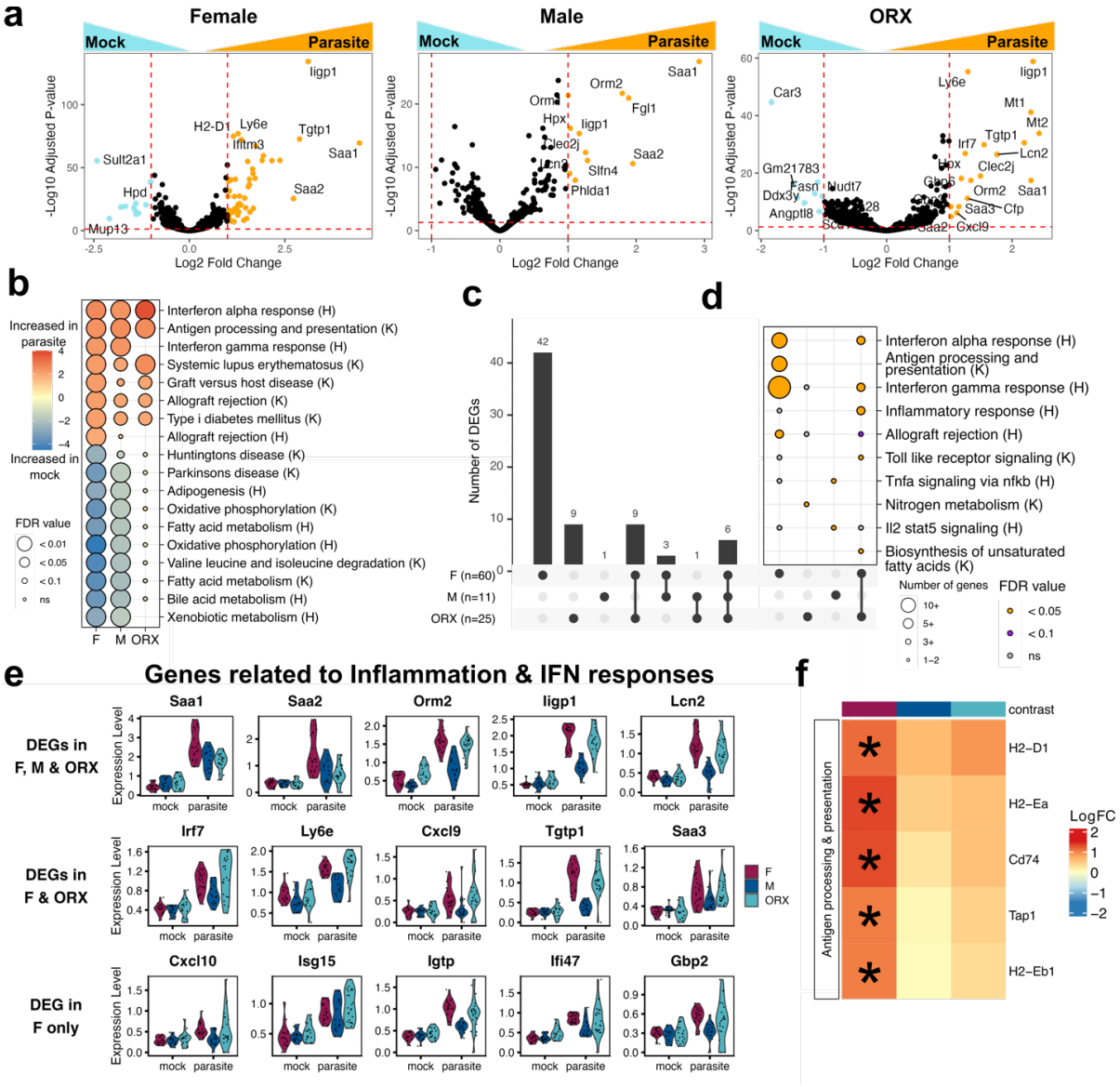

Figure 3.4: Inflammatory response to *P. yoelli* infection is influenced by sex and hormone status. a. Volcano plot showing differentially expressed genes between parasite and mock in females, males, and ORX males evaluated. The y-axis shows the $\log_{10}$ of the adjusted p value (Bonferonni corrected). The x-axis shows the $\log_2$ fold change relative to mock samples of each respective sex. Genes significantly increased or decreased in ROIs are plotted in orange or blue, respectively (false discovery rate (FDR) p-value < 0.05 and Log_2Fold Change +/- 1). Gene symbols are shown for selected genes. b. Gene set enrichment analysis (GSEA) shows pathways differentially regulated between parasite and mock for F, M, and ORX male mice. H, Hallmark gene sets; K, KEGG gene sets. c. Upset plot of genes shared between groups and in response to infection (FDR < 0.05 and Log_2Fold Change +/- 1). d. Gene enrichment analysis of genes unique to males, females, ORX males, and shared between ORX and F mice portray in upset plot (highlighted in yellow). e. Violin plots of expression levels of selected genes shared between F, M, and ORX males, between F & ORX alone, and F only. f. Heatmap of antigen processing and presentation related genes significantly induced within female mice in response to parasite infection. Fold change relative to mock of respective contrast (F, M, ORX) is depicted and * denotes a FDR< 0.05 and Log_2Fold Change +/- 1. Red marks marks upregulations and blue marks downregulation.

Genes associated with iron homeostasis were also differentially induced in response to *Plasmodium* infection between sexes. *Plasmodium* parasites are known to shift iron flux during hepatocyte invasion[147]. *Lsn2* was specifically increased within female and ORX male mice, which is constituently expressed by neutrophils mostly and is responsible for iron-trafficking from the cell. In contrast, *Hamp2,* hepcidin-2, which exports iron efflux into plasma, was specifically downregulated in female mice, which could be connected to low iron levels. Interestingly, *Scd1, G6pc,* and *Fasn,* genes involved in fatty acid metabolism, were reduced within ORX male mice, but not female and male mice. This may either indicate a potential regulatory role of ovarian hormones in fatty acid metabolism that drives a shift[262], or technical variability introduced by ORX surgery.

Biological sex impacts Kupffer cell and other immune cell responses in liver tissue

Finally, we sought to evaluate the impact of biological sex on immune cell proportions around parasites in infected tissues. We again used the single-cell RNAseq data set by Hildebrandt et al[150] to deconvolve the spatial gene expression data to estimate cell type proportion across the tissue. For this analysis, we compared immune cells between female, male and ORX male mice in the 200μm radius region around a parasite. We found female mice were enriched for Kupffer cells and monocytes & DCs (**Figure 3.5a**). However, we did not identify a significant difference in these immune cell densities between males and ORX males.

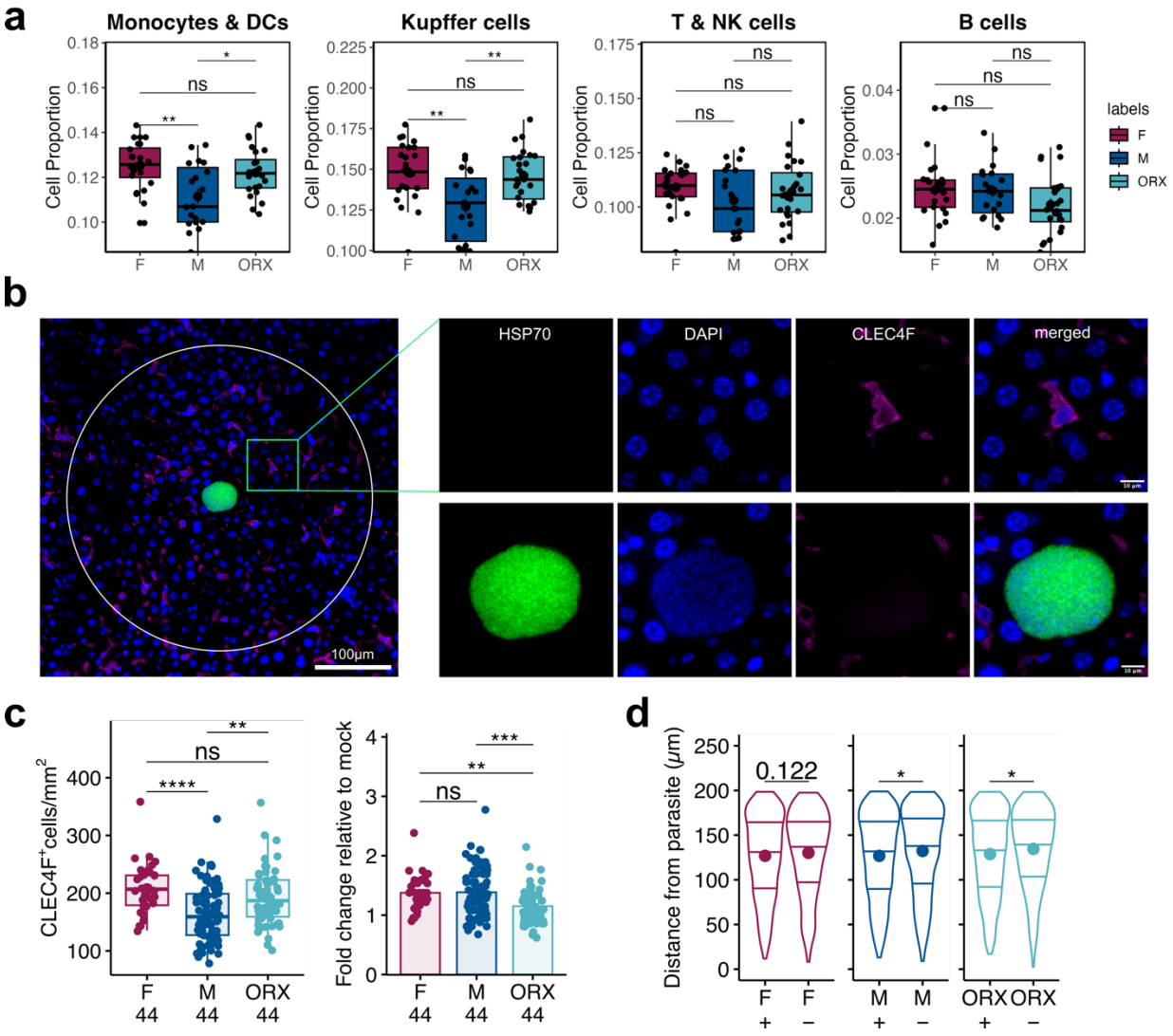

Figure 3.5: Microscopy and digital spatial profiling reveal baseline differences by sex skew enrichment of Kupffer cells and other innate immune cells. a. Immune cell type proportions for each ROI in *Py* parasite-infected mice, separated by biological sex and hormone status. An independent Wilcoxon test was used to compare the mean cell type proportions between female, male, and ORX male samples, and the resulting p values are shown. b. Representative image of CLEC4F^{+} staining within an infected liver. Nuclear DAPI staining is shown in blue, CLEC4F in red, and HSP70 staining in green. White ring portrays outer boundary of a 200µm radius. Additional CLEC4F staining of a single cell within the ring and representative image of a CLEC4F cell in close proximity to a parasite at 44hpi. c. Number of CELC4F^{+} cells normalized by area of ring in infected and uninfected tissue (left) and fold change of CLEC4F cells relative to respective mock-infected samples (right) at 44hpi. d. Calculated distance of CLEC4F^{+} cell from center of parasite. 5-10 ROI sets were counted for each of the mice. Data for c-d are shown from two independent experiments (n= 7 – 8; up to 10 circles per mouse). One-way ANOVA with Tukey multiple comparison was applied for c; unpaired t-test was applied to d. Error bar represents mean ± s.e.m; box plot depicts median with interquartile range. ***p<0.001, **p<0.01, *p<0.05, ns p>0.05.

To confirm the finding that females have higher density of KCs compared to males in infected tissues, we used fluorescent microscopy and quantified KC with a CLEC4F marker in a separate set of mice infected with 1x 10^5 *Py* sporozoites (**Figure 3.5b**). We further found that following infection, females and ORX males retain this increased density, while all groups increase overall density above mock-infected (**Figure 3.5c-d**). To determine if there was a difference in the magnitude of response between males and females, we calculated the fold difference relative to the mock infected samples of the respective sex. Interestingly, there was no significant difference in fold change between male and females nor in distance of KC from parasite (**Figure 3.5c**). This data overall indicates that sex difference in KC recruitment at 44 hpi is related to innate difference in baseline cell densities rather than an intrinsic activity difference between recruitment of KC toward site of infection.

Sex differences in *Plasmodium berghei* liver infection

To test the generalizability of these findings to other mouse models, we tested if we observed a sex difference in liver burden with *Plasmodium berghei,* a more inflammatory parasite. We used the established model in which adult male and female C57BL/6 mice were infected with 0.5 x10^5 *P. berghei* sporozoite intravenously. Forty-four hours post infection, the liver was isolated for quantification of a *Plasmodium* parasite RNA by 18S RT-qPCR as a surrogate for liver burden (**Figure 3.6a**). Interestingly, at 44 hpi, we did not detect a sex-specific difference in liver burden at this later timepoint (**Figure 3.6b**), indicating that the baseline factors driving set differences in *P. berghei* mice are not observed with *P. yoelli.*

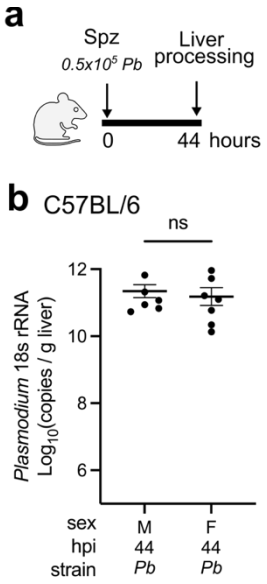

Figure 3.6: Sex bias in susceptibility to *Plasmodium berghei* infection in mice. a. Scheme of male and female C57BL/6 mice infected with $0.5x10^5$ Pb-WT intravenously (IV) and harvested at 44 hours post infection (hpi). b. Livers were excised for absolute pan-*Plasmodium* 18S rRNA copy numbers at 44 hpi. Data are shown from two independent experiments (n= 6). P-value with unpaired t-test ns $p>0.05$. mean ± s.e.m.

3.5 DISCUSSION

In this study, we investigated how biological sex and androgens influence host-parasite interactions during *Plasmodium yoelii* liver stage infection. We discovered that both biological sex and androgen levels significantly affect parasite survival. There is a notable difference in immune cell composition between females and ORX (castrated) males compared to intact males at baseline, with male mice having a reduced density of Kupffer cells (KCs) and other monocytes, and dendritic cells compared to female and ORX mice. We further show these baseline disparities were amplified during *Plasmodium* infection, as intact male mice exhibited impaired KC, monocyte, and DC recruitment and antigen presentation activity at 44 hours post infection. We further identify a robust, androgen-mediated Type I IFN response in females and ORX males, that is deficient in intact males. Yet, despite the impaired inflammatory response in males, the magnitude of KC recruitment was similar between males and females/ORX males. Thus, we conclude that a key driver of sex-specific differences in survival of parasites is likely linked to intrinsic difference in innate immune cell density between male and female mice, which is mediated by the presence of androgens.

Prior research in murine malaria models has aimed to unravel host-parasite interactions during the *Plasmodium* liver stage to guide liver-targeting interventions. Next-generation sequencing technologies have been used to map the spatial and single-cell host responses to *P. berghei* infection in female mice, revealing heterogeneity in host response to infection within liver tissue[136,150,156]. However, these studies overlook the impact of biological sex. As a sexually dimorphic organ, the liver's transcriptional patterns differ by sex in both mice[71,74,241] and humans[72,75]. By employing DSP with GeoMX on male, female, and castrated (ORX) male mice, here we were able to address this gap in the literature. In doing so, we uncover sex- and androgen-specific transcriptional programs that influence host metabolic processes, innate and adaptive immune responses, and localized inflammatory responses to *Plasmodium* liver stage infection.

We identified a difference in parasite survival by sex and sex hormone environment. Three possible mechanisms could explain this enhanced clearance in females and ORX male livers: (1) higher rates of innate immune cell recruitment and direct immune-cell clearing of infected hepatocytes, (2) increased cell-autonomous abortive pathways within infected hepatocytes, or (3) reduced metabolic sequestration and nutrient uptake by the parasite, limiting development and leading to clearance. Prior research has shown that innate immune responses in the liver play a crucial role in controlling *Plasmodium* infection[111,152,263,264]. Interferons (IFNs) are key regulators of these immune defenses[265]. Here, we demonstrate that while male mice produce a Type I IFN response during infection, it is significantly reduced in magnitude compared to female mice. Specifically, we were unable to identify a meaningful induction in males of some key genes important for potential T cell priming and propagation of further innate immune activation (e.g.

Irf7, Cxcl9, Cxcl10). Due to the non-single cell resolution of this dataset, we are unable to attribute this response to hepatocytes or innate immune cells. Regardless, a productive Type I IFN response in male mice is lacking, and this is modified by the presence of androgens. This finding parallels the known anti-inflammatory impact of androgens in other liver diseases[159,266,267].

Additionally, Type I IFNs, whether produced by hepatocytes or early innate immune responders, facilitate the recruitment of professional immune cells to the liver, where they can directly target infected hepatocytes[111]. Here we show recruitment of KCs, monocytes, and DCs toward infected tissues, confirming previously identified trends in innate immune cell recruitment around parasites[150,156]. Interestingly, we found similar immune cell proportions between parasites and bystander regions of infected mice, suggesting that immune cells may be uniformly distributed across the tissue. While activation was evident across all groups, males exhibited a lower total number of KCs near parasites compared to females and ORX males. This reduced KC density was also observed at baseline, where males consistently maintained fewer KCs than females and ORX males under steady-state conditions. Further evaluation of fold change between mock-infected samples and *P. yoelli* infected samples found that magnitude of KC recruitment is similar between sexes. We speculate that the stronger Type I IFN response in females and ORX males did not increase immune recruitment, but rather reflected a higher baseline density of KCs and monocytes/DCs surrounding infected hepatocytes that cascade to higher activation during infection. Furthermore, these APCs also likely have higher overall activity as linked to higher expression of genes associated with antigen processing (*Mpeg1* and *Tap1*). While further work would need to be executed to couple IFN response to cell source and direct hepatocyte clearance,

these data alone underscore the pivotal role of baseline cellular composition in shaping innate immune responses.

Alternatively, sex-specific and androgen-regulated cell-autonomous clearance within hepatocytes could be responsible for the difference in survival of infected hepatocytes between males and females. Abortive hepatocytes undergo a cell-autonomous abortive pathway that clears infection outcomes within itself[268–270]. Here we measured a more abortive-like gene expression profile in the infected tissue of female and ORX males, compared to intact males. *Cxcl10* and *Tgtp1* are both genes that are significantly reduced in males compared to females and have previously been connected to a more abortive-like profile[136]. Although the detected and measured parasites have evaded this process, we speculate that the increased abortive-like properties, tied to heightened inflammation, may contribute to greater infection clearance at earlier timepoints not captured in this analysis.

Previous studies have speculated a potential role for metabolism of lipid and fatty acid in facilitating *Plasmodium* liver stage development[150]. We also identified differences in baseline gene expression of lipid and fatty acid metabolism pathways, corroborating known sex-specific pathways between males and females. Previous studies in female mice found higher expression of genes involved in lipid metabolism close to the parasites, which in effect bring in an anti-inflammatory bubble around parasites that limits immune cell activity at the site of infection[150]. We were unable to detect a significant induction of lipid metabolism with GeoMX resolution, so we were able to answer this question, and further work should be done at increased resolution to identify a potential effect of metabolism on parasite survival. Further analysis, however, found a potential sex-specific effect on iron homeostasis. *Hamp2* and *Lcn2*, genes connected to iron flux

in hepatocytes[271,272], are not differentially induced in male mice. Other genes involved in metabolism in the liver were identified. One set of genes were *G6pc*, a Glucose-6-phosphate, and *Sult2a1*, a sulfotransferase known to metabolism DHEA to DHEA-S in the liver[273]. The liver is the main site of conversion of DHEA to its secretory form DHEA-S, and this conversion seems to be down regulated in response to *Plasmodium* infection[274]. Overall, this points to that female mouse and ORX mice are more metabolically plastic, which results in higher clearance of parasites and more robust anti-evasion mechanisms.

Thus, in our proposed model, the malaria parasite is better able to evade the innate immune mechanisms in males due to their lower immune cell density at steady state and restricted inflammatory response during infection. Likely, the intrinsic evasion mechanisms employed by the parasite are better suited to a testosterone-rich liver environment where anti-inflammatory mechanisms limit activation of genes associated with cell-autonomous clearance mechanisms. We did not observe that biological sex influenced zonal genes expression, however, we found that the resolution in which we conducted the GeoMX assay was not suited to capture these nuanced gene expression perturbations. Future investigations into the impact of biological sex on the *Plasmodium* liver stage should further deconvolute the impact of the microbiome, which is known to interact with the endocrine axis[275]. Further work will need to be undertaken to fully characterize the impact of biological sex and zone at earlier timepoints. Additionally, tandem measurement of parasite transcriptome in response to the sexually dimorphic liver would give insight into more sex-specific host-parasite interactions.

In conclusion, this study provides a comprehensive spatial transcriptomic analysis of host-parasite interactions during *Plasmodium* development within the sexually dimorphic liver.

Effective malaria eradication efforts depend on capturing the true heterogeneity of the human population. Thus, those engaged in generation of tissue-specific atlases might consider the intrinsic impact of biological sex and hormone environment on shifting immune responses to *Plasmodium* infection to design more inclusive interventions. Indeed, work by our lab has identified a significant sex-specific difference in protection from liver-stage vaccination (**Chapter 4**). Building on these findings, future research will aim to explore how results from rodent models translate to larger animal models, and determine how biological sex as a variable can be best considered in the development of interventions targeting malaria parasite liver stage.

3.6 ACKNOWLEDGMENTS

I would like to thank the co-authors on this manuscript: Alen Poleman, Ethan N. Conrad, Nilasha Sen, Aaron Ayenew, Becca Blyn, GW McElfresh, Elizabeth Glennon, Kenneth Boey, Anya C. Kalata, Alexis Kaushansky, Nana Minkah, Melanie J. Shears, and Sean C. Murphy.

We thank Brendy Fountaine and Marina Ivanova at the Histology and Imaging Center Support for support with histology preparation. We thank Dr. Emily Beirne and Dr. Ram Akilesh from the Department of Laboratory Medicine and Pathology (DLMP) Spatial Biology Core facility for technical assistance and execution of NanoString GeoMx Digital Spatial Profiler. We thank Cecilia Kalthoff at Seattle Children's Research Institute and Rebekah Reynolds at University of Washington insectary for assistance and support of *P. yoelii*–infected mosquito production. We thank the veterinary and husbandry staff of the UW Department of Comparative Medicine. This research was supported by NIH grant 1R01AI141857 to S. C. M and DSP was funded by the DLMP small grant award.

3.7 SUPPLEMENTAL FIGURES

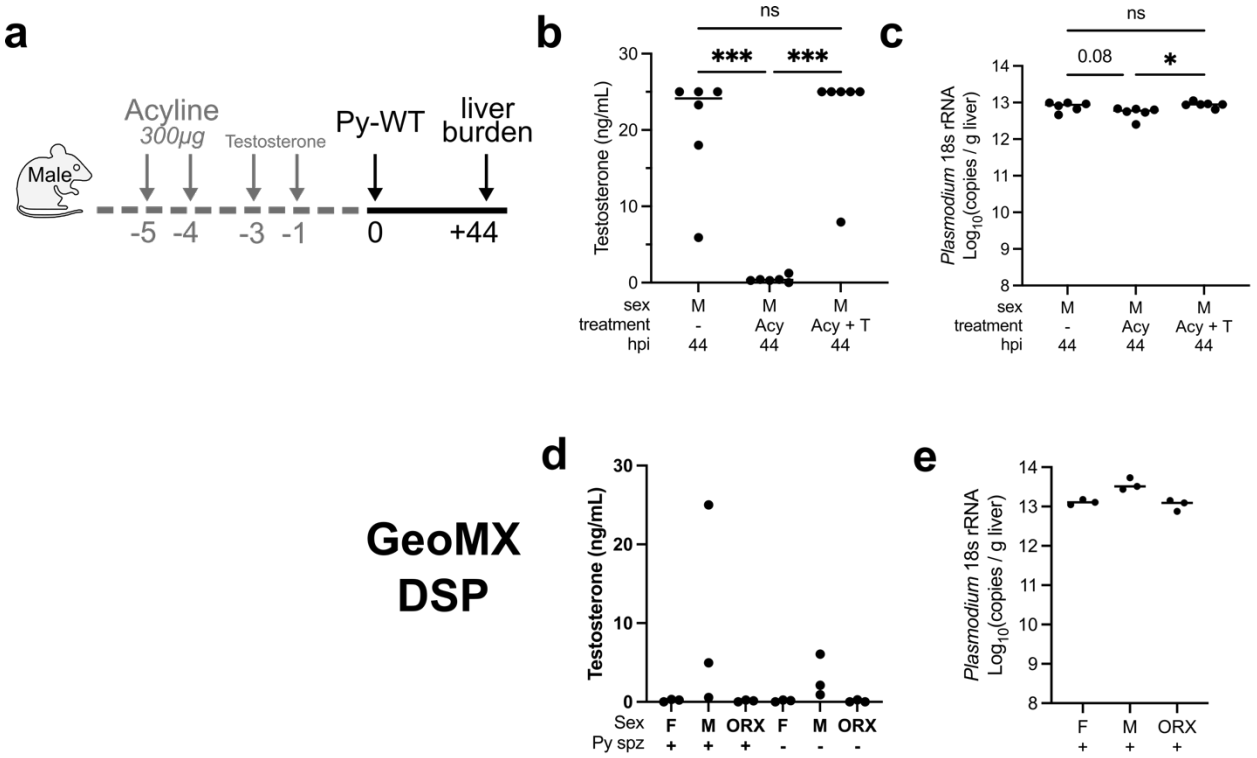

Supplemental Figure 3.7: Testosterone alters liver burden to *Plasmodium yoelli* infection in BALB/cJ mice. a. Scheme of male BALB/cJ mice infected with $1x10^5$ *Py*-WT spz by intravenously (IV) and harvested at 44hpi. Male mice received two doses 300µg Acyline, two doses of testosterone, or left untreated. b. Confirmatory testosterone measurements by ELISA of the mice. c. Liver burden as absolute pan-*Plasmodium* 18S rRNA copy numbers 44 hr post-challenge. Data are shown from two independent experiments (n= 6). d. Confirmatory testosterone measurements by ELISA of the mice in GeoMX experiment starting in Figure 2. e. Liver burden as absolute pan-*Plasmodium* 18S rRNA copy numbers 44 hr post-challenge in GeoMX experiment starting in Figure 2. Data are shown from one independent replication (n=3).

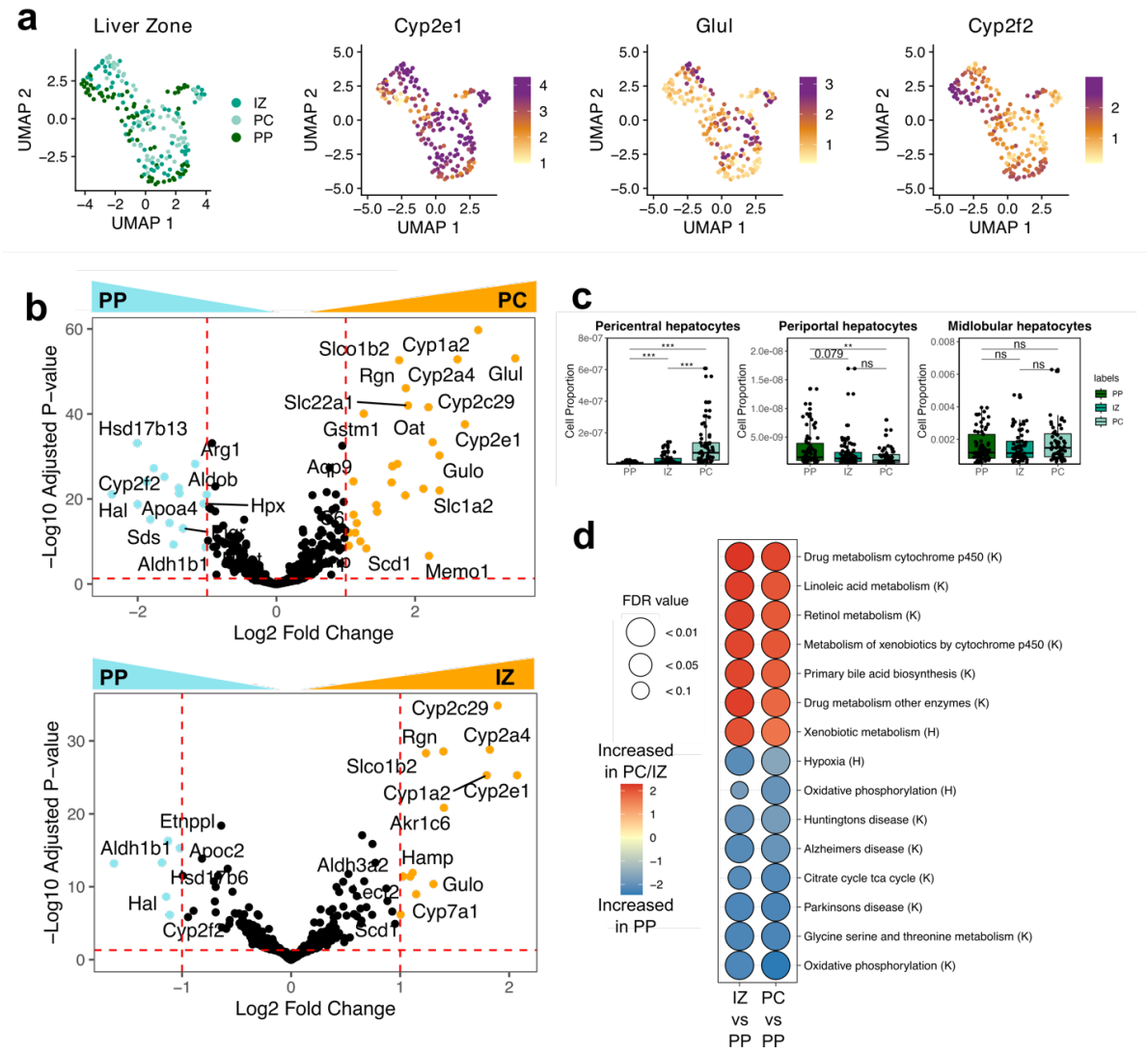

Supplemental Figure 3.8: Gene expression confirms accurate differentiation of liver zones during ROI selection. a. UMAP of ROIs, colored by liver zone (left), and by expression of the pericentral (PC) genes *Cyp2e1* and *Glul*, and periportal (PP) gene *Cyp2f2*. b. Volcano plot of showing differentially expressed genes conserved between periportal region or interzonal (IZ) region and PC region. The y-axis shows the $\log_{10}$ of the adjusted p value (bonferonni corrected). The x-axis shows the $\log_2$ fold change relative to periportal region. Gene significantly increased or decreased in ROIs are plotted in orange or blue, respectively (false discovery rate (FDR) p-value< 0.05 and Log_2Fold Change +/- 1). Gene symbols are shown for selected genes. c. Immune cell type proportions for each ROI in mock-infected mice, separated by liver zone. An independent Wilcoxon test was used to compare the mean cell type proportions between female, male, and ORX male samples, and the resulting p values are shown. ***p <0.001, **p<0.01, *p<0.05, ns p>0.05. d. Gene set enrichment analysis (GSEA) shows pathways differentially regulated between Females and Males, and ORX Males and Males. H, Hallmark gene sets; K, KEGG gene sets. Color scale denotes the Normalized Enrichment Score (NES).

a

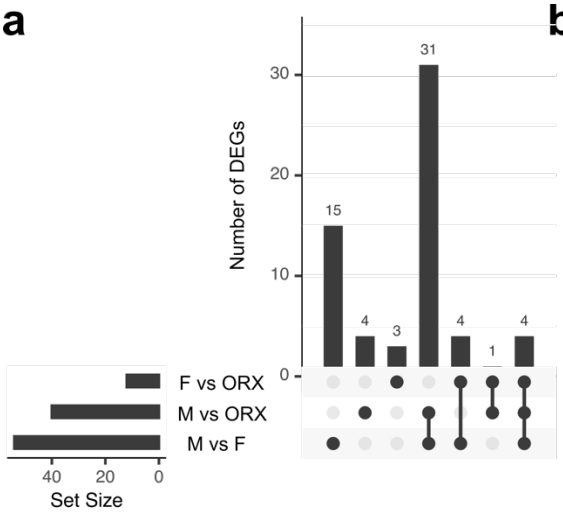

b

Comparison	Number of genes	DEGs
M vs F	15	Actg1, Aldh1a1, C6, C8a, Cbr1, Comt, Cyp2a4, Cyp2d12, Cyp2f2, Cyp8b1, Keg1, Lrg1, Mfsd2a, Sult1a1, Sult2a8
M vs ORX	4	Bhmt, H2-Ea, Orm2, Phyh
F vs ORX	3	Ddx3y, Gm21783, Igfbp2
Shared M vs F & M vs ORX	31	Acot3, Aox3, C4a, C8b, C9, Car3, Csad, Cyp2b13, Cyp2c37, Cyp2d10, Cyp4a10, Cyp4a12a, Cyp4a14, Cyp7b1, Egfr, Fgl1, Fmo3, Gstp1, Hamp2, Hao2, Hsd3b5, Nudt7, Prlr, Scp2, Selenbp1, Serpina1a, Serpina3k, Slc22a27, Slco1a1, Ttc39c, Ugt2b1
Shared M vs F & F vs ORX	4	Cyp7a1, Mt1, Mt2, Mup13
Shared M vs ORX & F vs ORX	1	Scd1
Shared between all	4	Ces3b, Sult2a1, Sult2a2, Sult2a5

Supplemental Figure 3.9: Differentially expressed genes between steady state F, M, and ORX mice. a. Upset plot of genes shared between groups (FDR < 0.05 and Log_2Fold Change +/- 1) from comparisons plotted in Figure 3b. b. Table of differentially expressed genes for each comparison.

a

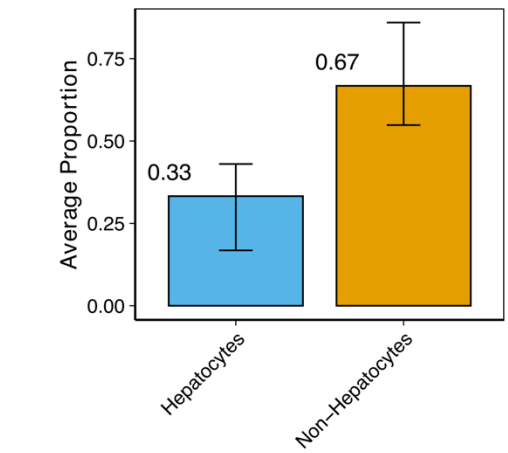

b

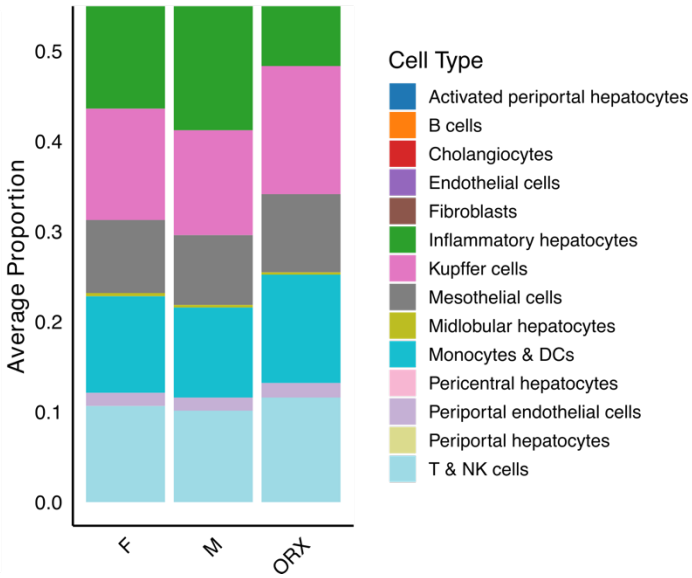

Supplemental Figure 3.10: Proportions of cell types across all samples. a. average proportion of hepatocytes across all conditions compared to the average proportion of all other cell types identified. b. average proportion of all cell types across all conditions. The number of samples used to calculate each cell type proportion was n = 3 (1 average value per condition).

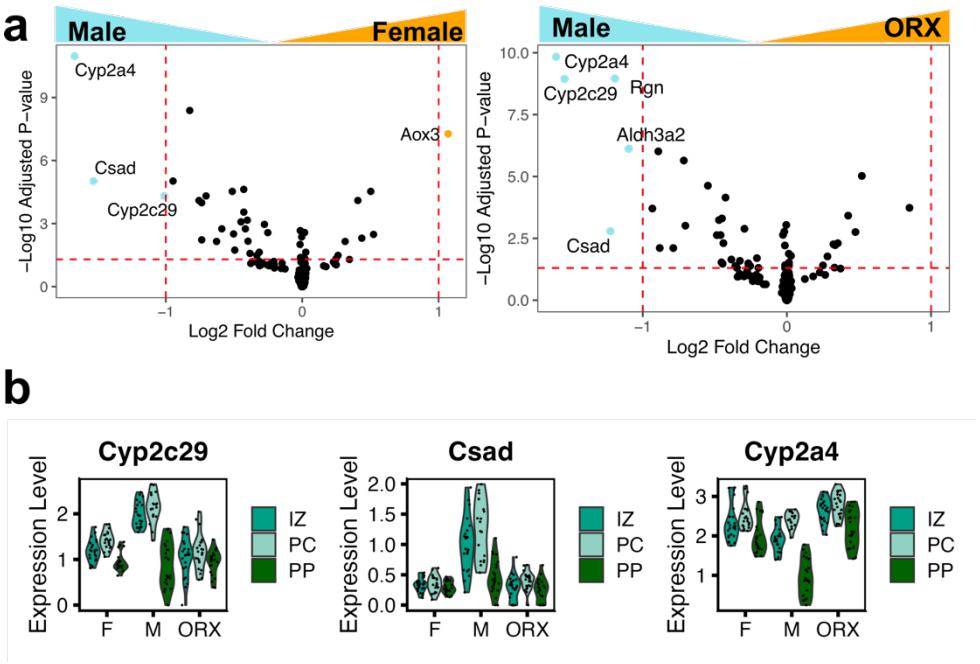

Supplemental Figure 3.11: Biological sex and hormone status minimally perturb gene expression profiles of liver zones at GeoMX resolution. a. Volcano plot of showing differentially boosted genes conserved between male and females (left) or ORX males and males (right) in the context of genes differentially expressed between periportal and pericentral. The y-axis shows the $\log_{10}$ of the adjusted p value (bonferonni corrected). The x-axis shows the Log Fold Change of differentially boosted between PP and PC in the context of biological sex and hormone status. Gene significantly increased or decreased in ROIs are plotted in orange or blue, respectively (false discovery rate (FDR) p-value< 0.05 and Log_2Fold Change +/- 1). Gene symbols are shown for significant genes. b. Violin plots of normalized and batch-corrected gene expression of gene *Cyp2c29*, *Csad*, and *Cyp2a4*.

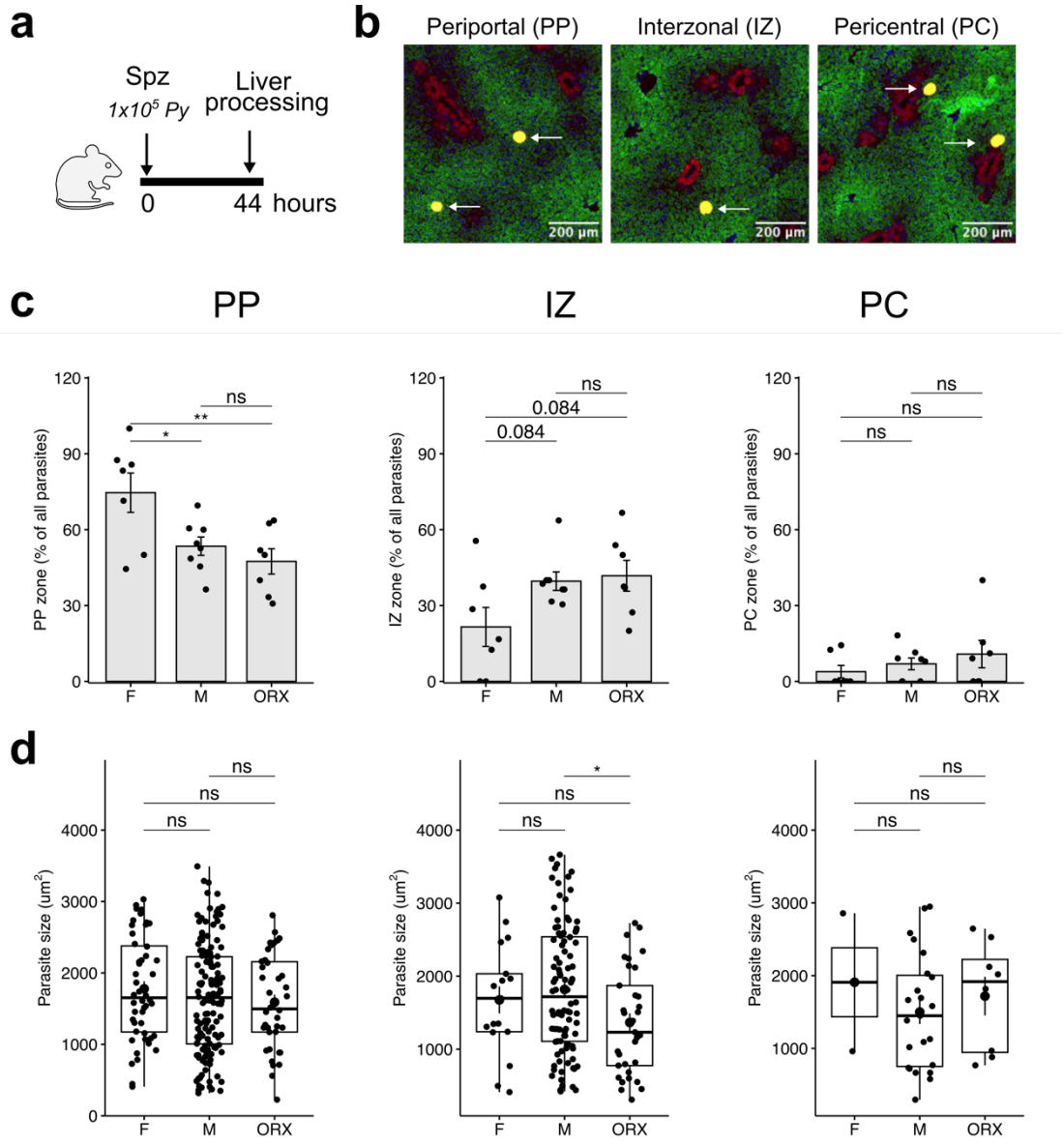

Supplemental Figure 3.12: Impact of sex and castration on zonation of *Plasmodium yoelli* infection in the liver. a. Scheme of male, female, and male orchiectomized BALB/cJ mice infected with 1x10^5 *Py*-WT spz by intravenously (IV) and harvested at 44 hours post infection (hpi). b. Representative image of the location of the parasite in the liver. Periportal (PP), interzonal (IZ), and pericentral were determined with the markers GS (red), ASS1(green), HSP70 (yellow), and DAPI (blue). c and d. Percentage of total parasite and size of parasites within the periportal (left), interzonal (middle), and pericentral (right) region of the liver as determined by fluorescent microscopy. Statistical significance for data was determined by One-way ANOVA with Tukey multiple comparison. Data are shown from two independent experiments (n= 7-8). Error bar represents mean ± s.e.m; box plots depict median with interquartile range. ***p<0.001, **p<0.01, *p<0.05, ns p>0.05.

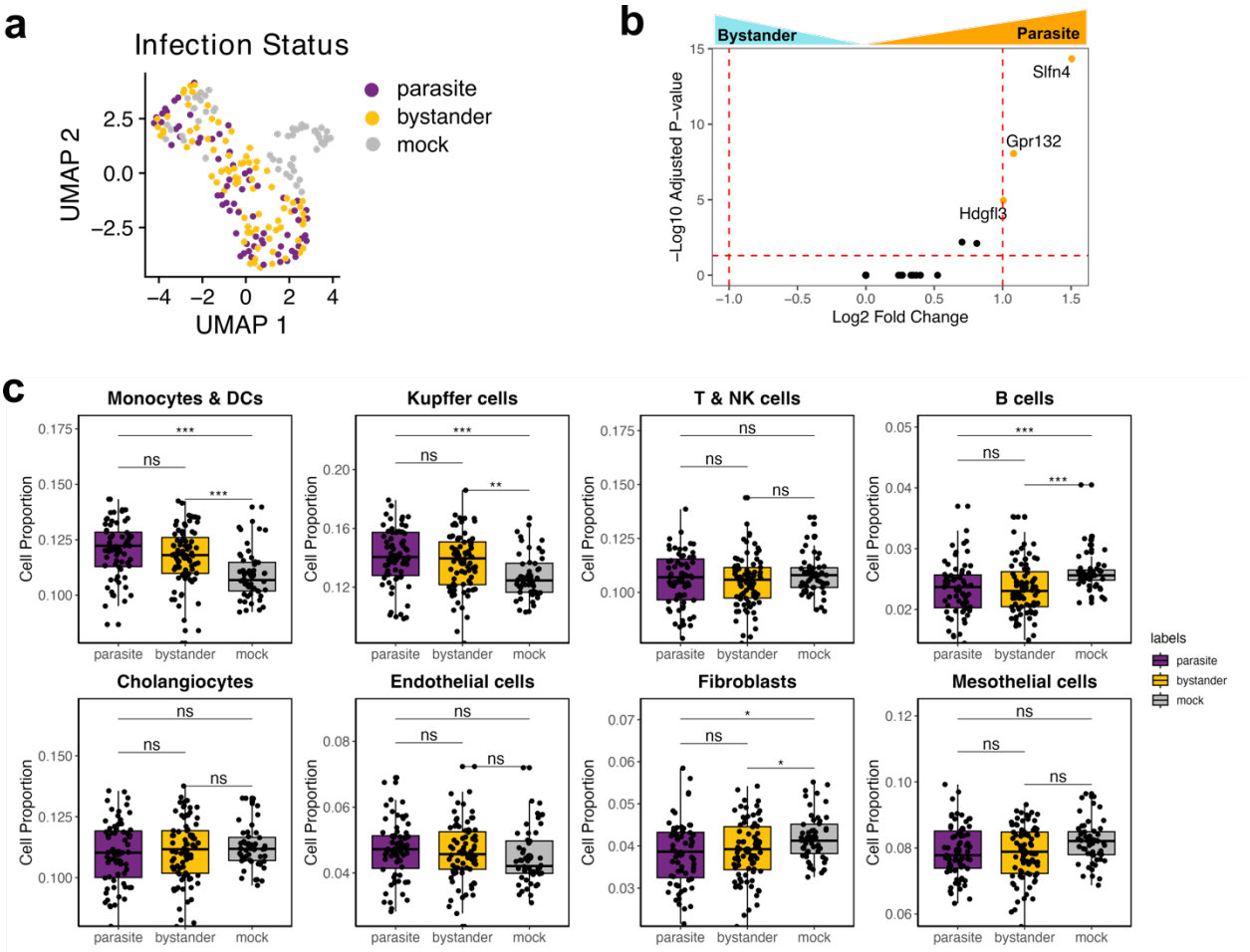

Supplemental Figure 3.13: *P. yoelli* infection impacts proximal and peripheral immune cell recruitment and genes expression in liver tissue. a. UMAP of ROIs, colored by infection type (parasite, bystander, or mock). b. Volcano plot of differentially boosted genes between parasite and bystander. The y-axis shows the $\log_{10}$ of the adjusted p value (bonferonni corrected). The x-axis shows genes differentially expressed relative to bystander. Gene significantly increased or decreased in ROIs are plotted in orange or blue, respectively (false discovery rate (FDR) p-value< 0.05 and Log_2Fold Change +/- 1). Gene symbols are shown for selected genes. c. Immune cell type proportions for each ROI in all mice, separated by infection type. An independent Wilcoxon test was used to compare the mean cell type proportions between female, male, and ORX male samples, and the resulting p values are shown. ***p <0.001, **p<0.01, *p<0.05, ns p>0.05.

Target	Primary	Secondary
DAPI	N/A	DAPI (Unlabeled aliquot) 1:2000
PyHsp70	Unlabeled aliquot mouse host 1:500 *Py*HSP70	Alexa Fluor 488 anti-mouse (A-11001) 1:1000
CLEC4F	N/A	Conjugated Alexa Fluor 647 anti-mouse CLEC4F (BioLegend 156804) 1:100

Supplemental Table 3.2: Table of antibodies for CLEC4F staining.

Comparison (Parasite vs. mock)	Number of genes	DEGs
ORX	9	Angptl8, Car3, Cfp, Ddx3y, Fasn, Mt1, Mt2, Nudt7, Slc22a28
F	42	Apcs, Apol9b, Bst2, Cd74, Ces3b, Cxcl10, Cyp2c37, Cyp3a41a, Cyp4a14, Cyp7a1, G6pc, Gbp2, Gbp2b, Gm20792, Gm4841, H2-D1, H2-Ea, H2-Eb1, H2-K1, Hamp2, Hp, Hpd, Ifi47, Ifitm3, Igfbp2, Igtp, Irgm1, Irgm2, Isg15, Lrg1, Mpeg1, Mup13, Psmb8, Serpina10, Serpina3g, Steap4, Sult2a1, Sult2a2, Sult2a5, Tap1, Tmsb4x, Zbp1
M	1	Phlda1
Shared between F & ORX	9	Cxcl9, Gbp3, Gbp6, Gm21783, Irf7, Ly6e, Saa3, Scd1, Tgtp1
Shared between M & ORX	1	Clec2j
Shared between F & M	3	Fgl1, Orm1, Slfn4
Shared between all	6	Hpx, Iigp1, Lcn2, Orm2, Saa1, Saa2

Supplemental Table 3.3: DEGs between mock and parasite ROIs.

Chapter 4. THE INFLUENCE OF BIOLOGICAL SEX AND SEX HORMONES ON LIVER STAGE VACCINATION IN MICE

4.1 ABSTRACT

Attenuated whole organism vaccines targeting the malaria liver stage reliably confer sterilizing immunity. These vaccines completely protect female mice from infection, but protection in male mice remains unproven. We discovered that male mice vaccinated with prime-and-trap, a whole organism-based vaccine strategy, exhibit poorer protection against *Plasmodium* sporozoite challenge than females. We investigated this sex difference, and discovered that vaccinated males have fewer hepatic memory $CD8^+$ T cells than females when scaling for liver biomass, and that they have reduced inflammatory responses post-vaccination. Surgical hormone manipulation clarified that the presence of testicular hormones hindered protection in male mice. The presence of androgens did not affect memory $CD8^+$ T cell quantity nor quality, but directly inhibited protective $CD8^+$ T cell effector response during sporozoite challenge via suppression of IFNγ. Here, we show both males and females form functional memory responses following prime-and-trap vaccination, but the presence of androgens during sporozoite challenge impair protection in male mice.

4.2 INTRODUCTION

Vaccines that are durably effective are urgently needed to combat malaria, which resulted in 249,000 infections and 608,000 deaths in 2022[29]. The complex lifecycle of *Plasmodium* parasites, the causative agent of malaria, begins with a bite from a mosquito carrying infectious sporozoites (spz). Spz migrate from the dermis to the bloodstream and are transported to the liver[34]. During this liver stage, spz invade hepatocytes. After replication, hepatocytes release the infectious exoerythrocytic merozoites into the bloodstream, initiating the disease-causing phase

of *Plasmodium* infection and enabling onward transmission[35]. Since halting the liver stage could prevent disease and transmission, it is considered an attractive target for vaccine design.

Repeated vaccination with radiation-attenuated sporozoites (RAS) is the most protective experimental malaria vaccine to date that confers sterile immunity against the liver stage in humans[162–164]. The ability of RAS to protect against infection was first demonstrated in mouse models of *Plasmodium*[165,276]. RAS-based vaccines leverage the natural ability of spz to home to the liver while lacking the ability to advance to blood stage infection. Since their discovery, decades of research have sought to deconvolute the mechanisms of immune protection conferred by RAS and other similar attenuated spz-based vaccines. The collective data indicate that memory $CD8^+$ T cells are a defining requirement for a protective immune response in the liver[168,169,277]. In particular, liver-targeted, tissue-resident memory $CD8^+$ T (Trm) cells and effector memory $CD8^+$ (Tem) cells are important for durable protection[164,166,278–280]. Knowledge of these immune correlates of protection inspired the design of next-generation liver stage targeting vaccines called 'prime-and-trap' (P&T). The priming component of the P&T vaccine is designed to induce peripheral antigen-specific $CD8^+$ T cells, and the trapping component is intended to recruit or 'trap' circulating antigen-specific memory $CD8^+$ T cells in the liver to become liver Trms[166,167]. Different iterations of this P&T strategy have protected female mice[167,281], but no data are so far available in male mice.

Sex-specific differences to vaccines are a well-documented phenomenon, with a general trend for females to mount more robust immune responses than males[1,5,112]. Three main sex-based factors drive differences in immune responses: sex hormones, sex-chromosome linked genes,

and physiological differences[5,112,282]. These three factors intrinsically modify the tissue microenvironment[72], leaving T cell-based vaccines especially susceptible to sex-divergent outcomes. The liver is also known to be one of the most sexually-dimorphic organs in mice[71] and humans[283]. Yet, pre-clinical studies of spz vaccines have almost exclusively relied on female mice. For example, in a review by Nganou-Makamdop and Sauerwein, of the 17 papers on spz immunization in mice, none reported using male mice, 12/17 reported using exclusively female mice, and 5/17 reported no sex information[115](**Supplemental Table 4.1**). This underscores the need to consider sex as a biological variable and delineate protection requirements in male mice.

The limited data we do have on the impact of sex on immune responses to liver stage malaria vaccines come from a single recent pre-clinical study[116]. Following repeated RAS vaccination, female mice were found to have more hepatic IFNγ-producing $CD8^+$ T cells and greater protection against *P. berghei* spz challenge than male mice. This reduced protection in males could be overcome by removal of testicular hormones prior to vaccination[116]. Male mice are also known to experience more severe blood stage malarial disease than female mice across several rodent *Plasmodium* spp[103,284]. Thus, there is at least some evidence that biological sex modifies immune responses to both attenuated and virulent *Plasmodium* parasites.

Given the paucity of information on liver stage malaria vaccination in male mice, here we will provide a comprehensive evaluation of P&T vaccine-induced responses on the basis of sex. Through a series of P&T immunization and challenge studies in male and female mice, we will evaluate sex-specific differences in protection outcomes and memory $CD8^+$ T cell populations. We will further assess the contribution of sex hormones in modifying protection and the quality

and quantity of P&T-induced memory $CD8^+$ T cell responses. Together, this study provides an in-depth characterization on the impact of biological sex and sex hormones on a liver stage malaria vaccine.

4.3 METHODS

Ethics statement

Animal studies were performed according to the regulations of the institutional animal care and use committee. Approval was obtained from the University of Washington (UW) Institutional Animal Care and Use Committee (IACUC) under protocol 4317-01. The UW IACUC adheres to the NIH Office of Laboratory Animal Welfare standards (OLAW welfare assurance # D16-00292).

Mice

Male and female BALB/cJ mice (4-6 wk old) were obtained from Jackson Laboratories and housed at UW in an IACUC-approved animal facility. All mice were used under an approved IACUC protocol (4317-01 to SCM).

DNA vaccine preparation

The *P. yoelii* (Py) circumsporozoite protein (CSP) DNA vaccine plasmids were constructed in the pUb.3 vector with an N-terminal ubiquitin tag and purified as described[167,285,286]. For all vaccinations, *Escherichia coli* heat-labile toxin (LT)-encoding plasmid was used as an adjuvant in a 1:10 ratio with the *Py*CSP vaccines[287]. The *Py* CSP-minigene plasmid encodes the codon-optimized SYVPSAEQI epitope and the *Py* CSP plasmid encodes the full-length codon-optimized CSP protein without the major repeat regions, $(GPGAPQ)_5$ and $(PPQQ)_4$. All plasmids

were Sanger sequenced at Azenta Life Sciences before use. Gene gun DNA vaccine cartridges were constructed by loading DNA onto gold powder and then coating loaded gold onto tubing as previously described[167,286]. Abdominal fur was trimmed and mice were vaccinated on the abdomen using a PowderJect-style gene gun using two cartridges per day on days 0 and 2 (0.5 μg DNA per cartridge).

Plasmodium sporozoites for challenge and vaccination

Female *Anopheles stephensi* mosquitoes infected with wild-type (WT) *P. yoelii* (strain 17XNL), GFP/luciferase-expressing *P. yoelii* 17XNL (*Py*-Luc)[288], or *P. berghei* (strain ANKA) were reared at Seattle Children's Research Institute (Seattle, WA) or UW (Seattle, WA). Fresh spz were obtained by salivary gland dissection 14-18 days post-infection followed by Accudenz gradient purification[68]. All spz were diluted in Schneider's insect media for administration (Gibco, Thermo Fisher Scientific). Figure legends specify the dose for each experiment. For *Py*-WT spz challenge, $1x10^3$ freshly dissected *Py*-WT spz were injected unless stated otherwise. For *Pb*-WT spz challenge, 200 freshly dissected *Pb*-WT spz were injected. Blood stage protection after spz challenge was assessed by Giemsa (Sigma-Aldrich,) stained thin blood smear microcopy on Days 3-14 post-challenge. Mice were deemed protected if blood smears remained negative for parasites up to Day 14.

For spz vaccinations, radiation attenuation of freshly dissected *Py* spz (*Py*-RAS) was done by exposing wild-type spz (*Py*-WT) to 10,000 rads via an X-ray source (Rad Source). Cryopreserved radiation-attenuated *Py* 17XNL spz (10,000 rads by C0-60) were produced, purified, and vialed by Sanaria Inc. (Rockville, MD) as described[289,290]. All spz used for immunization or challenge studies were administered intravenously (retro-orbital) in a volume of

100 µL per mouse. For *Py* and *Pb* RAS immunizations, the standard dose was $2x10^4$ spz, unless stated otherwise.

Parasite burden quantification

Luciferase-based *in vivo* parasite imaging of the liver was conducted with an *in vivo* bioluminescent imager (Xenogen IVIS Spectrum, Caliper Life Sciences)[288]. Briefly, mice previously infected with 10^4 *Py*-Luc spz were injected intraperitoneal (IP) with 5 mg of firefly D-Luciferin (Goldbio) prior to undergoing isoflurane anesthesia. Bioluminescence was acquired and measured as previously reported using a one-minute acquisition time. IVIS images were quantitatively evaluated using Living Image 3.0® software (Perkin Elmer) with regions of interest (ROI) placed around the abdominal area overlying the liver. ROI measurements were recorded in total flux (p/sec/cm^2/sr).

To quantify *Py* liver burden in BALB/cJ mice by reverse transcription polymerase chain reaction (RT-PCR), mice were sacrificed, half of the liver was excised and pulverized by bead beating in NucliSENS lysis buffer. For *Pb* liver burden in C57BL/6 mice, whole liver was excised, gently mashed through a 100-mm cell strainer and washed with RPMI mixture, and a fraction was collected into NucliSENS lysis buffer. Both methods, nucleic acids were extracted as previously described using a bioMérieux EasyMAG (bioMérieux)[222]. RNA was subjected to RT-PCR using the SensiFAST™ Probe Lo-ROX Kit (Bioline) using a predesigned HEX-labelled mouse GAPDH RT-PCR assay (IDT Inc) multiplexed with a Pan-*Plasmodium* 18S rRNA assay as described[222]. Cycling conditions consisted of one cycle of 45°C for 10 min, one cycle of 95°C for 2 min, and 45 cycles of 95°C for 5 s and 50°C for 35 s on a QuantStudio5 real-time PCR machine (Thermo Fisher Scientific). *Plasmodium* 18S rRNA copy numbers per reaction were

determined against a calibration curve of quantified Armored RNA encoding full-length *Plasmodium* 18S rRNA (Asuragen); data were also normalized to mouse GAPDH. Results were reported to a cycle threshold (CT) of 35 cycles. Mice were deemed completely protected if RT-PCR results were below the limit of detection (no cycle threshold detected or detected at >35 cycles).

Tissue processing for flow cytometry

Unperfused livers were collected into RPMI media containing, 5% fetal bovine serum (FBS), and supplemented with glutamine (RPMI mixture). Each liver was gently mashed through a 100-mm cell strainer and washed with RPMI mixture. Cell suspensions were centrifuged at 80 x g for 1 min at 22°C with no brake. Isolated supernatants were then centrifuged at 450 x g for 10 min to pellet cells. Cells were resuspended in 10 mL of 35% Percoll (GE Healthcare) in HBSS (Life Technologies) supplemented with 100 U heparin (Millipore Sigma) before centrifugation at 830 x g at 22°C with no brake. The cell pellet was incubated in 3 mL RBC lysis solution (150 mM NH4Cl, 10 mM KHCO3; 0.1 mM EDTA Na2·2H2O, pH 7.4) for 3 min before being washed with 10 mL of RPMI mixture and spun at 500 x g at 4°C for 8 min. Final pellets were resuspended in 200 µL of RPMI mixture and moved to 96-well plates for antibody staining. For hormone-free conditions observed in Figure 6, RPMI mixture was made without phenol red and used charcoal-stripped FBS.

Splenic lymphocytes were isolated by teasing tissue through a 100-mm cell strainer, washed with RPMI mixture and centrifuged at 460 x g at 4°C for 5 min. The cell pellet was incubated in 3 mL RBC lysis solution for 3 min before being washed with 10 mL of RPMI mixture and spun at 460 x g at 4°C for 5 min. Cells were resuspended in 1 mL of RPMI mixture and counted. Cells were

diluted, and one million splenocytes per sample were used for antibody staining. For ELISPOTS, splenocytes were cryopreserved in freezing media (FBS/10% DMSO) prior to thawing for ELISPOT procedures, except in the case of the C57BL/6 mice where splenocytes were not previously frozen.

Antibody staining and flow cytometry

Antibody panels used for staining were optimized to the BALB/cJ mouse model and are provided in Supplemental Table 2. For experiments corresponding to intracellular cytokine staining (ICS) in Figs **2** and **4**, lymphocytes were incubated at 37°C with *Py*CSP peptide SYVPSAEQI (10 μM final) (Genemed Synthesis) and CD107a antibody for 18 h. Brefeldin A was added (BD Biosciences, Franklin Lakes, NJ), and cells were incubated for an additional 4 h. Cells were washed, stained for live/dead designation, and resuspended in Fc-block for 15 min. Cells were washed and stained for cell surface markers and the intracellular markers IFNγ, TNFα, and Granzyme b using the BD Cytofix/Cytoperm reagent (BD Biosciences) according to manufacturer's instructions. For experiments corresponding to Figs **2** and **4,** following liver lymphocyte isolation, cells were immediately stained for live/dead designation and resuspended in Fc-block. Lymphocytes was incubated with H-2K^{d}-PyCSP$^{280\text{-}288}$ -specific tetramer for 30 min at 4°C prior to staining with surface antibodies and then intranuclear staining. Samples underwent intranuclear staining for marker TCF1 using the Foxp3/Transcription Factor buffer set (Thermo Fisher) for 30 min at 4°C. For experiments corresponding to Fig **6,** lymphocytes were incubated at 37°C with either 500nM of Dihydrotestosterone (DHT – Millipore Sigma) (or Methanol vehicle control) for 18 h. Cells were then stimulated with *Py*CSP peptide (or DMSO vehicle control). Brefeldin A was added after 2 h and cells were incubated for an additional 4 h.

ICS was then performed after stimulation as outline above. Flow cytometry data were acquired on a BD LSR Fortessa (BD Biosciences) equipped with a high-throughput sampler and configured with blue (488 nm), green (532 nm), red (628 nm), violet (405 nm), and ultraviolet (355 nm) lasers using standardized good clinical laboratory practice procedures to minimize variability.

Flow cytometry data analysis

Initial compensation, gating, and quality assessment of flow cytometry data were performed using FlowJo v.10 (TreeStar). Representative gating trees for ICS panel and intranuclear panel are shown in Supplemental Figures **2** and **3**. The surface marker and ICS flow cytometry data were then processed using the OpenCyto framework in the R programming environment[291].

Ex vivo IFNγ ELISPOT

PyCSP peptide (SYVPSAEQI) (Genemed Synthesis) was reconstituted in DMSO. Mouse IFNγ ELISPOT (eBioscience) was conducted by stimulating 5×10^5 splenocytes with *Py*CSP peptide (or DMSO vehicle control) at 1 μg/ml for 18 hr at 37°C followed by development following manufacturer guidelines as reported previously[292]. The number of spot-forming units (SFU) in each well was calculated using an ImmunoSpot 5.1 Analyzer (Cellular Technology Limited). SFU were normalized to DMSO control wells and reported as SFU per million splenocytes.

Orchiectomy and ovariectomy surgeries

For orchiectomy (ORX), male mice were anesthetized by isoflurane inhalation (Isoflurane, USP, Dechra Veterinary Products), with doses of 4-5% for induction and, 2-3% for maintenance. A 5 mg/kg dose of meloxicam (Pivetal® Alloxate™, Aspen Veterinary Resources®, LTD) was

administered subcutaneously (SC) to each mouse for systemic analgesia. Lubricant ophthalmic ointment (Pivetal® Artificial Tears, Aspen Veterinary Resources®, LTD) was applied to both eyes to prevent corneal desiccation. Thermal support was provided using a warm water circulating heating pad. The intended incision site was surgically prepped with three alternating scrubs of 10% povidone-iodine and 70% ethanol. A small, midline, scrotal incision was made with tissue scissors. Each testicle was identified singly, and the associated spermatic cord was clamped with hemostats for at least 10 seconds, and the testicle removed. The incision was closed using surgical tissue adhesive (3M™ Vetbond Tissue Adhesive 1469, 3M). Sham ORX surgeries were performed using the same surgical protocol without surgical removal of the testicles.

For ovariectomies (OVX), female mice were anesthetized by isoflurane inhalation with doses of 4-5% for induction and 2-3% for maintenance. A 5 mg/kg dose of meloxicam and 0.1 mg/kg dose of buprenorphine (generic Buprenorphine Hydrochloride for Injection, Par Sterile Products) were administered subcutaneously to each mouse for systemic analgesia. A 0.02 ml dose of 0.5% lidocaine/0.25% bupivacaine mixture (VEDCO Lidocaine Hydrochloride 2%, Sparhawk Laboratories; 0.25% Bupivacaine Hydrochloride Injection, USP, HF Acquisition Co., LLC) was also administered SC at each of the intended bilateral flank incision sites prior to incision for local anesthesia. The intended incision sites were surgically prepped with three alternating scrubs of 10% povidone-iodine and 70% ethanol. The first flank incision was made on one side of the mouse using iris tissue scissors, through the skin and abdominal muscle layers. The ovary was identified within the ovarian fat pad, exteriorized out of the skin incision, and a suture ligature was tied immediately proximal to the ovary using 4-0 or 5-0 absorbable suture. The ovary was

removed by incising through the oviduct immediately distal to the suture ligature. The abdominal wall was then closed using 4-0 or 5-0 absorbable suture. The skin incision was closed using surgical tissue adhesive (3M™ Vetbond Tissue Adhesive 1469, 3M). This process was repeated on the contralateral flank to remove the second ovary. Sham OVX surgeries were performed using the same surgical protocol without surgical removal of the ovaries.

Administration of acyline and testosterone

Acyline (lot # RDZ001) was provided by John K. Amory, MD, MPH at the University of Washington. The lyophilized vials were stored at -20°C until resuspension. At the time of use, Acyline was resuspend to a concentration of 2mg/mL with sterile Molecular Biology Grade Water (Cytiva). Resuspended vials were stored for a maximum of 1 week at 4°C. Unless stated otherwise, mice were subcutaneously injected 5 and 4 days prior to treatment (gene gun prime, RAS trap, or WT spz challenge) to give time for the hormone environment to equilibrate. For testosterone treatment, Testosterone propionate (Sigma Aldrich) was dissolved in sesame oil (Sigma Aldrich) at a concentration of 20 ug/uL. Mice were weighed to determine average weight per group, and then subcutaneously injected with 100 ug testosterone/g body weight at 3 timepoints (3- and 1-day pre-challenge and 1-day post-challenge), unless stated otherwise.

Testosterone quantification in serum

Serum was collected via chin bleed and stored in -20°C until testing. To measure testosterone levels in serum, Testosterone ELISA kits (Crystal Chem) were used per manufacturer guidelines. Singlet absorbance values of each sample were measured with CLARIOstar Plus Microplate Reader (BMG Labtech) and analyzed using MARS data analysis interface. A calibration curve

was generated using manufacturer provided standards (0,0.1, 0.4, 1.5, 6.0, and 25 ng/mL) and a four parametric logistic (4-PL) curve fit was used to calculate sample values.

Immunization with CSP Peptide-Pulsed DCs

Male BALB/c bone marrow-derived DCs were cultured and prepared for immunization as described[72]. On day 9 of culture, media was supplemented with lipopolysaccharide (0.1 μg/mL; Sigma) and *Py*CSP peptide (1 μg/mL)[72]. The next day, cells were washed in PBS and counted, and then $1x10^6$ cells were injected intradermally (ID) into mice. ID immunizations were administered as 100 μL per mouse split across two ID injections in the lower back near the base of the tail.

Glycolipid adjuvant preparation

Good manufacturing practice (GMP) grade glycolipid adjuvant 7DW8-5 powder was provided by Moriya Tsuji (Columbia U). 7DW8-5 was dissolved in DMSO, aliquoted, and stored at -20°C. Single use aliquots were thawed at 56°C for 10 min and then sonicated in an ultrasonic water bath for five min to break micelle formation. The 7DW8-5 was mixed with diluted *Py*RAS immediately before administration to mice. All mice received 2 μg of 7DW8-5 adjuvant.

Gene Expression Analysis

For RNA sequencing, the liver was perfused with perfusion buffer (PBS with 2 mM EDTA). Following perfusion, the left lateral lobe was sectioned and preserved in RNAlater. Total RNA was extracted from tissue and mRNA library was prepared with TruSeq stranded mRNA (Illumina). A sequencing depth of 40M total reads was performed on a NovaSeq6000 S4 150PE flowcell. RNA extraction and Illumina sequencing was performed by Psomagen. RNA

sequencing libraries were aligned with STAR aligner and quality filtered by median coefficient of variation coverage <0.75, duplicate mapped reads >0.75, total aligned sequences $\leq 10^6$. No samples were omitted after this process. Counts were normalized for RNA composition using the trimmed mean of M-values normalization method, filtered to protein-coding genes with ≥0.1 count per million in at least three samples, and converted to $\log_2$ count per million with quality weights using voom. This resulted in 15,120 genes for analysis. Differential expression was determined separately for each time point using the pairwise contrast model of: ~0 + group. Differentially expressed genes (DEGs) were defined as genes with a false-discovery rate (FDR) < 0.05 and |logFC| > 1.5. Hypergeometic enrichment against Broad MSigDBHallmark (H) and canonical pathway (C2) gene sets[293,294] was completed for significant genes, and here significant genes were defined at FDR less than 0.05. Gene set enrichment analysis (GSEA) was performed again H and C5 gene sets with contrast fold changes using fast GSEA.

Pathway score calculation

To identify the effect of the vaccine on the pathway response in female vs. male mice, we conducted a linear regression analysis separately for each time point (acute and adaptive). We took the normalized data and subsetted the data to the genes found in the MSigDB 2022.1.Mm mouse gene sets named in the figures. In order to use the lm function in R to perform the linear regression analysis, we first normalized the data to ensure that the geometric mean for each gene was 1. Next, we computed the geometric mean weight for each sample across gene sets and used these values as weights in the linear regression analysis. For each mouse, we then calculated the pathway gene score by taking a sum of gene expression across respective response gene sets. Next, we evaluated the significance of the interaction term between sex and vaccination status.

Confidence intervals for sex-specific differential expression were computed from the same linear regression. R 4.2.2 was used for all calculations.

Statistics

Details of the statistical tests applied to datasets shown in figures can be found in the above methods and in corresponding figure legends. All data points and n values reflect biological replicates. Data analyzed included outliers unless these could be explained by technical error. Data collection and analysis were not performed blind to the conditions of the experiments. Except as described above, non-parametric tests were employed. Where relevant, statistical tests were two-sided. Individual p values are provided in the figures. Statistical analyses were performed in R (version 3.5.1) or GraphPad Prism 9.1.2 Software. Plots used in this manuscript were generated with GraphPad Prism and the following R packages: ggplot2, ggpubr, and ComplexHeatmap.

4.4 RESULTS

Male mice exhibit less protection after prime-and-trap vaccination

To assess the influence of sex on the efficacy on liver stage malaria vaccines, we utilized a two-dose heterologous P&T regimen[167] in male and female BALB/cJ mice. This P&T regimen involves epidermal DNA plasmid vaccination by gene gun on days 0 and 2. The DNA encodes a *P. yoelii* circumsporozoite protein (CSP) minigene designed to maximize $CD8^+$ T cell activation and minimize antibody responses[167]. Twenty-eight days after DNA vaccination, a single dose of $2x10^4$ *P. yoelii* RAS was injected IV to trap circulating CSP-specific $CD8^+$ T cells in the liver. Mice were challenged 28 days later with IV administered $0.5\text{-}1.0x10^3$ infectious wild-type *Py* spz (*Py*-WT) (**Figure 4.1a**) and monitored for blood stage patency to assess protection. All

female mice were protected (19/19), whereas only 15% of male mice (3/20) were protected (**Figure 4.1b**). Regardless of sex, all naïve mice were susceptible to infection.

To determine if vaccinated male mice could achieve partial liver stage protection, we next monitored liver burden in P&T vaccinated mice of both sexes after virulent spz challenge. Mice were challenged 28 days after P&T using $1x10^4$ *P. yoelii* spz that constitutively express a GFP-luciferase fusion protein (*Py*-Luc)[288] and evaluated at 44 hours post-injection (hpi) by *in vivo* bioluminescent imaging**.** Naïve male and female mice were likewise challenged. Vaccinated female mice showed a 45-fold reduction in infection compared to naïve female mice, whereas vaccinated male mice showed only an 11-fold reduction compared to naïve males (**Figure 4.1c-d**). There was no difference in luminescence signal at 44 hpi between naïve female and male mice (**Figure 4.1 c-d**), suggesting that liver stage replication of the parasite was similar for both sexes. Additionally, augmenting P&T with a more potent prime or a co-administered RAS with the glycolipid adjuvant 7DW8-5[295] did not overcome the low rate of protection observed in male mice (**Supplemental Figure 4.17**).

To confirm that sex-specific protection was not unique to this mouse and parasite strain, we conducted similar P&T studies using C57BL/6 mice and *P. berghei* (Pb) parasites. DNA encoding *Pb*TRAP and *Pb*RPL6 was used for priming, since these two antigens can be recognized in C57BL/6, with *P. berghei* RAS used for trapping, and *Pb*-WT spz for challenge (**Supplemental Figure 4.9**). As expected, P&T vaccinated female C57BL/6 mice showed increased protection over vaccinated male mice. Thus, P&T vaccination induces sex-specific protection across two mouse models.

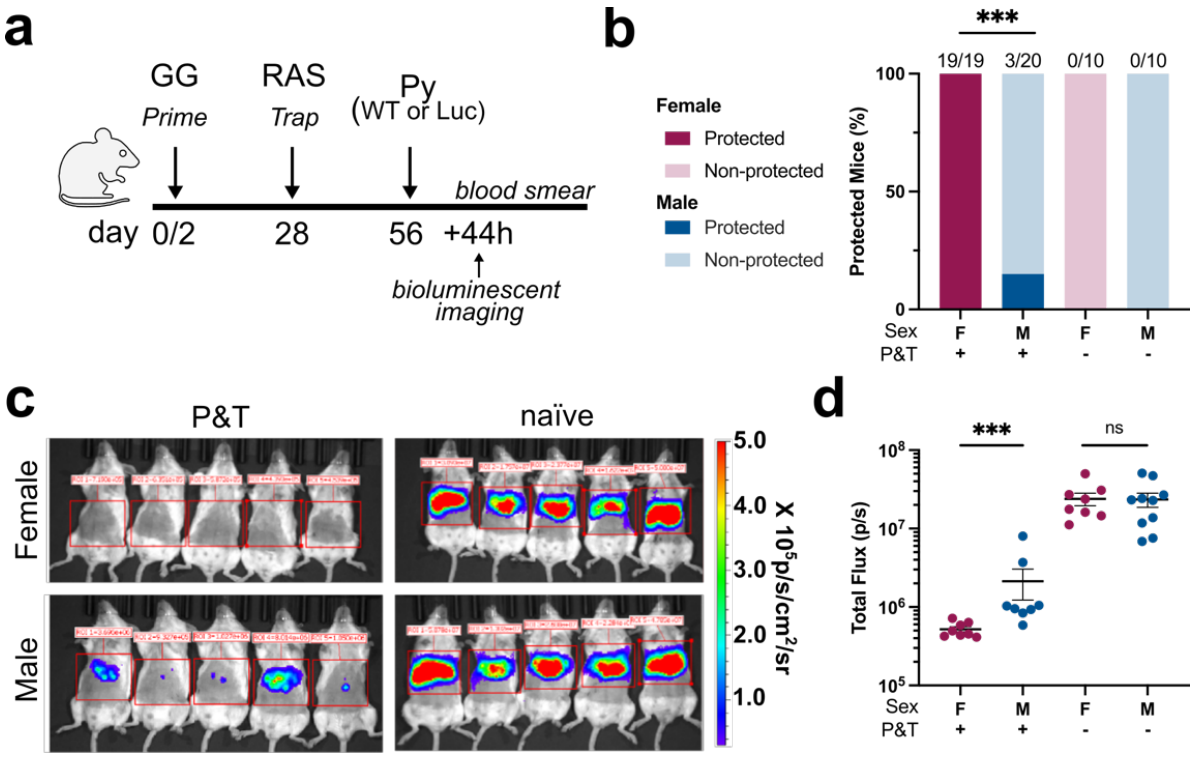

Figure 4.1: Prime-and-Trap malaria vaccination induces sex-specific protection against sporozoite challenge. a. Scheme of male and female BALB/cJ mice Prime-and-Trap (P&T) vaccination experiments. b. Percentages of mice protected or not protected against challenge with 0.5-1.0x10^3 *Py*-WT sporozoites, as measured by blood parasitemia up to day 14 post-challenge. Numbers above bars indicate numbers of protected mice out of total mice challenged, derived from four independent experiments. c. Representative rainbow images of luminescence in livers 44 hr post infection (hpi) with 1x10^4 *Py*-Luc sporozoites. Rainbow scales are expressed in radiance (p/s/cm^2/sr). d. Quantification of bioluminescent signal in log-transformed total flux (p/s) from mice in at 44 hpi (two independent replicates, n = 8-10/group; mean ± s.e.m). Groups in b were compared using Fisher's exact test and groups in d were compared by the Wilcoxon test; only relevant comparisons are depicted. ns = p > 0.05, ***p <0.001.

Female mice generate higher density of memory CD8$^+$ T cells in the liver

Given the importance of T cell responses to spz vaccines[166,172], we phenotyped memory CD8$^+$ T cells in male and female mice following P&T vaccination (**Fig 2a**). Twenty-eight days after vaccination, we isolated liver and spleen leukocytes and *ex vivo* stimulated with *Py*CSP$^{280-288}$ (SYVPSAEQI) peptide prior to intracellular cytokine staining (ICS) to evaluate CD8$^+$ T cells at

this memory timepoint. *Py*CSP$^{280\text{-}288}$ is a known immunodominant epitope in the *Py*RAS/BALB/cJ mouse model and responsive cells represent a major population of antigen-specific CD8$^+$ T cells after P&T vaccination[167]. A higher total CD4/CD8 ratio was observed in vaccinated male livers compared to female livers, but no significant differences in CD4/CD8 ratio were found in the spleen (**Figure 4.2b-c, Supplemental Figure 4.12a**). Male livers weighed significantly more than female livers in both naïve and vaccinated mice (**Figure 4.2e**); thus, liver weights were incorporated in an analysis (results expressed per gram of liver) to account for the impact of sex-difference in physical size on T cell numbers.

With differences in liver weight by sex acknowledged, we then evaluated the vaccine-induced memory CD8$^+$ T cell populations. Upon peptide stimulation, liver Trm cells generated by P&T vaccination are known to express IFNγ, TNFα, and the degranulation marker CD107a[166]. We evaluated the total cell number, frequency, and effector function of CSP-specific CD8$^+$ T cells isolated from the liver and spleen of male and female P&T-immunized mice. First, we examined the number of total cytokine-producing

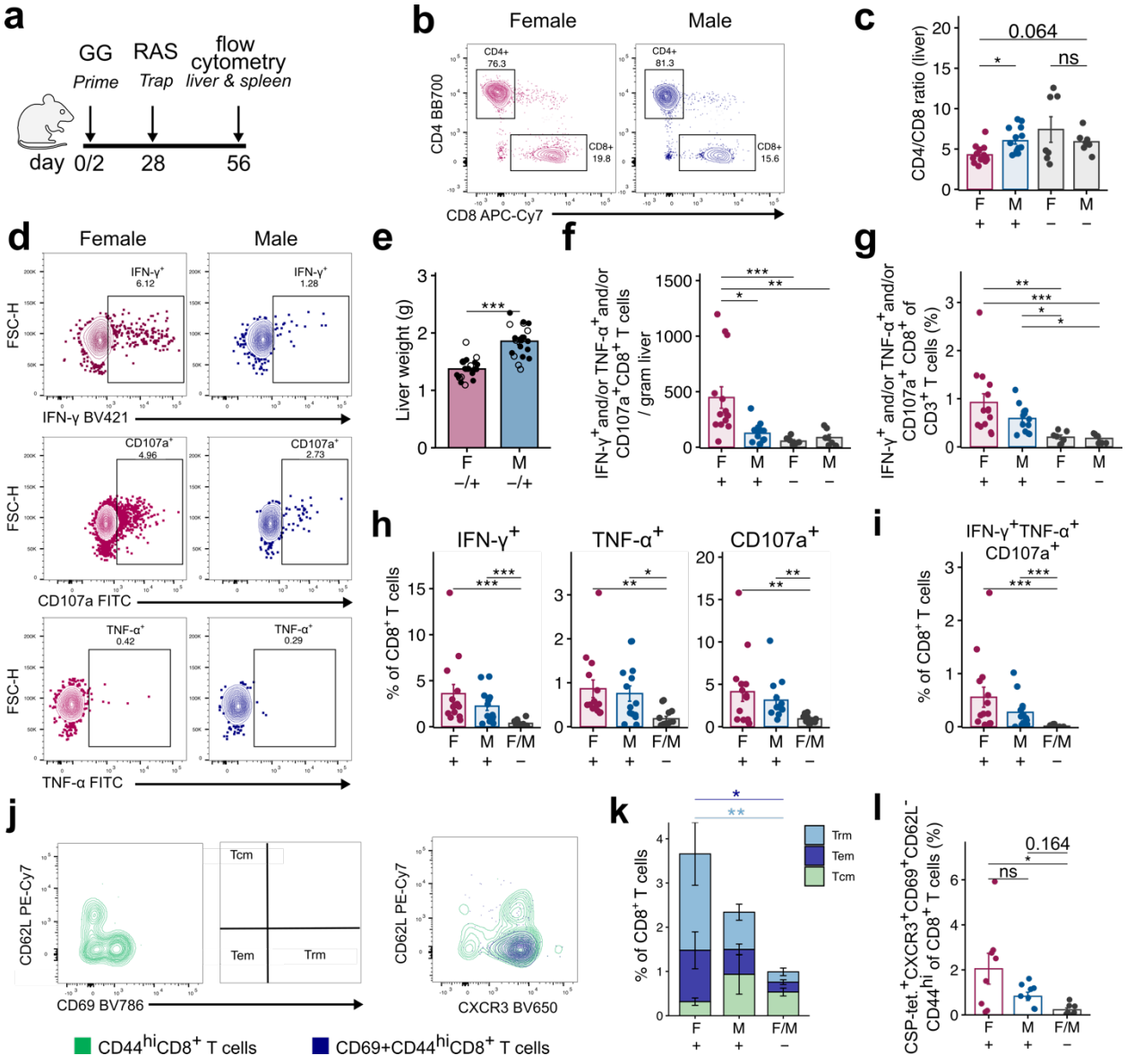

Figure 4.2: Higher density of hepatic memory CD8⁺ T cells in female mice. a. Male and female BALB/cJ mice were vaccinated with the prime-and-trap (P&T) regimen. 28 days later, liver cells were analyzed by flow cytometry. b. Representative flow plots of CD4 and CD8 surface markers on $CD3^+$ cells isolated from the liver of mice. c. Ratio of CD4-to-CD8 in the liver of P&T vaccinated (+) and unvaccinated mice (-) female (F) and male (M) BALB/cJ mice. d. Representative flow plots of IFN-γ (top), CD107a (middle), and TNF-α (bottom) on $CD8^+$ T cells isolated from the liver and *ex vivo* stimulated with *Py*CSP$^{280\text{-}288}$ peptide. e. Liver weights of unvaccinated (open circle) or P&T vaccinated (closed circle) mice. f-g. Quantification of $CD8^+$ T cells responding to *Py*CSP$^{280\text{-}288}$ (SYVPSAEQI) peptide defined by total number of IFN-γ^+ and/or TNF-α^+ and/or $CD107a^+$ producing $CD8^+$ T cells per gram of liver (f) and as proportion of $CD3^+$ T cells (g). h-i. Quantification of proportion of IFN-γ^+ (left), TNF-α^+ (middle), $CD107a^+$ (right) (h), and IFN-γ^+ TNF-α^+ $CD107a^+$ (i) producing $CD8^+$ T cells in the liver. Detailed gating information included in supplemental figures (Fig S2). Data for c - i are shown from 3 independent

experiments (n = 14 total mice/group). j. Representative flow cytometry plot depicting CSP-tet.$^{+}$CD44^{hi} CD8^{+} T cells Trm, Tem, and Trm phenotypes by markers CD69 (left) and CXCR3 (right). Gating calculations performed in R. See Supplemental Fig S3 for gating tree. k. Frequency of CSP tet.$^{+}$CD44^{hi} Tem (CD62L^{-}CD69^{+}CD44^{hi}), Tcm (CD62L^{+}CD69^{-} CD44^{hi}), Trm (CD62L^{-} CD69^{+}CD44^{hi}) subsets of CD8^{+} T cells in the liver. l. Frequency of CSP-tet.$^{+}$CXCR3^{+}CD62L^{-} CD69^{+}CD44^{hi} cells of CD8^{+} T cells in the liver. Data for j-l are shown from two independent experiments (n= 8-9). Error bar represents mean ± s.e.m. Statistical significance for data in c, f-i, k-I, was determined by Kruskal-Wallis test with Dunn's multiple comparison and data in e was evaluated with the Wilcoxon Test; ***p <0.001, **p<0.01, *p<0.05, ns p>0.05.

CSP-specific CD8^{+} T cells defined as any cell expressing IFNγ, TNFα, CD107a, or any combination of the three (**Figure 4.2d**). Females showed higher cell counts per gram of liver compared to males (**Figure 4.2f**). However, when evaluating total CSP-specific hepatic CD8^{+} T cells as a percent of CD3^{+} T cells, cytokine-producing CD8^{+} T cell frequencies did not significantly differ between male and female mice, though females trended toward more cells (**Figure 4.2g**). Second, we evaluated the relative production of IFNγ, TNFα, and CD107a within the respective CD8^{+} T cell population. Vaccinated male and female mice had similar frequencies of IFNγ, TNFα, and CD107a producing CD8+ cells in the liver, and the frequencies were significantly higher than what was seen in the naïve control group (**Figure 4.2h**). Third, we evaluated a putative cytotoxic 'functional' memory population defined as CD8^{+} IFNγ^{+} TNFα^{+}CD107a^{+} [296,297]. Hepatic CD8^{+} T cells expressing all three markers were detected at similar frequencies in both male and female mice (**Figure 4.2i**). In the spleen, there were also similar frequencies of IFNγ^{+} TNFα^{+}CD107a^{+} producing CD8^{+} T cells in male and female mice (**Supplemental Figure 4.12b-e**).

We also evaluated antigen-specific memory $CD8^+$ T cells induced by P&T vaccination in another experiment using the H-$2k^d$ tetramer specific for MHC class I peptide K^d-$PyCSP^{280-288}$. We defined putative Trms as $CD44^{hi}CD62L^-CD69^+$ or $CD44^{hi}CD62L^-CD69^+CXCR3^+$ (**Fig 2j**). P&T vaccinated females showed a trend for increased frequency of CSP-$tetramer^+CD44^{hi}$ $CD8^+$ T cells in the liver at 28 days post-immunization, but this was non-significant (**Supplemental Figure 4.13c**). Across either definition of *Py*CSP-specific tissue resident memory in the liver, there was no significant difference in Trm frequency between vaccinated male and female mice (**Figure 4.3k-l, Supplemental Figure 4.13d-e**). In the spleen, most cells had an effector memory phenotype (Tem: $CD44^{hi}CD62L^-CD69^-$) and there were also no significant differences in the proportion of *Py*CSP-specific Tem cells in the spleen between vaccinated male and female mice (**Supplemental Figure 4.13**).

Taken together, P&T vaccination induces more CSP-specific memory $CD8^+$ T cells per gram of liver by ICS in female mice compared to male mice. However, the frequency of these cells as a proportion of $CD3^+$ T cells did not differ between male and female mice. Also, there were no detectable difference in effector function between male and female mice based on expression of IFNγ, TNFα, and/or CD107a. Finally, there was no detectable difference in frequency of tissue resident memory T cells. Thus, sex divergent outcomes in P&T vaccinated mice are associated with differences in density, but not quality, of vaccine-induced memory $CD8^+$ T cells.

Livers of male and female mice differ in inflammatory response to RAS immunization

We examined gene expression profiles following RAS immunization to contextualize the sex-specific liver localized microenvironment directing the formation of memory $CD8^+$ T cells. The acute inflammatory response of the liver following attenuated spz immunization mediates the

formation of functional hepatic spz-specific $CD8^+$ T cell responses[184]. Thus, to capture the transcriptional profile during initial innate phase and peak $CD8^+$ T cell production phase, bulk mRNA sequencing was performed on whole livers isolated 44 hours or 6 days post-RAS immunization. Prior to RAS immunization, mice were either primed with DNA encoding *Py*CSP or were naïve (**Figure 4.3a**). Principal component analysis (PCA) identified sex as a major driver of variation in the transcriptome, mapping to the first principal component (PC1) that explained 35.6% of variation (**Figure 4.3b**), even when omitting sex chromosomal-linked contributions (**Supplemental Figure 4.14**) and stratifying by vaccination status (**Figure 4.3c**). Differential expression analysis of mock-infected male and female mice confirmed differentially expressed genes (DEGs) in the Cytochrome P450 (*Cyp*) enzyme superfamily (**Supplemental Figure 4.14b**), aligning with known sex differences in the liver[298]. DEGs were examined relative to mock-infected controls within sex to account for this baseline variability between sexes (**Supplemental Figure 4.14d**).

Prior studies comparing early and late arresting whole spz vaccines in female mice have determined that type I IFN gene signature at time of immunization impairs hepatic $CD8^+$ T cell memory via a $CD8^+$ T cell-extrinsic mechanism[184]. IFN signaling pathways have also been documented in response to wild-type[152,176] and attenuated spz[111]. Yet, despite a well-established female bias toward heightened interferon signaling responses upon inflammation[282], a direct comparison between sexes following attenuated spz delivery remains to be reported. Thus, we performed gene sequence enrichment analysis (GSEA) on previously defined transcriptional patterns[293,299]. During the initial innate immune response phase at 44 hrs post-immunization, male and female mice responded similarly for several pathways, including IFN-α response

regardless of vaccination status (**Figure 4.3d**). Further evaluation of differentially expressed genes identified a gene signature shared between male and female mice related to liver inflammation (*Saa1, Saa3*) (**Supplemental Figure 4.15c**).

The day 6 timepoint captures the transcriptome during peak T cell recruitment, proliferation, and ongoing innate immune cell recruitment in the liver following clearance of RAS from infected hepatocytes[162,172]. Consistent with this, the gene ontology pathway for T cell activation was significantly induced in both vaccinated male and female mice at this timepoint (**Figure 4.3d**), though females experienced a significantly higher response than male mice (**Figure 4.3e-f).** The T cell activation gene ontology pathway includes genes indicative of a $CD8^+$ T cell response, including key genes encoding CD8, CD3, and CD28 surface markers. It is notable that there was a lack of detectable *Plasmodium* 18S rRNA at 6 days post-immunization, indicating that transcriptomes were driven by inflammation resulting from RAS clearance and the onset of adaptive cellular responses (**Supplemental Figure 4.14f**). Indeed, unsupervised clustering revealed that liver gene expression signatures clustered first by sex, then by timepoint and vaccine type (**Figure 4.3c**)**.**

Finally, further evaluation of the inflammatory environment during this T cell response at day 6 was conducted. Networks associated with responses to IFN-a were upregulated in female mice, but not in male mice at this timepoint (**Figure 4.3d**). Further investigation of the genes involved in IFN-a response found

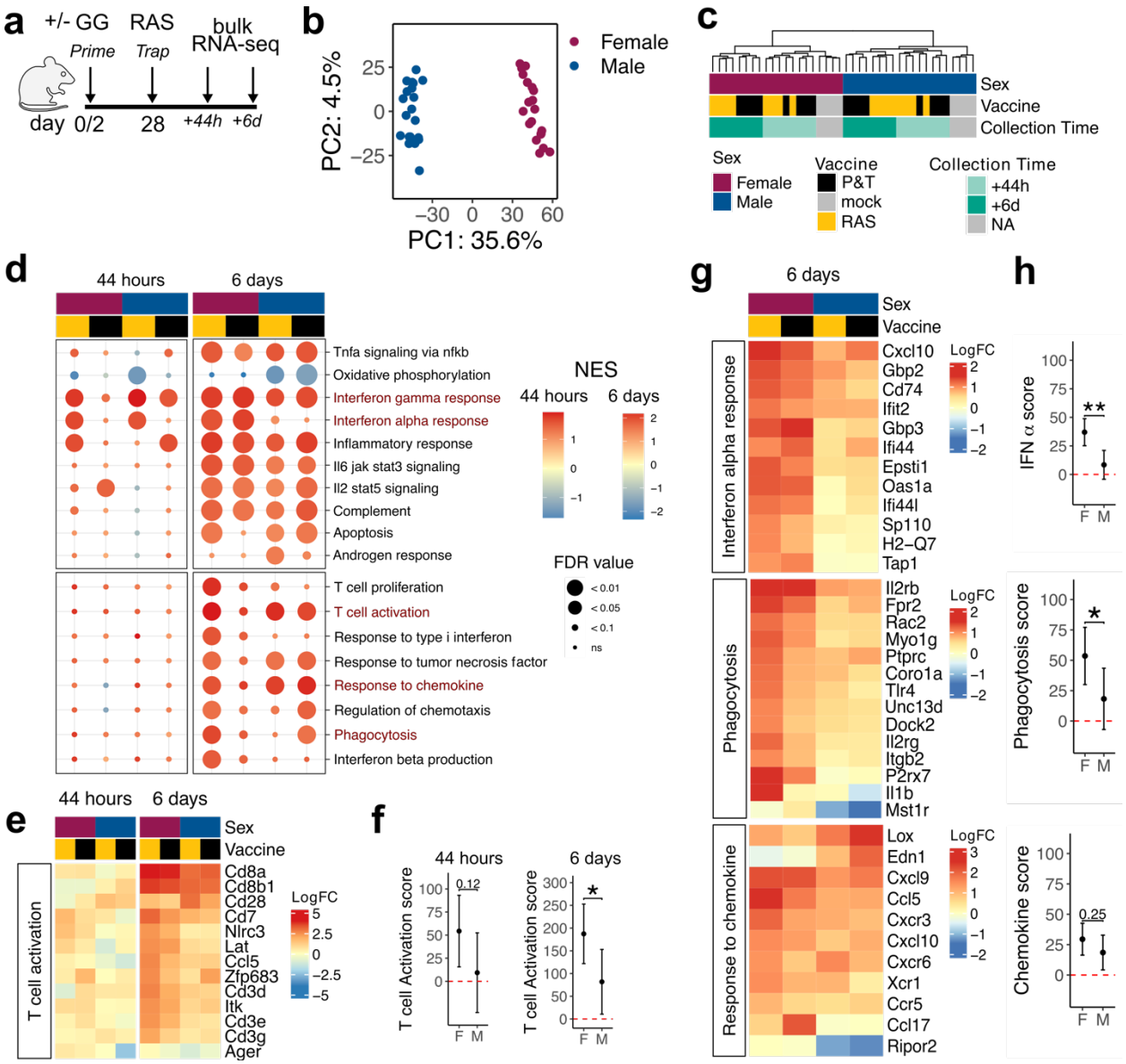

Figure 4.3: Male mice experience a restricted inflammatory response compared to females after Radiation Attenuated Sporozoite (RAS) immunization. a. Experimental schematic. Livers from mock vaccinated, P&T vaccinated (P&T), or RAS-only (RAS) vaccinated male and female BALB/cJ mice were collected 44 hours or 6 days after the indicated vaccine for RNAseq (n=4 per group). b. Principal Component (PC) analysis of male and female transcriptomes following vaccination (containing all vaccinated and mock-vaccinated mice). c. Hierarchical clustering on differentially expressed genes (FDR < 0.05 and |LogFC| > 1.5) and unique to response to vaccination (not shared with baseline differences between the mock-vaccinated male and female mice) with column annotations for sex, vaccine status, and timepoint. Euclidean distance metric was used for sample clustering. d. GSEA of Hallmark (top) and Gene Ontology Biological Processes pathways (bottom) with genes ranked by fold-change values relative to mock injected mice by sex. NES = normalized enrichment score. Column annotations depict sex and vaccine status as designated in panel c. e. Heatmap and hierarchal clustering of genes that contain

at least one differentially expressed gene in either timepoint (44 hours or 6 days) (BH-adjusted p <0.01, |LogFC| > 2) and appear in the Gene Ontology Biological Processes pathway 'T cell activation'. Column annotations depict sex, timepoint, and vaccine status. f. Calculated pathway score of aggregate samples by T cell activation pathways depicted in e for the 44 hour and 6-day timepoint. Detailed explanation of calculation in *Methods* section. g. Heatmap and hierarchal clustering of genes that contain at least one differentially expressed gene at the 6 days timepoint (BH-adjusted p <0.05, |LogFC| > 1) and appear in the Hallmark 'Interferon-α response', or Gene Ontology Biological Processes pathways 'phagocytosis', 'response to chemokine'. Column annotations depict sex and vaccine status as in panel c. j. Calculated pathway score of aggregate samples by Interferon-α response, response to chemokine, and phagocytosis pathways depicted in panel g at day 6 post-immunization. Error bars in f and h represent 95% confidence intervals. **p<0.01, *p<0.05, ns p>0.05.

little to no induction of genes related to proteins associated with a type I IFN response (*Gbp2, Gbp3, ifi44, ifit2*) and CXCR3 ligands (*Cxcl9, Cxcl10*) in male mice (**Figure 4.3i**). Female mice also experienced an increased IFNγ response compared to male mice (**Figure 4.3d, Supplemental Figure 4.14g-h**). Several other pathways were evaluated due to their potential to influence hepatic $CD8^+$ T cell memory responses[176]: phagocytosis was upregulated in females but not males, whereas both male and female mice induced responses to chemokines at this timepoint (**Figure 4.3i-j**). Overall, this suggests that while male mice can form chemokine cues important for $CD8^+$ T cells, and there is a diminished response to inflammatory signals, like interferons, when compared to female mice. This data indicates that the difference in hepatic $CD8^+$ T cell number is potentially related to reduced inflammatory and T cell activation in the liver following immunization.

Androgens alter protection from malaria challenge

Given the known effects of sex hormones on altering adaptive immune responses, we sought to evaluate the impact of sex hormones on protection from P&T vaccination. To evaluate whether estrogens in females or androgens in males contributed to the discordance in protection by sex

following vaccination, we removed the gonads in adult mice at least 14 days prior to P&T vaccination and then later quantified liver burden 44 hours post-spz challenge by *Plasmodium* 18S rRNA RT-PCR to assess protection (**Figure 4.4a**). For females, ovariectomy (OVX, removing estrogens and progestins) had no effect on protection outcome, with OVX females maintaining protection (**Figure 4.4b, Supplemental Figure 4.15a**). For males, orchiectomy (ORX, removing androgens) led to protection, a reversal of the outcome in intact males (**Figure 4.4c, Supplemental Figure 4.15b**). IFNγ ELISPOT on splenocytes obtained at post-challenge timepoints did not demonstrate significant differences in IFNγ producing cells between intact and OVX females or intact and ORX males (**Supplemental Figure 4.15c**). Taken together, these data illustrate that among female mice, ovariectomy to ablate circulating estrogens does not affect protection outcomes, whereas orchiectomy to ablate androgens prior to vaccination significantly improves protection in male mice.

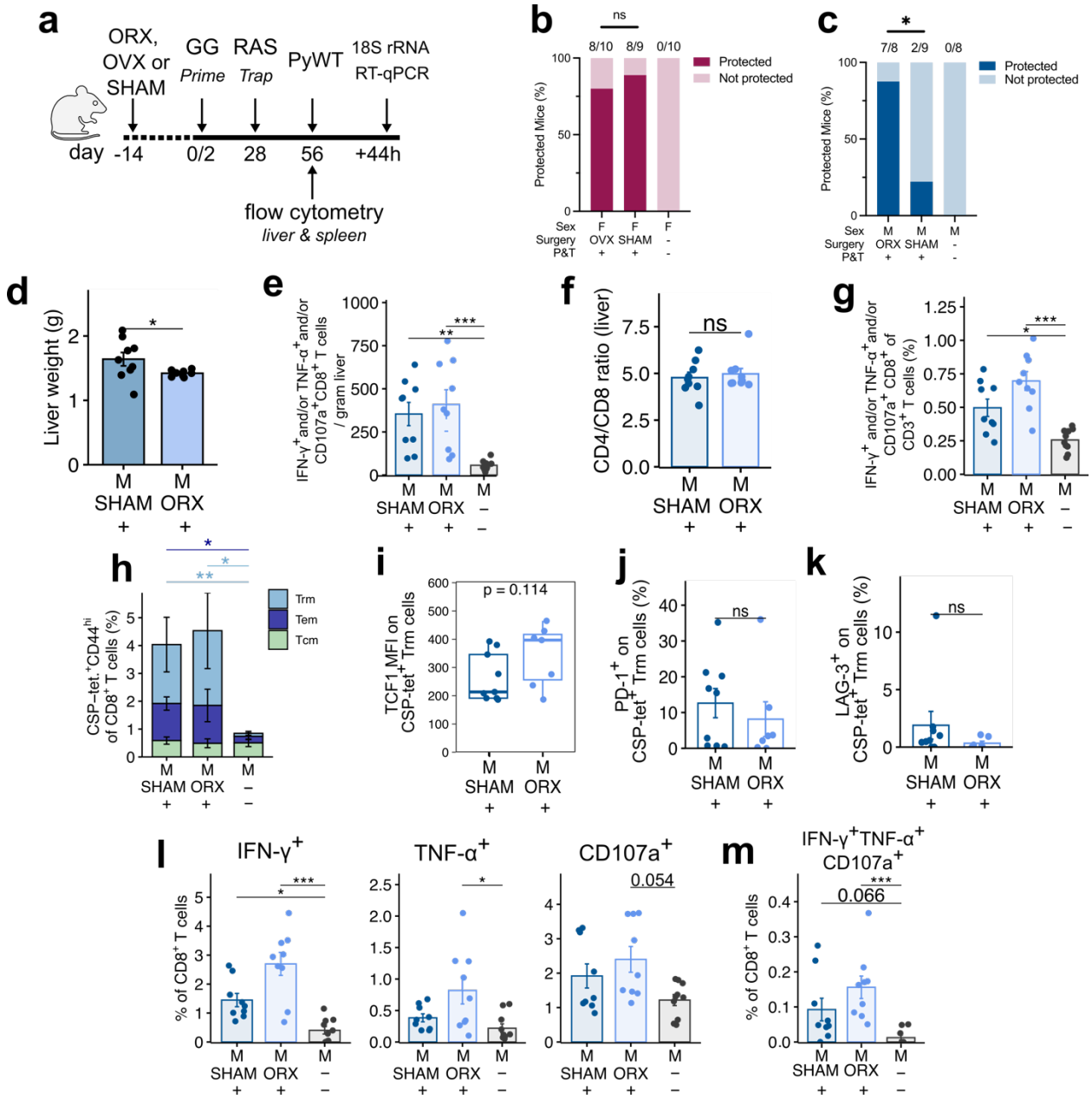

Figure 4.4: Androgens decrease protection from challenge, but do not alter markers of memory CD8⁺ T cell fate and function. a. Experimental regimen with orchiectomy (ORX) in males, ovariectomy (OVX) in females, or sham surgery followed by P&T vaccination. 28 days later, mice were challenged and liver and spleen lymphocytes were analyzed by flow cytometry. b-c. Protection following 1x10^3 *Py*-WT sporozoite challenge defined as no detectable pan-*Plasmodium* 18S rRNA copies 44 hours post-challenge. c and e. Liver burden as absolute pan-*Plasmodium* 18S rRNA copy numbers 44 hr post-challenge. Data are shown from two independent experiments (n = 8 - 10/group). Only relevant comparisons are shown. d. Liver weight of ORX and SHAM operated male BALB/cJ mice vaccinated with P&T regimen and harvest 28 days later. e. Quantification of total responsive CD8$^+$ T cells to *Py*CSP$^{280\text{-}288}$ (SYVPSAEQI) peptide defined by total number of IFN-γ$^+$ and/or TNF-α$^+$ and/or CD107a$^+$ producing CD8$^+$ T cells corrected by weight of liver. f. Ratio of CD4-to-CD8 in the liver. g. Quantification of total responsive CD8$^+$ T

cells to *Py*CSP$^{280-288}$ (SYVPSAEQI) peptide defined by total number of IFN-γ^+ and/or TNF-α^+ and/or CD107a$^+$ producing CD8$^+$ T cells as proportion of CD3$^+$ T cells in the liver. h. Frequency of CSP tetramer$^+$CD44^{hi} Tem (CD62L$^-$CD69$^+$), Tcm (CD62L$^+$CD69$^-$), Trm (CD62L$^-$CD69$^+$) subsets of total CD8$^+$ T cell. i. Quantitative evaluation of TCF1 MFI on CSP-tet.$^+$ Trm cells in the liver (CSP-tet.$^+$CD62L$^-$CD69$^+$CD44^{hi}CD8$^+$ T cells). j. Proportion of PD-1$^+$ on liver Trm cells. k. Proportion of LAG-3$^+$ on liver Trm cells. Data for h – k are shown from two independent experiments (n = 7-10/group). l-m. Quantification of proportion of IFN-γ^+ (left), TNF-α^+ (middle), and CD107a$^+$ (right), and IFN-γ^+ TNF-α^+ CD107a$^+$ (m) producing CD8$^+$ T cells in the liver. Data for d-g and l-m are shown from two independent experiments (n = 9-10/group). Statistical significance for data in b and d was determine by Fisher exact test; data in e, g-h, and l-m was determined by Kruskal-Wallis test with Dunn's multiple comparison and data in d, f, and i-k was evaluated with Wilcoxon Test. In h, individual p values for significant differences are shown, colored to correspond to memory T cell subsets where relevant. Error bar represents mean ± s.e.m; ***p <0.001, **p<0.01, *p<0.05, ns p>0.05.

Androgens do not alter hepatic CD8$^+$ T cell memory populations

Next, we characterized the impact of androgens on the memory CD8$^+$ T cell repertoire in male mice after P&T immunization by ICS. Male mice underwent ORX or equivalent sham surgeries (SHAM), were P&T vaccinated, and then vaccines response at 28 days post-immunization was evaluated as above. As previously reported[300], we observed that livers from vaccinated ORX mice were significantly smaller compared to the vaccinated SHAM mice (**Figure 4.4d**). We analyzed the number CSP-specific CD8$^+$ T cells per gram of tissue, and did not find a significant difference between ORX and SHAM mice (**Figure 4.4e**). There was no difference in the CD4/CD8 T cell ratio in the livers of ORX and SHAM mice (**Figure 4.4f**). Additionally, there was no significant difference in the frequency of CSP-specific CD8$^+$ T cells as a percent of CD3$^+$ T cells in the liver (**Figure 4.4g**) and the spleen (**Supplemental Figure 4.16d-e**). Thus, androgens do not appear to alter the total number or frequency of CSP-specific CD8$^+$ T cells memory cells in the liver as measured by ICS.

In a separate experiment, we characterized the impact of androgens on memory CD8$^+$ T cell responses in male mice after P&T vaccination by tetramer staining. ORX and SHAM male mice

showed similar frequencies of memory CSP-tetramer^{+}CD44^{hi}CD8^{+} T cells in the liver and spleen, with frequencies higher than naïve mice (**Figure 4.4h**). Although Trm and Tem phenotypes were present in both ORX and SHAM vaccinated mice livers and spleen, there were no differences in Trm or Tem composition (**Figure 4.4h-i, Supplemental Figure 4.16a-c**)**.** Taken together, androgens do not appear to alter the frequency of CSP-specific CD8^{+} T cells memory subsets in the liver.

Since there was no difference in the number and proportion of CSP-specific CD8^{+} T cells in the livers of immunized ORX and SHAM male mice 28 days post-immunization, other factors must mediate the improved protection that occurs after withdrawal of androgens. We next evaluated the quality of CSP-tetramer^{+} Trm cells for markers of dysfunction. Androgen receptor signaling has been linked to a more dysfunctional T cell state via the transcription factor TCF1[199,200,301,302]. Thus, we hypothesized that the presence of androgens may alter TCF1 expression and increase expression of co-inhibitory molecules like programmed cell death protein (PD-1) and lymphocyte activation gene 3 (LAG-3) that have also been connected to dysfunctional states[303]. As expected, higher expression of TCF1 was observed on central memory CD8^{+} T cells (Tcm) in the liver than on Tem and Trm cells (**Supplemental Figure 4.16d**). However, importantly, there was no difference in TCF1, PD-1, and LAG-3 expression on tissue resident CD8^{+} T cells (defined as CSP-tetramer^{+}CD62L^{-}CD69^{+}CD44^{hi} CD8^{+} T cells) in ORX compared to SHAM vaccinated mice (**Figure 4.4i-k**, **Supplemental Figure 4.16g**).

Next, we assessed whether there are more cytokine-producing CD8^{+} T cells in ORX P&T immunized mice upon re-stimulation compared to SHAM mice. Both P&T vaccinated groups

had increased levels of cytokine producing $CD8^+$ T cells as compared to the naïve controls, but there was not a significant difference in the frequency of $IFN\gamma^+$, $TNF\alpha^+$, or $CD107a^+$ cells in the liver or the spleen between the ORX and SHAM groups (**Figure 4.4l, Supplemental Figure 4.16h**). A similar pattern was seen when comparing the frequency of $IFN\gamma^+TNF\alpha^+CD107a^+$ cells (**Figure 4.4m, Supplemental Figure 4.16i**).

In all, there was no detectable difference between the frequency, exhaustion/dysfunction status, or polyfunctionality profiles of antigen-specific $CD8^+$ T cells in male mouse livers at 28 days post-immunization following ORX or SHAM surgeries.

Hormone environment at time of challenge impacts protection outcomes

The question remained, why are intact male mice not protected by vaccination? Theoretically, androgens could influence the efficacy of P&T vaccination during two potential phases: 1) the production phase of immune memory at time of vaccination, or 2) the recall phase of immune memory at time of challenge. To identify at what stage androgens alter protection outcomes, ORX was performed before or after P&T vaccination and then mice were challenged three weeks after the post-P&T ORX procedures (**Figure 4.5a**) to allow the hormone environment in the liver to re-equilibrate. SHAM mice received surgery at the post-P&T timepoint. As in previous experiments, male mice were protected by P&T when ORX was performed prior to vaccination. Remarkably, when ORX was performed after P&T vaccination, the mice were also protected (**Figure 4.5b, Supplemental Figure 4.17b**). However, since ORX is irreversible, this method of hormone manipulation did not allow for evaluation of the effect of androgens uniquely at the time of vaccination.

To allow us to further interrogate at which phase of vaccination and challenge androgens were exerting immune effects, we developed an acute and reversible model to suppress testosterone production in male mice. Acyline is a gonadotropin releasing hormone (GnRH) antagonist that suppresses downstream production of testosterone in a dose-dependent manner and has previously been applied in mice[250], and humans[251,252]. We optimized the dose of acyline for the BALB/cJ mouse model by selecting the dose that most consistently retained suppressed testosterone levels for over 7 days but under 14 days to ensure that hormone levels were maintained during peak immune responses of the P&T regimen (**Supplemental Figure 4.18a-b**).

Next, we depleted testosterone prior to both steps of P&T vaccination, prior to spz challenge, or both (**Figure 4.5c**). We found reducing testosterone during either vaccination or challenge was sufficient to increase protection outcomes in male mice (**Figure 4.5d**). To further confirm that testosterone at time of challenge changes protection outcomes, we added back testosterone and once again saw a reduction in protection (**Figure 4.5d**). We further confirmed that administration of acyline, testosterone, and ORX surgery did not alter liver burden in unvaccinated mice (**Supplemental Figure 4.18e-f**). Together with the above liver $CD8^+$ T cell characterization data, these findings lead us to conclude that the hormone environment at time of challenge is a driving factor behind limited vaccine-induced protection in intact male mice.

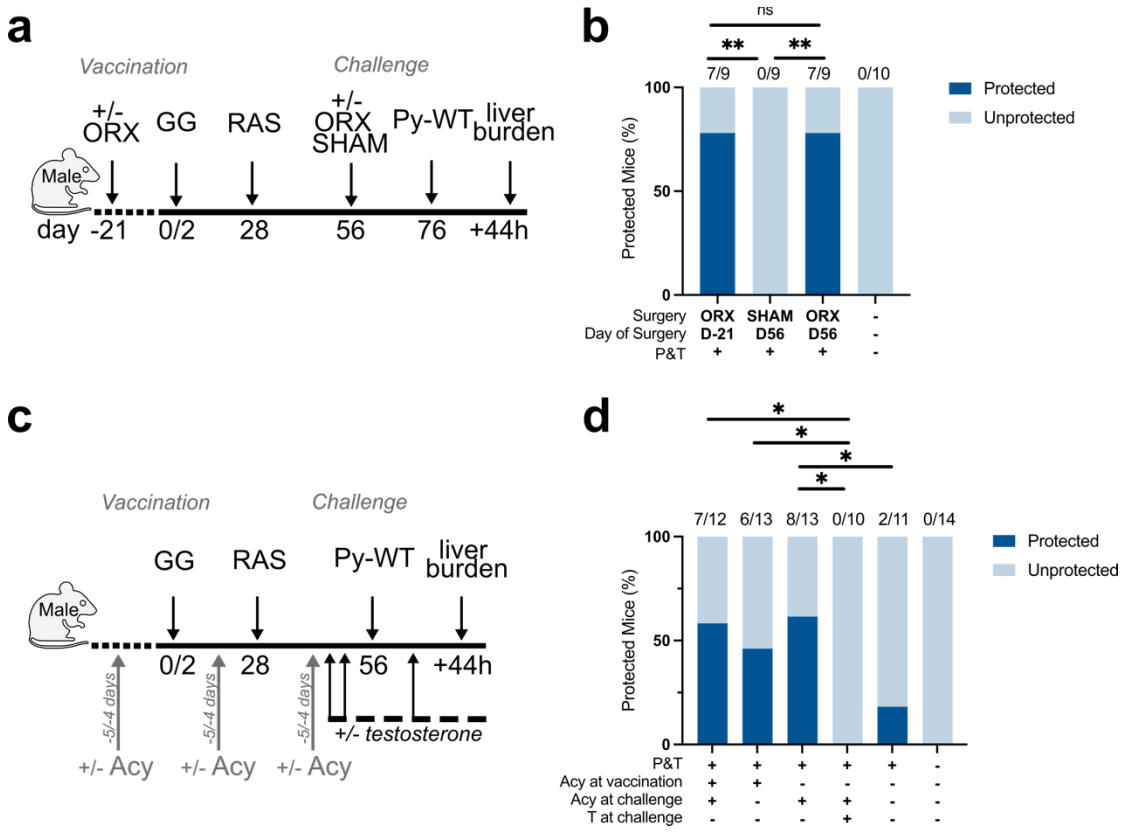

Figure 4.5: Protection of male mice depends on hormone environment at time of challenge. a. Schedule of orchiectomy (ORX) in male mice 21 days before or 28 days after P&T vaccination as shown. After the completion of vaccinations, mice were rested 21 days to establish a new hormone equilibrium and then were challenged with $1x10^3$ *Py*-WT sporozoites. b. Protection after *Py*-WT sporozoite challenge by pan-*Plasmodium* 18S rRNA RT-PCR from livers collected 44 hours post-challenge. Data are shown from two independent experiments (n= 9-10/group). c. Schedule of administration of Acyline (Acy) in male mice at day 5 and 4 prior to either P&T vaccination (prior to gene gun and RAS) or prior to challenge, or both. Testosterone add-back group received 3 injections of testosterone on day 3 and 1 prior to challenge and 1 day following challenge. d. Protection after *Py*-WT sporozoite challenge by pan-*Plasmodium* 18S rRNA RT-PCR from livers collected 44 hours post-challenge. Data are shown from two - three independent experiments (n= 10-14/group). Statistical significance for data in b and e was determined by the Fisher exact test. Only relevant comparisons are shown. Error bar represents mean ± s.e.m; ***p<0.001, **p<0.01, *p<0.05, ns p>0.05.

Androgens inhibit $CD8^+$ T cell recall response

To further identify the impact of androgens on $CD8^+$ T cells during recall at time of challenge, we established an *ex vivo* stimulation model where we exogenously supply dihydrotestosterone (DHT), the metabolically active form of the testosterone, and evaluated the impact on $CD8^+$ T cells in altered hormone environment. Intact male and female mice, and ORX male mice were P&T vaccinated as previously described (**Figure 4.6a**) and lymphocytes were isolated from the liver and stimulated with *Py*$CSP^{280-288}$ peptide in the presence or in the absence of DHT (**Figure 4.6b**). $CD8^+$ T cells from ORX male mice showed a reduction in IFNγ and Granzyme B, but not TNFα, in the presence of DHT (**Figure 4.6b**). Furthermore, in the presence of DHT, there was a reduction in proportion of $CD8^+$ T cells expressing $IFN\gamma^+$ Granzyme B^+ or a putative polyfunctional T cell expressing $IFN\gamma^+$ Granzyme $B^+TNF\alpha^+CD107a^+$ in cells from the ORX male group and female group (**Figure 4.6d,f**). Granzyme B^+ expression was reduced only in cells from the female mice (**Figure 4.6e-g**). Thus, overall, the presence of DHT reduced activity of $CD8^+$ T cells via inhibition of $IFN\gamma^+$ and Granzyme B^+.

As a secondary analysis, within the above experiment we also queried the frequency of γδ T cells by biological sex. Interestingly, we identified that females also have a higher frequency of γδ T cells at both baseline and in response to P&T vaccination **(Supplemental Figure 4.19)**.

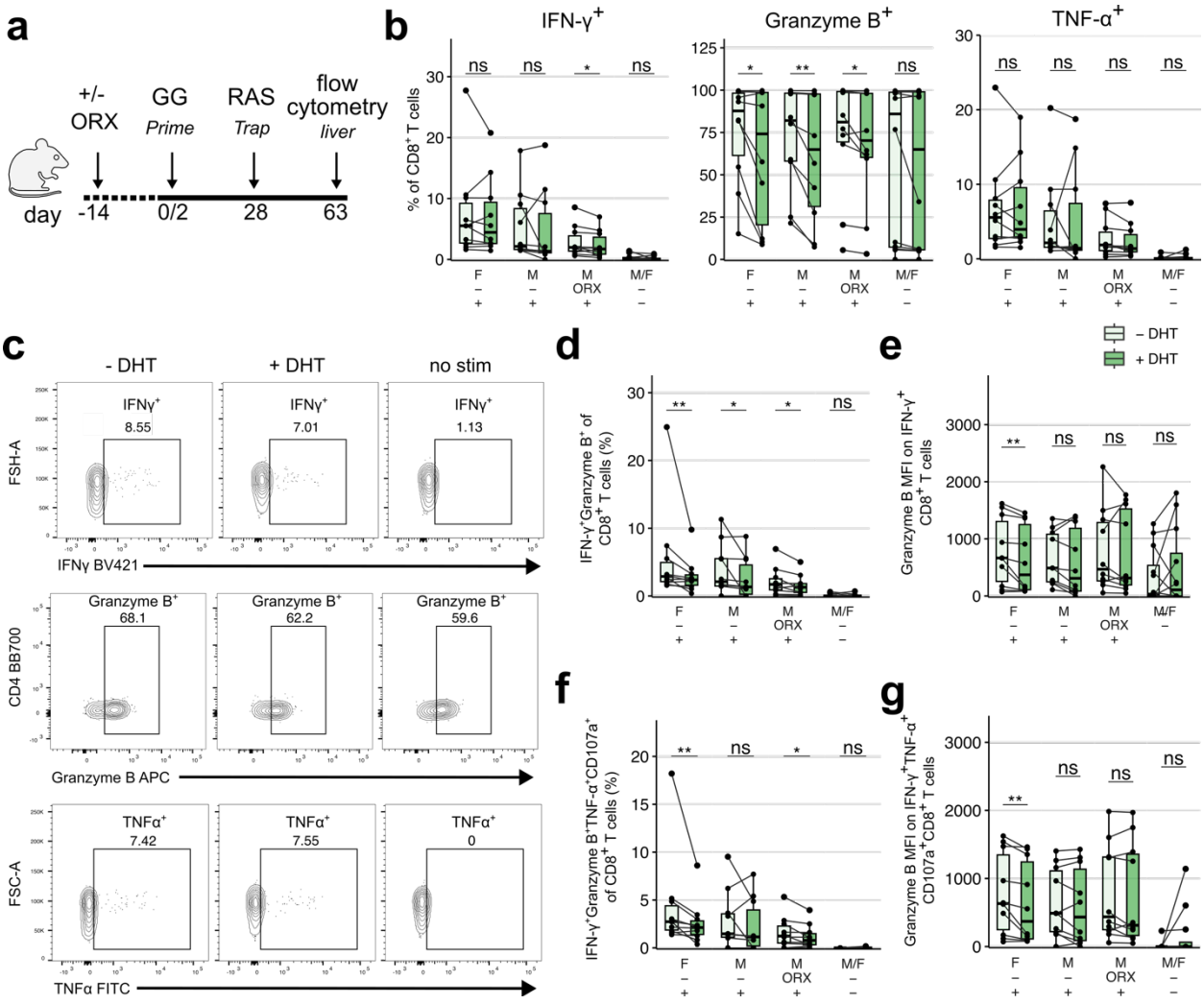

Figure 4.6. Androgens inhibit protective CD8$^+$ T cell activity via inhibition of IFN-γ and Granzyme B production during recall response. a. Female, male, and ORX male BALB/cJ mice were vaccinated with the prime-and-trap (P&T) regimen. 35 days later, liver cells were analyzed by flow cytometry. b. Quantification of proportion of IFN-γ (left), Granzyme B (middle), and TNF-α (right) producing CD8$^+$ T cells in the liver. c. Representative flow plots of IFN-γ (top), Granzyme B (middle), and TNF-α (bottom) on CD8$^+$ T cells isolated from the liver and *ex vivo* stimulated with *Py*CSP$^{280\text{-}288}$ peptide in hormone free condition with dihydrotestosterone (DHT) added to media. d and f. Quantification of proportion of IFN-γ$^+$Granzyme B$^+$ (d) and IFN-γ$^+$Granzyme B$^+$ TNF-α$^+$CD107a$^+$ (f) producing CD8$^+$ T cells in the liver. e and g. Quantification of Granzyme B MFI on IFN-γ$^+$ (e) and IFN-γ$^+$Granzyme B$^+$ TNF-α$^+$CD107a$^+$ (g) producing CD8$^+$ T cells in the liver. Data are shown from 2 independent experiments (n = 10-12 total mice/group, naïve composed of n=6 per sex). Statistical significance for data in b, d-g was determined by a paired Wilcoxon Test; ***p <0.001, **p<0.01, *p<0.05, ns p>0.05.

4.5 DISCUSSION

Liver stage malaria vaccine research has predominantly been conducted in female mice. Through a series of P&T immunization and challenge studies in male and female BALB/cJ mice, we identified sex-specific differences in protection outcomes, $CD8^+$ T cell density, and inflammation in the liver. We further show that although androgens modulate protection outcomes, the number of $CD8^+$ T cells was not correlated with sex hormone-mediated protection. Instead, through a step-wise assessment of modified vaccination regimens to overcome reduced protection, we ultimately determined that androgens at the time of challenge impede an otherwise protective adaptive immune response via suppression of IFNγ production by vaccine-induced $CD8^+$ T cells in male mice.

Sex hormones, physiology, and sex chromosomes are factors potentially contributing to sex-specific malaria liver stage vaccine outcomes. These three factors have important implications for the production, function, and recall responses of memory $CD8^+$ T cells in liver. First, with respect to sex hormones, it is well established that sex hormones influence many immune system functions[5,112,282]. Both androgens and estrogens have been linked to altering inflammation, interferon signaling, and $CD8^+$ T cell frequency and function[14,16,20,104,159,207,304]. One prior report also found that sex hormones alter protection outcomes in adult C3H/HeNCr MTV mice vaccinated with two doses of radiation attenuated *P. berghei* expressing *P. falciparum* CSP[116]. They further identified testosterone as a key modulator of protection through a series of orchiectomies, ovariectomies, and add-back hormone studies[116]. Here, we found a similar trend in response to P&T vaccination – that androgens and not estrogens are the driver behind differential protection to P&T vaccination in the *Py*/BALB/cJ model.

Theoretically, androgens could influence the efficacy of P&T vaccination during two potential phases: 1) the production phase of immune memory at time of vaccination, or 2) the recall phase of immune memory at time of challenge. Some of our data does suggest androgens may influence the "production phase" of vaccination, since by acutely and reversibly altering hormone environment at time of vaccination, we were able to increase protection in male mice. However, other evidence points to that poor protection in intact male mice is not directly related the "production phase" of vaccination. First, increasing $CD8^+$ T cell responses with more immunogenic priming or adjuvanted trapping methods did not significantly increase protection in males. Second, a non-significant difference in the quality and quantity of the vaccine-induced $CD8^+$ T cell repertoire between ORX and SHAM male mice indicated that differences in $CD8^+$ T cell programs could not explain the outcome. This was surprising, as there is literature describing how the androgen receptor accelerates terminally exhausted $CD8^+$ T cells via direct transcriptional activation of TCF1/*Tcf7*[302]. We hypothesized that intact male mice would have more dysfunctional $CD8^+$ T cells as shown by increased LAG-3^+, PD-1^+, and TCF1^{lo} expression and/or reduced production of IFNγ, TNFα, and CD107a. Yet, neither direct *ex vivo* phenotyping nor *in vitro* stimulation under normal media conditions followed by ICS could establish a connection between androgens and T cell dysfunction. One potential explanation for why administering acyline at time of vaccination altered protection outcomes could be related to CD8-T cell extrinsic factors within the liver. Therefore, while we can affirm that androgens do not alter the permanent $CD8^+$ T cell program, we cannot exclude their potential impact on $CD8^+$ T cell effector function *in vivo.*

The alternative explanation was that immune effects of androgens at the "recall phase" were driving sex-bias in protection outcomes from P&T vaccination. Remarkably, when we reduced androgens levels *after* P&T vaccination but *prior* to spz challenge, high levels of protection in males was achieved, confirming this was the key driver of the sex-specific outcomes in our model. Prior literature has shown that androgens could be suppressing protection by direct and indirect mechanisms. Given this, we hypothesized that androgens could directly reduce effector $CD8^+$ T cell activity at time of challenge (**Figure 4.7**)[305]. The major caveat to previous *in vitro* stimulation conditions was the non-physiologic hormone environment found in cell culture media[306]. When we repeated *ex vivo* stimulation in hormone-free conditions and exogenously added DHT into the media, we saw a reduction in expression of IFNγ and granzyme B. This supports prior literature that had identified that androgen receptor (AR) interacts with the open chromatin regions associated with Ifng and Gzmb in effector memory $CD8^+$ T cells and regulates rapid production of IFNγ and granzyme B upon TCR stimulation[199]. The lack of reduction after DHT treatment observed within male intact mice is likely related to an already activated AR that is refractory to further activity, unlike the case in female and ORX male mice. While not directly evaluated, at the indirect level, androgens could reconfigure the tissue microenvironment[80] to restrict sensing[109], alter innate immune cell activity[14], and suppress inflammation[14,307]. Indeed, in line with this, we observed markedly reduced cellular and inflammatory responses in the male liver following RAS immunization. Further investigations into how reduction in IFNγ and granzyme B might modulate recognition and further immune cell recruitment toward infected hepatocytes will thus be a key focus of our future work.

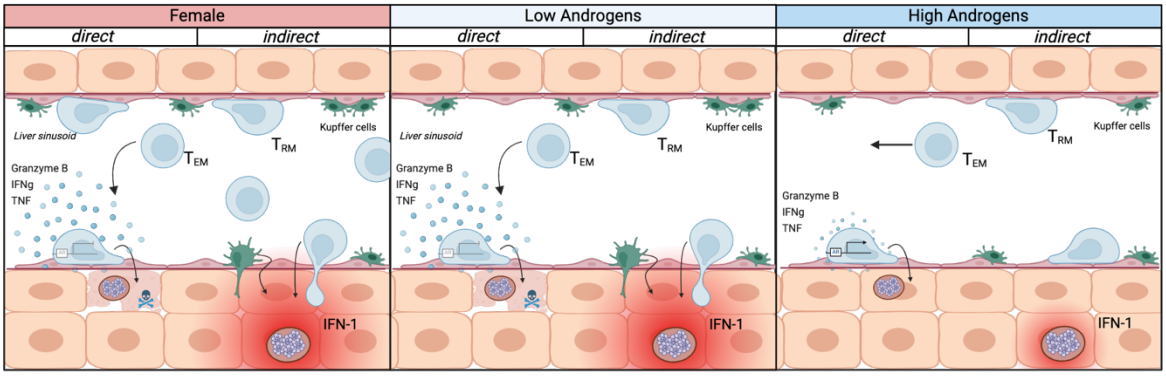

Figure 4.7. Proposed model of the impact of biological sex and androgens on Trm cell recruitment during the effector phase at time of challenge. In female mice there is a higher density of memory CD8 T cells that are able to more quickly respond to signaling produced by infected hepatocytes. Both in female and ORX male mice there is also a higher density of Kupffer cells and other innate immune cells that are also more quickly activated to clear infected hepatocytes. Under high androgen conditions, there is reduced Type I IFN response and less density of memory $CD8^+$ T cells. Additionally, the presence of androgens at time of challenge also reduces secretions of cytokines and cytolytic compounds, hereby limiting recruitment toward infected hepatocytes and leaving male mice less protected from *Plasmodium* challenge. Created with BioRender.com.

While physiological differences by sex were not a focus here, we also observed the male mouse liver was about 35% larger than that of female mice (**Figure 4.2e**). Previous work found a balance between the number of infected hepatocytes and effector $CD8^+$ T cells needed to confer sterile protection[172]. While we did not identify a difference in parasite biomass between naïve male and female mice 44 hours after spz challenge, vaccine-induced $CD8^+$ T cell number after accounting for differences in liver mass revealed a higher density in females. Future research could thus also seek to explore whether physical size influences malaria liver stage vaccine efficacy in pre-clinical models.

Equally, while sex chromosomes were not directly evaluated here, the X and Y chromosomes encode a wide array of immune response-linked proteins[20]. The presence of two X chromosomes (XX) and absence of the Y chromosome is clearly not a requirement for protection since we were

able to protect male mice by altering the hormone environment. However, genes mapped to the X-chromosome exhibited sex-specific expression in response to P&T, such as *Cxcr3* and *Il2rg*. CXCR3 is an important homing marker and is constitutively expressed on Trm cells during homeostasis[308]. IL-2Rγ transduces common γ-chain cytokine signals such IL-2, IL-7, and IL-15, which are important signals for the survival of memory $CD8^+$ T cells[309]. These genes therefore also warrant further evaluation for sex biased regulation. However, since male mice were capable of being protected, we can conclude these sex-linked genes were not the major driver of differential protection to P&T vaccination.

Finally, a critical question is how these findings may relate to human vaccination and infection. A recent meta-analysis of the attenuated spz vaccine PfSPZ identified higher levels of antigen-specific antibodies in females compared to males. However, no difference in PfSPZ vaccine efficacy based on sex was identified[114]. Although sex-specific immunogenicity is observed in humans and mice, the absence of sex specific protection outcomes in humans may be linked to inherent differences, such as the longer liver stage in humans and distinct endocrine systems. Given the paucity of information about how biological sex interacts with the immune-parasite axis during *Plasmodium* liver stage infection in mice and humans, further evaluation of the basic biology of how males and females respond to attenuated and virulent *Plasmodium* parasites is warranted.

Taken together, our results indicate that there are sex-specific differences in protection outcomes and hepatic memory $CD8^+$ T cell number relative to liver size. However, direct inhibition of $CD8^+$ T cell activity via IFNγ is the driving factor behind the inability to protect male mice.

Although ovariectomies did not decrease protection, we could not assess if there was an increase in efficacy because intact female mice are already completely protected, leaving the potential role of ovarian hormones uncertain. Additionally, the gene expression data are limited by measuring the mRNA levels and no protein level analysis was conducted. This work highlights why male mice serve as a more stringent model for malaria liver stage vaccine evaluation. While we were unable to overcome the natural androgen-mediated barrier of the male liver with alternative P&T strategies, a malaria liver stage vaccine that can elicit complete sterile immunity in males may be an indicator of a promising malaria vaccine. Beyond malaria liver stage vaccines, capturing sex differences in pre-clinical and clinical studies is a National Institute of Health mandate and an important step towards understanding intrinsic biases in vaccine development.

4.6 EXTENDED INFORMATION ON ESTROGENS

The focus of the dissertation naturally shifted to the impact of androgens on restricting protection in male mice. The reason for this was two-fold. First, preliminary data first identified the dramatic modifying effect of androgens in reducing protection in P&T vaccinated male mice. Second, there were practical limitations. The time period to conduct on orchiectomy lasted around ~ 5 minutes per mouse by the board-certified vet within the laboratory. In contrast, an ovariectomy took around 20 - 30 minutes per mouse, due to the added complication of two incision routes and a smaller target. Thus, in the end this thesis focused on androgens. However, we have also identified an important role of ovarian hormones, estrogens and progesterone, in mediating protection outcomes.

Here we report that the main **ovarian hormones, estrogens and progesterone, increase protection from secondary sporozoite challenge**. Given the pro-inflammatory features of estrogen in mediating immune responses[4], we hypothesized that an intact female mouse has higher protection. Since the P&T vaccine regimen already confers 100% protection, a sub-optimal vaccine model would be necessary to capture the beneficial effect of estrogens and progesterone on protection. Given the known effects of sex hormones on altering adaptive immune responses, we sought to evaluate the impact of sex hormones on protection from the sub-optimal single dose of RAS vaccine model. To evaluate whether estrogen in females or androgens in males contributed to the discordance in protection between male and female mice following vaccination, we removed the gonads in adult mice at least 14 days prior to RAS vaccination and then later quantified liver burden 44 hours post-spz challenge by *Plasmodium* 18S rRNA RT-PCR to assess protection (**Figure 4.8a**). For females, ovariectomy (OVX, removing estrogens and progestins) decreased protection outcome, with OVX females only 10% protection compared to the 50% protected in the SHAM female group (**Figure 4.8b-c**). For males, orchiectomy (ORX, removing androgens) led to higher levels of protection as expected from previous P&T experiments (**Figure 4.8b**). This data shows that ovariectomy reduces protection in female mice, while orchiectomy improves protection in male mice.

We further examined the impact of estrogen (E2) delivered via pellet implantation on liver gene expression profiles. In this study, male mice underwent orchiectomy (ORX) and were implanted with either an estrogen or testosterone pellet subcutaneously (see **Chapter 4** for detailed methods). Liver samples were collected 44 hours after injection with 10,000 cryopreserved spz (**Figure 4.8b**). Due to the inclusion of only one mock control—an intact male mouse—this differential gene expression analysis reflects a combination of baseline hormonal effects and the

response to spz. However, the hormone-induced changes are likely the primary drivers of the observed gene expression patterns. E2-treated ORX mice displayed significant shifts in baseline gene expression profiles. Compared to ORX alone, E2 treatment led to elevated IFN-β levels, enhanced regulation of chemotaxis, activation of IL-2/STAT signaling, and a general increase in inflammatory responses (**Figure 4.8b -f**). These findings highlight that estrogen dramatically alters the baseline immune homeostasis in male mice under controlled conditions, whereas testosterone suppresses immune responses (**Figure 4.8e -f**), corroborating spatial transcriptomic findings in **Chapter 3**.

This work establishes a foundation for future studies to investigate the effects of estrogen and progesterone on innate and adaptive immune responses in the murine liver. Exploring the dose-dependent impact of estrogen could potentially uncover novel correlates of infection in humans, offering valuable insights into sex-specific immune mechanisms.

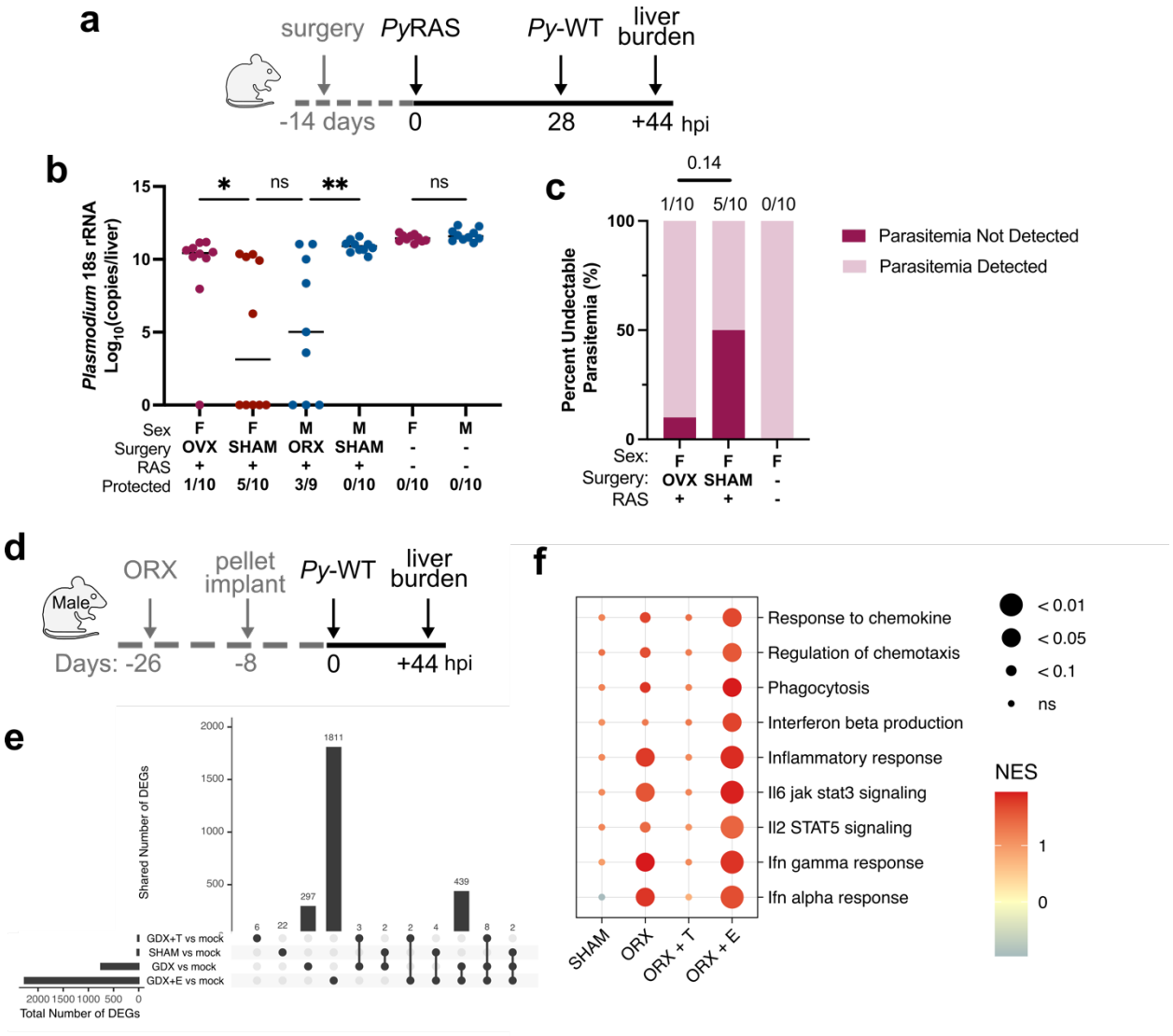

Figure 4.8: Estrogen increases protection for liver stage vaccines and inflammation. **a**. Experimental regimen with orchiectomy (ORX) in males, ovariectomy (OVX) in females, or sham surgery followed by RAS only ($2x10^4$ *Py*RAS) vaccination. **b**. Protection following $1x10^3$ *Py*-WT sporozoite challenge defined as no detectable pan-*Plasmodium* 18S rRNA copies 44 hours post-challenge. **c**. Liver burden as absolute pan-*Plasmodium* 18S rRNA copy numbers 44 hr post-challenge. Data are shown from two independent experiments (n = 9 - 10/group). Only relevant comparisons are shown. **d.** Experimental schematic for surgery and pellet implantation in male mice. **e**. Upset plot of differentially expressed genes (FDR < 0.05 and |LogFC| > 1**).** between each treatment group compared to mock infected intact male mice. d. GSEA of selected Hallmark and KEGG pathways with genes ranked by fold-change values relative to mock injected male mouse collected at the 44-hour timepoint. Pathways with an BH-adjusted FDR<0.05 are shown. NES = normalized enrichment score.

4.7 ACKNOWLEDGMENTS

I would like to thank the co-authors on this manuscript: Nilasha Sen, Alen Poleman, Felicia N. Watson, Erik D. Layton, Kenneth Boey, Ethan N. Conrad, Anya C. Kalata, A. Mariko Seilie, Kimberly A. Dill-McFarland, Chetan Seshadri, Melanie J. Shears, and Sean C. Murphy. We thank Tess Seltzer, Veronica Primavera, Cecilia Kalthoff, and Alexis Kaushansky (Seattle Children's Research Institute) and staff at University of Washington insectary for assistance and support of *P. yoelii*–infected mosquito production and the NIH Tetramer Core Facility (contract number75N93020D00005) for providing *Py*CSP monomers. We thank the veterinary and husbandry staff of the UW Department of Comparative Medicine. We thank Paul Edlefsen, Ewelina Kosmider, and Danica Shao (Fred Hutch) for statistical support and Moriya Tsuji for the 7DW8-5 adjuvant. This research was supported by NIH grant 1R01AI141857 to S. C. M.

4.8 SUPPLEMENTAL FIGURES

Parasite strain	Mouse strain	Sporozoite attenuation strategy	Biological Sex	Ref
P. yoelii (17XNL), P. berghei (ANKA)	BALB/c	RAS, CPS-CN	Female	1
P. yoelii (265BY)	BALB/c; 129P2Sv/ev	RAS, CPS-CQ, CPS-PQ	Female (BALB/c); Sex not reported (129P2Sv/ev)	2
P. yoelii (17XNL), *P. berghei* (NK65)	BALB/c; C57BL/6; Swiss Webster	RAS, CPS-PQ	Sex not reported	3
P. yoelii (17XNL)	BALB/c; Swiss Webster	GAP ΔSAP1	Female	4
P. yoelii (17XNL)	BALB/c	GAP ΔSAP1	Female	5
P. yoelii (17XNL), P. yoelii (YM), P. berghei	BALB/c; C57BL/6; Swiss Webster	GAP ΔSAP1, GAP ΔFABB/F, RAS	Sex not reported	6
P. yoelii (17XNL)	BALB/c	GAP ΔUIS3, GAP ΔUIS4	Female	7
P. yoelii (17XNL)	BALB/c;C.129S7(B6)	GAP ΔUIS3, GAP ΔUIS4	Female	8
P. yoelii (265 BY), *P. berghei* (ANKA)	BALB/c; C57BL/6	GAP Δp36p, RAS	Sex not reported	9
P. berghei (ANKA)	BALB/c; C57BL/6	GAP Δp36p, RAS	Female	10
P. berghei (ANKA)	C57BL/6	GAP ΔUIS3, GAP Δp36p, RAS, CPS-PQ, CPS-AZ, CPS-CQ, CPS-PYR	Female	11
P. berghei (ANKA)	C57BL/6	RAS, CPD-CQ	Sex not reported	12
P. berghei (ANKA)	C57BL/6	GAP ΔSLARP	Female	13
P. yoelii (17XNL), P. berghei (ANKA)	BALB/c; C57BL/6	CPS-PQ	Sex not reported	14
P. berghei (ANKA)	BALB/c; C57BL/6	CPS-CN	Female	15
P. berghei (NK65)	C57BL/6	GAP ΔPKG	Female	16
P. berghei (ANKA)	C57BL/6; μMT	CPS-AZ, CPS-CM	Female	17

Supplemental Table 4.1: Was mouse sex listed in key papers about murine sporozoite vaccines?

References from Nganou-Makamdop and Sauerwein[18] with respect to whether or not biological sex of the mice were noted by reviewed paper.

1 Purcell, L. A. *et al.* Chemically attenuated *Plasmodium* sporozoites induce specific immune responses, sterile immunity and cross-protection against heterologous challenge. *Vaccine* **26**, 4880-4884, doi:10.1016/j.vaccine.2008.07.017 (2008).

2 Belnoue, E. *et al.* Protective T cell immunity against malaria liver stage after vaccination with live sporozoites under chloroquine treatment. *J Immunol* **172**, 2487-2495, doi:10.4049/jimmunol.172.4.2487 (2004).

3 Schmidt, N. W., Butler, N. S., Badovinac, V. P. & Harty, J. T. Extreme CD8 T cell requirements for anti-malarial liver-stage immunity following immunization with radiation attenuated sporozoites. *PLoS Pathog* **6**, e1000998, doi:10.1371/journal.ppat.1000998 (2010).

4 Aly, A. S., Lindner, S. E., MacKellar, D. C., Peng, X. & Kappe, S. H. SAP1 is a critical post-transcriptional regulator of infectivity in malaria parasite sporozoite stages. *Mol Microbiol* **79**, 929-939, doi:10.1111/j.1365-2958.2010.07497.x (2011).

5 Aly, A. S. *et al.* Targeted deletion of SAP1 abolishes the expression of infectivity factors necessary for successful malaria parasite liver infection. *Mol Microbiol* **69**, 152-163, doi:10.1111/j.1365-2958.2008.06271.x (2008).

6 Butler, N. S. *et al.* Superior antimalarial immunity after vaccination with late liver stage-arresting genetically attenuated parasites. *Cell Host Microbe* **9**, 451-462, doi:10.1016/j.chom.2011.05.008 (2011).

7 Tarun, A. S. *et al.* Protracted sterile protection with *Plasmodium* yoelii pre-erythrocytic genetically attenuated parasite malaria vaccines is independent of significant liver-stage persistence and is mediated by CD8+ T cells. *J Infect Dis* **196**, 608-616, doi:10.1086/519742 (2007).

8 Trimnell, A. *et al.* Genetically attenuated parasite vaccines induce contact-dependent CD8+ T cell killing of *Plasmodium* yoelii liver stage-infected hepatocytes. *J Immunol* **183**, 5870-5878, doi:10.4049/jimmunol.0900302 (2009).

9 Douradinha, B. *et al.* Genetically attenuated P36p-deficient *Plasmodium berghei* sporozoites confer long-lasting and partial cross-species protection. *Int J Parasitol* **37**, 1511-1519, doi:10.1016/j.ijpara.2007.05.005 (2007).

10 van Dijk, M. R. *et al.* Genetically attenuated, P36p-deficient malarial sporozoites induce protective immunity and apoptosis of infected liver cells. *Proc Natl Acad Sci U S A* **102**, 12194-12199, doi:10.1073/pnas.0500925102 (2005).

11 Friesen, J. & Matuschewski, K. Comparative efficacy of pre-erythrocytic whole organism vaccine strategies against the malaria parasite. *Vaccine* **29**, 7002-7008, doi:10.1016/j.vaccine.2011.07.034 (2011).

12 Nganou-Makamdop, K., van Gemert, G. J., Arens, T., Hermsen, C. C. & Sauerwein, R. W. Long term protection after immunization with *P. berghei* sporozoites correlates with sustained IFNgamma responses of hepatic CD8+ memory T cells. *PLoS One* **7**, e36508, doi:10.1371/journal.pone.0036508 (2012).

13 Silvie, O., Goetz, K. & Matuschewski, K. A sporozoite asparagine-rich protein controls initiation of *Plasmodium* liver stage development. *PLoS Pathog* **4**, e1000086, doi:10.1371/journal.ppat.1000086 (2008).

14 Putrianti, E. D., Silvie, O., Kordes, M., Borrmann, S. & Matuschewski, K. Vaccine-like immunity against malaria by repeated causal-prophylactic treatment of liver-stage *Plasmodium* parasites. *J Infect Dis* **199**, 899-903, doi:10.1086/597121 (2009).
15 Purcell, L. A., Yanow, S. K., Lee, M., Spithill, T. W. & Rodriguez, A. Chemical attenuation of *Plasmodium berghei* sporozoites induces sterile immunity in mice. *Infect Immun* **76**, 1193-1199, doi:10.1128/IAI.01399-07 (2008).
16 Falae, A. *et al.* Role of *Plasmodium berghei* cGMP-dependent protein kinase in late liver stage development. *J Biol Chem* **285**, 3282-3288, doi:10.1074/jbc.M109.070367 (2010).
17 Friesen, J. *et al.* Natural immunization against malaria: causal prophylaxis with antibiotics. *Sci Transl Med* **2**, 40ra49, doi:10.1126/scitranslmed.3001058 (2010).
18 Nganou-Makamdop, K. & Sauerwein, R. W. Liver or blood-stage arrest during malaria sporozoite immunization: the later the better? *Trends Parasitol* **29**, 304-310, doi:10.1016/j.pt.2013.03.008 (2013).

Marker	Fluorochrome	Clone	Source	Catalog	Titer (in 50 µL MM)
Live/Dead	Zombie yellow		Biolegend		1:250
CD3E	BUV395	145-2C11	BD Bioscience	563565	1 µL
B220	BV711	RA3-6B2	Biolegend	103255	0.25µL
CD4	BB700	GK1.5	BD Bioscience	745922	0.5µL
CD8a	APC-H7	53-6.7	BD Bioscience	560182	0.5µL
CD44	BUV737	IM7	BD Bioscience	612799	0.5µL
CD62L	PE-CY7	MEL-14	BD Bioscience	560516	0.5µL
CD69	BV786	H1-2F3	BD Bioscience	564683	1µL
CXCR3	BV650	CXCR3-173	BD Bioscience	740630	1µL
PD1	PE/DAZZLE594	29F.1A12	Biolegend	135228	0.5µL
LAG3	BB515	C9B7W	BD Bioscience	564672	0.5µL
TCF1	BV421	S33-966	BD Bioscience	566692	1µL
CD107a	PE	1D4B	BD Bioscience	558661	0.5µl (in 200µL MM)
IFNG	BV421	XMG1.2	Biolegend	505830	1µL
TNFa	FITC	MP6-XT22	BD Bioscience	554418	1µL
Granzyme B	AF647	GB11	BD Bioscience	560212	0.5µL
CSP-tetramer	APC		NIH tetramer facility		1µL

Supplemental Table 4.2: Flow cytometry antibody manifest.

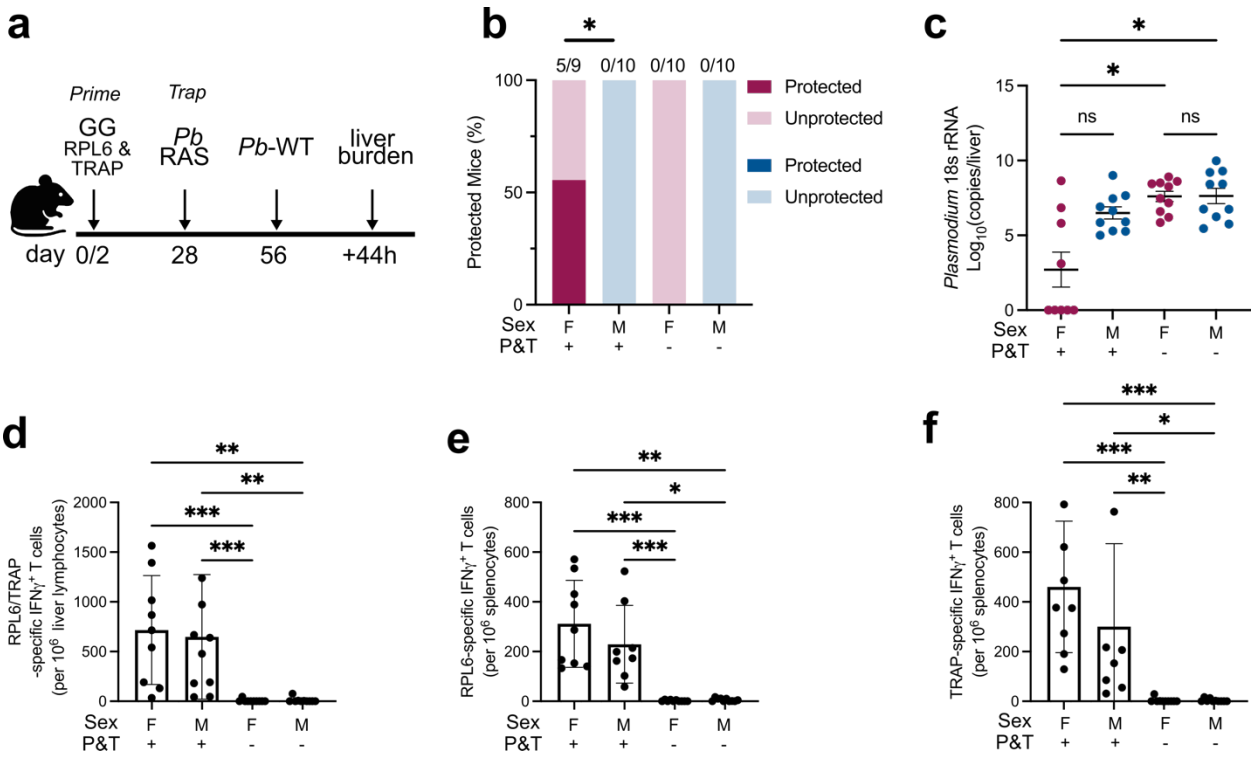

Supplemental Figure 4.9: Prime-and-Trap malaria vaccination induces sex-specific protection against sporozoite challenge in a *Plasmodium berghei* and C57BL/6 rodent malaria model. a. Scheme of male and female C57BL/6 mice Prime-and-Trap (P&T) vaccination experiment. b. Protection following $1x10^3$ *Py*-WT sporozoite challenge defined as no detectable pan-*Plasmodium* 18S rRNA copies 44 hours post-challenge. c. Liver burden as absolute pan-*Plasmodium* 18S rRNA copy numbers 44 hr post-challenge. d - f. Liver and spleen were harvested from the mice at the 44 hours post-challenge timepoint and IFN-γ ELISPOT was performed in the presence of either RPL6 peptide (e), TRAP peptide (f), or both (d). IFN-γ spot forming units (SFU) are shown per million liver (d) and spleen (e-f) lymphocytes for each mouse normalized to the corresponding media control. Error bar are mean normalized SFU per million lymphocytes ± s.e.m. n= 9 -10 mice across two independent experiments. Statistical significance for data in b was determined by the Fisher exact test. Only relevant comparisons are shown. Statistical significance for data in c - f was determined by the Kruskal-Wallis test with Dunn's multiple comparison. Error bar represents mean ± s.e.m; ***p<0.001, **p<0.01, *p<0.05, ns p>0.05.

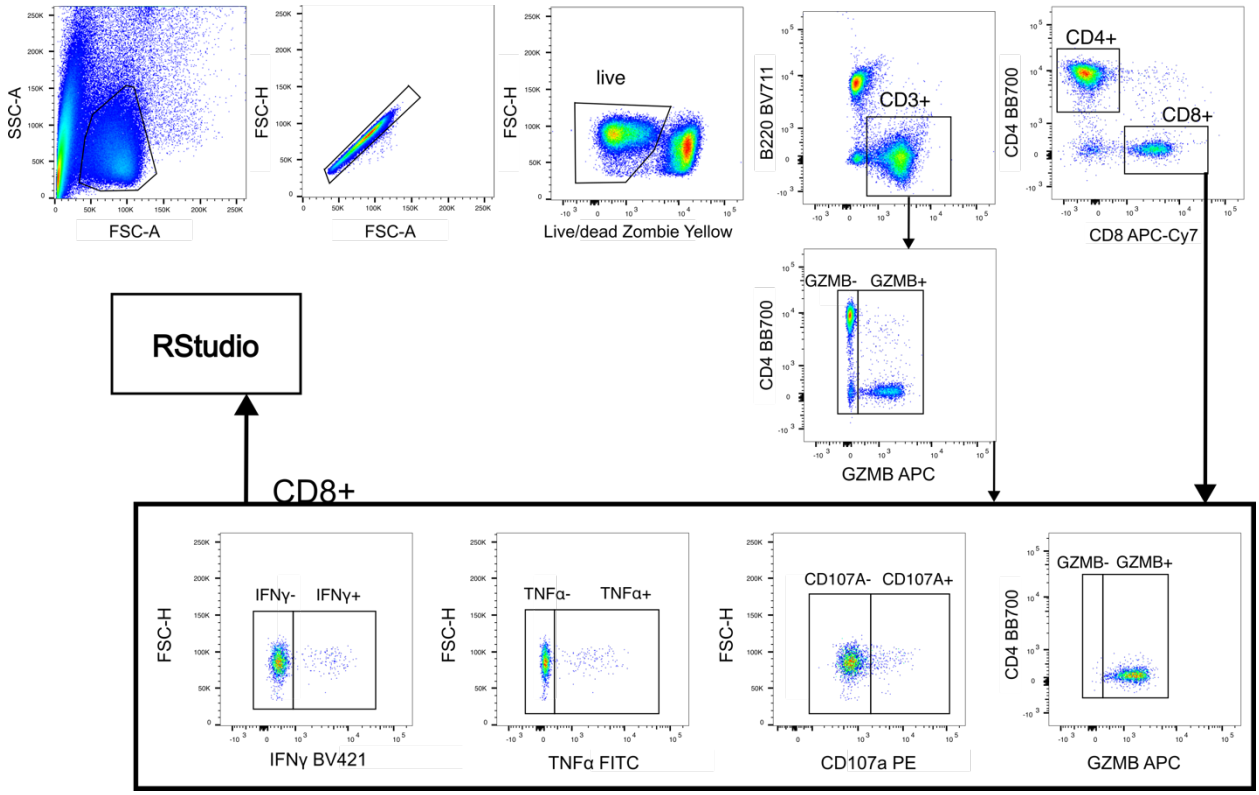

Supplemental Figure 4.10. Gating strategy for T cell Intracellular Cytokine Staining. Data in Figures 2 (b-i), 4 (d-g and l-m), and 6 were obtained using a 9-color multiparameter flow cytometry panel following intracellular cytokine staining (ICS). Events were selected using a lymphocyte gate, then a singlet event gate, and then a live/dead stain. CD3 and B220 were next used to identify T cells and exclude B cells. $CD3^+$ cells were subsequently evaluated for either granzyme B (GZMB) or for CD4 and CD8. $CD8^+$ cells were further chracterized for expression of IFN-γ, TNF-α, and the CD107a degranulation marker. Further downstream heiracheal and boolean gating was performed in RStudio.

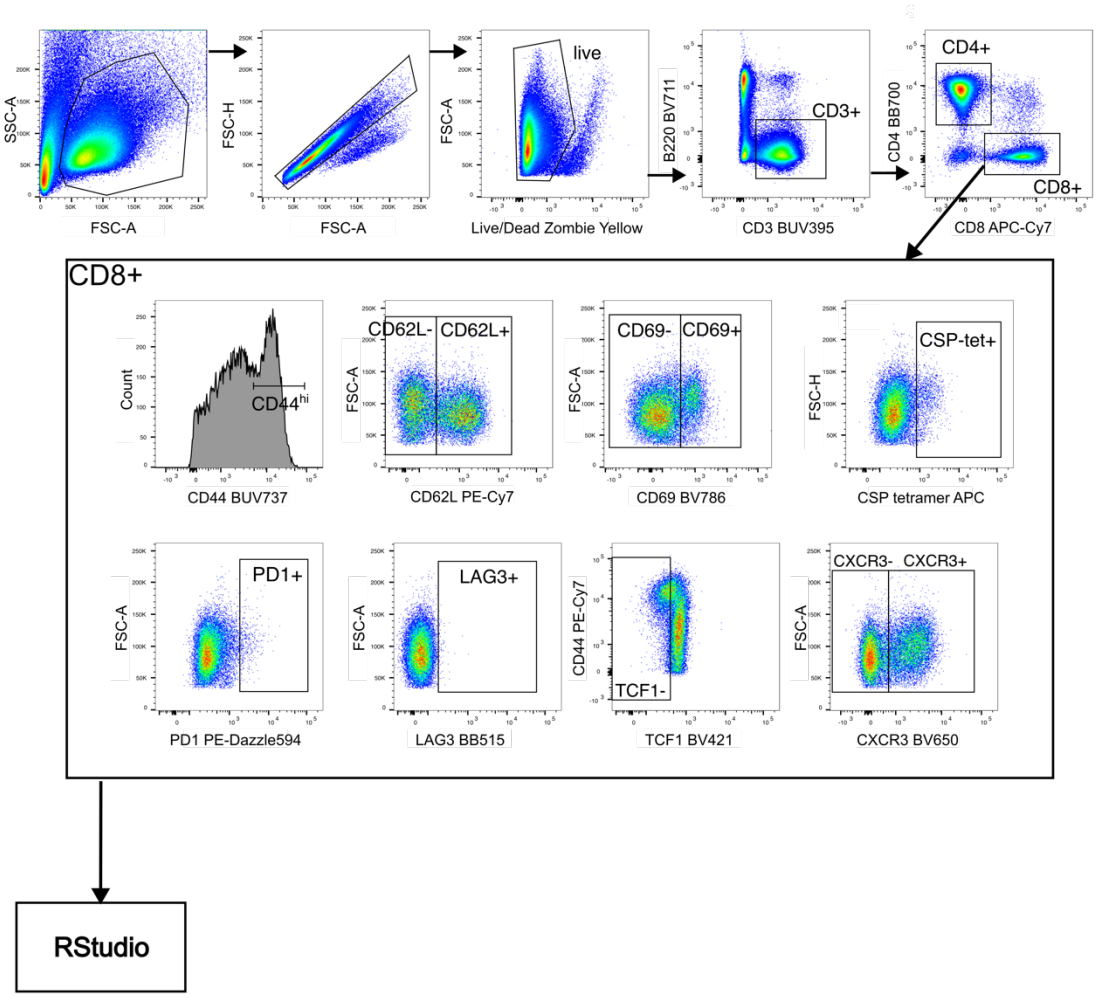

Supplemental Figure 4.11. Gating strategy for T cell flow cytometry. Data presented in Figures 2 (j-l), and 4 (h-k) were obtained using a 13-color multiparameter flow cytometry panel. Events were selected using a lymphocyte gate, then a singlet event gate, and then a live/dead stain. CD3 and B220 were next used to identify T cells and exclude B cells. $CD3^+$ cells were gated for CD4 and CD8 co-receptor expression. For $CD8^+$ populations, cell were further characterized for expression of CD44, CD62L, CD69, CSP-tetramer, LAG-3, PD-1, TCF1, and CXCR3. Further downstream heiracheal gating was performed in RStudio.

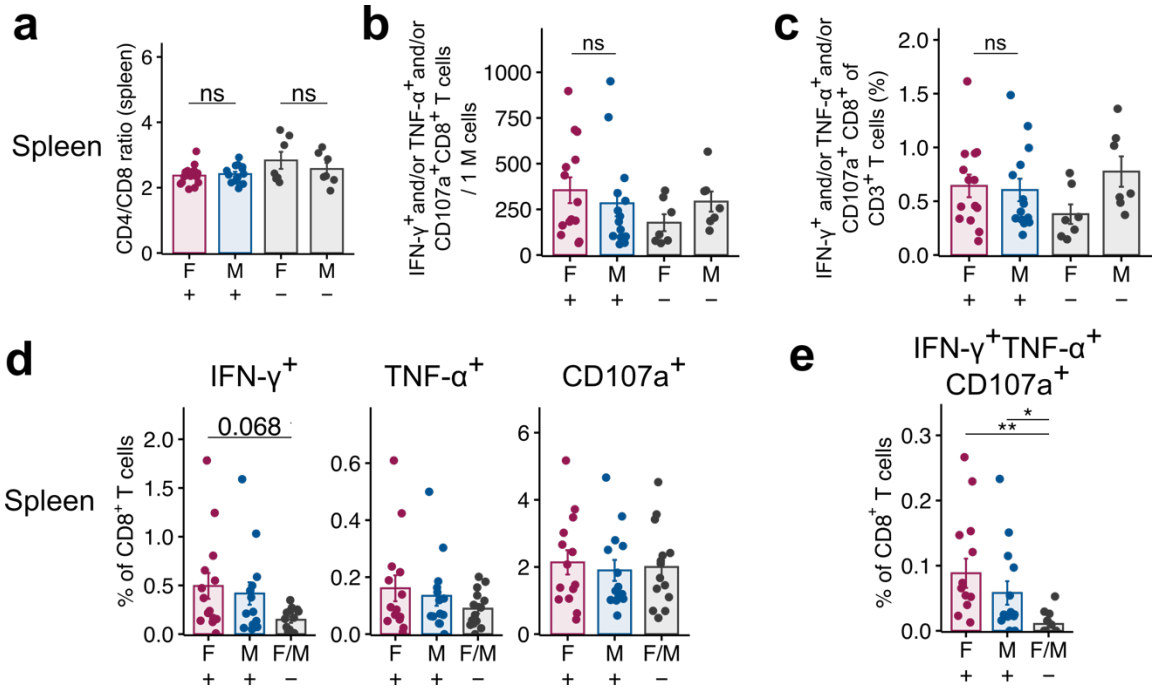

Supplemental Figure 4.12: Evaluation of vaccine-induced CD8$^+$ T cells in the spleen between males and females. Female and male BALB/cJ mice were vaccinated with the prime-and-trap (P&T) regimen. 28 days later, spleen cells were analyzed by flow cytometry. a. Ratio of CD4-to-CD8 in the spleen of P&T vaccinated (+) and unvaccinated mice (-) female (F) and male (M) BALB/cJ mice. b-c. Quantification of total CSP^{280}-specific CD8$^+$ T cells as total number of IFN-γ$^+$ and/or TNF-α$^+$ and/or CD107a$^+$ producing CD8$^+$ T cells per million splenocytes (b) and as a proportion of CD3$^+$ splenic T cells (c). d-e. Quantification of proportion of IFN-γ$^+$ (d - left), TNF-α$^+$ (d - middle), CD107a$^+$ (d - right) and IFN-γ$^+$ TNF-α$^+$ CD107a$^+$ (e) producing CD8$^+$ T cells in the spleen. Error bars are mean ± s.e.m. Statistical significance for data was determined by Kruskal-Wallis tests with Dunn's multiple comparison; **p<0.01, *p<0.05, ns p>0.05.

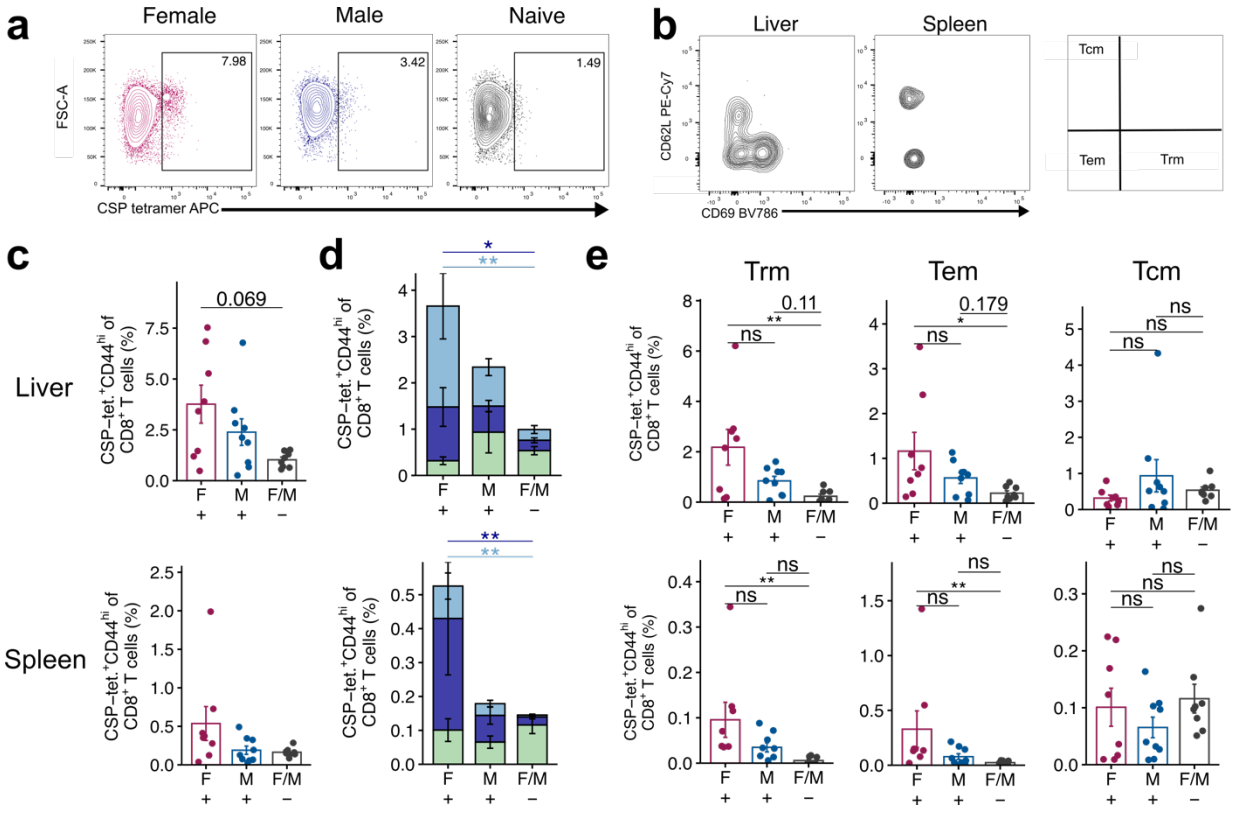

Supplemental Figure 4.13: Extended evaluation sex differences in CD8$^+$ T cells memory subsets. a. Representative flow cytometry plot (gated on CD8$^+$ T cells) depicting H-2K^d-PyCSP$^{280\text{-}288}$ tetramer positive (CSP-tet.$^+$) cells isolated from the liver of P&T vaccinated female (left) and male (middle) mice and an unvaccinated control mouse collected 28 days after the last immunization. b. Representative flow cytometry plot depicting CSP-tet.$^+$CD44^{hi} CD8$^+$ T cells Trm, Tem, and Trm phenotypes. Gating calculations performed in R. See Supplemental Fig S3 for gating tree. c. Frequency of CSP-tet.$^+$CD44^{hi} cells of CD8$^+$ T cells in livers (top) and spleens (bottom). d-e. Frequency of CSP tet.$^+$CD44^{hi} memory subsets, Trm (CD62L$^-$CD69$^+$; left), Tem (CD62L$^-$CD69$^+$; middle), Tcm (CD62L$^+$CD69$^-$; right), of total CD8$^+$ T cell in livers (top – also depicted in Fig 2k) and spleens (bottom). Data are shown from two independent experiments (n= 8-9). Error bar represents mean ± s.e.m. Statistical significance for data was determined by Kruskal-Wallis test with Dunn's multiple comparison. Individual p values for significant differences are shown, colored to correspond to memory T cell subsets where relevant; **p<0.01, *p<0.05, ns p>0.05.

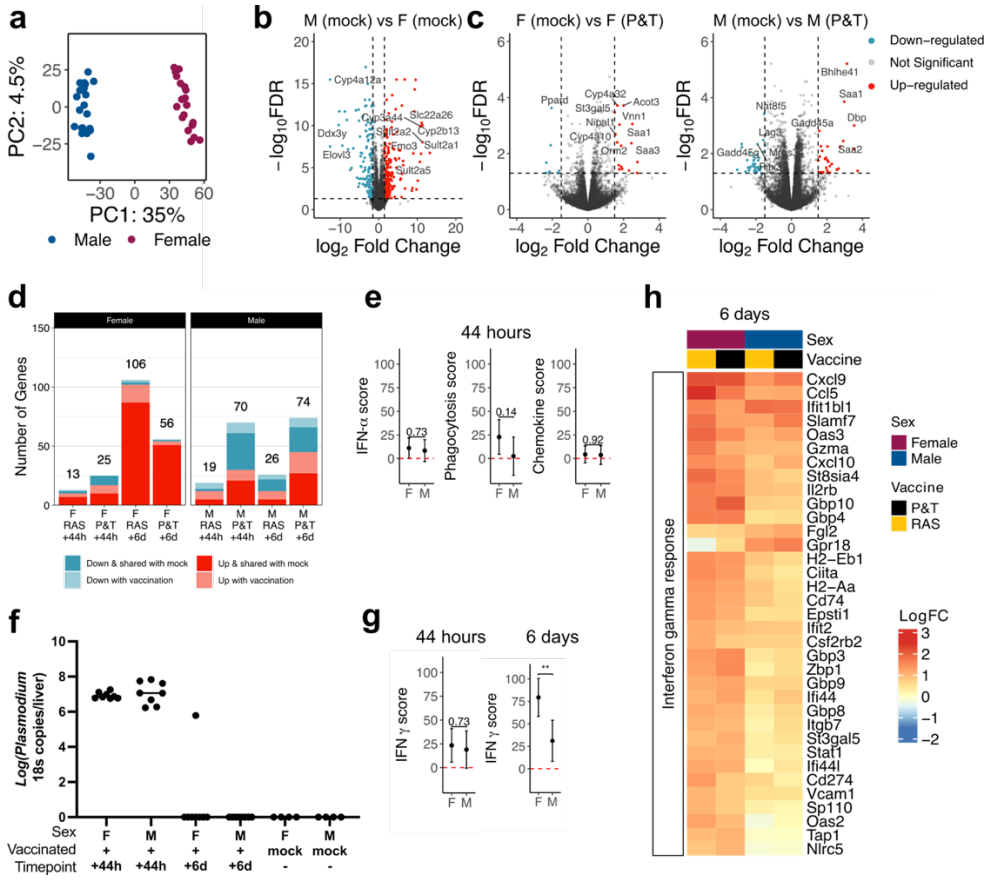

Supplemental Figure 4.14: Male mice experience a restricted inflammatory response compared to females after Radiation Attenuated Sporozoite (RAS) immunization (extended). a. Principal Component (PC) plot after exclusion of sex-chromosome-linked genes of male and female transcriptomes following RAS immunization. b - c. Volcano plot of differentially expressed genes between mock-injected male and female mice (b), P&T vaccinated female and mock females (c - left), and P&T vaccinated males and mock-injected males (c – right). Red indicates genes up-regulated in female and blue indicates genes down-regulated relative to male mock (b, c - right) to female mock (c – left) with FDR < 0.05 and |LogFC| > 1.5. The top ten most significant differentially expressed genes are depicted. d. Depiction of number of differentially expressed genes for each comparison (FDR < 0.05 and |LogFC| > 1.5). Dark blue and dark red indicate down-regulated and up-regulated genes that are unique to the response to sporozoites respectively. Light blue and light red indicate genes that are also differentially expressed between mock male and female mice. e. Pathway score of aggregate samples by Interferon-α response, phagocytosis, and response to chemokines pathways at 44 hours post-immunization. f. Livers dissected for RNAseq were processed for *Plasmodium* 18S rRNA reverse transcription polymerase chain reaction (RT-PCR) to measure parasite burden. Data are shown as absolute 18S rRNA $\log_{10}$ copy numbers per liver. g. Pathway score of aggregate samples by Interferon-γ pathways at 44 hours (left) and 6 days (right) post-immunization. h. Heatmap and hierarchal clustering of genes that contain at least one differentially expressed gene at the 6 day timepoint (BH-adjusted p <0.05, |LogFC| > 1) and appear in the Hallmark 'Interferon-γ response'. Column annotations depict biological sex and vaccine status. Error bars in e and g represent 95% confidence intervals. **p<0.01, *p<0.05, ns p>0.05.

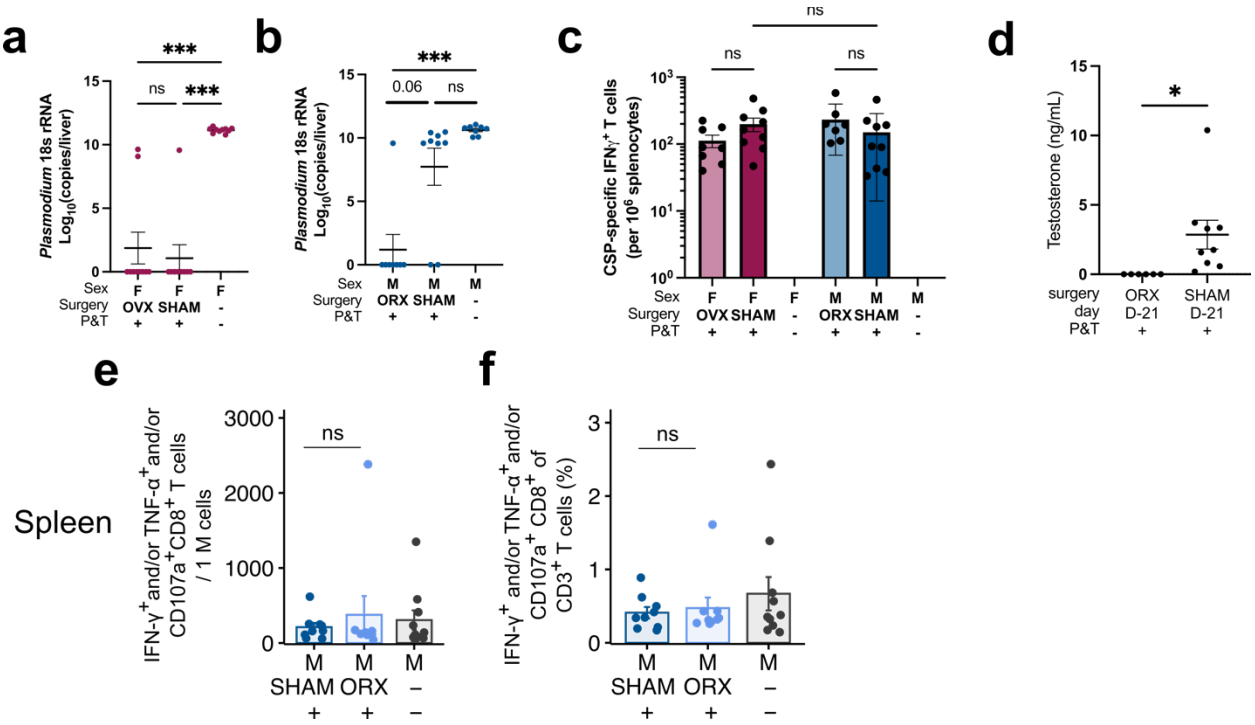

Supplemental Figure 4.15: Further evaluation the impact of ORX and OVX on splenic CD8$^+$ T cells. a. Liver burden values from Fig 4a-b as absolute pan-*Plasmodium* 18S rRNA copy numbers 44 hr post-challenge. Data are shown from two independent experiments (n = 8 - 10/group). Spleens were harvested from a subset of the mice in Fig. 4a-c at the 44 hours post-challenge timepoint and IFN-γ ELISPOT was performed in the presence of CSP$^{280-288}$ peptide. IFN-γ spot forming units (SFU) are shown per million splenocytes for each mouse normalized to the corresponding media control. Error bar are mean normalized SFU per million splenocytes ± s.e.m. n=6-9 mice across two independent experiments. d. Confirmatory testosterone measurements in serum by ELISA of a subset of mice in Fig 4c. e. ICS quantification of total CSP responsive CD8$^+$ T cells as total IFN-γ$^+$ and/or TNF-α$^+$ and/or CD107a$^+$ producing CD8$^+$ T cells per million splenocytes (e) and as proportion of splenic CD3$^+$ T cells (f). Data for e-f are shown from two independent experiments (n = 9-10/group). Error bars are mean ± s.e.m. Statistical significance for data in a-c and e-f was determined by Kruskal-Wallis test with Dunn's multiple comparison and data in d was evaluated with unpaired Wilcoxon Test; ***p<0.001, **p<0.01, *p<0.05, ns p>0.05.

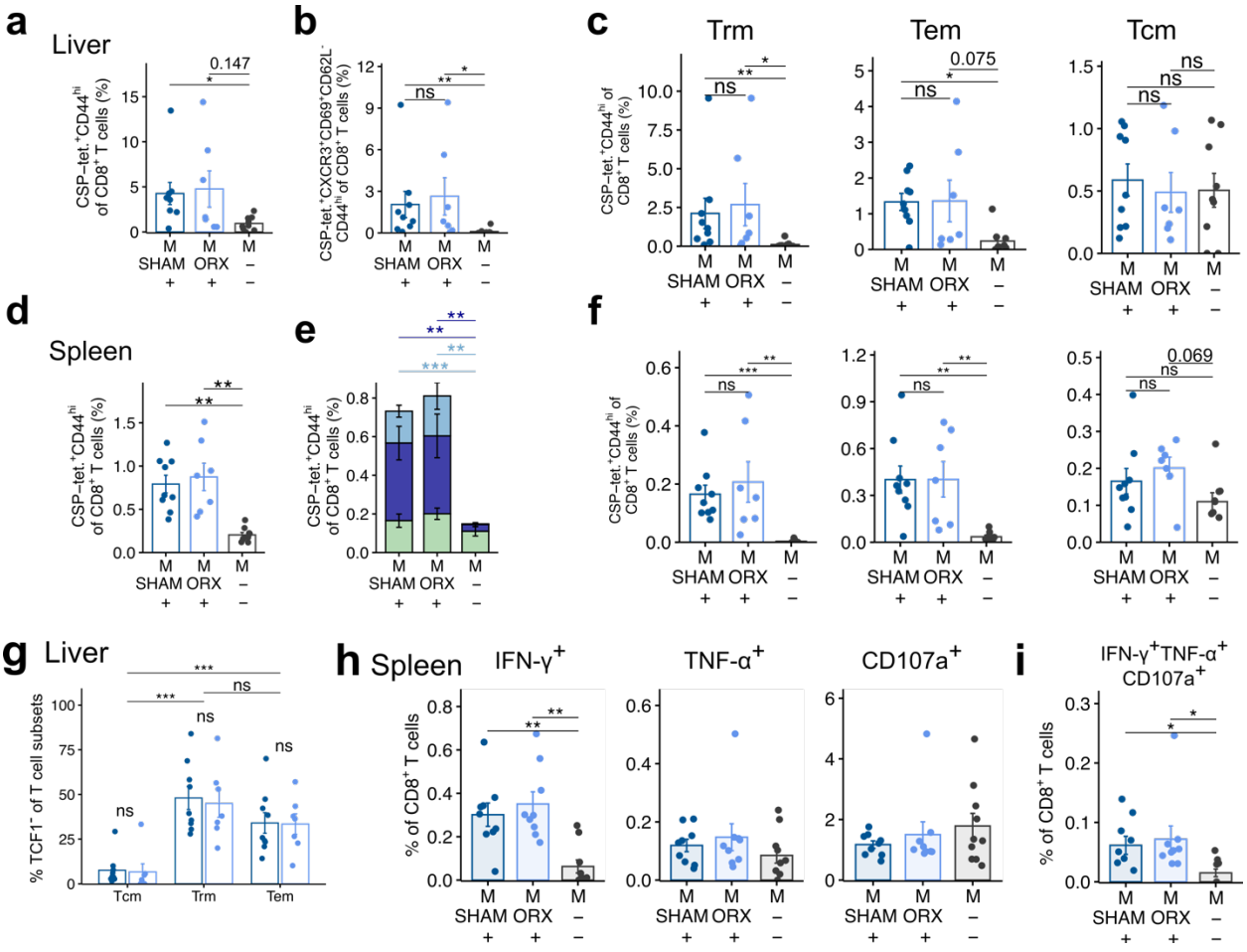

Supplemental Figure 4.16: Further evaluation of impact of ORX on CD8$^+$ T cell fate in male mice. ORX- or SHAM-operated male BALB/cJ mice were vaccinated by the P&T regimen. 28 days later, liver and spleen lymphocytes were analyzed by flow cytometry. a and d. Frequency of CSP tetramer$^+$CD44^{hi} cells of CD8$^+$ T cells in the liver (a) and the spleen (d). b - c and e - f. Frequency of CSP tetramer$^+$CD44^{hi} Trm (CXCR3$^+$CD62L$^-$CD69$^+$- b; CD62L$^-$CD69$^+$- c and f), Tem (CD62L$^-$CD69$^+$), Tcm (CD62L$^+$CD69$^-$) subsets of total CD8$^+$ T cell in the liver (b-c) and spleen (e-f). g. Quantitative evaluation of proportion of TCF1$^-$ on CSP-tet.$^+$CD44^{hi} CD8 T cells phenotypically defined as Trm, Tem, and Tcm cells in the liver. Data are shown from two independent experiments (n = 7-10/group). h. Quantification of proportion of IFN-γ$^+$ (left), TNF-α$^+$ (middle), CD107a$^+$ (right), and IFN-γ$^+$ TNF-α$^+$ CD107a$^+$ (i) producing CD8$^+$ T cells in the spleen. Data for h-i are shown from two independent experiments (n = 9-10). Statistical significance for data in a-f, h-i and between T cell memory phenotypes in g was determined by Kruskal-Wallis tests with Dunn's multiple comparison and data between SHAM and ORX within a T cell memory phenotype in g was evaluated with Wilcoxon Test; ***p<0.001, **p<0.01, *p<0.05, ns p>0.05.

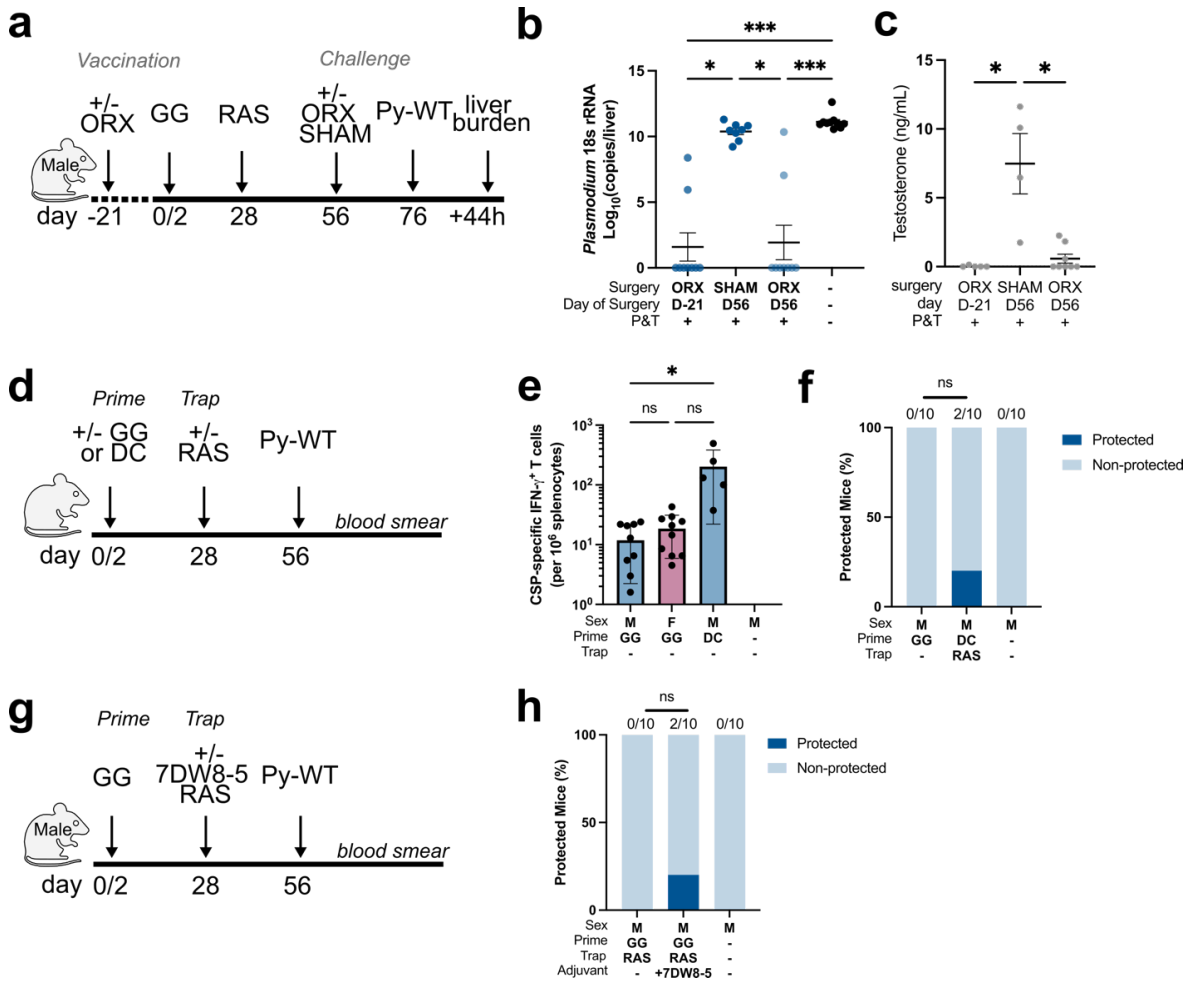

Supplemental Figure 4.17: Enhancing P&T vaccination does not overcome hormone environment. a. Schedule of orchiectomy (ORX) in male mice 21 days before or 28 days after P&T vaccination as shown. After the completion of vaccinations, mice were rested 21 days to establish a new hormone equilibrium and then were challenged with 1x10^3 *Py*-WT sporozoites. b. Liver burden values from Fig 5b as absolute pan-*Plasmodium* 18S rRNA copy numbers 44 hr post-challenge. Data are shown from two independent experiments (n= 9-10/group). c. Confirmatory testosterone measurements in serum by ELISA of a subset of mice in Fig 5b. d. Male and female BALB/cJ mice were vaccinated with gene gun (GG) CSP DNA vaccination alone or left as naïve mice or primed with CSP peptide-pulsed dendritic cells (DC) followed by 2x10^4 radiation attenuated sporozoites (RAS), or remained naïve to RAS. e. CSP-specific IFN-γ+ T cells in the spleen by ELISPOT on samples collected 28 days following priming steps. Data shown are from 1-2 experiments. f. Percentages of mice protected against challenge with 1x10^3 *Py*-WT sporozoites by blood smears through 14 days post-challenge. g. P&T vaccination with the addition of the glycolipid adjuvant 7DW8-5 to the RAS trapping step. h. Percentages of mice protected against challenge with 1x10^3 *Py*-WT sporozoites by blood smears through 14 days post-challenge. Data are shown from two independent experiments (n= 10/group). Statistical significance for data in f and h was determined by the Fisher exact test. Only relevant comparisons are shown. Statistical significance for data in b-c, and e was determined by the Kruskal-Wallis test with Dunn's multiple comparison. Error bar represents mean ± s.e.m; ***p<0.001, **p<0.01, *p<0.05, ns p>0.05.

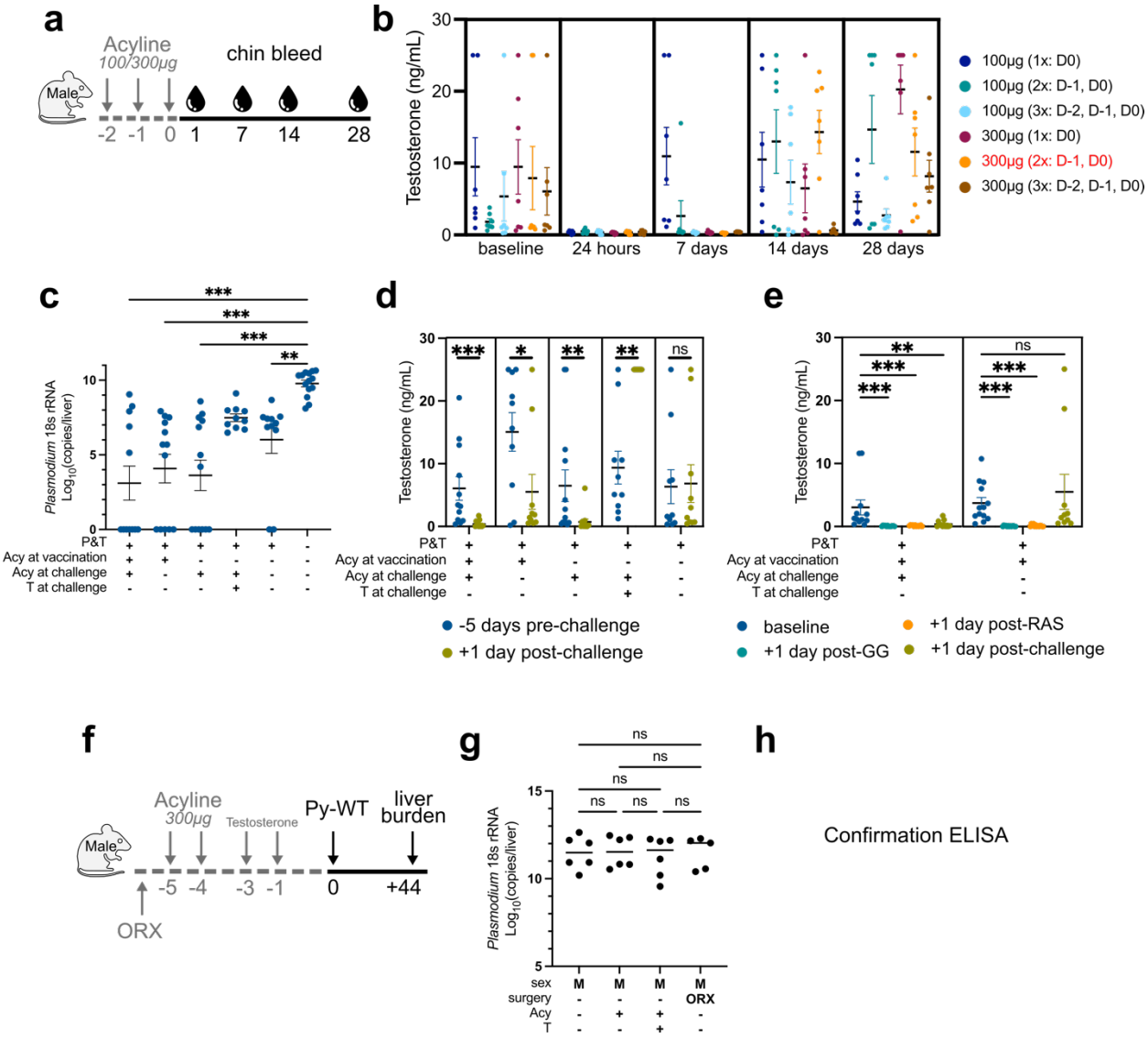

Supplemental Figure 4.18: Acyline as a model for acute, reversible reduction of testosterone levels. a - b. Male mice received one or multiple doses of 100µg or 300µg Acyline and were monitored for testosterone levels measured by ELISA up to 28 days post last dose. c. Liver burden values from Fig 5c as absolute pan-*Plasmodium* 18S rRNA copy numbers 44 hr post-challenge. d-e Confirmatory testosterone measurements by ELISA of the mice in Figure 5d. f. Male mice either were orchiectomized (ORX), received Acyline and/or testosterone, or left untreated, then challenged with 1000 *Py*-WT spz. g. Liver burden as absolute pan-*Plasmodium* 18S rRNA copy numbers 44 hr post-challenge. h. Confirmatory testosterone measurements by ELISA of mice in Fig S10g. Statistical significance for data in c, e, and g-h was determined by the Kruskal-Wallis test with Dunn's multiple comparison; data in d was determined by a paired Wilcoxon Test. No statistical test was conducted for b due to an observatory readout. Error bar represents mean ± s.e.m; ***p<0.001, **p<0.01, *p<0.05, ns p>0.05.

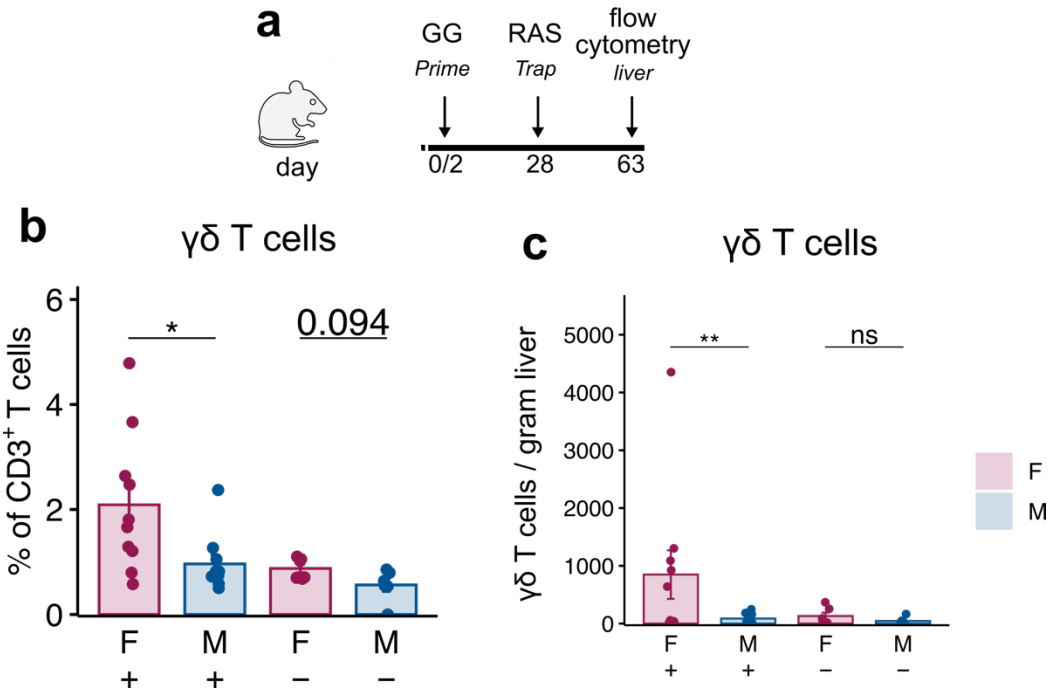

Supplemental Figure 4.19: Female mice have increased number of γδ T cells following vaccination. a. Female and male BALB/cJ mice were vaccinated with the prime-and-trap (P&T) regimen. 35 days later, liver cells were analyzed by flow cytometry. b-c. Quantification of γ/δ T cells defined by total number of γδ TCR^+ as proportion of $CD3^+$ T cells (b) and per gram of liver (c). Data are shown from 2 independent experiments (n = 10-6 total mice/group). Statistical significance for data in b-c was determined by a paired Wilcoxon Test; ***p <0.001, **p<0.01, *p<0.05, ns p>0.05.

Chapter 5. DISCUSSION AND CONCLUSIONS

5.1 SUMMARY OF FINDINGS

Understanding the heterogeneity in host responses to pathogens and vaccines is essential for designing interventions effective across diverse populations. Until recently, there was a knowledge gap in how biological sex – through sex hormones, sex chromosomes, and physiology – influences the *Plasmodium* liver stage (**Figure 5.1**). Two key observations underpin this gap: 1) The liver is a sexually dimorphic organ[71,241,310], and 2) *Plasmodium* parasites are hepatotropic and interact dynamically with their microenvironment during liver stage infection[136,150,156]. To fill this gap, we hypothesized that biological sex alters the *Plasmodium* liver stage. We then tested this in humans and mice and contributed to substantially new knowledge about how biological sex mediates the host response to *Plasmodium* parasites.

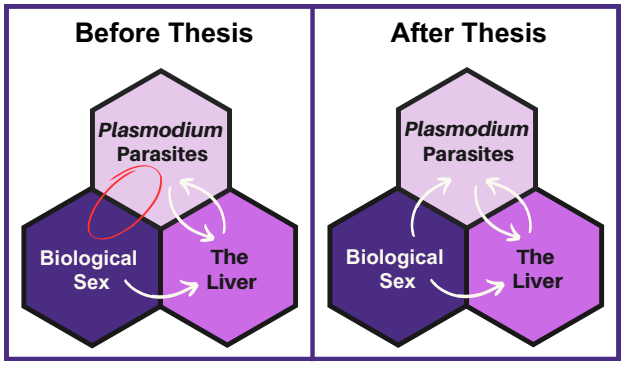

Figure 5.1: State of the literature before and after this thesis is published.

This thesis demonstrates that male humans experience a delayed liver stage infection compared to females (**Chapter 2**). In contrast, male mice show an increased liver burden, attributed to enhanced parasite survival due to restricted innate immune responses, with this effect influenced by androgens (**Chapter 3**). Additionally, our work identified sex differences in liver stage vaccine protection, linked to the presence of androgens, and uncovered the mechanisms through which androgens alter memory $CD8^+$ T cell responses (**Chapter 4**). Through these studies, we revealed a cascade of sex-specific host responses, shaped by baseline differences and amplified

throughout different stages of the host-parasite interaction – from primary *Plasmodium* infection in the liver, to vaccination with attenuated spz-based vaccines, and to secondary infection during challenge (See **Figure 5.2** for a summary). At each stage, biological sex through sex hormones modifies host responses critical for innate and adaptive control of *Plasmodium* liver stage infection.

In this discussion, we will explore the implications and limitations of these findings. Here we will discuss sex differences between mice and humans (**Chapter 5.2**), implications for liver stage vaccine development (**Chapter 5.3**), interpretations from the endocrinologist perspective (**Chapter 5.4**), and lessons learned from studying biological sex with omics-based data (**Chapter 5.5**). We will also address future research directions throughout each section.

5.2 CONNECTING SEX DIFFERENCES IN MICE AND MEN

At first glance, the sex-based differences in the duration of the human liver stage appear to contradict those observed in murine models. In humans, males are 3.7 times more likely to experience ***delayed parasitemia***, suggesting decreased parasite survival in the liver. Conversely, in mice, males exhibit a ***higher liver parasite burden***, which is associated with increased parasite survival in the liver. The apparent discordance between the trends observed in mice and humans may stem from fundamental differences in host-parasite interactions between these species. Rodent malaria models are widely used to understand *Plasmodium* biology and inform intervention strategies for humans. Comparing these models highlights both similarities and differences, which can provide insights into the sex-based variations observed in humans and mice.

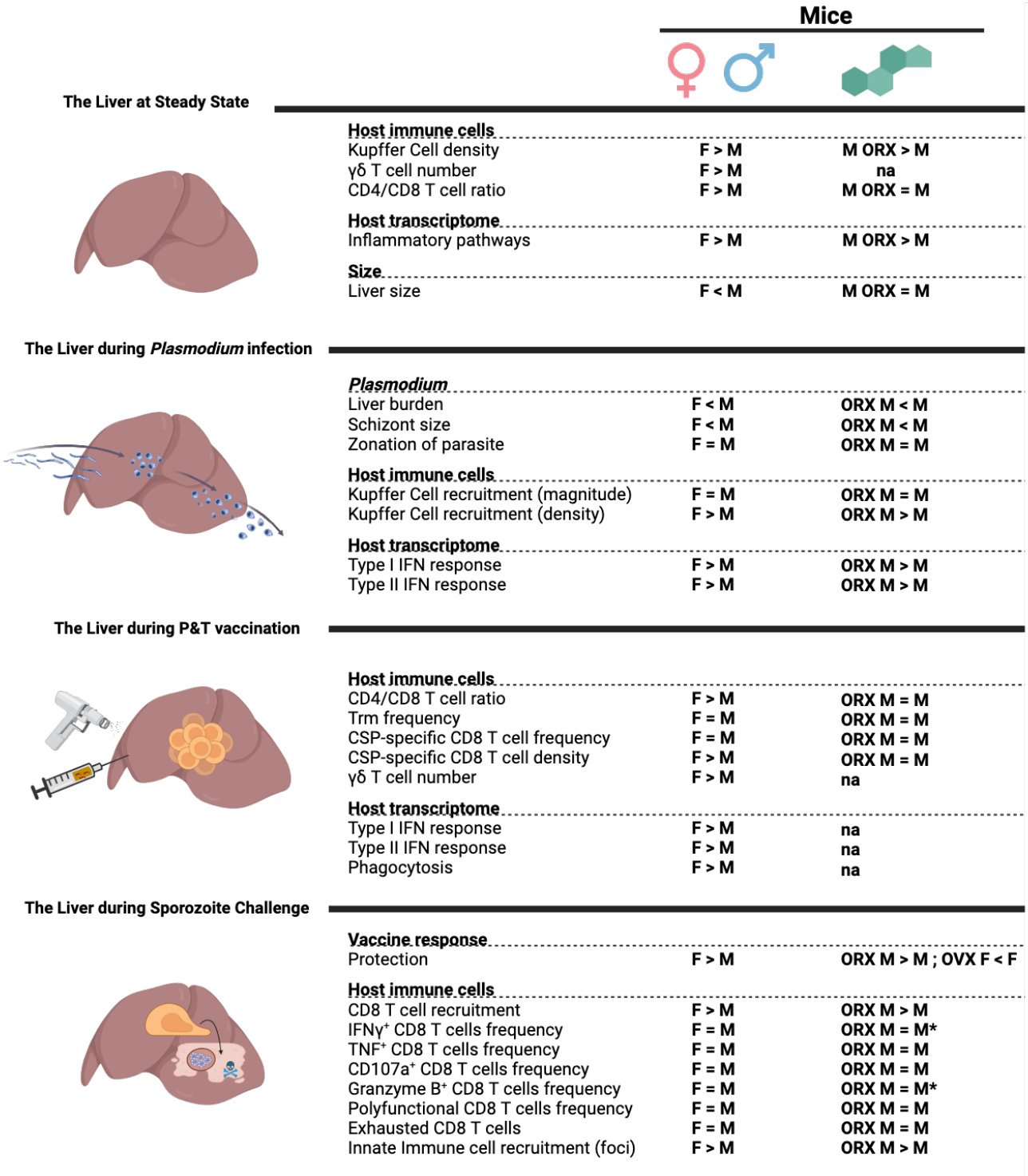

Figure 5.2: Summary of thesis findings in mice. This figure summarizes the main immunological findings on the impact of biological sex and sex hormones across four stages of the *Plasmodium* liver stage in mice: (1) the liver at steady state (baseline); (2) the liver during *Plasmodium* infection; (3) the liver during vaccination; and (4) the liver during sporozoite

challenge. Findings from human studies have also been integrated for additional context. Created with BioRender.com.

This section first calls attention to the limitations of the murine model in representing human biology, focusing on differences in sex hormones, liver biology, immune systems, and *Plasmodium* strains and vaccine dosage. Next, we explore how these differences can be leveraged to inform our understanding of potential underlying biology in humans. Finally, we propose future research directions to deepen understanding of biological sex in malaria biology and bridge the translational gap between murine models and human studies.

Differences in sex hormones

Connecting sex-based differences in mice to those in humans requires a nuanced understanding of their respective endocrine systems, particularly regarding sex hormones. While both species produce the same types of sex hormones, their concentrations vary by age and sex[311]. Male mice, on average, have higher testosterone levels than humans, whereas female mice and humans exhibit similar estradiol (E2) concentrations[311]. Differences in tissue availability of sex hormones arise due to species-specific production of sex hormone-binding globulin (SHBG), which regulates bioactive hormone levels[312]. Interestingly, although the SHBG gene is present in all mammals, adult rats and mice do not express or secrete SHBG from their liver cells, resulting in the absence of circulating SHBG in adult male mice[313]. Additional differences include the length of the female estrous cycle — 4–7 days in mice versus 28 days in humans[314]—and the pulsatile testosterone release cycle, which occurs in both species but at different frequencies[7,315]. Despite these differences, no time-dependent effects on susceptibility or protection during liver-stage malaria challenges were observed in mice (unpublished observation). This suggests that acute

hormone fluctuations may play a limited role, whereas prolonged hormonal changes may be more relevant for aligning human and murine sex hormone dynamics.

The limitation in natural steady state between murine and human endocrine system is further exacerbated under hormone manipulation methods employed here in this thesis. The methods developed and employed here in the thesis are three-fold: surgical (orchiectomy and ovariectomy), chemical (acyline as a gonadotropin antagonist), and supplemental (T, DHT & E2 reintroduction via pellets and injections). All of these methods overwhelm the system with either complete removal or supraphysiological hormone levels to that beyond natural steady state. While these methods are useful to determine the effect of sex hormones at the extreme, they are not exact parallel models to natural hormone fluctuations in humans over their lifespan, from infancy to puberty to adulthood to old age. This disparity could be especially pronounced in the liver, where evidence suggests sex hormone storage may occur. For example, one study demonstrated that castration had no effect on the bioactive DHT levels in the liver, even as T and DHT levels in the serum decreased, as expected[316]. Given that sex hormones have an effect beyond just the liver, reproducing natural concentrations and cycle patterns would allow for identification of parallel processes in humans. Overall, while there are notable similarities and differences in sex hormone concentrations and regulation between mice and humans, the largest limitation remains the lack of liver-specific information on sex hormone flux.

Further research is needed to elucidate human sex hormone-mediated liver processes. Models like the four-core genotype (FCG) mouse could offer more physiologically relevant hormone concentrations[317]. The FCG mouse model was developed to investigate the impact of sex chromosomes (XX versus XY) and gonadal type (testes versus ovaries) on phenotypes[318].

Deletion of *Sry* from the Y chromosome, a gene that causes testes formation and testosterone synthesis, results in XY^- mice with ovaries (gonadally female). In contrast, insertion of the *Sry* transgenes onto an autosome in XX mice generates the production of testes[318]. Application of FCG mice could permit identification of the relative contribution of sex chromosomes and sex hormones at more physiological concentrations on sex differences[319] in *Plasmodium* liver stage infection and protection conferred by P&T vaccination.

Differences in liver biology

Additional differences exist between liver size, liver architecture, and gene regulation between mice and humans that could instill sex-specific outcomes. First, the liver in humans is much larger than the liver in mice. While the microarchitecture of the liver is very similar among mammalian species, with increasing size in humans comes increasing number of lobules and slightly larger lobules, with increasing portocentral distance in humans compared to mice[49]. Second, the liver in humans is generally considered to not have clearly delineated lobes (non-lobulated), compared to mouse livers with six clearly distinct lobes (**Figure 5.3**). This difference is primarily related to the amount of connective tissue separating the liver sections in each species[49]. Third, gene specific regulation differs between humans and mice. One study sought to identify gene specific network in the liver between mice and humans by comparing regulation under fatty acid disease in both hosts. Interestingly, they identified around 50% of commonly regulated genes exhibited opposite regulation, even when tightly controlling for the environment of expression *in vitro*[320]. Together, their data implied that differences in gene regulation between humans and mice in the liver could induce divergent immune responses.

The impact of these three differences (liver size, architecture, and gene expression) all limit applicability between mice and humans. Liver size may directly influence IFN-1 signaling-mediated homing mechanisms by introducing longer physical distances for chemokine gradients[321]. Additionally, the distinct lobulation component is a factor given that all microscopy was performed on the left lateral lobe in mice within this thesis, demonstrates that any lobe-specific effect on sporozoite homing and delivery might not be translatable to human liver. Third, the opposite gene regulation trends in humans may reflect differential processes that alter liver immune responses compared to mice[320]. Future work should explore a biophysical evaluation of liver size and distance from stimuli on inflammation. Additionally, sex-informed organoid models based on human livers[322] may also help in the better representation of human anatomy over that of mice.

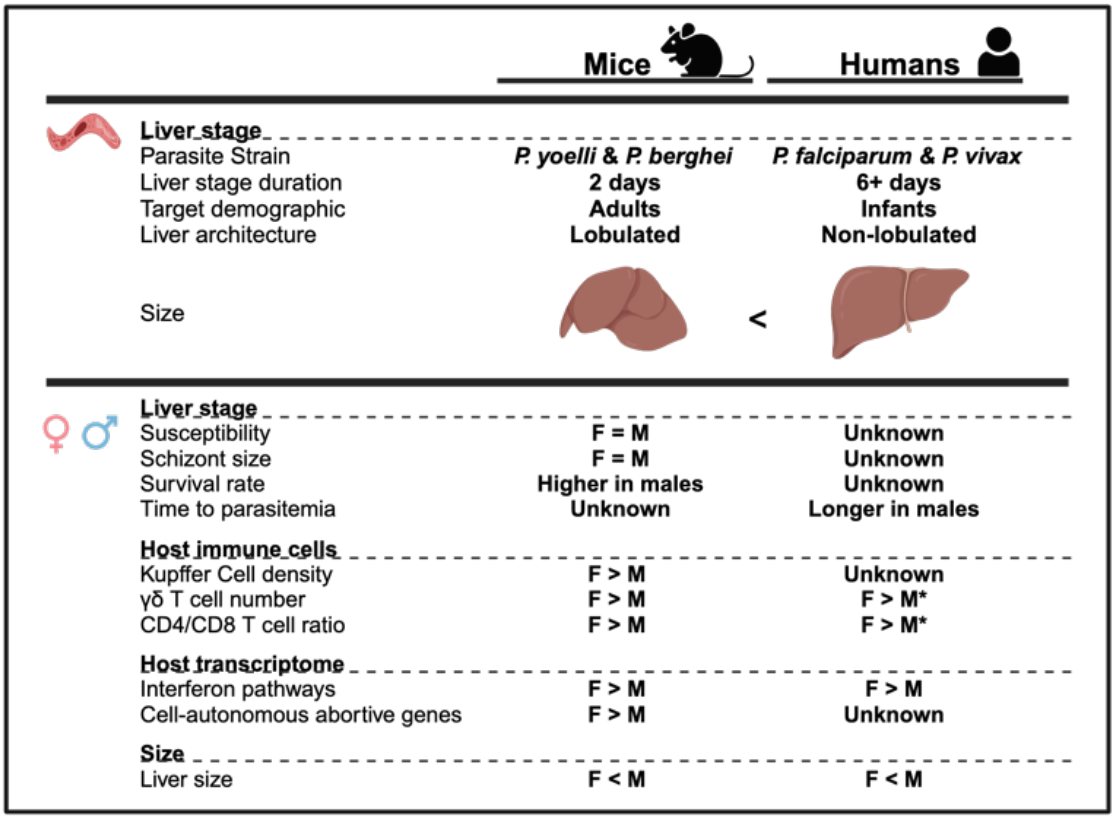

Figure 5.3: Summary table of known differences between mice and humans. The figure highlights key differences between mice and humans during *Plasmodium* liver stage infection. It also includes a summary of findings on sex-based differences. An asterisk (*) indicates literature-supported observations that were not confirmed within this thesis. Created with BioRender.com.

Differences in immune systems

The immune systems of mice and humans differ significantly, particularly in immune cell composition and pathogen-sensing mechanisms[323]. Murine livers are enriched in NK and NKT cells compared to humans[324], which may influence their responses to adjuvants and downstream correlates of protection[325]. Differences also extend to populations of γδ T cells[326], potentially altering innate mechanisms that bridge to adaptive immunity. Mice and humans express distinct Toll-like receptor (TLR) repertoires, with humans having 10 TLRs and mice 12[327]. Sex-specific variations in TLR activation have been documented, though the patterns and hormonal regulation differ between mice and humans[66,323,328]. While this thesis identifies several sex-specific differences in liver immune cell composition (**Figure 5.2**), much work remains to map the baseline immune cell landscape of the human liver by biological sex. Creating comprehensive, accessible atlases of human liver immune composition during *Plasmodium* infection will be critical for future tissue-specific sex difference research.

Differences in *Plasmodium* liver stage strain and dose

The translation of mouse models of *Plasmodium* infection and vaccination to humans is constrained by several differences, including: (1) differences in parasite biology, (2) discrepancies in mimicking the natural host immune response. First, a critical difference is the duration of the liver stage. *P. falciparum* takes between 6 – 7 days in humans, whereas *Py* or *Pb*

completes a liver stage in 2 – 3 days in mice[33]. Second, the natural host of *Pb* and *Py* are thicket rats (*Grammomys surdaster* and *Thamnomys rutilans*, respectively) and not laboratory mice (*Mus musculus*)[329], which may limit an accurate portrayal of an evolutionarily evolved sex-specific host response. Additionally, inbred rodent models do not represent the genetic diversity differences of human populations, which could alter host responses to infection[330].

There were two main limitations of the models employed: (1) differences in the administered dose of spz, and (2) variations in the route of sporozoite delivery. First, field studies using naturally reared mosquitoes in humans have shown that a single mosquito injects less than 100 spz, whereas laboratory-reared mosquitoes deliver an inoculum of approximately 125 spz per bite[331]. In contrast, mouse experiments to test vaccines typically involve administering 1×10^3 *P. yoelli* spz, a dose significantly higher than what is delivered by a mosquito bite. Furthermore, within the microscopy studies employed here, a dose up to 3×10^5 was used, a vastly supraphysiological dose to the murine liver that could limit downstream translational application[150]. Interestingly, at lower doses, we did not observe a sex difference in liver burden by RT-PCR in mice. The 2-3 fold sex-based difference in parasite survival was only measurable with a higher challenge dose of $1x10^5$ spz. Second, the challenge route is a critical factor to consider. Spz are naturally transmitted to humans via mosquito bites, requiring migration through the skin before reaching the liver[35]. In this study, the intravenous (IV) challenge route was utilized in mice, bypassing the skin and directly delivering spz to the liver. The IV approach was chosen for its stringency and reliability in assessing the liver stage and T cell-mediated efficacy of liver stage vaccines. Notably, throughout the study, 100% of naïve control animals were successfully infected, confirming the effectiveness of the IV challenge in mice. Our

analysis of IV versus mosquito bite challenges in human CHMI, the latter of which involved the bites of five infectious mosquitos that presumably delivered a variable injection dosage, revealed that biological sex influenced the delay in time to positivity, regardless of the route. For future directions, further investigation is warranted to examine the effects of inoculation routes and spz dosage on liver stage survival, especially at low doses. Additionally, including an evaluation of mosquito bite challenge by biological sex would be warranted.

Proposed model for sex-based differences in humans

Considering the combined differences in the human endocrine system, liver biology, immune system, parasite strain, and dose—factors that may not accurately reflect human biology—a leading hypothesis emerges. We propose that variations in liver stage infection between mice and humans play a pivotal role in measured liver burdens. In both mice and humans, an early innate immune response is induced. However, humans have an additional four or more days to mount an early adaptive immune response, which may be critical in controlling lower-density infections. During this extended time, an early adaptive T cell response begins to develop, which could significantly influence infection outcomes. Additionally, differences in TLR signaling between mice and humans may further contribute to these discrepancies. It is possible that TLR differences limit the ability to detect liver stage infections in female mice to a measurable extent, whereas such differences may be more detectable in humans. Lastly, other factors such as diet and microbiome may further modulate outcomes by species[128,332,333].

In summary, differences in the endocrine system, liver biology, immune response, parasite strains, and dose likely contribute to variations in *Plasmodium* liver stage infection. Future research should focus on measuring liver burden by host sex using models that more closely

mimic natural host liver biology, such as *P. knowlesi* in pigtail macaques (*Macaca nemestrina*) or cynomolgus macaques (*Macaca fascicularis*)[334,335]. Additionally, primary human hepatocyte culture systems could be used to investigate the influence of sex and sex hormones on parasite invasion and replication, while preserving a natural hormonal environment[336]. Immortalized hepatocyte cell lines are unsuitable for studying sex differences, as they lack the sex-specific gene expression and physiological hormone conditions essential for such investigations. Humanized mouse models would also be appropriately applied to study the impact of liver stage biology on human-infecting *Plasmodium* strains[320,337], however, often these models lack an effective immune system to measure differences in host responses.

5.3 IMPLICATIONS ON LIVER STAGE VACCINE DEVELOPMENT

An effective malaria vaccine is urgently needed to alleviate the global burden of the disease. Currently, no vaccine offers complete protection, but three promising candidates—RTS,S, R21, and PfSPZ—can reduce malaria mortality after multiple booster shots[44–46,221]. The primary target demographic for these vaccines is children in malaria-endemic areas, who account for approximately 85% of global malaria mortality[29]. RTS,S and R21 have been shown to prevent severe malaria disease and mortality, but they do not significantly prevent infection or transmission in field studies in endemic regions[42]. They are most effective in infants and children in endemic setting. On the other hand, PfSPZ (irradiated spz) can completely prevent infection in malaria-naïve populations[164] but has shown limited efficacy in children and infants[338]. The onset of sex hormones in adults impacts vaccine efficacy but is not yet fully understood [196]. This thesis shows that biological sex and hormones shape innate and adaptive immune responses to liver stage infection in mice. However, their role in *Plasmodium* liver stage immunity and vaccine

protection in humans remains unclear. This section explores the implications for preclinical murine studies and CHMI human trials.

In pre-clinical mouse studies, biological sex significantly affects vaccine efficacy. We demonstrated that across several liver-targeting vaccine regimens (P&T, RAS only, adjuvanted P&T, DC-pulsed prime) in two mouse strains (BALB/cJ, C57BL6) and two rodent malaria strains (*P. yoelli* and *P. berghei*), females were more protected than males. This higher protection likely explains one reason why most pre-clinical trials use female mice. We identified two main mechanisms contributing to this: higher baseline $CD8^+$ T cell density in females and a restricted type I IFN response in males, which limits the recruitment of Trm cells needed for parasite clearance. While females are easier to protect, we could not design a more effective vaccine to overcome these sex-specific differences. This raises the question: should male mice be used as a more stringent model for T-cell mediated liver vaccines? In theory, this sounds reasonable, but the strain differences between mouse and human malaria parasites complicate translating results from mice to humans. From a vaccinology perspective, using only female mice may be sufficient to inform human vaccine development. However, if the goal is to understand the mechanisms of protection in the liver stage, inclusion of both sexes is crucial. For instance, we could not determine if IFNγ was a key mediator of protection in androgen-deficient males, even though it is known to play a role in protection in females across multiple studies.

In malaria vaccine CHMI trials, the effect of biological sex and sex hormones is less well defined. A recent meta-analysis of clinical trials on the attenuated spz vaccine PfSPZ found higher levels of antigen-specific antibodies in adult females compared to males, but no difference in vaccine efficacy based on sex[114]. However, no analysis of $CD8^+$ T cells, the presumed

mechanism of protection, was conducted due to technical limitations of peripheral sampling. This suggests that males can achieve complete protection from an attenuated-parasite vaccine, a stark contrast to the significant sex-based differences we observed in mice. In **Chapter 5.2**, we discussed the potential differences in liver stage responses between male and female mice and humans. We also identified differences in liver stage duration between male and female humans in CHMI studies (**Chapter 2**). Notably, vaccine efficacy in the meta-analysis above was determined by the presence of blood-stage infection, without considering the time to parasitemia. So, does the time to parasitemia matter if the final protection outcome is the same? While clinical trials are not typically powered to assess sex-based differences in protection, further studies should explore this. A potential implication could be the need to adjust dosing for males in case of inefficacy. Regardless, clinical trials should aim for balanced sex representation or include a sex-weighted metric to assess its modifying effect on vaccine efficacy. Stratifying human trials by sex, as recommended for mice, would clarify immune differences and guide interventions effective for diverse populations.

Overall, when evaluating vaccine translational capacity in mice—where the focus is on preliminary immunogenicity and efficacy—sex balancing may be less critical. However, when investigating underlying immunological mechanisms, accounting for biological sex is essential. In humans, it is important to balance and design trials capable of capturing sex-specific effects on protection. Additional consideration should also be done to account for various characteristics that might alter sex hormone levels, for example hormonal contraception and hormone therapy.

5.4 ENDOCRINE PERSPECTIVE: CONSIDERATIONS FOR STEROIDOGENESIS

There are two ways to evaluate the intersection of the endocrine-immune interface in the liver. One way to evaluate this is from the perspective of an immunologist. Here, an immunologist would ask the question: *how do sex hormones impact the immune system?* The bulk of this thesis focuses on the perspective of the immunologist. We have identified that testosterone suppresses inflammation, restricts innate and adaptive immune cell recruitment, and completely shifts the liver immunogenic state at steady state. However, the perspective from the lens of the endocrinologist is lacking. An endocrinologist is focused on the question*: how does the immune system impact sex hormone biosynthesis?* Steroidogenesis is a complex series of events that result in the production of steroid molecules[339]. The liver is the site of some essential steroidogenic pathways, such as conversion of testosterone to its metabolically active form, DHT[340], and the sulfation of DHEA to DHEA-S[54], the most abundant hormone in the human body (**Figure 1.6**). Here we will discuss two potential points: do we see evidence of a shift in gene expression patterns around infected Py-infected hepatocytes and what liver cells could be attributed to this potential function. Additionally, we will explore if there is preliminary evidence to further investigation of parasite-induced nutrient sequestration from hepatocytes.

Differentially expressed genes in response to infection (**Figure 5.4**), as detailed in the GeoMX experiment, revealed notable changes in sulfotransferases, particularly *Sult2a1*, *Sult2a2*, and *Sult1a1*[341], which regulate the sulfation of DHEA and estrogens. In female mice, *Sult1a1* was uniquely downregulated, likely reflecting elevated estrogen levels compared to males and ORX males. Interestingly, the induction of *Esr2* (estrogen receptor 2) suggests a potential interplay between sulfotransferase activity and estrogen signaling, warranting further investigation. Other

genes of interest include *Cyp11a1*, which may indicate a parasite-driven shift in *de novo* steroid synthesis, and *Hsd17b1*, a key player in sex steroid metabolism, establishing estrogen gradients between serum and tissues. Additionally, *Cyp19a1*, an aromatase, was uniquely downregulated in ORX males, potentially reflecting a shift towards a more inflammatory hepatic environment. Contrary to initial hypotheses, no strong evidence was observed for *Srd5a2*-mediated testosterone conversion, suggesting differential regulation of androgen pathways during infection.

Future work should further consider that the strongest evidence for a steroidogenic role of *Plasmodium* infection in the liver lies in the activation and inactivation of hormones via sulfotransferases and *Hsd17b1*, indicating a complex metabolic flux. However, other pathways appear less affected by hormone presence, possibly due to minimal baseline differences in hormone states. While hepatocytes likely drive most of these gene expression patterns, the observed shifts could also be partially attributed to the influx of monocytes, dendritic cells, and Kupffer cells near parasites. From an endocrine perspective, *Plasmodium* appears to influence steroidogenesis, particularly hormone deactivation pathways in hepatocytes, but further investigation is required to pinpoint the cellular contributors and fully elucidate these mechanisms. This highlights the need for integrating a metabolomic perspective with gene expression data to capture the full scope of nutrient flux leveraged by the parasite during infection.

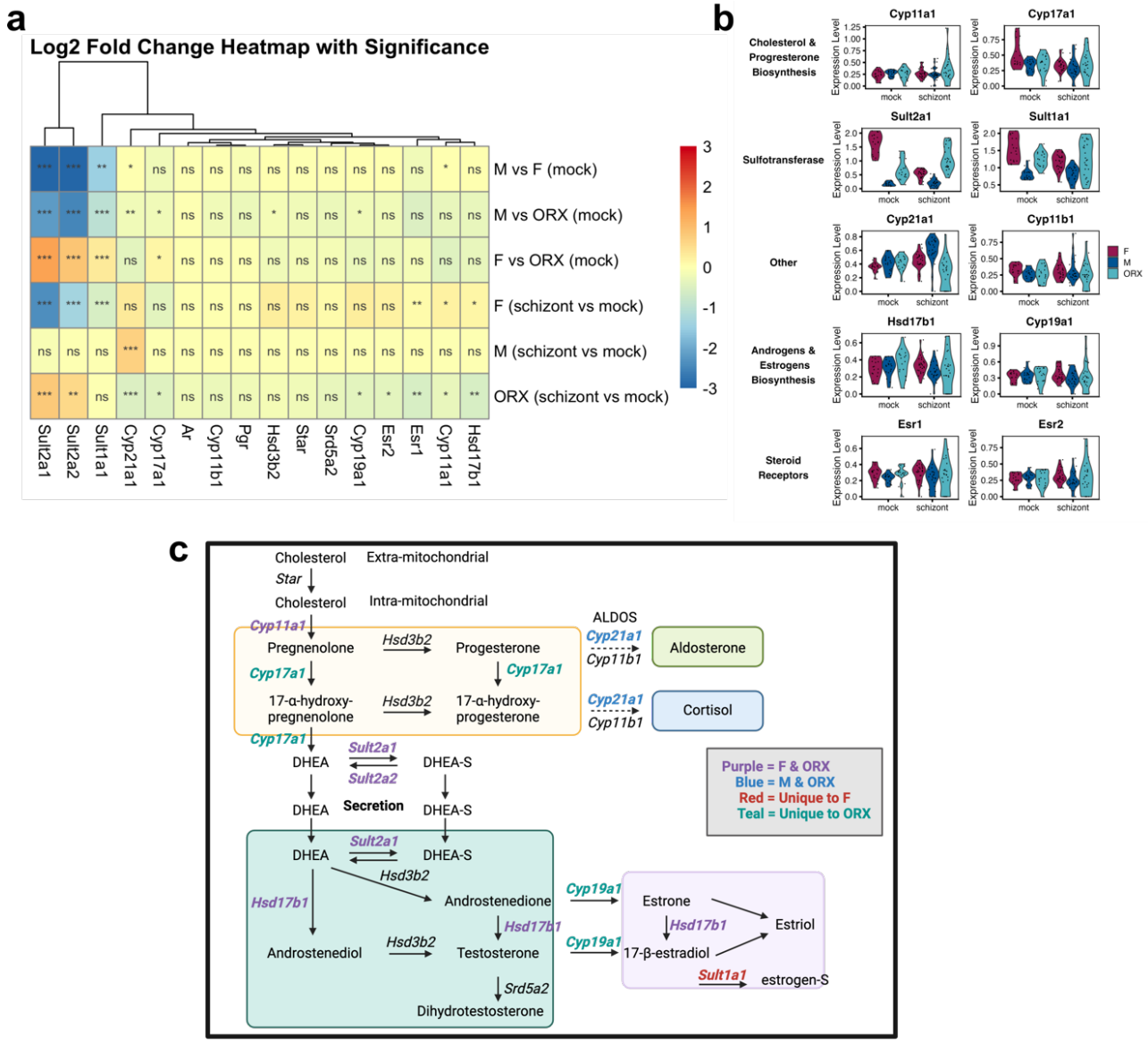

Figure 5.4: Figure of selected steroidogenesis-related genes. **a.** Heatmap of differential gene expression on liver tissue produced in Chapter 3 GeoMX experiment. Scale bar marks the Log Fold Change in gene expression for selected contrasts (rows) and for selected genes (x-axis). Significance of comparison is marker on heatmap (***FDR <0.001, **FDR<0.01, *FDR<0.05, ns FDR>0.05). **b.** Violin plots of differential gene expression profiles for selected genes in mock and within 200um around parasite at 44 hours post infection with *Plasmodium yoelli.* **c.** Schematic of sex hormone biosynthesis with genes highlighted that were differentially induced by administration of *Py*. Purple indicates a gene that was differentially expressed in both female and ORX males. Blue indicates a gene that was differentially expressed in both male and ORX males. Red and teal indicates a differentially expressed gene only in female mice and ORX mice respectively. Created with BioRender.com.

5.5 LESSONS LEARNED ABOUT SEX DIFFERENCES IN OMICS DATA

Throughout the exploration of the endocrine-immune-parasite axis within a tissue microenvironment, a wide range of immunological techniques were utilized, including flow cytometry, microscopy, and ELISPOT assays. Among these, the most transformative approach was the integration of omics-based data, which required extensive trial-and-error steps to effectively capture the influence of biological sex in a murine model. While this thesis primarily focuses on bulk RNA sequencing (**Chapter 4.4**) and spatial transcriptomics with GeoMX (**Chapter** Error! Reference source not found.) to investigate the role of biological sex, additional efforts considered incorporating metabolomics to accurately quantify sex hormones in a tissue-specific context. This section highlights the key lessons learned from designing and analyzing omics-based data to accurately capture the impact biological sex and sex hormones on an immunological system.

First and foremost, it is crucial to include appropriate steady-state controls for each sex and hormone state in study designs. Biological sex and sex hormones significantly modulate baseline gene expression and the metabolome, making non-stimulated or mock controls essential for distinguishing baseline variations from stimulus-induced effects. These controls also help map the baseline impact of biological sex. Sex-based analyses should begin with a clear understanding of baseline differences in gene expression and cellular composition, as these can vary across mouse strains[342] and environmental conditions[343]. This foundational knowledge is key to accurate interpretation and reproducibility.

Carefully consider the resolution of your chosen omics assay. In this thesis, single-cell resolution was achieved only through flow cytometry, which allowed for assessing sex hormone impacts on

individual immune cells. However, its targeted panel design focused on memory T cell responses, overlooking other cell types. Bulk RNA sequencing provided a broad overview of liver responses but lacked spatial resolution and cell-type specificity. Spatial transcriptomics with GeoMX added spatial context but did not achieve single-cell resolution, preventing distinctions between infected and uninfected hepatocytes. Additionally, metabolic shifts within the liver microenvironment remained unmeasured, limiting detection of subtle, sex-specific expression profiles. The techniques used here had inherent resolution limitations, and the lack of integration between metabolomics and spatial transcriptomics further restricted mapping of steroidogenic pathways. Future studies should combine high-resolution methods or apply techniques like Single-cell Spatial Metabolomics (ScSpaMet)[344] to better capture sex-specific processes in tissue microenvironments.

Caution is needed when interpreting gene ontology pathways related to sex hormone responses. A key limitation exists with widely used Broad Institute MPEG collections of pathways, employed in this thesis and many other analyses. These pathways provide valuable insights into system-level functions but often fail to capture the effects of sex hormone fluctuations. For instance, KEGG pathways broadly describe gene functions[345], but do not account for hormone states or biological sex, despite including most genes involved in sex hormone biosynthesis. Similarly, the Androgen and Estrogen Response pathways in the HALLMARK database[293] have notable gaps. The Androgen Response pathways were derived from cell line treatments in prostate adenocarcinoma cells treated with DHT (likely male), while the Estrogen Response pathways were based on breast cancer cells treated with E2 (likely female)[293]. Neither is defined for mice or tissue-specific contexts like the liver. These limitations highlight the need for sex-

informed gene sets categorized by biological sex and mapped to capture sex-biased and hormone-mediated processes more precisely.

Finally, to conduct a sex-informed analysis, one must frame your research questions within the context of the impact of sex hormones, sex chromosomes, and physiological differences. By categorizing these factors, you can focus on how each contributes to the biology of the system. Together, these lessons emphasize the importance of careful and targeted omics-based approaches that account for the nuanced effects of biological sex. This ensures a more accurate and comprehensive understanding of the system's true biology, leading to more insightful and targeted analyses.

5.6 CONCLUSIONS

This thesis unequivocally demonstrates that the sexually dimorphic liver significantly influences the *Plasmodium* parasite liver stage and liver stage vaccine outcomes, shaped by intrinsic baseline cellular differences and sex hormones. This work addresses a critical gap in understanding how biological sex alters the *Plasmodium* liver stage, and also highlights several future directions, including employing alternative models to better study immune responses and re-analyzing CHMI trial data to stratify outcomes by biological sex. Overall, this work underscores the importance of considering biological sex as a key variable in liver stage malaria research and vaccine development, and countering historical biases that have previously obscured biologically relevant sex-based trends.

Chapter 6. BIBLIOGRAPHY

1. Khramtsova, E. A., Davis, L. K. & Stranger, B. E. The role of sex in the genomics of human complex traits. *Nat. Rev. Genet.* **20**, 173–190 (2019).
2. Polderman, T. J. C. *et al.* The Biological Contributions to Gender Identity and Gender Diversity: Bringing Data to the Table. *Behav. Genet.* **48**, 95–108 (2018).
3. Khramtsova, E. A., Davis, L. K. & Stranger, B. E. The role of sex in the genomics of human complex traits. *Nat. Rev. Genet.* **20**, 173–190 (2019).
4. Klein, S. L. & Flanagan, K. L. Sex differences in immune responses. *Nat. Rev. Immunol.* **16**, 626–638 (2016).
5. Flanagan, K. L., Fink, A. L., Plebanski, M. & Klein, S. L. Sex and Gender Differences in the Outcomes of Vaccination over the Life Course. *Annu. Rev. Cell Dev. Biol.* **33**, 577–599 (2017).
6. Miller, W. L. & Auchus, R. J. The Molecular Biology, Biochemistry, and Physiology of Human Steroidogenesis and Its Disorders. *Endocr. Rev.* **32**, 81–151 (2011).
7. Klein, C. E. The Hypothalamic-Pituitary-Gonadal Axis. in *Holland-Frei Cancer Medicine. 6th edition* (BC Decker, 2003).
8. Labrie, F. All sex steroids are made intracellularly in peripheral tissues by the mechanisms of intracrinology after menopause. *J. Steroid Biochem. Mol. Biol.* **145**, 133–138 (2015).
9. Rubinow, K. B. An intracrine view of sex steroids, immunity, and metabolic regulation. *Mol. Metab.* **15**, 92–103 (2018).
10. Klein, S. L. The effects of hormones on sex differences in infection: from genes to behavior. *Neurosci. Biobehav. Rev.* **24**, 627–638 (2000).

11. Hägg, S. & Jylhävä, J. Sex differences in biological aging with a focus on human studies. *eLife* **10**, e63425 (2021).
12. Sever, R. & Glass, C. K. Signaling by Nuclear Receptors. *Cold Spring Harb. Perspect. Biol.* **5**, a016709–a016709 (2013).
13. Schwartz, N., Verma, A., Bivens, C. B., Schwartz, Z. & Boyan, B. D. Rapid steroid hormone actions via membrane receptors. *Biochim. Biophys. Acta BBA - Mol. Cell Res.* **1863**, 2289–2298 (2016).
14. Shepherd, R., Cheung, A. S., Pang, K., Saffery, R. & Novakovic, B. Sexual Dimorphism in Innate Immunity: The Role of Sex Hormones and Epigenetics. *Front. Immunol.* **11**, 604000 (2021).
15. Kadel, S. & Kovats, S. Sex Hormones Regulate Innate Immune Cells and Promote Sex Differences in Respiratory Virus Infection. *Front. Immunol.* **9**, 1653 (2018).
16. Pujantell, M. & Altfeld, M. Consequences of sex differences in Type I IFN responses for the regulation of antiviral immunity. *Front. Immunol.* **13**, 986840 (2022).
17. Straub, R. H. The Complex Role of Estrogens in Inflammation. *Endocr. Rev.* **28**, 521–574 (2007).
18. Information (US), N. C. for B. Chromosome Map. in *Genes and Disease [Internet]* (National Center for Biotechnology Information (US), 1998).
19. Wilkinson, N. M., Chen, H.-C., Lechner, M. G. & Su, M. A. Sex Differences in Immunity. *Annu. Rev. Immunol.* **40**, 75–94 (2022).
20. Fish, E. N. The X-files in immunity: sex-based differences predispose immune responses. *Nat Rev Immunol* **8**, 737–44 (2008).

21. Migeon, B. R. The role of X inactivation and cellular mosaicism in women's health and sex-specific diseases. *JAMA* **295**, 1428–1433 (2006).

22. Youness, A., Miquel, C.-H. & Guéry, J.-C. Escape from X Chromosome Inactivation and the Female Predominance in Autoimmune Diseases. *Int. J. Mol. Sci.* **22**, 1114 (2021).

23. Case, L. K. *et al.* Chromosome Y Regulates Survival Following Murine Coxsackievirus B3 Infection. *G3 GenesGenomesGenetics* **2**, 115 (2012).

24. Body Weight Information for B6 (000664). *The Jackson Laboratory* https://www.jax.org/jax-mice-and-services/strain-data-sheet-pages/body-weight-chart-000664.

25. Abdullah, M. *et al.* Gender effect on in vitro lymphocyte subset levels of healthy individuals. *Cell. Immunol.* **272**, 214–219 (2012).

26. Afshan, G., Afzal, N. & Qureshi, S. CD4+CD25(hi) regulatory T cells in healthy males and females mediate gender difference in the prevalence of autoimmune diseases. *Clin. Lab.* **58**, 567–571 (2012).

27. Bhargava, A. *et al.* Considering Sex as a Biological Variable in Basic and Clinical Studies: An Endocrine Society Scientific Statement. *Endocr. Rev.* **42**, 219–258 (2021).

28. Spangelo, B. L., Judd, A. M., Call, G. B., Zumwalt, J. & Gorospe, W. C. Role of the Cytokines in the Hypothalamic-Pituitary-Adrenal and Gonadal Axes. *Neuroimmunomodulation* **2**, 299–312 (1995).

29. By-Nc-Sa, C. World malaria report 2023.

30. Sarma, N., Patouillard, E., Cibulskis, R. E. & Arcand, J.-L. The Economic Burden of Malaria: Revisiting the Evidence. (2019) doi:10.4269/ajtmh.19-0386.

31. Global Malaria Programme operational strategy 2024-2030. *World Health Organ.* (2024).

32. Sato, S. Plasmodium-a brief introduction to the parasites causing human malaria and their basic biology. *J. Physiol. Anthropol.* **40**, 1 (2021).

33. De Niz, M. & Heussler, V. T. Rodent malaria models: insights into human disease and parasite biology. *Curr. Opin. Microbiol.* **46**, 93–101 (2018).

34. Sinnis, P. & Zavala, F. The skin: where malaria infection and the host immune response begin. *Semin. Immunopathol.* **34**, 787–792 (2012).

35. Cowman, A. F., Healer, J., Marapana, D. & Marsh, K. Malaria: Biology and Disease. *Cell* **167**, 610–624 (2016).

36. Wangdi, K. *et al.* Comparative effectiveness of malaria prevention measures: a systematic review and network meta-analysis. *Parasit. Vectors* **11**, 210 (2018).

37. Daily, J. P. Monoclonal Antibodies — A Different Approach to Combat Malaria. *N Engl J Med* **387**, 460–461 (2022).

38. Duffy, P. E. & Patrick Gorres, J. Malaria vaccines since 2000: progress, priorities, products. *Npj Vaccines* **5**, 48 (2020).

39. Mahmoudi, S. & Keshavarz, H. Malaria Vaccine Development: The Need for Novel Approaches: A Review Article. *Iran. J. Parasitol.* **13**, 1 (2018).

40. Marques-da-Silva, C., Peissig, K. & Kurup, S. P. Pre-Erythrocytic Vaccines against Malaria. *Vaccines* **8**, 400 (2020).

41. Laurens, M. B. RTS,S/AS01 vaccine (Mosquirix^{TM}): an overview. *Hum. Vaccines Immunother.* **16**, 480 (2019).

42. Zavala, F. RTS,S: the first malaria vaccine. *J. Clin. Invest.* **132**, e156588 (2022).

43. Collins, K. A., Snaith, R., Cottingham, M. G., Gilbert, S. C. & Hill, A. V. S. Enhancing protective immunity to malaria with a highly immunogenic virus-like particle vaccine. *Sci. Rep.* **7**, 46621 (2017).

44. Malaria vaccines (RTS,S and R21). https://www.who.int/news-room/questions-and-answers/item/q-a-on-rts-s-malaria-vaccine.

45. The RTS,S Clinical Trials Partnership. First Results of Phase 3 Trial of RTS,S/AS01 Malaria Vaccine in African Children. *N. Engl. J. Med.* **365**, 1863–1875 (2011).

46. Datoo, M. S. *et al.* Safety and efficacy of malaria vaccine candidate R21/Matrix-M in African children: a multicentre, double-blind, randomised, phase 3 trial. *The Lancet* **403**, 533–544 (2024).

47. Overstreet, M. G., Cockburn, I. A., Chen, Y. & Zavala, F. Protective CD8 $^{+}$ T cells against *Plasmodium* liver stages: immunobiology of an 'unnatural' immune response. *Immunol. Rev.* **225**, 272–283 (2008).

48. Itsara, L. S. *et al.* The Development of Whole Sporozoite Vaccines for Plasmodium falciparum Malaria. *Front. Immunol.* **9**, 2748 (2018).

49. Kruepunga, N., Hakvoort, T. B. M., Hikspoors, J. P. J. M., Köhler, S. E. & Lamers, W. H. Anatomy of rodent and human livers: What are the differences? *Biochim. Biophys. Acta BBA - Mol. Basis Dis.* **1865**, 869–878 (2019).

50. Blouin, A., Bolender, R. P. & Weibel, E. R. Distribution of organelles and membranes between hepatocytes and nonhepatocytes in the rat liver parenchyma. A stereological study. *J. Cell Biol.* **72**, 441–455 (1977).

51. Gibert-Ramos, A. *et al.* The Hepatic Sinusoid in Chronic Liver Disease: The Optimal Milieu for Cancer. *Cancers* **13**, 5719 (2021).

52. Holz, L. E., Fernandez-Ruiz, D. & Heath, W. R. Protective immunity to liver-stage malaria. *Clin. Transl. Immunol.* **5**, e105 (2016).

53. Trefts, E., Gannon, M. & Wasserman, D. H. The liver. *Curr. Biol.* **27**, R1147–R1151 (2017).

54. Rhyu, J. & Yu, R. Newly discovered endocrine functions of the liver. *World J. Hepatol.* **13**, 1611–1628 (2021).

55. Bram, Y. *et al.* Cell and Tissue Therapy for the Treatment of Chronic Liver Disease. *Annu. Rev. Biomed. Eng.* **23**, 517–546 (2021).

56. Heymann, F. & Tacke, F. Immunology in the liver — from homeostasis to disease. *Nat. Rev. Gastroenterol. Hepatol.* **13**, 88–110 (2016).

57. Robinson, M. W., Harmon, C. & O'Farrelly, C. Liver immunology and its role in inflammation and homeostasis. *Cell. Mol. Immunol.* **13**, 267–276 (2016).

58. Protzer, U., Maini, M. K. & Knolle, P. A. Living in the liver: hepatic infections. *Nat. Rev. Immunol.* **12**, 201–213 (2012).

59. Bilzer, M., Roggel, F. & Gerbes, A. L. Role of Kupffer cells in host defense and liver disease. *Liver Int.* **26**, 1175–1186 (2006).

60. Su, G. L. *et al.* Kupffer cell activation by lipopolysaccharide in rats: Role for lipopolysaccharide binding protein and toll-like receptor 4. *Hepatology* (2000) doi:10.1053/he.2000.5634.

61. Elsegood, C. L. *et al.* Kupffer cell-monocyte communication is essential for initiating murine liver progenitor cell-mediated liver regeneration. *Hepatol. Baltim. Md* **62**, 1272–1284 (2015).

62. Thomson, A. W. & Knolle, P. A. Antigen-presenting cell function in the tolerogenic liver environment. *Nat. Rev. Immunol.* **10**, 753–766 (2010).

63. Xu, R., Huang, H., Zhang, Z. & Wang, F.-S. The role of neutrophils in the development of liver diseases. *Cell. Mol. Immunol.* **11**, 224–231 (2014).

64. Pruvot, F. R. *et al.* Characterization, quantification, and localization of passenger T lymphocytes and NK cells in human liver before transplantation. *Transpl. Int. Off. J. Eur. Soc. Organ Transplant.* **8**, 273–279 (1995).

65. Norris, S. *et al.* Resident human hepatic lymphocytes are phenotypically different from circulating lymphocytes. *J. Hepatol.* **28**, 84–90 (1998).

66. Wu, J. *et al.* Toll-like receptor-induced innate immune responses in non-parenchymal liver cells are cell type-specific. *Immunology* **129**, 363 (2010).

67. Crispe, I. N. Immune Tolerance in Liver Disease. *Hepatol. Baltim. Md* **60**, 2109 (2014).

68. Knolle, P. *et al.* Human Kupffer cells secrete IL-10 in response to lipopolysaccharide (LPS) challenge. *J. Hepatol.* **22**, 226–229 (1995).

69. Tokita, D. *et al.* Poor allostimulatory function of liver plasmacytoid DC is associated with pro-apoptotic activity, dependent on regulatory T cells. *J. Hepatol.* **49**, 1008–1018 (2008).

70. Sander, L. E. *et al.* Hepatic acute-phase proteins control innate immune responses during infection by promoting myeloid-derived suppressor cell function. *J. Exp. Med.* **207**, 1453–1464 (2010).

71. Yang, X. *et al.* Tissue-specific expression and regulation of sexually dimorphic genes in mice. *Genome Res.* **16**, 995–1004 (2006).

72. Oliva, M. *et al.* The impact of sex on gene expression across human tissues. *Science* **369**, eaba3066 (2020).

73. Marcos, R. *et al.* Stereological assessment of sexual dimorphism in the rat liver reveals differences in hepatocytes and Kupffer cells but not hepatic stellate cells. *J. Anat.* **228**, 996–1005 (2016).

74. Goldfarb, C. N., Karri, K., Pyatkov, M. & Waxman, D. J. Interplay Between GH-regulated, Sex-biased Liver Transcriptome and Hepatic Zonation Revealed by Single-Nucleus RNA Sequencing. *Endocrinology* **163**, bqac059 (2022).

75. Lopes-Ramos, C. M. *et al.* Sex Differences in Gene Expression and Regulatory Networks across 29 Human Tissues. *Cell Rep.* **31**, 107795 (2020).

76. Zheng, D., Wang, X., Antonson, P., Gustafsson, J.-Å. & Li, Z. Genomics of sex hormone receptor signaling in hepatic sexual dimorphism. *Mol. Cell. Endocrinol.* **471**, 33–41 (2018).

77. Waxman, D. J. & O'Connor, C. Growth Hormone Regulation of Sex-Dependent Liver Gene Expression. *Mol. Endocrinol.* **20**, 2613–2629 (2006).

78. Trapani, L., Segatto, M. & Pallottini, V. Regulation and deregulation of cholesterol homeostasis: The liver as a metabolic 'power station'. *World J. Hepatol.* **4**, 184–190 (2012).

79. Eacker, S. M. *et al.* Hormonal regulation of testicular steroid and cholesterol homeostasis. *Mol. Endocrinol. Baltim. Md* **22**, 623–635 (2008).

80. Kasarinaite, A., Sinton, M., Saunders, P. T. K. & Hay, D. C. The Influence of Sex Hormones in Liver Function and Disease. *Cells* **12**, 1604 (2023).

81. Toda, K., Toda, A., Ono, M. & Saibara, T. Lack of 17β-estradiol reduces sensitivity to insulin in the liver and muscle of male mice. *Heliyon* **4**, e00772 (2018).

82. Livingstone, D. E. W. *et al.* 5α-Reductase type 1 deficiency or inhibition predisposes to insulin resistance, hepatic steatosis, and liver fibrosis in rodents. *Diabetes* **64**, 447–458 (2015).

83. Ding, E. L., Song, Y., Malik, V. S. & Liu, S. Sex differences of endogenous sex hormones and risk of type 2 diabetes: a systematic review and meta-analysis. *JAMA* **295**, 1288–1299 (2006).

84. Bruce-Chwatt, L. J. Molineaux, L. and Gramiccia, G. (1980). The Garki Project. Research on the epidemiology and control of malaria in the Sudan savanna of West Africa. Geneva: World Health Organization, 311 pp. 33 tables, 83 figs. Price: Sw. Fr. 33. *Trans. R. Soc. Trop. Med. Hyg.* **75**, 190–191 (1981).

85. Luxemburger, C. *et al.* The epidemiology of severe malaria in an area of low transmission in Thailand. *Trans. R. Soc. Trop. Med. Hyg.* **91**, 256–262 (1997).

86. Pathak, S. *et al.* Age-dependent sex bias in clinical malarial disease in hypoendemic regions. *PloS One* **7**, e35592 (2012).

87. McDonald, C. R. *et al.* Sex as a determinant of disease severity and clinical outcome in febrile children under five presenting to a regional referral hospital in Uganda. *PloS One* **17**, e0276234 (2022).

88. Kesteman, T. *et al.* Nationwide evaluation of malaria infections, morbidity, mortality, and coverage of malaria control interventions in Madagascar. *Malar. J.* **13**, 465 (2014).

89. Mendis, C. *et al.* Characteristics of malaria transmission in Kataragama, Sri Lanka: a focus for immuno-epidemiological studies. *Am. J. Trop. Med. Hyg.* **42**, 298–308 (1990).

90. Camargo, L. M. *et al.* Hypoendemic malaria in Rondonia (Brazil, western Amazon region): seasonal variation and risk groups in an urban locality. *Am. J. Trop. Med. Hyg.* **55**, 32–38 (1996).

91. Abdalla, S. I., Malik, E. M. & Ali, K. M. The burden of malaria in Sudan: incidence, mortality and disability--adjusted life--years. *Malar. J.* **6**, 97 (2007).

92. Creasey, A. *et al.* Eleven years of malaria surveillance in a Sudanese village highlights unexpected variation in individual disease susceptibility and outbreak severity. *Parasitology* **129**, 263–271 (2004).

93. Landgraf, B., Kollaritsch, H., Wiedermann, G. & Wernsdorfer, W. H. Parasite density of Plasmodium falciparum malaria in Ghanaian schoolchildren: evidence for influence of sex hormones? *Trans. R. Soc. Trop. Med. Hyg.* **88**, 73–74 (1994).

94. Tiedje, K. E. *et al.* Seasonal Variation in the Epidemiology of Asymptomatic Plasmodium falciparum Infections across Two Catchment Areas in Bongo District, Ghana. *Am. J. Trop. Med. Hyg.* **97**, 199–212 (2017).

95. Houngbedji, C. A. *et al.* Disparities of Plasmodium falciparum infection, malaria-related morbidity and access to malaria prevention and treatment among school-aged children: a national cross-sectional survey in Côte d'Ivoire. *Malar. J.* **14**, 7 (2015).

96. Golassa, L. *et al.* Microscopic and molecular evidence of the presence of asymptomatic Plasmodium falciparum and Plasmodium vivax infections in an area with low, seasonal and unstable malaria transmission in Ethiopia. *BMC Infect. Dis.* **15**, 310 (2015).

97. Briggs, J., Murray, M., Nideffer, J. & Jagannathan, P. Sex-Linked Differences in Malaria Risk Across the Lifespan. *Curr. Top. Microbiol. Immunol.* **441**, 185–208 (2023).

98. Okiring, J. *et al.* Gender difference in the incidence of malaria diagnosed at public health facilities in Uganda. *Malar. J.* **21**, 22 (2022).

99. Olson, S. H., Gangnon, R., Silveira, G. A. & Patz, J. A. Deforestation and Malaria in Mâncio Lima County, Brazil. *CDC Emerg. Infect. Dis. J.* **16**, (2010).

100. Sumner, K. M. *et al.* Impact of asymptomatic Plasmodium falciparum infection on the risk of subsequent symptomatic malaria in a longitudinal cohort in Kenya. *eLife* **10**, e68812 (2021).

101. Briggs, J. *et al.* Sex-based differences in clearance of chronic Plasmodium falciparum infection. *eLife* **9**, e59872 (2020).

102. Wunderlich, F. *et al.* Testosterone and other gonadal factor(s) restrict the efficacy of genes controlling resistance to Plasmodium chabaudi malaria. *Parasite Immunol.* **13**, 357–367 (1991).

103. Cernetich, A. *et al.* Involvement of Gonadal Steroids and Gamma Interferon in Sex Differences in Response to Blood-Stage Malaria Infection. *Infect. Immun.* **74**, 3190–3203 (2006).

104. Cervantes-Candelas, L. A. *et al.* 17β-Estradiol Is Involved in the Sexual Dimorphism of the Immune Response to Malaria. *Front. Endocrinol.* **12**, 643851 (2021).

105. Legorreta-Herrera, M. *et al.* Sex-Associated Differential mRNA Expression of Cytokines and Its Regulation by Sex Steroids in Different Brain Regions in a *Plasmodium berghei* ANKA Model of Cerebral Malaria. *Mediators Inflamm.* **2018**, 1–15 (2018).

106. Klein, P. W., Easterbrook, J. D., Lalime, E. N. & Klein, S. L. Estrogen and progesterone affect responses to malaria infection in female C57BL/6 mice. *Gend. Med.* **5**, 423–433 (2008).

107. Zhang, Z.-H., Chen, L., Saito, S., Kanagawa, O. & Sendo, F. Possible Modulation by Male Sex Hormone of Th1/Th2 Function in Protection against *Plasmodium chabaudi chabaudi* AS Infection in Mice. *Exp. Parasitol.* **96**, 121–129 (2000).

108. Krücken, J. *et al.* Testosterone Suppresses Protective Responses of the Liver to Blood-Stage Malaria. *Infect. Immun.* **73**, 436–443 (2005).

109. Benten, W. P. M., Ulrich, P., Kühn-Velten, W. N., Vohr, H.-W. & Wunderlich, F. Testosterone-induced susceptibility to Plasmodium chabaudi malaria: persistence after withdrawal of testosterone. *J. Endocrinol.* **153**, 275–281 (1997).

110. Delić, D. *et al.* Testosterone-induced permanent changes of hepatic gene expression in female mice sustained during Plasmodium chabaudi malaria infection. *J. Mol. Endocrinol.* **45**, 379–390 (2010).

111. Miller, J. L., Sack, B. K., Baldwin, M., Vaughan, A. M. & Kappe, S. H. I. Interferon-Mediated Innate Immune Responses against Malaria Parasite Liver Stages. *Cell Rep.* **7**, 436–447 (2014).

112. Aaby, P. *et al.* The non-specific and sex-differential effects of vaccines. *Nat. Rev. Immunol.* **20**, 464–470 (2020).

113. Weinstein, Y., Ran, S. & Segal, S. Sex-associated differences in the regulation of immune responses controlled by the MHC of the mouse. *J. Immunol.* **132**, 656–661 (1984).

114. Kc, N. *et al.* Increased levels of anti-PfCSP antibodies in post-pubertal females versus males immunized with PfSPZ Vaccine does not translate into increased protective efficacy. *Front. Immunol.* **13**, 1006716 (2022).

115. Nganou-Makamdop, K. & Sauerwein, R. W. Liver or blood-stage arrest during malaria sporozoite immunization: the later the better? *Trends Parasitol.* **29**, 304–310 (2013).

116. Vom Steeg, L. G., Flores-Garcia, Y., Zavala, F. & Klein, S. L. Irradiated sporozoite vaccination induces sex-specific immune responses and protection against malaria in mice. *Vaccine* **37**, 4468–4476 (2019).

117. Acuna-Soto, R., Maguire, J. H. & Wirth, D. F. Gender distribution in asymptomatic and invasive amebiasis. *Am. J. Gastroenterol.* **95**, 1277–1283 (2000).

118. Blessmann, J. & Tannich, E. Treatment of asymptomatic intestinal Entamoeba histolytica infection. *N. Engl. J. Med.* **347**, 1384 (2002).

119. Lewis, F. A. & Tucker, M. S. Schistosomiasis. in *Digenetic Trematodes* (eds. Toledo, R. & Fried, B.) 47–75 (Springer, New York, NY, 2014). doi:10.1007/978-1-4939-0915-5_3.

120. Pinot de Moira, A. *et al.* Analysis of Complex Patterns of Human Exposure and Immunity to Schistosomiasis mansoni: The Influence of Age, Sex, Ethnicity and IgE. *PLoS Negl. Trop. Dis.* **4**, e820 (2010).

121. Mohamed-Ali, Q. *et al.* Susceptibility to periportal (Symmers) fibrosis in human schistosoma mansoni infections: evidence that intensity and duration of infection, gender, and inherited factors are critical in disease progression. *J. Infect. Dis.* **180**, 1298–1306 (1999).

122. Nicolls, D. J. *et al.* Characteristics of schistosomiasis in travelers reported to the GeoSentinel Surveillance Network 1997-2008. *Am. J. Trop. Med. Hyg.* **79**, 729–734 (2008).

123. What is Viral Hepatitis? | CDC. https://www.cdc.gov/hepatitis/abc/index.htm (2024).

124. Abdel-Gawad, M. *et al.* Gender differences in prevalence of hepatitis C virus infection in Egypt: a systematic review and meta-analysis. *Sci. Rep.* **13**, 2499 (2023).

125. Ayano, G. *et al.* A systematic review and meta-analysis of gender difference in epidemiology of HIV, hepatitis B, and hepatitis C infections in people with severe mental illness. *Ann. Gen. Psychiatry* **17**, 16 (2018).

126. Wang, A. C., Geng, J.-H., Wang, C.-W., Wu, D.-W. & Chen, S.-C. Sex difference in the associations among risk factors with hepatitis B and C infections in a large Taiwanese population study. *Front. Public Health* **10**, (2022).

127. Brown, R., Goulder, P. & Matthews, P. C. Sexual Dimorphism in Chronic Hepatitis B Virus (HBV) Infection: Evidence to Inform Elimination Efforts. *Wellcome Open Res.* **7**, 32 (2022).

128. Burra, P. *et al.* Clinical impact of sexual dimorphism in non-alcoholic fatty liver disease (NAFLD) and non-alcoholic steatohepatitis (NASH). *Liver Int. Off. J. Int. Assoc. Study Liver* **41**, 1713–1733 (2021).

129. Hagström, H. *et al.* Etiologies and outcomes of cirrhosis in a large contemporary cohort. *Scand. J. Gastroenterol.* **56**, 727–732 (2021).

130. Chen, Y.-L. *et al.* Prevalence of and risk factors for metabolic associated fatty liver disease in an urban population in China: a cross-sectional comparative study. *BMC Gastroenterol.* **21**, 212 (2021).

131. Amino, R. *et al.* Quantitative imaging of Plasmodium transmission from mosquito to mammal. *Nat. Med.* **12**, 220–224 (2006).

132. Prudêncio, M., Rodriguez, A. & Mota, M. M. The silent path to thousands of merozoites: the Plasmodium liver stage. *Nat. Rev. Microbiol.* **4**, 849–856 (2006).

133. Frevert, U. *et al.* Intravital observation of Plasmodium berghei sporozoite infection of the liver. *PLoS Biol.* **3**, e192 (2005).

134. Baer, K. *et al.* Kupffer cells are obligatory for Plasmodium yoelii sporozoite infection of the liver. *Cell. Microbiol.* **9**, 397–412 (2007).

135. Carrolo, M. *et al.* Hepatocyte growth factor and its receptor are required for malaria infection. *Nat. Med.* **9**, 1363–1369 (2003).

136. Afriat, A. *et al.* A spatiotemporally resolved single-cell atlas of the Plasmodium liver stage. *Nature* **611**, 563–569 (2022).

137. Schulze, R. J., Schott, M. B., Casey, C. A., Tuma, P. L. & McNiven, M. A. The cell biology of the hepatocyte: A membrane trafficking machine. *J. Cell Biol.* **218**, 2096–2112 (2019).

138. Vaughan, A. M. *et al.* Type II fatty acid synthesis is essential only for malaria parasite late liver stage development. *Cell. Microbiol.* **11**, 506–520 (2009).

139. Vial, H. J., Philippot, J. R. & Wallach, D. F. H. A reevaluation of the status of cholesterol in erythrocytes infected by *Plasmodium knowlesi* and *P. falciparum*. *Mol. Biochem. Parasitol.* **13**, 53–65 (1984).

140. Polet, H. & Conrad, M. E. Malaria: Extracellular Amino Acid Requirements for in Vitro Growth of Erythrocytic Forms of Plasmodium knowlesi∗. *Proc. Soc. Exp. Biol. Med.* **127**, 251–253 (1968).

141. Vaughan, A. M. & Kappe, S. H. I. Malaria Parasite Liver Infection and Exoerythrocytic Biology. *Cold Spring Harb. Perspect. Med.* **7**, a025486 (2017).

142. Meireles, P. *et al.* GLUT1-mediated glucose uptake plays a crucial role during Plasmodium hepatic infection. *Cell. Microbiol.* **19**, e12646 (2017).

143. Toro-Moreno, M., Sylvester, K., Srivastava, T., Posfai, D. & Derbyshire, E. R. RNA-Seq Analysis Illuminates the Early Stages of Plasmodium Liver Infection. *mBio* **11**, e03234-19 (2020).

144. Posfai, D. *et al.* Plasmodium parasite exploits host aquaporin-3 during liver stage malaria infection. *PLOS Pathog.* **14**, e1007057 (2018).

145. Albuquerque, S. S. *et al.* Host cell transcriptional profiling during malaria liver stage infection reveals a coordinated and sequential set of biological events. *BMC Genomics* **10**, 270 (2009).

146. Schroeder, E. A., Chirgwin, M. E. & Derbyshire, E. R. Plasmodium's fight for survival: escaping elimination while acquiring nutrients. *Trends Parasitol.* **38**, 544–557 (2022).

147. Lahree, A., Mello-Vieira, J. & Mota, M. M. The nutrient games – Plasmodium metabolism during hepatic development. *Trends Parasitol.* **39**, 445–460 (2023).

148. Yang, A. S. P. *et al.* Zonal human hepatocytes are differentially permissive to *Plasmodium falciparum* malaria parasites. *EMBO J.* **40**, e106583 (2021).

149. Rodríguez-Montes, L. *et al.* Sex-biased gene expression across mammalian organ development and evolution. *Science* **382**, eadf1046 (2023).

150. Hildebrandt, F. *et al.* Host-pathogen interactions in the Plasmodium-infected mouse liver at spatial and single-cell resolution. *Nat. Commun.* **15**, 7105 (2024).

151. Cunningham, R. P. & Porat-Shliom, N. Liver Zonation – Revisiting Old Questions With New Technologies. *Front. Physiol.* **12**, (2021).

152. Liehl, P. *et al.* Host-cell sensors for Plasmodium activate innate immunity against liver-stage infection. *Nat. Med.* **20**, 47–53 (2014).

153. Marques-da-Silva, C. *et al.* AIM2 sensors mediate immunity to Plasmodium infection in hepatocytes. *Proc. Natl. Acad. Sci.* **120**, e2210181120 (2023).

154. Roland, J. *et al.* NK Cell Responses to Plasmodium Infection and Control of Intrahepatic Parasite Development1. *J. Immunol.* **177**, 1229–1239 (2006).

155. Kurup, S. P. *et al.* Monocyte-Derived CD11c+ Cells Acquire Plasmodium from Hepatocytes to Prime CD8 T Cell Immunity to Liver-Stage Malaria. *Cell Host Microbe* **25**, 565-577.e6 (2019).

156. Glennon, E. K. K. *et al.* Elucidating Spatially-Resolved Changes in Host Signaling During Plasmodium Liver-Stage Infection. *Front. Cell. Infect. Microbiol.* **11**, 804186 (2022).

157. Bae, H. R. *et al.* The interplay of type I and type II interferons in murine autoimmune cholangitis as a basis for sex-biased autoimmunity. *Hepatology* **67**, 1408–1419 (2018).

158. Bergsbaken, T., Bevan, M. J. & Fink, P. J. Local Inflammatory Cues Regulate Differentiation and Persistence of CD8+ Tissue-Resident Memory T Cells. *Cell Rep.* **19**, 114–124 (2017).

159. Henze, L., Schwinge, D. & Schramm, C. The Effects of Androgens on T Cells: Clues to Female Predominance in Autoimmune Liver Diseases? *Front. Immunol.* **11**, 1567 (2020).

160. Mohammad, I. *et al.* Estrogen receptor α contributes to T cell–mediated autoimmune inflammation by promoting T cell activation and proliferation. *Sci. Signal.* **11**, eaap9415 (2018).

161. Chakravarty, S. *et al.* CD8+ T lymphocytes protective against malaria liver stages are primed in skin-draining lymph nodes. *Nat. Med.* **13**, 1035–1041 (2007).

162. Schmidt, N. W., Butler, N. S., Badovinac, V. P. & Harty, J. T. Extreme CD8 T Cell Requirements for Anti-Malarial Liver-Stage Immunity following Immunization with Radiation Attenuated Sporozoites. *PLoS Pathog.* **6**, e1000998 (2010).

163. Scheller, L. F. & Azad, A. F. Maintenance of protective immunity against malaria by persistent hepatic parasites derived from irradiated sporozoites. *Proc. Natl. Acad. Sci. U. S. A.* **92**, 4066–4068 (1995).

164. Ishizuka, A. S. *et al.* Protection against malaria at 1 year and immune correlates following PfSPZ vaccination. *Nat. Med.* **22**, 614–623 (2016).

165. Nussenzweig, R. S., Vanderberg, J., Most, H. & Orton, C. Protective immunity produced by the injection of x-irradiated sporozoites of plasmodium berghei. *Nature* **216**, 160–162 (1967).

166. Fernandez-Ruiz, D. *et al.* Liver-Resident Memory CD8 + T Cells Form a Front-Line Defense against Malaria Liver-Stage Infection. *Immunity* **45**, 889–902 (2016).

167. Olsen, T. M., Stone, B. C., Chuenchob, V. & Murphy, S. C. Prime-and-Trap Malaria Vaccination To Generate Protective CD8+ Liver-Resident Memory T Cells. *J. Immunol. Baltim. Md 1950* **201**, 1984–1993 (2018).

168. Schofield, L. *et al.* Gamma interferon, CD8+ T cells and antibodies required for immunity to malaria sporozoites. *Nature* **330**, 664–666 (1987).

169. Weiss, W. R., Sedegah, M., Beaudoin, R. L., Miller, L. H. & Good, M. F. CD8+ T cells (cytotoxic/suppressors) are required for protection in mice immunized with malaria sporozoites. *Proc. Natl. Acad. Sci. U. S. A.* **85**, 573–576 (1988).

170. Doolan, D. L. & Hoffman, S. L. The Complexity of Protective Immunity Against Liver-Stage Malaria. *J. Immunol.* **165**, 1453–1462 (2000).

171. Sano, G. *et al.* Swift Development of Protective Effector Functions in Naive Cd8+ T Cells against Malaria Liver Stages. *J. Exp. Med.* **194**, 173–180 (2001).

172. Spencer, A. J. *et al.* The Threshold of Protection from Liver-Stage Malaria Relies on a Fine Balance between the Number of Infected Hepatocytes and Effector CD8+ T Cells Present in the Liver. *J. Immunol.* **198**, 2006–2016 (2017).

173. Schmidt, N. W., Butler, N. S. & Harty, J. T. Plasmodium–Host Interactions Directly Influence the Threshold of Memory CD8 T Cells Required for Protective Immunity. *J. Immunol.* **186**, 5873–5884 (2011).

174. Schenkel, J. M. & Masopust, D. Tissue-Resident Memory T Cells. *Immunity* **41**, 886–897 (2014).

175. Schmidt, N. W. *et al.* Memory CD8 T cell responses exceeding a large but definable threshold provide long-term immunity to malaria. *Proc. Natl. Acad. Sci. U. S. A.* **105**, 14017–14022 (2008).

176. Lefebvre, M. N. *et al.* Expeditious recruitment of circulating memory CD8 T cells to the liver facilitates control of malaria. *Cell Rep.* **37**, 109956 (2021).

177. Martin, M. D. & Badovinac, V. P. Defining Memory CD8 T Cell. *Front. Immunol.* **9**, 2692 (2018).

178. Schenkel, J. M., Fraser, K. A., Vezys, V. & Masopust, D. Sensing and alarm function of resident memory CD8+ T cells. *Nat. Immunol.* **14**, 509–513 (2013).

179. Corradin, G. & Levitskaya, J. Priming of CD8+ T Cell Responses to Liver Stage Malaria Parasite Antigens. *Front. Immunol.* **5**, 527 (2014).

180. Joshi, N. S. *et al.* Inflammation directs memory precursor and short-lived effector CD8(+) T cell fates via the graded expression of T-bet transcription factor. *Immunity* **27**, 281–295 (2007).

181. Pipkin, M. E. *et al.* Interleukin-2 and inflammation induce distinct transcriptional programs that promote the differentiation of effector cytolytic T cells. *Immunity* **32**, 79–90 (2010).

182. Tsuji, M. *et al.* Development of antimalaria immunity in mice lacking IFN-gamma receptor. *J. Immunol. Baltim. Md 1950* **154**, 5338–5344 (1995).

183. Villegas-Mendez, A. *et al.* Heterogeneous and tissue-specific regulation of effector T cell responses by IFN-gamma during Plasmodium berghei ANKA infection. *J. Immunol. Baltim. Md 1950* **187**, 2885–2897 (2011).

184. Minkah, N. K. *et al.* Innate immunity limits protective adaptive immune responses against pre-erythrocytic malaria parasites. *Nat. Commun.* **10**, 3950 (2019).

185. Duffy, F. J. *et al.* Early whole blood transcriptional responses to radiation-attenuated Plasmodium falciparum sporozoite vaccination in malaria naïve and malaria pre-exposed adult volunteers. *Malar. J.* **20**, 308 (2021).

186. Du, Y. *et al.* Systems analysis of immune responses to attenuated P. falciparum malaria sporozoite vaccination reveals excessive inflammatory signatures correlating with impaired immunity. *PLoS Pathog.* **18**, e1010282 (2022).

187. Zaidi, I. *et al.* γδ T Cells Are Required for the Induction of Sterile Immunity during Irradiated Sporozoite Vaccinations. *J. Immunol.* **199**, 3781–3788 (2017).

188. Ryg-Cornejo, V. *et al.* NK cells and conventional dendritic cells engage in reciprocal activation for the induction of inflammatory responses during Plasmodium berghei ANKA infection. *Immunobiology* **218**, 263–271 (2013).

189. Carvalho, L. H. *et al.* IL-4-secreting CD4+ T cells are crucial to the development of CD8+ T-cell responses against malaria liver stages. *Nat. Med.* **8**, 166–170 (2002).

190. Murphy, K. M. Janeway's immunobiology /. (2017).

191. Noah S. Butler; Nathan W. Schmidt; John T. Harty. Differential Effector Pathways Regulate Memory CD8 T Cell Immunity against Plasmodium berghei versus P. yoelii Sporozoite. *J Immunol (2010) 184 (5): 2528–2538.* doi:https://doi.org/10.4049/jimmunol.0903529.

192. Kurup, S. P., Butler, N. S. & Harty, J. T. T cell-mediated immunity to malaria. *Nat. Rev. Immunol.* **19**, 457–471 (2019).

193. Cockburn, I. A. *et al.* In vivo imaging of CD8 $^{+}$ T cell-mediated elimination of malaria liver stages. *Proc. Natl. Acad. Sci.* **110**, 9090–9095 (2013).

194. Cockburn, I. A., Tse, S.-W. & Zavala, F. CD8+ T Cells Eliminate Liver-Stage Plasmodium berghei Parasites without Detectable Bystander Effect. *Infect. Immun.* **82**, 1460–1464 (2014).

195. Brown, M. A. & Su, M. A. An Inconvenient Variable: Sex Hormones and Their Impact on T Cell Responses. *J. Immunol.* **202**, 1927–1933 (2019).

196. Fish_NatureImmReview_2008_The X-files in immunity- sex-based differences predispose immune responses.pdf.

197. Chi, L. *et al.* Sexual dimorphism in skin immunity is mediated by an androgen-ILC2-dendritic cell axis. *Science* **384**, eadk6200 (2024).

198. Wierman, M. E. Sex steroid effects at target tissues: mechanisms of action. *Adv. Physiol. Educ.* **31**, 26–33 (2007).

199. Guan, X. *et al.* Androgen receptor activity in T cells limits checkpoint blockade efficacy. *Nature* **606**, 791–796 (2022).

200. Kwon, H. *et al.* Androgen conspires with the CD8 $^{+}$ T cell exhaustion program and contributes to sex bias in cancer. *Sci. Immunol.* **7**, eabq2630 (2022).

201. Fox, H. S., Bond, B. L. & Parslow, T. G. Estrogen regulates the IFN-gamma promoter. *J. Immunol.* **146**, 4362–4367 (1991).

202. Shen, Z., Rodriguez-Garcia, M., Patel, M. V. & Wira, C. R. Direct and Indirect endocrine-mediated suppression of human endometrial CD8+T cell cytotoxicity. *Sci. Rep.* **11**, 1773 (2021).

203. Yee Mon, K. J. *et al.* Differential Sensitivity to IL-12 Drives Sex-Specific Differences in the CD8+ T Cell Response to Infection. *ImmunoHorizons* **3**, 121–132 (2019).

204. Lai, J.-J. *et al.* Androgen Receptor Influences on Body Defense System via Modulation of Innate and Adaptive Immune Systems. *Am. J. Pathol.* **181**, 1504–1512 (2012).

205. Klein, S. L. Hormonal and immunological mechanisms mediating sex differences in parasite infection. *Parasite Immunol.* **26**, 247–264 (2004).

206. *Sex and Gender Differences in Infection and Treatments for Infectious Diseases*. vol. 441 (Springer International Publishing, Cham, 2023).

207. Jacobsen, H. & Klein, S. L. Sex Differences in Immunity to Viral Infections. *Front. Immunol.* **12**, 720952 (2021).

208. Hodgson, S. H. *et al.* Increased sample volume and use of quantitative reverse-transcription PCR can improve prediction of liver-to-blood inoculum size in controlled human malaria infection studies. *Malar. J.* **14**, 33 (2015).

209. Murphy, J. R., Baqar, S., Davis, J. R., Herrington, D. A. & Clyde, D. F. Evidence for a 6.5-day minimum exoerythrocytic cycle for Plasmodium falciparum in humans and confirmation that immunization with a synthetic peptide representative of a region of the circumsporozoite protein retards infection. *J. Clin. Microbiol.* **27**, 1434–1437 (1989).

210. Hermsen, C. C. *et al.* Testing vaccines in human experimental malaria: statistical analysis of parasitemia measured by a quantitative real-time polymerase chain reaction. *Am. J. Trop. Med. Hyg.* **71**, 196–201 (2004).

211. Stanisic, D. I., McCarthy, J. S. & Good, M. F. Controlled Human Malaria Infection: Applications, Advances, and Challenges. *Infect. Immun.* **86**, e00479-17 (2018).

212. Em, B. *et al.* Sporozoite immunization of human volunteers under mefloquine prophylaxis is safe, immunogenic and protective: a double-blind randomized controlled clinical trial. *PloS One* **9**, (2014).

213. Bijker, E. M. *et al.* Cytotoxic Markers Associate With Protection Against Malaria in Human Volunteers Immunized With Plasmodium falciparum Sporozoites. *J. Infect. Dis.* **210**, 1605–1615 (2014).

214. Healy, S. A. *et al.* Chemoprophylaxis Vaccination: Phase I Study to Explore Stage-specific Immunity to Plasmodium falciparum in US Adults. *Clin. Infect. Dis.* **71**, 1481–1490 (2020).

215. Murphy, S. C. *et al.* A Randomized Trial Evaluating the Prophylactic Activity of DSM265 Against Preerythrocytic Plasmodium falciparum Infection During Controlled Human Malarial Infection by Mosquito Bites and Direct Venous Inoculation. *J. Infect. Dis.* **217**, 693–702 (2018).

216. Murphy, S. C. *et al.* A genetically engineered Plasmodium falciparum parasite vaccine provides protection from controlled human malaria infection. *Sci. Transl. Med.* **14**, eabn9709 (2022).

217. Hermsen, C. C. *et al.* Detection of Plasmodium falciparum malaria parasites in vivo by real-time quantitative PCR. *Mol. Biochem. Parasitol.* **118**, 247–251 (2001).

218. Talley, A. K. *et al.* Safety and comparability of controlled human Plasmodium falciparum infection by mosquito bite in malaria-naïve subjects at a new facility for sporozoite challenge. *PloS One* **9**, e109654 (2014).

219. Kublin, J. G. *et al.* Safety, Pharmacokinetics, and Causal Prophylactic Efficacy of KAF156 in a *Plasmodium falciparum* Human Infection Study. *Clin. Infect. Dis.* **73**, e2407–e2414 (2021).

220. Roestenberg, M. *et al.* A double-blind, placebo-controlled phase 1/2a trial of the genetically attenuated malaria vaccine PfSPZ-GA1. *Sci. Transl. Med.* **12**, eaaz5629 (2020).

221. Murphy, S. C. *et al.* PfSPZ-CVac efficacy against malaria increases from 0% to 75% when administered in the absence of erythrocyte stage parasitemia: A randomized, placebo-controlled trial with controlled human malaria infection. *PLOS Pathog.* **17**, e1009594 (2021).

222. Murphy, S. C. *et al.* Real-time quantitative reverse transcription PCR for monitoring of blood-stage Plasmodium falciparum infections in malaria human challenge trials. *Am. J. Trop. Med. Hyg.* **86**, 383–394 (2012).

223. Roozen, G.V.T. et al. Single immunisation with genetically attenuated PfΔmei2 (GA2) parasites leads to high level protection against a controlled human malaria infection. (2025).

224. Lamers, O. A. C. *et al.* Safety and Efficacy of Immunization with a Late-Liver-Stage Attenuated Malaria Parasite. *N. Engl. J. Med.* **391**, 1913–1923 (2024).

225. Despommier, D. D., Griffin, D. O., Gwadz, R. W., Hotez, P. J. & Knirsch, C. A. *Parasitic Diseases 7th Edition*. (Independently published, 2019).

226. R Core Team. R: A Language and Environment for Statistical Computing. R Foundation for Statistical Computing (2023).

227. Anderson-Bergman, C. icenReg: Regression Models for Interval Censored Data in R. *J. Stat. Softw.* **81**, 1–23 (2017).

228. Fay, M. P. & Shaw, P. A. Exact and Asymptotic Weighted Logrank Tests for Interval Censored Data: The interval R Package. *J. Stat. Softw.* **36**, 1–34 (2010).

229. Bates, D., Maechler, M., Bolker, B. & Walker, S. lme4: Linear Mixed-Effects Models using 'Eigen' and S4. 1.1-35.5 https://doi.org/10.32614/CRAN.package.lme4 (2003).

230. Gómez-Pérez, G. P. *et al.* Controlled human malaria infection by intramuscular and direct venous inoculation of cryopreserved Plasmodium falciparum sporozoites in malaria-naïve volunteers: effect of injection volume and dose on infectivity rates. *Malar. J.* **14**, 306 (2015).

231. Laurens, M. B. *et al.* Dose-Dependent Infectivity of Aseptic, Purified, Cryopreserved Plasmodium falciparum 7G8 Sporozoites in Malaria-Naive Adults. *J. Infect. Dis.* **220**, 1962–1966 (2019).

232. Seilie, A. M. *et al.* Beyond Blood Smears: Qualification of Plasmodium 18S rRNA as a Biomarker for Controlled Human Malaria Infections. *Am. J. Trop. Med. Hyg.* **100**, 1466–1476 (2019).

233. Spring, M., Polhemus, M. & Ockenhouse, C. Controlled Human Malaria Infection. *J. Infect. Dis.* **209**, S40–S45 (2014).

234. Hoffman, S. Experimental challenge of volunteers with malaria. *Ann. Intern. Med.* **127**, 233–235.

235. Ferrer, P. *et al.* Repeat controlled human Plasmodium falciparum infections delay bloodstream patency and reduce symptoms. *Nat. Commun.* **15**, 5194 (2024).

236. Cummings, J. F. *et al.* A phase IIa, randomized, double-blind, safety, immunogenicity and efficacy trial of Plasmodium falciparum vaccine antigens merozoite surface protein 1 and

RTS,S formulated with AS02 adjuvant in healthy, malaria-naïve adults. *Vaccine* **42**, 3066–3074 (2024).

237. Bennett, J. W. *et al.* Phase 1/2a Trial of Plasmodium vivax Malaria Vaccine Candidate VMP001/AS01B in Malaria-Naive Adults: Safety, Immunogenicity, and Efficacy. *PLoS Negl. Trop. Dis.* **10**, e0004423 (2016).
238. Hickey, B. W. *et al.* Mosquito bite immunization with radiation-attenuated Plasmodium falciparum sporozoites: safety, tolerability, protective efficacy and humoral immunogenicity. *Malar. J.* **15**, 377 (2016).
239. Tamminga, C. *et al.* Human adenovirus 5-vectored Plasmodium falciparum NMRC-M3V-Ad-PfCA vaccine encoding CSP and AMA1 is safe, well-tolerated and immunogenic but does not protect against controlled human malaria infection. *Hum. Vaccines Immunother.* **9**, 2165–2177 (2013).
240. Schats, R. *et al.* Heterologous Protection against Malaria after Immunization with Plasmodium falciparum Sporozoites. *PloS One* **10**, e0124243 (2015).
241. Brie, B. *et al.* Brain Control of Sexually Dimorphic Liver Function and Disease: The Endocrine Connection. *Cell. Mol. Neurobiol.* **39**, 169–180 (2019).
242. Kasarinaite, A., Sinton, M., Saunders, P. T. K. & Hay, D. C. The Influence of Sex Hormones in Liver Function and Disease. *Cells* **12**, 1604 (2023).
243. Friedman-Klabanoff, D. J. *et al.* The Controlled Human Malaria Infection Experience at the University of Maryland. *Am. J. Trop. Med. Hyg.* (2019) doi:10.4269/ajtmh.18-0476.
244. Charni-Natan, M., Aloni-Grinstein, R., Osher, E. & Rotter, V. Liver and Steroid Hormones—Can a Touch of p53 Make a Difference? *Front. Endocrinol.* **10**, 374 (2019).

245. Ben-Moshe, S. & Itzkovitz, S. Spatial heterogeneity in the mammalian liver. *Nat. Rev. Gastroenterol. Hepatol.* **16**, 395–410 (2019).

246. Marcos, R. *et al.* Stereological assessment of sexual dimorphism in the rat liver reveals differences in hepatocytes and Kupffer cells but not hepatic stellate cells. *J. Anat.* **228**, 996–1005 (2016).

247. Hu, M. & Chikina, M. InstaPrism: an R package for fast implementation of BayesPrism. *Bioinformatics* **40**, btae440 (2024).

248. Lex, A., Gehlenborg, N., Strobelt, H., Vuillemot, R. & Pfister, H. UpSet: Visualization of Intersecting Sets. *IEEE Trans. Vis. Comput. Graph.* **20**, 1983–1992 (2014).

249. Rowe, A. A., Issioui, Y., Johnny, B. & Wert, K. J. Murine Orchiectomy and Ovariectomy to Reduce Sex Hormone Production. *J. Vis. Exp. JoVE* e64379 (2023) doi:10.3791/64379.

250. Sanz, E. *et al.* RiboTag Analysis of Actively Translated mRNAs in Sertoli and Leydig Cells In Vivo. *PLoS ONE* **8**, e66179 (2013).

251. Herbst, K. L., Anawalt, B. D., Amory, J. K. & Bremner, W. J. Acyline: the first study in humans of a potent, new gonadotropin-releasing hormone antagonist. *J Clin Endocrinol Metab* **87**, 3215–20 (2002).

252. Herbst, K. L. *et al.* A single dose of the potent gonadotropin-releasing hormone antagonist acyline suppresses gonadotropins and testosterone for 2 weeks in healthy young men. *J Clin Endocrinol Metab* **89**, 5959–65 (2004).

253. AlOgayil, N. *et al.* Distinct roles of androgen receptor, estrogen receptor alpha, and BCL6 in the establishment of sex-biased DNA methylation in mouse liver. *Sci. Rep.* **11**, 13766 (2021).

254. Heintza, M. M., Kumar, R., Rutledge, M. M. & Baldwin, W. S. Cyp2b-null male mice are susceptible to diet-induced obesity and perturbations in lipid homeostasis. *J. Nutr. Biochem.* **70**, 125–137 (2019).

255. Creasy, K. T., Jiang, J., Ren, H., Peterson, M. L. & Spear, B. T. Zinc Fingers and Homeoboxes 2 (Zhx2) Regulates Sexually Dimorphic Cyp Gene Expression in the Adult Mouse Liver. *Gene Expr.* **17**, 7–17 (2016).

256. Blencowe, M. *et al.* Relative contributions of sex hormones, sex chromosomes, and gonads to sex differences in tissue gene regulation. *Genome Res.* **32**, 807–824 (2022).

257. Chu, T., Wang, Z., Pe'er, D. & Danko, C. G. Cell type and gene expression deconvolution with BayesPrism enables Bayesian integrative analysis across bulk and single-cell RNA sequencing in oncology. *Nat. Cancer* **3**, 505–517 (2022).

258. Scotland, R. S., Stables, M. J., Madalli, S., Watson, P. & Gilroy, D. W. Sex differences in resident immune cell phenotype underlie more efficient acute inflammatory responses in female mice. *Blood* **118**, 5918–5927 (2011).

259. Becu-Villalobos, D. Liver Sex Dimorphism and Zonation Shaped by Growth Hormone. *Endocrinology* **163**, bqac087 (2022).

260. Ebrahimnezhaddarzi, S. *et al.* Mpeg1 is not essential for antibacterial or antiviral immunity, but is implicated in antigen presentation. *Immunol. Cell Biol.* **100**, 529–546 (2022).

261. Rodríguez, P. The role of a pore-forming protein, Mpeg1, in cytosolic import. (2022) doi:10.17863/CAM.81743.

262. Campbell, S. E., Mehan, K. A., Tunstall, R. J., Febbraio, M. A. & Cameron-Smith, D. 17beta-estradiol upregulates the expression of peroxisome proliferator-activated receptor alpha and lipid oxidative genes in skeletal muscle. (2003) doi:10.1677/jme.0.0310037.

263. Gazzinelli, R. T., Kalantari, P., Fitzgerald, K. A. & Golenbock, D. T. Innate sensing of malaria parasites. *Nat. Rev. Immunol.* **14**, 744–757 (2014).

264. He, X., Xia, L., Tumas, K. C., Wu, J. & Su, X.-Z. Type I Interferons and Malaria: A Double-Edge Sword Against a Complex Parasitic Disease. *Front. Cell. Infect. Microbiol.* **10**, 594621 (2020).

265. Marques-da-Silva, C. *et al.* Direct type I interferon signaling in hepatocytes controls malaria. *Cell Rep.* **40**, 111098 (2022).

266. Park, E.-S. *et al.* Gender-specific alteration of steroid metabolism and its impact on viral replication in a mouse model of hepatitis B virus infection. *Anim. Cells Syst.* **28**, 466–480 (2024).

267. Sellau, J. *et al.* Immunological clues to sex differences in parasitic diseases. *Trends Parasitol.* **40**, 1029–1041 (2024).

268. Kim, N. *et al.* Interferon-inducible protein SCOTIN interferes with HCV replication through the autolysosomal degradation of NS5A. *Nat. Commun.* **7**, 10631 (2016).

269. Zhang, Y. *et al.* The in vivo ISGylome links ISG15 to metabolic pathways and autophagy upon Listeria monocytogenes infection. *Nat. Commun.* **10**, 5383 (2019).

270. Checroun, C., Wehrly, T. D., Fischer, E. R., Hayes, S. F. & Celli, J. Autophagy-mediated reentry of Francisella tularensis into the endocytic compartment after cytoplasmic replication. *Proc. Natl. Acad. Sci.* **103**, 14578–14583 (2006).

271. Huang, H., Akira, S. & Santos, M. M. Is the iron donor lipocalin 2 implicated in the pathophysiology of hereditary hemochromatosis?†. *Hepatology* **49**, 1012 (2009).

272. Truksa, J., Lee, P. & Beutler, E. The role of STAT, AP-1, E-box and TIEG motifs in the regulation of hepcidin by IL-6 and BMP-9: Lessons from human *HAMP* and murine *Hamp1* and *Hamp2* gene promoters. *Blood Cells. Mol. Dis.* **39**, 255–262 (2007).

273. Kim, M. S., Shigenaga, J., Moser, A., Grunfeld, C. & Feingold, K. R. Suppression of DHEA sulfotransferase (Sult2A1) during the acute-phase response. *Am. J. Physiol.-Endocrinol. Metab.* **287**, E731–E738 (2004).

274. Longcope, C. Metabolism of Dehydroepiandrosterone. *Ann. N. Y. Acad. Sci.* **774**, 143–148 (1995).

275. Santos-Marcos, J. A., Mora-Ortiz, M., Tena-Sempere, M., Lopez-Miranda, J. & Camargo, A. Interaction between gut microbiota and sex hormones and their relation to sexual dimorphism in metabolic diseases. *Biol. Sex Differ.* **14**, 4 (2023).

276. El-Moamly, A. A. & El-Sweify, M. A. Malaria vaccines: the 60-year journey of hope and final success-lessons learned and future prospects. *Trop Med Health* **51**, 29 (2023).

277. Weiss, W. R. & Jiang, C. G. Protective CD8+ T lymphocytes in primates immunized with malaria sporozoites. *PLoS One* **7**, e31247 (2012).

278. Seder, R. A. *et al.* Protection against malaria by intravenous immunization with a nonreplicating sporozoite vaccine. *Science* **341**, 1359–65 (2013).

279. Tse, S. W., Radtke, A. J. & Zavala, F. Induction and maintenance of protective CD8+ T cells against malaria liver stages: implications for vaccine development. *Mem Inst Oswaldo Cruz* **106 Suppl 1**, 172–8 (2011).

280. Holz, L. E. *et al.* CD8(+) T Cell Activation Leads to Constitutive Formation of Liver Tissue-Resident Memory T Cells that Seed a Large and Flexible Niche in the Liver. *Cell Rep* **25**, 68-79 e4 (2018).

281. Valencia-Hernandez, A. M. *et al.* A Natural Peptide Antigen within the Plasmodium Ribosomal Protein RPL6 Confers Liver TRM Cell-Mediated Immunity against Malaria in Mice. *Cell Host Microbe* **27**, 950-962.e7 (2020).

282. Klein, S. L. & Flanagan, K. L. Sex differences in immune responses. *Nat Rev Immunol* **16**, 626–38 (2016).

283. Kur, P., Kolasa-Wołosiuk, A., Misiakiewicz-Has, K. & Wiszniewska, B. Sex Hormone-Dependent Physiology and Diseases of Liver. *Int. J. Environ. Res. Public. Health* **17**, 2620 (2020).

284. Legorreta-Herrera, M. *et al.* Sex hormones modulate the immune response to Plasmodium berghei ANKA in CBA/Ca mice. *Parasitol. Res.* **114**, 2659–2669 (2015).

285. Imai, J., Otani, M., Sakai, T. & Hatta, S. Purification of the subcellular compartment in which exogenous antigens undergo endoplasmic reticulum-associated degradation from dendritic cells. *Heliyon* **2**, e00151 (2016).

286. Stone, B. C. *et al.* Complex Minigene Library Vaccination for Discovery of Pre-Erythrocytic Plasmodium T Cell Antigens. *PLoS One* **11**, e0153449 (2016).

287. Arrington, J. *et al.* Plasmid vectors encoding cholera toxin or the heat-labile enterotoxin from Escherichia coli are strong adjuvants for DNA vaccines. *J Virol* **76**, 4536–46 (2002).

288. Miller, J. L. *et al.* Quantitative bioluminescent imaging of pre-erythrocytic malaria parasite infection using luciferase-expressing Plasmodium yoelii. *PLoS One* **8**, e60820 (2013).

289. Kennedy, M. *et al.* A rapid and scalable density gradient purification method for Plasmodium sporozoites. *Malar J* **11**, 421 (2012).

290. Billman, Z. P., Seilie, A. M. & Murphy, S. C. Purification of Plasmodium Sporozoites Enhances Parasite-Specific CD8+ T Cell Responses. *Infect Immun* **84**, 2233–2242 (2016).

291. Finak, G. *et al.* OpenCyto: an open source infrastructure for scalable, robust, reproducible, and automated, end-to-end flow cytometry data analysis. *PLoS Comput Biol* **10**, e1003806 (2014).

292. Murphy, S. C., Kas, A., Stone, B. C. & Bevan, M. J. A T-cell response to a liver-stage Plasmodium antigen is not boosted by repeated sporozoite immunizations. *Proc Natl Acad Sci U A* **110**, 6055–60 (2013).

293. Liberzon, A. *et al.* The Molecular Signatures Database Hallmark Gene Set Collection. *Cell Syst.* **1**, 417–425 (2015).

294. Subramanian, A. *et al.* Gene set enrichment analysis: a knowledge-based approach for interpreting genome-wide expression profiles. *Proc Natl Acad Sci U A* **102**, 15545–50 (2005).

295. Coelho-Dos-Reis, J. G., Li, X. & Tsuji, M. Development of a novel mechanism-based glycolipid adjuvant for vaccination. *F1000Res* **7**, (2018).

296. Butler, N. S., Schmidt, N. W. & Harty, J. T. Differential effector pathways regulate memory CD8 T cell immunity against Plasmodium berghei versus P. yoelii sporozoites. *J Immunol* **184**, 2528–38 (2010).

297. Cooney, L. A. *et al.* Short-lived effector CD8 T cells induced by genetically attenuated malaria parasite vaccination express CD11c. *Infect Immun* **81**, 4171–81 (2013).

298. Waxman, D. J. & Holloway, M. G. Sex differences in the expression of hepatic drug metabolizing enzymes. *Mol Pharmacol* **76**, 215–28 (2009).

299. Ashburner, M. *et al.* Gene ontology: tool for the unification of biology. The Gene Ontology Consortium. *Nat Genet* **25**, 25–9 (2000).

300. Hall, K. & Korenchevsky, V. Liver Changes in Male Rats after Castration and Injection of Sex Hormones. *Br Med J* **1**, 438–41 (1938).

301. Wolfl, M., Kuball, J., Eyrich, M., Schlegel, P. G. & Greenberg, P. D. Use of CD137 to study the full repertoire of CD8+ T cells without the need to know epitope specificities. *Cytom. A* **73**, 1043–9 (2008).

302. Yang, C. *et al.* Androgen receptor-mediated CD8+ T cell stemness programs drive sex differences in antitumor immunity. *Immunity* **55**, 1268-1283.e9 (2022).

303. Wherry, E. J. & Kurachi, M. Molecular and cellular insights into T cell exhaustion. *Nat Rev Immunol* **15**, 486–99 (2015).

304. Brown, M. A. & Su, M. A. An Inconvenient Variable: Sex Hormones and Their Impact on T Cell Responses. *J. Immunol.* **202**, 1927–1933 (2019).

305. Araneo, B. A., Dowell, T., Diegel, M. & Daynes, R. A. Dihydrotestosterone exerts a depressive influence on the production of interleukin-4 (IL-4), IL-5, and gamma-interferon, but not IL-2 by activated murine T cells. *Blood* **78**, 688–99 (1991).

306. De Souza Santos, R., Frank, A. P., Palmer, B. F. & Clegg, D. J. Sex and media: Considerations for cell culture studies. *ALTEX* **35**, 435–440 (2018).

307. Gubbels Bupp, M. R. & Jorgensen, T. N. Androgen-Induced Immunosuppression. *Front. Immunol.* **9**, 794 (2018).

308. Masopust, D. & Soerens, A. G. Tissue-Resident T Cells and Other Resident Leukocytes. *Annu Rev Immunol* **37**, 521–546 (2019).

309. Chin, S. S. *et al.* T cell receptor and IL-2 signaling strength control memory CD8(+) T cell functional fitness via chromatin remodeling. *Nat Commun* **13**, 2240 (2022).

310. Saito, K., Negishi, M. & James Squires, E. Sexual dimorphisms in zonal gene expression in mouse liver. *Biochem. Biophys. Res. Commun.* **436**, 730–735 (2013).

311. Nilsson, M. E. *et al.* Measurement of a Comprehensive Sex Steroid Profile in Rodent Serum by High-Sensitive Gas Chromatography-Tandem Mass Spectrometry. *Endocrinology* **156**, 2492–2502 (2015).

312. Sedelaar, J. M., Dalrymple, S. S. & Isaacs, J. T. Of Mice and Men-Warning: Intact Versus Castrated Adult Male Mice as Xenograft Hosts Are Equivalent to Hypogonadal Versus Abiraterone Treated Aging Human Males, Respectively. *The Prostate* **73**, 1316 (2013).

313. Jänne, M., Deol, H. K., Power, S. G., Yee, S. P. & Hammond, G. L. Human sex hormone-binding globulin gene expression in transgenic mice. *Mol. Endocrinol. Baltim. Md* **12**, 123–136 (1998).

314. Staley, K. & Scharfman, H. A woman's prerogative. *Nat. Neurosci.* **8**, 697–699 (2005).

315. Herbison, A. E. The Gonadotropin-Releasing Hormone Pulse Generator. *Endocrinology* **159**, 3723–3736 (2018).

316. Colldén, H. *et al.* Comprehensive Sex Steroid Profiling in Multiple Tissues Reveals Novel Insights in Sex Steroid Distribution in Male Mice. *Endocrinology* **163**, bqac001 (2022).

317. 010905 - Four Core Genotypes (FCG) Strain Details. https://www.jax.org/strain/010905.

318. Arnold, A. P. & Chen, X. What does the 'four core genotypes' mouse model tell us about sex differences in the brain and other tissues? *Front. Neuroendocrinol.* **30**, 1–9 (2009).

319. Arnold, A. P. Mouse Models for Evaluating Sex Chromosome Effects that Cause Sex Differences in Non-Gonadal Tissues. *J. Neuroendocrinol.* **21**, 377–386 (2009).

320. Jiang, C. *et al.* Comparative Transcriptomics Analyses in Livers of Mice, Humans, and Humanized Mice Define Human-Specific Gene Networks. *Cells* **9**, 2566 (2020).

321. Schwarz, J. *et al.* A microfluidic device for measuring cell migration towards substrate-bound and soluble chemokine gradients. *Sci. Rep.* **6**, 36440 (2016).

322. Nuciforo, S. & Heim, M. H. Organoids to model liver disease. *JHEP Rep.* **3**, 100198 (2020).

323. Zschaler, J., Schlorke, D. & Arnhold, J. Differences in innate immune response between man and mouse. *Crit. Rev. Immunol.* (2014) doi:10.1615/CritRevImmunol.2014011600.

324. Tian, Z., Chen, Y. & Gao, B. Natural killer cells in liver disease. *Hepatology* **57**, 1654 (2013).

325. Watson, F. N. *et al.* Cryopreserved Sporozoites with and without the Glycolipid Adjuvant 7DW8-5 Protect in Prime-and-Trap Malaria Vaccination. *Am. J. Trop. Med. Hyg.* **106**, 1227–1236 (2022).

326. Qu, G. *et al.* Comparing Mouse and Human Tissue-Resident γδ T Cells. *Front. Immunol.* **13**, (2022).

327. Bjornson-Hooper, Z. B. *et al.* A Comprehensive Atlas of Immunological Differences Between Humans, Mice, and Non-Human Primates. *Front. Immunol.* **13**, 867015 (2022).

328. Berghöfer, B. *et al.* TLR7 Ligands Induce Higher IFN-α Production in Females1. *J. Immunol.* **177**, 2088–2096 (2006).

329. Conteh, S. *et al.* Grammomys surdaster, the Natural Host for Plasmodium berghei Parasites, as a Model to Study Whole-Organism Vaccines Against Malaria. *Am J Trop Med Hyg* (2017) doi:10.4269/ajtmh.16-0745.

330. Mestas, J. & Hughes, C. C. W. Of Mice and Not Men: Differences between Mouse and Human Immunology. *J. Immunol.* **172**, 2731–2738 (2004).

331. Medica, D. L. & Sinnis, P. Quantitative dynamics of Plasmodium yoelii sporozoite transmission by infected anopheline mosquitoes. *Infect. Immun.* **73**, 4363–4369 (2005).

332. Mainz, R. E. *et al.* NLRP6 Inflammasome Modulates Disease Progression in a Chronic-Plus-Binge Mouse Model of Alcoholic Liver Disease. *Cells* **11**, 182 (2022).

333. Yang, M., Ma, F. & Guan, M. Role of Steroid Hormones in the Pathogenesis of Nonalcoholic Fatty Liver Disease. *Metabolites* **11**, 320 (2021).

334. Shears, M. J., Seilie, A. M., Kim Lee Sim, B., Hoffman, S. L. & Murphy, S. C. Quantification of Plasmodium knowlesi versus Plasmodium falciparum in the rhesus liver: implications for malaria vaccine studies in rhesus models. *Malar. J.* **19**, 313 (2020).

335. Peterson, M. S. *et al.* Clinical recovery of Macaca fascicularis infected with Plasmodium knowlesi. *Malar J.* **20**, 486 (2021).

336. Hochmuth, L. *et al.* Sex-dependent dynamics of metabolism in primary mouse hepatocytes. *Arch. Toxicol.* **95**, 3001–3013 (2021).

337. Minkah, N. K., Schafer, C. & Kappe, S. H. I. Humanized Mouse Models for the Study of Human Malaria Parasite Biology, Pathogenesis, and Immunity. *Front. Immunol.* **9**, (2018).

338. Zaidi, I. & Duffy, P. E. PfSPZ Vaccine learns a lesson. *Med* **2**, 1289–1291 (2021).

339. Chakraborty, S., Pramanik, J. & Mahata, B. Revisiting steroidogenesis and its role in immune regulation with the advanced tools and technologies. *Genes Immun.* **22**, 125–140 (2021).

340. Kinter, K. J., Amraei, R. & Anekar, A. A. Biochemistry, Dihydrotestosterone. in *StatPearls [Internet]* (StatPearls Publishing, 2023).

341. Dawson, P. A. & Setchell, K. D. R. Will the real bile acid sulfotransferase please stand up? Identification of Sult2a8 as a major hepatic bile acid sulfonating enzyme in mice1. *J. Lipid Res.* **58**, 1033–1035 (2017).

342. Noyes, H. A. *et al.* Genotype and expression analysis of two inbred mouse strains and two derived congenic strains suggest that most gene expression is trans regulated and sensitive to genetic background. *BMC Genomics* **11**, 361 (2010).

343. Willis-Owen, S. A. G. & Valdar, W. Deciphering gene-environment interactions through mouse models of allergic asthma. *J. Allergy Clin. Immunol.* **123**, 14–23 (2009).

344. Hu, T. *et al.* Single-cell spatial metabolomics with cell-type specific protein profiling for tissue systems biology. *Nat. Commun.* **14**, 8260 (2023).

345. Kanehisa, M. & Goto, S. KEGG: Kyoto Encyclopedia of Genes and Genomes. *Nucleic Acids Res.* **28**, 27–30 (2000).

VITA

Caroline Duncombe, born in 1996, grew up in Appleton, WI and attended Appleton North High School. She earned her Bachelor of Arts degree in Chemistry with a concentration in Community and Global Health from Macalester College in 2018. During her undergraduate years, she gained diverse research and global health experience through internships in Quito, Ecuador; Fort Collins, Colorado; and Geneva, Switzerland. Following graduation, Caroline joined the Laboratory of Dr. Clifton Barry in the Tuberculosis Research Section at the National Institute of Allergy and Infectious Diseases (NIAID), part of the National Institutes of Health (NIH) in Bethesda, Maryland, where she investigated the mechanisms of action of tuberculosis treatments. In 2020, she began her doctoral studies in the Pathobiology Program at the University of Washington. Caroline completed her dissertation research in the Laboratory of Dr. Sean C. Murphy where she studied the impact of biological sex on the *Plasmodium* parasite liver stage.